Functions and interactions of Sec61β/Sbh1

Dissertation

zur Erlangung des Grades

des Doktors der Naturwissenschaften

der Naturwissenschaftlich-Technischen Fakultät

der **Universität des Saarlandes**

von

Lalitha Yadhanapudi

Saarbrücken

2024

Tag des Kolloquiums:	19.02.2025
Dekan:	Prof. Dr.-Ing. Dirk Bähre
Berichterstatter:	Prof. Dr. Karin Römisch Prof. Dr. Martin van der Laan
Akad. Mitglied:	Dr. Björn Diehl
Vorsitz:	Prof. Dr. Volkhard Helms

TABLE OF CONTENTS

LIST OF FIGURES

LIST OF TABLES

LIST OF ABBREVIATIONS

A	Alanine
Ala	Alanine
Amp	Ampicillin
APS	Ammonium persulfate
Asn	Asparagine
B88	Buffer 88
BiP	Immunoglobulin binding protein
BSA	Bovine serum albumin
C	Cysteine
C-terminal	Carboxy terminal
C-terminus	Carboxy terminus
$CaCl_2$	Calcium chloride
CMP	Conserved membrane proximal
ConA	Concanavalin A
COPI/II	Coat protein complex I/II
CPY	Carboxypeptidase Y
Cryo-EM	Cryo-electron microscopy
Cys	Cysteine
D	Aspartic acid
DBC	Deoxy-Big CHAP
Der1	Degradation in the ER protein 1
Digi	Digitonin
DMSO	Dimethyl sulfoxide
DNA	Deoxyribonucleic acid
Doa10	Degradation of alpha 2 protein 10
DPAPB	Diaminopeptidase B
DTT	Dithiothreitol
E	Glutamic acid
EDTA	Ethylene diamine tetra acetic acid
ER	Endoplasmic reticulum
ERAD	ER-associated degradation
F	Phenylalanine
Fwd	Forward primer
G	Glycine
Gls1/2	Glucosidase 1
GTP	Guanosine triphosphate
H	Histidine
h	Hour(s)

Hac1	Homolog to Atf/Creb1
HCl	Hydrochloric acid
HEPES	4-(2-hydroxyethyl)-1-piperazineethanesulfonic acid
Hrd1	HMG-CoA reductase degradation protein 1
HRP	Horse radish peroxidase
Hsp70/40	Heat shock protein 70/40
Htm1	Homolog to ER mannosidase 1
I	Isoleucine
IDR	Intrinsically disordered region
IPTG	Isopropyl-β-D-thiogalactopyranosidase
Irc22	Increase recombination centers 22
Ire1	Inositol-requiring protein 1
K	Lysine
Kar2	Karyogamy protein 2
KCl	Potassium chloride
kDa	Kilodalton
KOAc	Potassium acetate
KOH	Potassium hydroxide
L	Leucine
LB	Lysogeny broth
Leu	Leucine
LiAc	Lithium acetate
Lys	Lysine
M	Methionine
MD	Molecular dynamics
MES	2-(N-morpholino) ethanesulfonic acid
$Mg(OAc)_2$	Magnesium acetate
$MgSO_4$	Magnesium sulfate
min	Minute(s)
$MnCl_2$	Manganese chloride
Mns1	Mannosidase 1
MOPS	3-(N-morpholino) propanesulfonic acid
MoRF	Molecular recognition feature
MP	Megaprimer
MQ	MilliQ
mRNA	Messenger RNA
N	Asparagine
N-terminal	Amino terminal
N-terminus	Amino terminus
NaCl	Sodium chloride
NaN_3	Sodium azide

o/n	Overnight
OD	Optical density
OST	Oligosaccharyl transferase
P	Proline
PAGE	Polyacrilamide gel electrophoresis
PCC-α-M	4-trans-(4-trans-Propylcyclohexyl)-cyclohexyl α-maltoside
PCR	Polymerase chain reaction
PDB	Protein Databank
PDI	Protein disulfide isomerase
PEG	Polyethylene glycol
PMSF	Phenylmethylsulfonyl chloride
Pmt	Protein *O*-mannosyltransferase
ppαF	Prepro alpha factor
Pro	Proline
ProtA	Protein A
Q	Glutamine
QC	Quality control
R	Arginine
RAMP	Ribosome-associated membrane protein
Rev	Reverse primer
RNA	Ribonucleic acid
RNC	Ribosome-nascent chain complex
RpL17a	Ribosomal protein of the large subunit L17A
rpm	Rotations per minute
RT	Room temperature
S	Serine
Sbh1/2	Sec61 beta homolog 1/2
SDM	Site-directed mutagenesis
SDS	Sodium dodecyl sulfate
Sec	Secretory transport protein
Sec61/62/63/71/72	Secretory transport protein 61/62/71/72
Ser	Serine
SNARE	Soluble NSF attachment protein receptor
SP	Signal peptide
SRP	Signal recognition particle
Ssh1	Sec sixty-one homolog 1
Sss1	Sec sixty-one suppressor 1
T	Threonine
TBST	Tris-buffered saline – 0.1 % Tween20
TCA	Trichloroacetic acid

TE	Tris-EDTA
TEMED	N, N, N’, N’-Tetramethylethylenediamine
TGN	Trans Golgi network
Thr	Threonine
TM	Trans-membrane
tRNA	Transfer RNA
TX-100	Triton X-100
UPR	Unfolded protein response
Ura	Uracil
V	Valine
W	Tryptophan
Y	Tyrosine
Yos9	Yeast OS-9 homolog
YPD	Yeast peptone dextrose
YPG	Yeast peptone glycerol

Functions and interactions of Sec61β/Sbh1

ABSTRACT

Secretory and transmembrane proteins depend on the universally conserved Sec61 complex for their translocation into the endoplasmic reticulum (ER) or membrane insertion. The function of the non-essential β subunit of the Sec61 channel, called Sbh1 in yeast, is not fully understood and the existing data predominantly covers its conserved transmembrane domain. The interactions and functions of the Sbh1 cytosolic domain, including its conserved membrane proximal (CMP) region, and its intrinsically disordered N-terminal region with multiple phosphorylation sites, remain unclear. In this work, I characterised defects of yeast mutants that lack *SBH1* and its paralog *SBH2*. I investigated the role of Sbh1 in the heptameric Sec complex responsible for posttranslational ER protein import and found it to not be essential for the complex stability. Based on molecular dynamics simulations that identified the Sbh1 CMP region as a potential interaction site, I generated and functionally characterised CMP mutants. I studied the interactions of the Sbh1 cytosolic domain and found that the CMP region interacts directly and specifically with Sbh1-dependent signal peptides. Based on my data, I hypothesise that the Sbh1 CMP domain selectively facilitates Sec61 channel insertion of specific signal peptides.

Functions and interactions of Sec61β/Sbh1

Zusammenfassung

Sekretorische und Transmembranproteine sind für ihre Translokation ins Endoplasmatische Retikulum (ER) oder bzw. Membraninsertion auf den universell konservierten Sec61-Komplex angewiesen. Die Funktion der nicht-essenziellen β-Untereinheit des Sec61-Kanals, in der Hefe Sbh1 genannt, ist nicht vollständig geklärt, und die vorhandenen Daten befassen sich vorwiegend mit der konservierten Transmembrandomäne. Die Interaktionen und Funktionen der zytosolischen Domäne von Sbh1, einschliesslich der konservierten membranproximalen (CMP) Region und dem intrinsisch ungeordneten, mehrfach phosphorylierten N-terminalen Bereich sind nach wie vor unklar. In dieser Arbeit habe ich funktionelle Defekte von Hefemutanten charakterisiert, denen *SBH1* und sein Paralog *SBH2* fehlen. Ich habe die Rolle von Sbh1 im heptameren, für posttranslationalen ER-Import verantwortlichen Sec-Komplex untersucht und festgestellt, dass Sbh1 zur Stabilität des Komplexes nicht wesentlich beiträgt. Auf der Grundlage von Molekulardynamiksimulationen, die die CMP-Region von Sbh1 als potenzielle Interaktionsstelle identifizierten, habe ich CMP-Mutanten erzeugt und funktionell charakterisiert. Außerdem habe ich die Interaktionen der zytosolischen Domäne von Sbh1 untersucht. Ich konnte zeigen, dass die CMP-Region direkt und spezifisch mit Sbh1-abhängigen Signalpeptiden interagiert. Auf der Grundlage meiner Daten stelle ich die Hypothese auf, dass die CMP-Domäne von Sbh1 selektiv die Sec61-Kanal-Insertion spezifischer Signalpeptide erleichtert.

Introduction

1

1. Introduction

1.1. Secretory Pathway in Eukaryotes

In eukaryotic cells, biochemical functions are compartmentalised in membrane bound organelles. The diversity between organelles allows for biochemical environments of varied protein compositions, pH, and inorganic ions to exist simultaneously [1]. These organelles receive their localised proteins and communicate with each other by protein secretion, enabling them to coordinate their functions and maintain cell homeostasis [2]. Protein secretion is an essential process in both prokaryotes and eukaryotes, and its mechanisms have been extensively studied. Figure 1.1 depicts a simplified version of events in the secretory pathway, its components and organelles that participate in it.

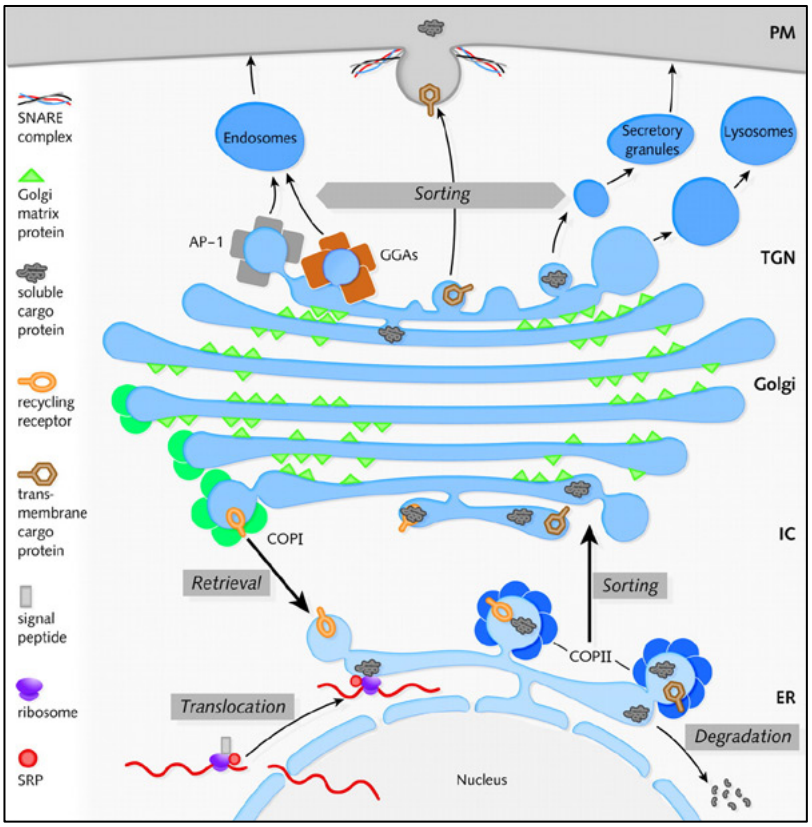

Figure 1.1 Schematic representation of the secretory pathway. Figure from Reynaud and Simpson, 2002. Components of the secretory pathway are shown. The pathway begins at the translocation of newly synthesised polypeptides into the ER where they are folded, modified and transported to the Golgi for futher processing, sorting and transport to their designated intracellular or extracellular location. Misfolded proteins in the ER are detected and transported to the cytosol for degradation. ER, Endoplasmic Reticulum; IC, Intermediate Complex; TGN, Trans Golgi Network; PM, Plasma Membrane.

The endoplasmic reticulum (ER) serves as the entry point into the secretory pathway for newly translated proteins where, upon translocation, they undergo maturation and folding and are transported to the Golgi. They are further processed in the Golgi and targeted to their destination where they are functional, within the cell, plasma membrane or extracellular space [3].

Newly synthesised proteins enter the secretory pathway by translocating into the ER either co-translationally or post-translationally (Figure 1.1). In *Saccharomyces cerevisiae*, co-translational translocation is mediated by the trimeric Sec61 complex consisting of subunits Sec61, Sbh1 and Sss1, while post-translational translocation is mediated by the heptameric Sec complex composed of Sec62, Sec63, Sec71, Sec72 and the Sec61 complex [4]. Protein translocation in mammalian cells is similarly performed the homologs of Sec61 complex and Sec complex [5]. The components and mechanisms of protein translocation into the ER will be discussed further in Section 1.2.

The ER serves as a processing hub for newly synthesised proteins, where they undergo a series of modifications, including cleavage of the signal peptide by the signal peptidase complex, *N*-glycosylation by oligosaccharyl transferase complex, *O*-mannosylation by protein mannosyltransferases, and disulfide bond formation by the enzyme protein disulfide isomerase (PDI) in the ER lumen [6,7]. Molecular chaperones, such as Kar2, assist in folding proteins and serve as critical checkpoints to detect misfolded proteins [8]. ER quality control mechanisms, triggered by the recognition of misfolded or unfolded proteins, prevent their exit from the ER by initially inhibiting aggregation, then attempting to facilitate correct refolding, or ultimately marking them for degradation [9,10]. One such mechanism is the

unfolded protein response (UPR), which upregulates chaperone expression to promote folding efficiency [11]. When misfolded proteins continue to accumulate, the cell initiates ER associated degradation (ERAD), whereby misfolded proteins are retro-translocated to the cytosol for proteasome-mediated degradation [12]. These processes will be further discussed in Section 1.3.

Following modification and quality control processes, ER resident proteins remain in the ER, while proteins targeted to other organelles or for secretion will continue in this pathway to enter the Golgi apparatus via vesicular transport (Figure 1.1). This transport can occur in anterograde (forward, ER to Golgi) or retrograde (Golgi to ER) as shown in Figure 1.2 [13–15].

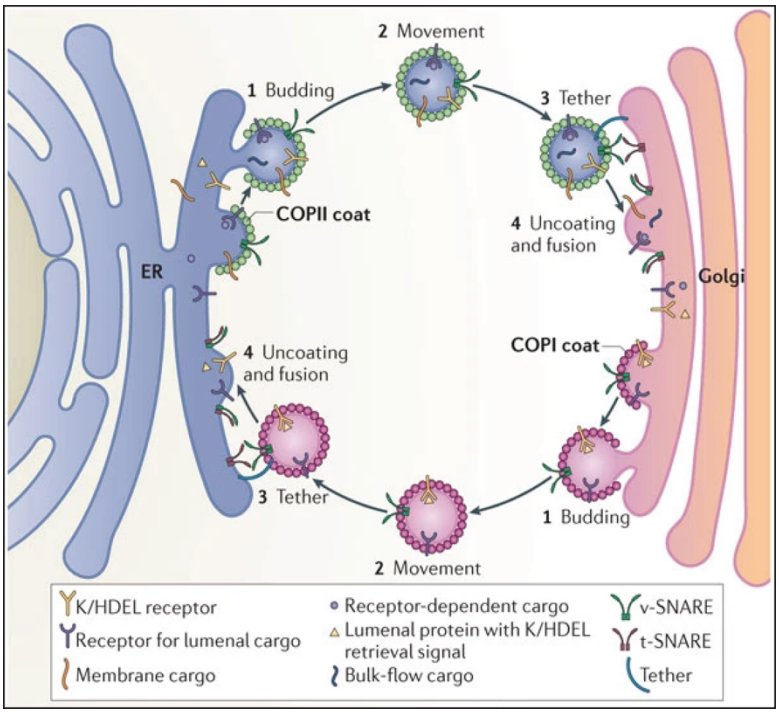

Figure 1.2 Simplified model for bidirectional transport and fusion of vesicles. Figure from Brandizzi and Barlowe, 2013. In anterograde transport from ER to Golgi, cargo proteins are packaged into COPII coated vesicles, while in retrograde transport from Golgi to ER, the vesicles are coated with COPI. Upon transport, the fusion of the vesicles to the target membrane is mediated by SNARE proteins.

In *S. cerevisiae,* the proteins to be exported accumulate at ER exit sites where they are packaged into transport vesicles coated with coat protein complex II (COPII), composed of

five subunits Sar1-GTPase, Sec23, Sec24, Sec13 and Sec31 [16,17]. Mammalian cells have a specialised transitional ER, in addition to ER exit sites, where cargo proteins accumulate to be packaged into COPII vesicles [18]. Sec12, a nucleotide exchange factor on the ER membrane, activates Sar1 GTPase, which triggers membrane-bound Sec23 and Sec24 to sort protein cargos into a prebudding cargo complex, and subsequently recruit the soluble Sec13-Sec31 outer layer coat complex to bend the membrane and form the COPII-coated vesicles [19–21]. The multiple binding sites on the Sec24 subunit recognise sorting signals on correctly folded transmembrane (TM) cargo proteins and selectively concentrate them into COPII vesicles, thereby acting as a checkpoint [22].

Transported COPII vesicles in yeast directly fuse with *cis*-Golgi cisternae. In contrast, in mammalian cells multiple COPII vesicles fuse to form the ER-Golgi intermediate compartment before transport to *cis*-Golgi [23,24]. When COPII vesicles reach the *cis*-Golgi membrane in *S. cerevisiae,* they are first tethered to the surface by TRAPPI complex. The membrane bound soluble NSF attachment protein receptor (SNARE) proteins on the vesicle interact with those on the membrane to mechanically pull the vesicle close to the membrane and create a fusion pore as shown in Figure 1.2 [25,26].

In eukaryotes Golgi cisternae are typically arranged in stacks, while the Golgi complex in *S. cerevisiae* is made of isolated cisternae scattered in the cytoplasm that associate together [27,28]. Golgi cisternae are classified based on their protein content into *cis-,* median-, *trans*-Golgi or the *trans*-Golgi network (TGN) [29,30]. The cargo proteins delivered to the *cis*-Golgi are gradually transported between the cisternae while undergoing compartment specific modifications such as *O*-glycosylation, sulfation, proteolytic processing, and outer chain

carbohydrate modifications [8]. Mature proteins reach the TGN and are sorted into secretory vesicles targeted to their final location in the plasma membrane, endosomes or the vacuole, as shown in Figure 1.1 [24]. Proteins that reside in the Golgi are retained in the TGN, while ER proteins are transported back to the ER in COPI-coated vesicles by the retrograde transport pathway.

In retrograde transport from Golgi to the ER, the seven subunits, α, β, β', γ, δ, ε and ζ-COP, form the intact COPI which is recruited to the Golgi membrane and forms the vesicle containing mature protein, which is transported to the ER, shown in Figure 1.2 [31]. COPI coated vesicles are also responsible for inter-Golgi transport between different cisternae [24,32,33].

Approximately one-third of the eukaryotic proteome consists of TM and secretory proteins, which rely on the secretory pathway both for their structural modifications and functional localisation [34]. Modulation of early secretory pathway is essential for maintenance of cellular function and proteostasis. Accumulation of misfolded proteins in the ER results in the formation of hazardous aggregates and leads to several diseases in humans [35]. Several neurodegenerative disorders, such as Alzheimer's disease, Parkinson's disease and Huntington's disease, are caused by the aggregation of immature proteins leading to neuron death [36]. An increase in ERAD has been linked to Cystic Fibrosis and is often treated by proteostasis-enhancing therapeutic drugs [37,38]. Understanding the secretory pathway, and factors that affect it, is thus important not only for advancing our knowledge of fundamental cell biology, but also to develop new approaches to treat related human diseases.

1.2. Protein Translocation into the ER

Nearly 30 % of all proteins synthesised by a cell are translocated into the ER before folding occurs, either co-translationally or post-translationally [39]. These proteins are recognised by the signal peptide (SP) at their N-terminus, or a hydrophobic N-terminal helix in the case of membrane proteins [40]. Central to both translocation processes is the Sec61 channel, which is the pore-forming unit of the translocon [41]. The components and mechanisms of translocation will be discussed in this section.

1.2.1. Signal Peptides

The SP is a short peptide located at the N-terminus of a protein that acts as a molecular address to direct the protein into the secretory pathway as well as to indicate its final location [42]. SPs are typically 25-30 residues long and are cleaved by signal peptidase at their C-terminal ends [43,44]. Longer SPs (~140 residues) and internally located, no-cleaved signal anchored sequences also exist in eukaryotes [43,45]. SPs typically consist of three distinct structural regions as shown in Figure 1.3: the positively charges N-region at the N-terminus, H-region containing the helical hydrophobic core, and the C-region at the C-end containing the cleavage site [44]. Although the structure of SPs is conserved, their amino acid composition and length may vary considerably [46]. This variability in SP not only influences translocation efficiency, cleavage sites, and post-cleavage processes but is also believed to allow them to withstand mutations while maintaining high translocation efficiency [42,47]. Such SPs may differ in their interaction with the translocon or the signal cleavage machinery [40].

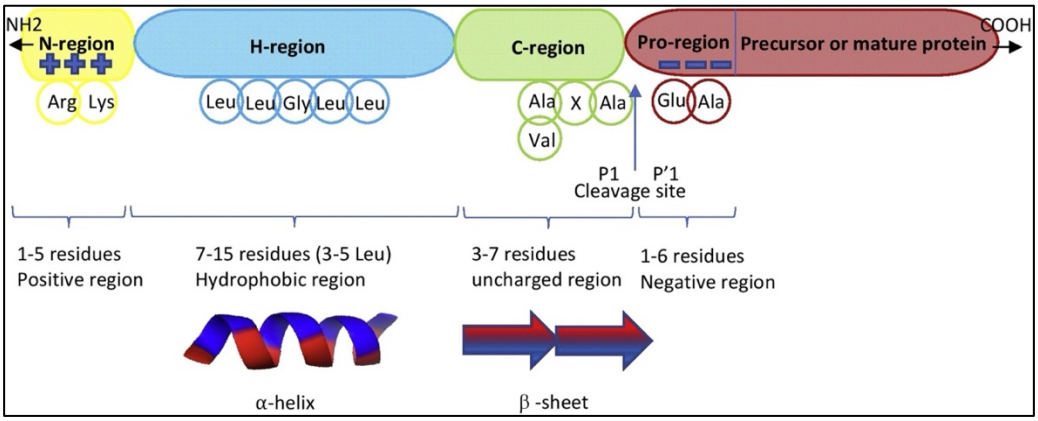

Figure 1.3 Structure of a signal peptide. Figure from Owji et al., 2018. Signal peptides, in general, have a positively charged N-terminus (N-region), a hydrophobic core forming an α-helix (H-region), and a β-sheet forming cleavage site at the C-terminal region (C-region). The signal peptide is followed by a pro-region, which is the initial part of the protein.

Residues at positions -1 and -3 relative to the SP cleavage site determine where cleavage occurs, and the SPs regulate the timing of the process [40,48]. This timing control, which differs between substrates, influences downstream events such as protein folding, glycosylation, and their ER exit [40,49]. Cleavage timing might also influence if the glycosylation sites at the N-terminus are used, and reciprocally the presence of glycosylation sites or TM domains following the SP can modulate its function [50,51].

SPs translocate into the ER through the Sec61 channel. The structural and physicochemical properties of SPs optimise them for this process. The high glycine and/or proline content, variable in length, in the H-region increase its hydrophobicity, forming an α-helix with the hydrophobic side chains exposed to the outside and hydrophilic peptide backbone hidden inside [52,53]. The charge bias between the N- and C-regions facilitates the SP orientation during channel insertion [52]. The “positive-inside rule” governs the TM insertion of both the SP and, to a lesser degree, downstream TM domians through the influence of charge-flanking residues [54].

1.2.2. Sec61 Complex

The universally conserved Sec61 channel is the chief pore forming unit of the ER translocon. It serves a dual function: it allows soluble polypeptides to pass through the ER membrane and allows hydrophobic TM domains of proteins to integrate laterally into the lipid bilayer co-translationally or post-translationally [41]. During co-translational translocation the Sec61 complex acts as a receptor for the ribosome and allows the nascent polypeptide chain to directly cross into the ER lumen [55–57]. In post-translational translocation, it forms the Sec complex by interacting with the Sec62-63 subcomplex [4], mechanisms of which will be address later in this section. Sec61 channel can readily alternate between the two modes of translocation by switching its interaction partners [58]. The Sec61 channel has also been suggested as the central component of the protein export channel and as the proteasome receptor during ERAD [59,60]. The mammalian Sec61 channel is composed of α, β and γ subunits. The homologs of Sec61 channel subunits in *S. cerevisiae* are Sec61, Sbh1, and Sss1, respectively [61]. The SecYEG channel located in the inner membrane is the homolog of the Sec61 channel in bacteria and archaea, composed of homologous subunits SecY/Sec61, SecG/Sbh1 and SecE/Sss1 [62]. The genes coding for *SEC61* and *SSS1* in yeast are essential [43]. The Sec61 channel is inherently passive and relies on auxiliary proteins to facilitate translocation [41].

Figure 1.4 shows the cryo-electron microscopy (cryo-EM) structure of Sec61 complex as a part of the Sec complex in *S. cerevisiae* [63]. The central Sec61/Sec61α subunit (shown in cyan in Figure 1.4) consists of a hydrophilic pore surrounded by 10 TM helix bundle, with both of its termini in the cytosol. It can be considered as having an N-terminal half and a C-terminal half [64]. The channel pore is formed between TM5 and TM6 with a constriction at the

midpoint of the membrane, called pore ring. The pore ring is formed by the hydrophobic side chains of 6 aliphatic amino acids projecting inwards, giving it a characteristic hourglass shape [61]. The cytosolic end of the pore remains open, but the luminal side is obstructed by a helical plug domain that, together with the pore ring limits transmembrane movement [41,65]. At the interface of TM2/TM3 and TM7/TM8 lies the Sec61 lateral gate that serves as a SP binding site in the initial stages of translocation and facilitates the integration of TM domains of membrane proteins [64,66]. This gate, which is closed when idle, opens into the surrounding membrane when the channel is opened [67]. The tail anchored Sbh1/Sec61β subunit, shown in yellow in Figure 1.4, is peripherally associated with Sec61 [43]. This subunit will be discussed in detail in Section 1.4. Sss1/Sec61γ, an essential subunit of the Sec61 complex (magenta in Figure 1.4), consists of an amphipathic helix on the cytosolic face of the ER membrane and a diagonal TM segment [61,64] . Together, these helices form a stabilising 'clamp' around the Sec61 helix bundle [68].

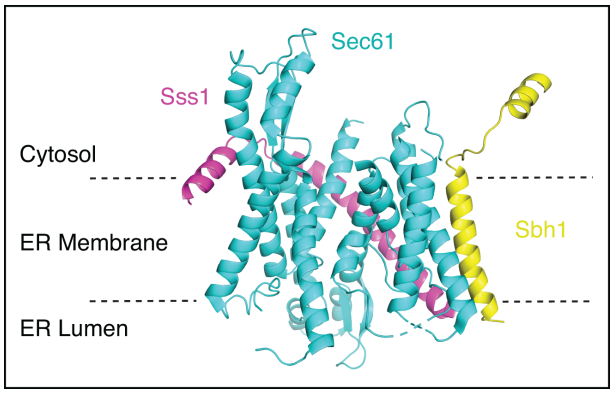

Figure 1.4 The Sec61 Complex. The Cryo-EM structure of Sec61 complex within the Sec complex in *S. cerevisiae,* published by Wu et al., 2019 (PDB code 6ND1). Sec61 is shown in cyan, Sss1 in magenta and Sbh1 in yellow. The unstructured cytosolic domain of Sbh1 is not visible.

As mentioned earlier, in the idle state the pore ring and the plug domain seal the Sec61 channel pore, and its lateral gate is closed. A sequence of interactions with partner proteins and conformational changes is required to open the Sec61 channel for its functions, shown in

Figure 1.5. First, a partner protein, such as the ribosome or the Sec62-63 complex, binds to the cytosolic loops of Sec61α/Sec61 and primes the channel for opening [63,66,69]. This interaction restricts the mobility of the C-terminal half of Sec61α/Sec61, inducing a conformational change across the TM helix bundle. As a result, the pore ring expands, and the lateral gate partly cracks open on the cytosolic side [70]. The plug shifts from its central position in the pore to the front, creating a barrier to prevent phospholipids from seeping through the lateral gate [71]. The positively charged N-termini of SPs or TM domains remain in the cytosol while the SPs or subsequent TM sequences move into the partially opened lateral gate and dock to a site between TM2 and TM7 creating a wide opening in the lateral gate [64,66,72]. At this point, SPs stay in the hydrophobic groove of the lateral gate and newly synthesised polypeptide chains insert through the channel as a hairpin loop [64,73]. Hydrophobic TM segments, on the other hand, displace TM2 to widen the lateral gate and start to move into the membrane [64,74].

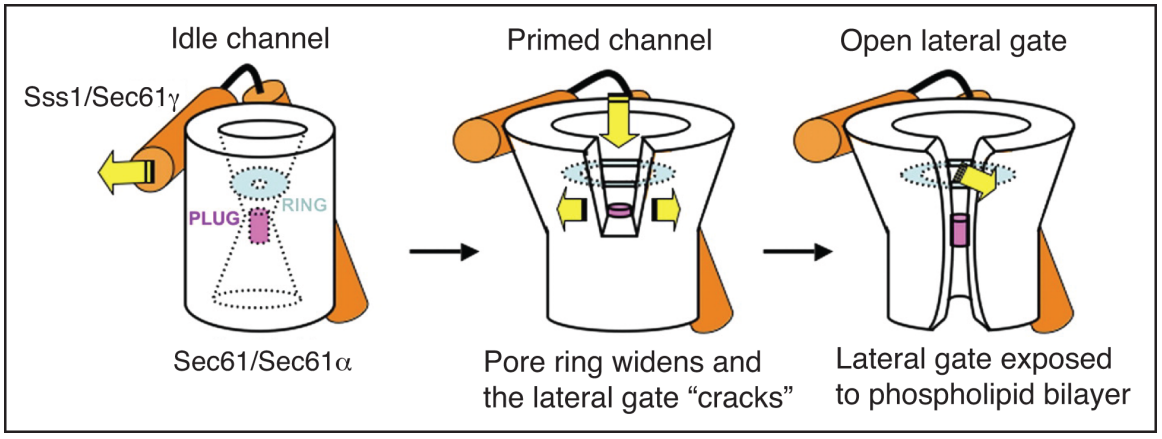

Figure 1.5 Opening of the Sec61 channel lateral gate. Schematic modified from Egea and Stroud, 2010. Idle Sec61 channel is characterised by an obstructed central pore and closed lateral gate. The channel is primed for polypeptide entry when the pore ring widens and the lateral gate partially opens on the cytoplasmic side. As an SP of a secretory protein or N-terminal helix of a membrane protein engages the lateral gate, the lateral gate widens to fully open.

The Ssh1 complex in *S. cerevisiae* is a homolog of the Sec61 complex, which forms a trimeric complex with Sbh2 and Sss1 [75]. Despite being non-essential and only sharing 30% sequence identity with Sec61, the Ssh1 complex demonstrates similar ribosome affinity [76–78]. Its inability to assemble with the Sec62-Sec63 complex, combined with its binding to certain co-translationally translocated protein SPs, indicates an exclusive function in co-translational translocation [75,79,80].

1.2.3. Co-translational Translocation of Proteins into the ER

Co-translational translocation of ribosome-bound nascent polypeptides is mediated by signal recognition particle (SRP) and occurs mainly through the Sec61 channel in eukaryotes, or the SecYEG channel in bacteria [81]. The SRP can also associate with the Ssh1 complex for co-translational translocation [75]. While the properties of substrates marked for co-translational translocation are not fully understood, SRP recognises highly hydrophobic SPs [39]. Figure 1.6 summarises the main steps that occur during co-translational translocation through the Sec61 channel.

The SRP complex is a ribonucleoprotein composed of a 7S RNA and six protein subunits, two of which are not essential in *S. cerevisiae* [8,82]. In the cytosol, the SRP screens translating ribosomes for suitable SPs [83,84]. Within the ribosome, mRNA is translated in the groove of the large subunit and the nascent polypeptide chain is elongated through the peptide exit tunnel, forming the ribosome-nascent chain complex (RNC) (Step 1 in Figure 1.6) [85,86]. The SRP detects and binds preferentially to highly hydrophobic SPs of nascent chains exiting the ribosome (Step 2 in Figure 1.6) [40,87–90]. The SP is engaged in the hydrophobic groove of the 54 kDa subunit of SRP by the electrostatic interactions between the basic sidechains of its

N-terminal residues and the phosphate backbone of the 7S RNA in the SRP [40,91]. In absence of an SP, SRP binds to the hydrophobic N-terminal signal anchor or the first TM domain of the nascent chains [44].The substrate specificity of SRP in yeast is also influenced by the RNC [92,93]. The SP-bound SRP further binds to GTP, delaying or halting the chain elongation [94]. This temporary arrest is necessary as the rate of translation is slower than protein folding, and allows for the nascent chain to remain unfolded until it is translocated [95–97]. SRP-mediated arrest of translation has not been observed in *S. cerevisiae* [83].

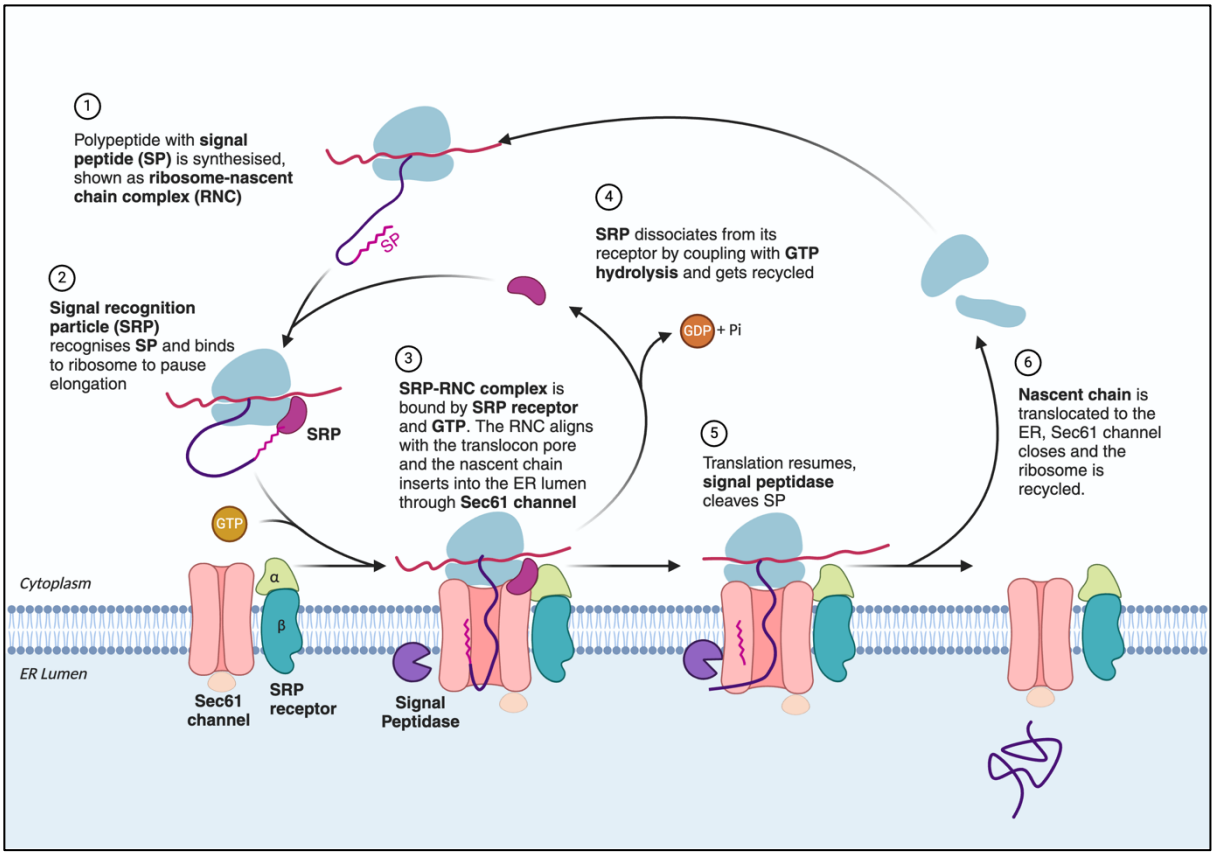

Figure 1.6 Co-translational translocation through the Sec61 channel. The steps involved in SRP-mediated co-translational translocation through Sec61 channel in *S. cerevisiae* are described. Created with BioRender.com

Following the translation arrest, the SRP interacts with the α subunit of the heterodimeric SRP receptor adjacent to the Sec61 complex in the ER membrane and relegates the RNC to the translocon (Step 3 in Figure 1.6) [88,98,99]. The SRP is released from both the SRP receptor and the RNC by GTP hydrolysis, and is recycled (Step 4 in Figure 1.6) [100,101]. The

ribosome interacts with the cytosolic loops of Sec61α/Sec61 between TM6/7 and TM8/9 [57,69,79]. This interaction places the peptide exit tunnel of the ribosome directly over the Sec61 channel pore and enables the direct passage of the nascent chain across or into the ER membrane [55,56]. The lateral gate of Sec6 is opened to engage the SP or to allow the insertion of membrane proteins into the bilayer [74]. Translation resumes, and the nascent chain elongates into the ER, while the SP is cleaved by signal peptidase, an ER resident enzyme (Steps 5 and 6 in Figure 1.6) [74].

1.2.4. Post-translational Translocation of Proteins into the ER

Post-translational translocation is employed by secretory proteins bearing SPs of low hydrophobicity, which evade recognition by the SRP and are only translocated after their complete ribosomal synthesis and release [89,102]. In eukaryotes, translated proteins are predominantly translocated through the Sec complex which is formed by the association of the Sec61 channel with Sec62-63 complex [58,103]. Other post-translational pathways have also been identified [104].

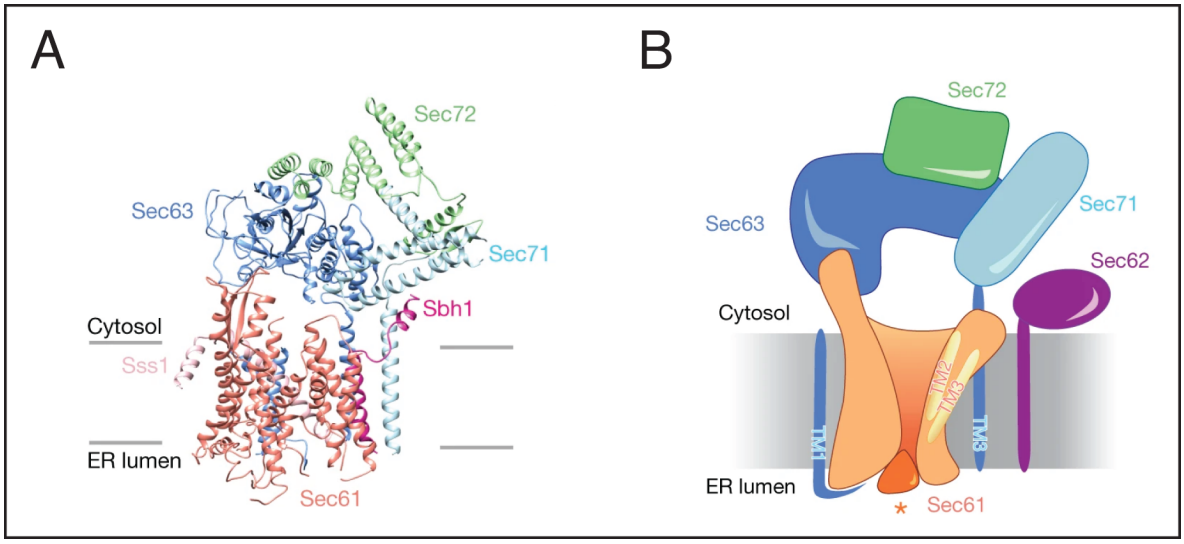

Figure 1.7 Structure of the Sec complex. Modified figure from Wu et al., 2019. **A)** Side view of the cryo-EM structure of the Sec complex in *S. cerevisiae* (PDB code 6ND1). Sec62 is not shown. **B)** Schematic depicting the association of Sec complex subunits. Plug domain of Sec61 is indicated by *. Subunits of Sec61 complex are not shown.

Figure 1.7 shows the structure of the Sec complex in *S. cerevisiae*, where the membrane-bound Sec61 complex (described in Section 1.2.2) associates with the tetrameric Sec62-63 complex composed of the subunits Sec62, Sec63, Sec71 and Sec72 [63]. Of the Sec62-63 complex subunits, Sec62 and Sec63 are essential while Sec71 and Sec72 are non-essential in yeast and are absent in higher eukaryotes [58,103,105]. Sec62 consists of two TM segments and a cytosolic domain that binds to the C-terminus of Sec63 [63,106,107]. Sec63 consists of a large cytosolic domain, three TM segments, and a flexible luminal J domain [63,108,109]. Sec61 and Sec63 interact at multiple sites and these interactions play a crucial role in maintaining the association between the subcomplexes of the Sec complex and the opening of the Sec61 lateral gate [108]. The Brl domain of Sec63 interacts with the cytosolic loops between TM6/7 and TM8/9 on the C-terminal half of Sec61 in the cytosol, and in the ER membrane, TM3 of Sec63 interacts with TM1 and TM5 of Sec61 in its N-terminal half as well as the TM domains of Sec61 complex subunits Sbh1 and Sss1 [63,108]. Sec71 tethers the soluble Sec72 to the ER membrane, and these proteins together clamp the Sec63 cytosolic domain [63,108].

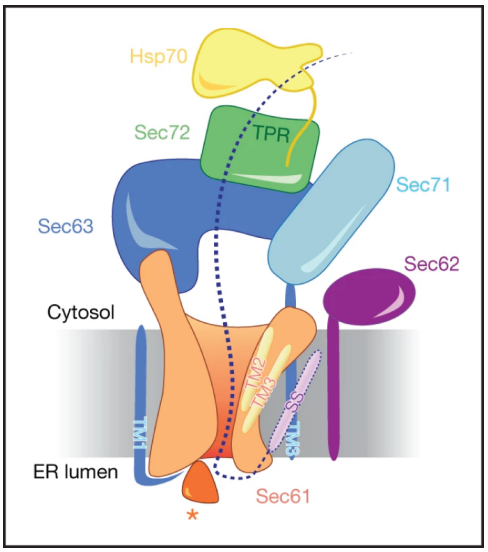

Figure 1.8 Sec complex during post-translational translocation. Schematic from Wu et al., 2019 showing the Sec complex engaged in the insertion of Hsp70 bound polypeptide chain into the ER. The SP, shown here as signal sequence (SS), is engaged in the lateral gate of Sec61 while the polypeptide displaces the channel plug, marked with *, and is inserted as a loop.

Upon translation, cytosolic chaperones such as Hsp70 bind to the newly synthesised polypeptide to maintain it in an unfolded state for translocation [110]. Sec62-63 complex binds to the Sec61 complex and the Sec63 Brl domain obstructs ribosomes from binding to the Sec61 complex [63]. Interactions of Sec63 and Sec61 open the lateral gate, and it is held in that conformation by Sec63 which acts as a scaffold [63,108]. The Sec63 Brl domain also recruits Sec71 and Sec72 to the Sec complex [111]. As shown in Figure 1.8, substrate-bound Hsp70 interacts with Sec72 and orients the polypeptide to enter the translocon [112]. In the absence of Sec71 and Sec72, this substrate transfer step is mediated by calmodulin in higher eukaryotes [113]. Sec62 identifies the incoming SP and transfers it to the Sec61 channel pore where it enters the lateral gate and the cytosolic chaperones bound to the polypeptide dissociate as in Figure 1.8 [64,73,110,114]. The wide opening of the lateral gate allows for the SP, and subsequent TM helices for insertion, to freely enter the lipid bilayer despite their low hydrophobicity [63]. The J domain of Sec63 activates Kar2, a luminal ATPase called BiP in mammals, which binds to the polypeptide and drives its insertion [115].

1.2.5. Insertion of membrane proteins into ER

Membrane proteins are inserted into their designated membranes predominantly through translocons [116]. In eukaryotes, integral membrane proteins are directly inserted into the ER membrane through the Sec61 channel, almost exclusively co-translationally [117]. Like co-translational translocation, polypeptides for insertion are recognised by SRP by their hydrophobic N-terminal helix and targeted to the Sec61 channel for insertion through the lateral gate. Figure 1.9 shows the schematic representation of membrane insertion of a multi-span membrane protein. The TM helix segments dislodge the Sec61 plug domain by moving TM7 towards TM10, widen the lateral gate by displacing Sec61 TM2, and begin to move into

the surrounding lipid phase [64,108,118]. TM segments are inserted sequentially with the initial N-terminal segment determining the orientation of all subsequent TM segments, following the positive-inside rule [119]. Inserted segments move further into the lipid phase and away from the Sec61 channel as the polypeptide inside the channel elongates to a sufficient length [64,120,121]. Insertion takes place iteratively until all the TM segments in the polypeptide are inserted [113].

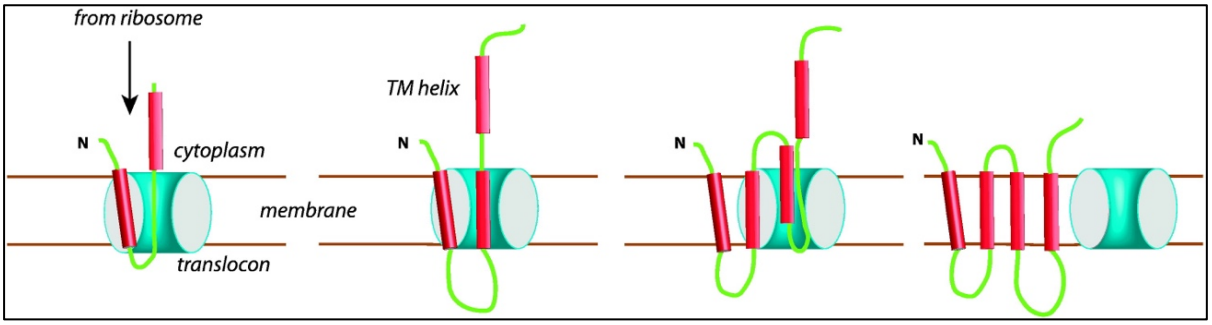

Figure 1.9 General scheme for the assembly of multi-span membrane proteins. Schematic representation from Cymer et al., 2015. Nascent polypeptide sequence is N-terminally inserted into the Sec61 translocon while being elongated at the C-terminal end. The TM segments enter the ER membrane through the lateral gate of Sec61 and move further away from the translocon as the polypeptide is elongated.

1.2.6. Diseases related to protein translocation

Protein translocation into the ER is an essential cellular function. Disruptions in translocation machinery have been linked to several diseases and disorders. Defects in functioning and cleavage of SPs result in certain disease pathologies. Point mutations adjacent to the cleavage site can disrupt SP cleavage and subsequent protein folding, resulting in ER stress and cytotoxicity [122–124]. Hereditary diabetes has been associated with impaired SP cleavage of preproinsulin [125].

Sec61 channel dysfunctions, called Sec61 channelopathies, are associated with various inherited disorders and cancers. In humans, tubule-interstitial kidney disease and common

variable immune deficiency have been linked to mutations in the gene encoding Sec61α [126]. Sec61 impairs biosynthesis of protein components of influenza virus, and also suppresses replication of HIV and dengue virus [127], suggesting the potential of Sec61 as a target for antiviral therapies. Mutations in mice lead to the development of diabetes [126]. Polycystic liver disease is caused by mutations in *SEC61B* gene [128]. The *SEC61G* gene is essential for the survival of glioblastoma tumour cells [129].

Mutations in genes coding for Sec62 and Sec63 are frequently mutated or overexpressed in several cancers, indicating their role in oncogenesis [130]. Specifically, mutations in SEC63 have also been linked to polycystic kidney disease [130]. Research into Sec complex and Sec61 channel function is crucial not only for elucidating mechanisms of these diseases, but also for exploring its potential as a therapeutic target.

1.3. Protein Processing in the ER

1.3.1. Protein modifications and folding in the ER

Proteins are translocated into the ER in an unfolded chain conformation. Once in the ER lumen, polypeptide chains with hydrophobic domains are at risk of aggregation if left unfolded in the aqueous environment. To prevent aggregation, molecular chaperones non-covalently bind to the hydrophobic patches on the polypeptide chain as it exits the translocon pore [131,132]. These chaperones, present in high concentrations in the ER lumen, also aid in folding of both, soluble and membrane proteins, act as a quality control mechanism to ensure correct folding, and prevent early ER exit of unfolded and misfolded proteins [133,134].

A principal family of molecular chaperones is the 70 kDa heat shock proteins (Hsp70), that are ubiquitous in eukaryotes and widely prevalent in prokaryotes [132,135]. Hsp70s play key roles in protein folding, transportation and target misfolded or aggregated proteins for degradation [136]. Hsp70s also exhibit low intrinsic ATPase activity, which is enhanced by DNAJ or Hsp40 co-chaperones and nucleotide exchange factors (NEFs) [137–139]. Kar2 or BiP, as mentioned in Section 1.2.4, is the predominant Hsp70 chaperone which also participates in protein folding [140]. Kar2 employs Sec63, Scj1 and Jem1 as co-chaperones for ATP hydrolysis when binding to partially folded proteins, shown in Figure 1.10 [141–143]. This activity of Kar2 doubles as a protein quality control checkpoint, as will be discussed in later sections.

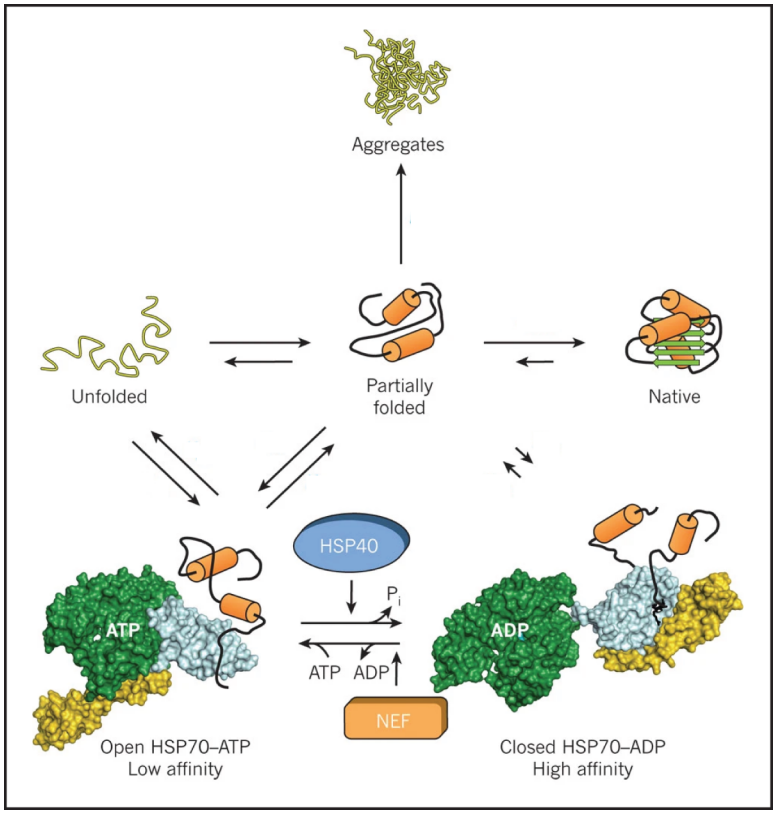

Figure 1.10 Hsp70 assissted protein folding. Modified diagram from Hartl et al., 2011 depicting the protein folding function of Hsp70 family chaperones.

Protein disulfide isomerases (PDI) are another ER resident chaperone family which are involved in disulfide bond formation [144]. PDI family participate in protein folding and quality

control through their interactions with Kar2, Calnexin and Htm1 [145–147]. ER resident PDI chaperones in yeast include Pdi1, Mdp1, Mdp2, Eug1 and Eps1 [148]. Pdi1 acts as a chaperone by binding to polypeptides prone to self-assembly, preventing their aggregation [149,150]. Though the chaperone function and isomerase activity are interlinked, Pdi1 also assists in folding of polypeptides that lack disulfide bonds [150–152].

Glycosylation is an essential post-translational modification that most secretory proteins undergo in yeast [8]. Addition of carbohydrate moieties or glycans not only increases the solubility of a polypeptide, but also serves as a signal for lectin chaperones during folding by its conformation [153]. While considerable diversity exists among glycans and their linkages, *N*-linked glycosylation and *O*-mannosylation are the most common and occur upon entry into the ER lumen [7,154]. Proteins are *N*-glycosylated at Asn-Xxx-Ser/Thr motifs, Xxx being any residue except Pro, by oligosaccharyl transferase (OST) complex [155]. In the ER lumen, OST interacts with the Sec61 translocon and catalyses the transfer of the glycan from a lipid-linked donor during co-translational translocation [156,157]. Protein *O*-mannosyl transferases (Pmts) also associate with the Sec61 channel and add a mannose residue to Ser/Thr residues [158].

1.3.2. Protein quality control in the ER

Despite the accuracy of polypeptide synthesis, factors such as mutations and environmental factors leading to cell stress may cause proteins to misfold [159]. Accumulation and aggregation of misfolded proteins disturbs cellular homeostasis and has been linked to diseases such as Alzheimer's disease, amyotrophic lateral sclerosis, and aging [160]. Sophisticated quality control (QC) mechanisms in the ER identify and retain misfolded

proteins in the ER and attempt to refold them into their native state [161]. Retention in the ER prolongs the exposure of proteins to folding machinery and increases the probability of correct folding [162]. When attempts to salvage misfolded proteins fail, they are retained in the ER and targeted for degradation (Figure 1.11) [12].

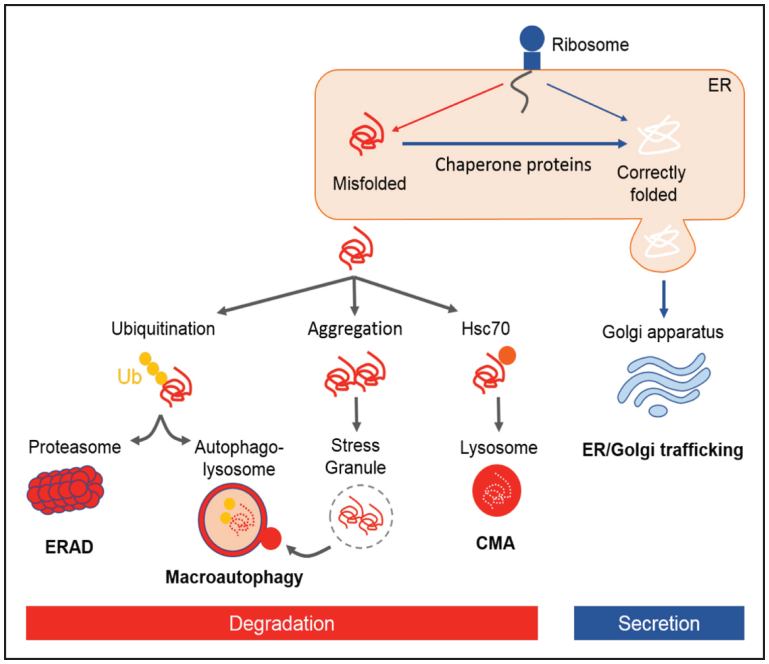

Figure 1.11 Mechanisms of protein quality control in the ER. Illustration from Shahheydari et al., 2017.

Chaperones in the ER play an additional role as protein quality sensors by detecting misfolded proteins [141]. Their high concentration in the ER lumen enables them to maintain a constant surveillance of protein folding. The presence, absence, or delay of post-translational modifications signal the conformational status of the protein to chaperone sensors, which then covalently tag misfolded proteins with glucose or ubiquitin and are subsequently recognised by folding or degradation machinery, respectively [163].

The modification of *N*-glycan moiety by sequential trimming of glucose and mannose residues and specific addition of glucose residues governs the maturation and degradation of proteins in mammals and yeasts [164]. This is performed by glucosidases Gls1 and Gls2, and

yeast specific mannosidases Mns1 and Htm1 [165]. The presence of glucose residues in N-linked glycans serves as a signal to retain the protein in the ER [166]. N-terminal M8GlcNAc2, which is formed by Mns1 trimming the terminal mannose residue in M9GlcNAc2, signals the fully folded glycoprotein to be exported [167]. Terminally misfolded proteins are further trimmed by Htm1 to form M7GlcNAc2, which is targeted for ERAD by the lectin Yos9 [168,169]. The calnexin/calreticulin cycle in mammalian cells retain and redirect non-ER resident glycoproteins for refolding or degradation [170]. However, this cycle is not essential in *S. cerevisiae* [171].

1.3.3. Unfolded Protein Response in the ER

Accumulation of unfolded or misfolded proteins in the ER causes an imbalance in proteostasis and triggers the unfolded protein response (UPR) [11]. During UPR in yeast, protein synthesis is decreased, and the production of chaperones and degradation machinery is increased to enhance folding and eliminate misfolded proteins [172].

Figure 1.12 provides an overview of the UPR mechanism in yeast. Ire1 is an ER membrane protein that interacts with Kar2 at proteostasis conditions and with unfolded or misfolded proteins when stressed [173,174]. Accumulation of proteins in the ER lumen disrupts its interaction with Kar2, leading Ire1 to oligomerise and subsequently activating its kinase and ribonuclease domains [175]. Activated Ire1 splices the pre-mRNA of *HAC1* gene and Rlg1, a tRNA ligase, ligates the splicing product to produce mature *HAC1* mRNA which is subsequently translated to Hac1p [176]. Hac1p is a transcription factor which activates genes coding for UPR components such as chaperones, leading to upregulation of their synthesis and induction

of UPR. Ire1p, Hac1p and Rlg1p regulate the transcription of a significant number of genes related to protein folding and biosynthesis, thus playing a central role in ER proteostasis [177].

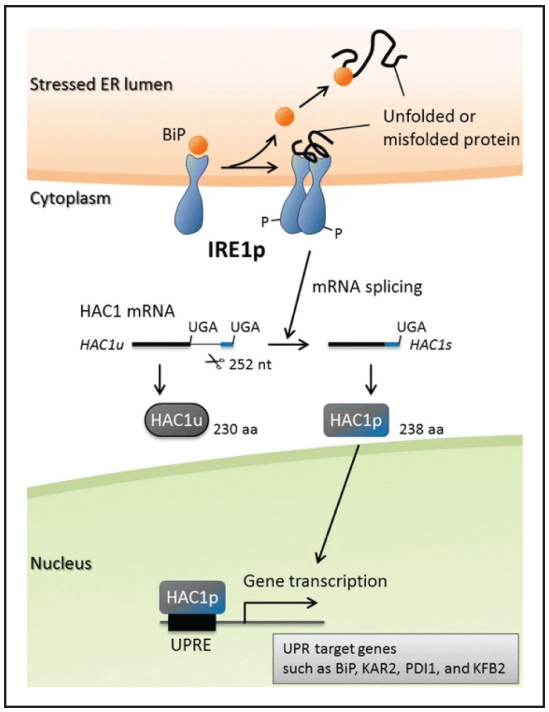

Figure 1.12 UPR mechanism in yeast. Schematic illustration from Chakraborty et al., 2016. When ER undergoes stress due to protein accumulation, Kar2/BiP dissociates from Ire1 , causing Ire1 to bind to the unfolded/misfolded proteins and oligomerise. This activates the cytosolic ribonuclease domain of Ire1 leading to the splicing and Rlg1 mediated maturation of *HAC1* mRNA. Translated Hac1p upregulates the production of UPR elements (UPRE) such as chaperones and protein modification enzymes which subsequently manage the accumulated proteins and restore ER homeostasis.

1.3.4. ER-Associated Degradation of Proteins

Irreparably misfolded proteins are degraded through the conserved ER-associated degradation (ERAD) mechanism [178]. This process involves the ubiquitination misfolded proteins, their retrotranslocation to the cytosol, and subsequent degradation by the proteosome [179]. Disruptions in ERAD can lead increased ER stress and compromised cellular proteostasis [12]. The ERAD system in yeast comprises three main pathways, ERAD-L, -M, and -C, each targeting proteins with the misfolding located in the luminal, membrane or cytosolic domain [168,180]. These pathways are also characterised by their use of distinct ubiquitin ligase, such as Hrd1 or Doa10 [145,181]

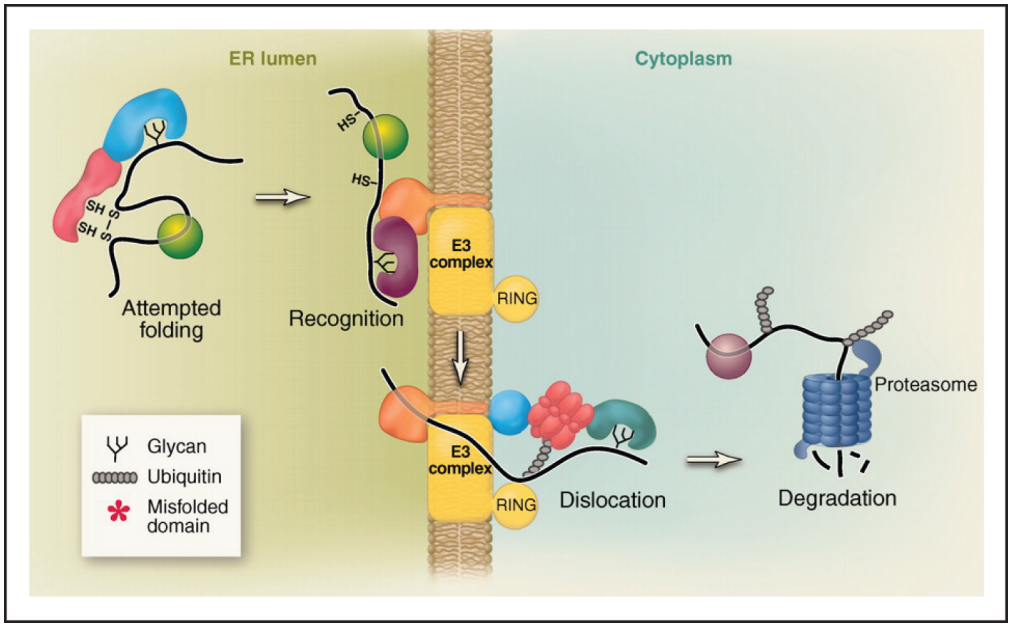

Figure 1.13 Key steps of ERAD in yeast. Schematic illustration from Smith et al., 2011. Misfolded proteins stably bound to chaperones in the ER lumen are recognised by their trimmed N-glycan and retrotranslocated into the cytosol where they are ubiquitylated and subsequently degraded by the proteasome.

Figure 1.13 shows the key steps involved in the three ERAD pathways in yeast. Misfolded proteins in the ER lumen are stably associated with chaperones and retained in the ER, where their N-terminal glycan is de-mannosylated by Mns1 and Htm1 to Man7GlcNAc2 [182–184]. This glycan acts as an intrinsic signal targeting the protein for ERAD and binds to the lectin Yos9 [165,185]. Yos9 then interacts with Kar2 and membrane-bound Hrd1 ubiquitin ligase and the proteins are retrotranslocated into the cytosol [169,186]. Three complexes, Sec61, Hrd1 and Der1, have been proposed as the retrotranslocon [187–189].

Once in the cytosol, the misfolded proteins are degraded by the ubiquitin-protease system [190]. First, ubiquitin chains are added to lysine residues of target substrates by an enzyme cascade involving ubiquitin activating (E1), ubiquitin conjugating (E2) and ubiquitin ligase (E3) enzymes [191,192]. The polyubiquitinated proteins are then directed to the 26S

proteasome, a large multi-subunit complex that degrades the proteins and cleaves the ubiquitin chains for reuse [193].

1.4. Intrinsically Disordered Proteins and Protein Regions

Intrinsically disordered proteins and intrinsically disordered protein regions (IDRs) cannot independently form a stable tertiary structure. In eukaryotes, 10-20% of full-length proteins and 25-40% of all residues are intrinsically disordered and exhibit more mutations than structured proteins/regions [82,194]. IDRs have reduced sequence complexity, abundant charged and hydrophilic residues, and fewer hydrophobic residues [195]. Their skewed amino acid distribution the residues extensively exposed to the solvent resulting in flexible structures [196,197]. In this work, I will be focussing on IDRs.

Molecular recognition features (MoRFs) are specific motifs within the IDR that tend to form a secondary structure to interact with proteins as well as nucleic acids and lipids, conferring function to the IDR [198]. MoRFs are islands of about 20 amino acids in length within the IDR, typically containing conserved aromatic and hydrophobic residues [199]. Based on the structure they adopt, MoRFs are classified as follows: α-helix forming α-MoRFs, β-sheet forming β-MoRFs, irregular structures with non-repeating psi- and phi- angles called ι-MoRFs, and complex MoRFs with multiple, equally distributed secondary structures [200].

IDRs transition into a stable secondary structure on binding with their interaction partners by undergoing coupled folding and binding interactions [201,202]. Figure 1.14 shows the two models that explain this process: induced fit and conformational selection. In the induced fit model, IDRs first form weak interactions with their partners which, also influenced by the

binding partner's surface residues, drive the transition to their final conformation with strong intramolecular contacts [203]. The conformation selection model, on the other hand, suggests that IDRs transiently adopt a range of structures which are selectively recognised and bound by their interaction partners [204].

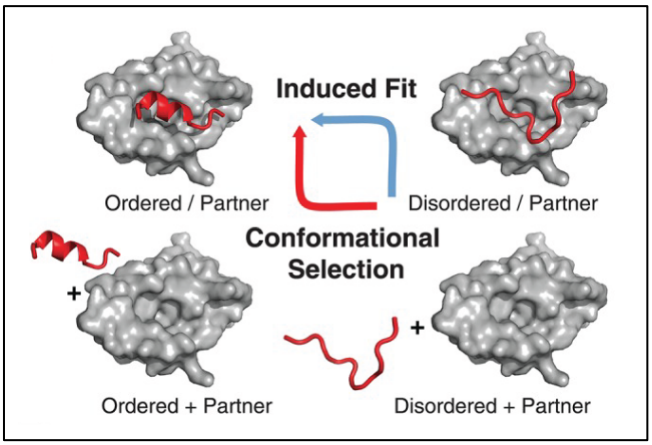

Figure 1.14 Mechanisms of coupled folding and binding interactions. Schematic from Theillet et al., 2014 representing the two models for disorder-to-order transitions. In induced fit model (blue arrow), IDRs are influenced by their initial weak interactions with their binding partner to mold into a conformation with stronger interactions. In conformational selection model (red arrow), IDRs exist in a range of conformations, which are then preferentially bound by their interaction partner to form a complex.

The structural plasticity of IDRs allows them to engage in versatile interactions with diverse set of binding partners [199]. This flexibility also exposes sites for post-translational modifications and allow IDRs to bind partners with high specificity but a moderate affinity that facilitates rapid association/dissociation [205,206]. Collectively, these properties make IDRs ideal for controlling and regulating intracellular signalling and are present in 75% of signalling proteins [1,207]. Conformational transitions of IDRs modify binding site affinity and interaction surfaces, amplifying signal complexity [208]. IDRs are also crucial in protein biosynthesis and are essential structural components in chaperones [1]. During co-translational translocation in mammalian cells, a MoRF in the linker domain of the SRP receptor is critical for ribosome detection [209].

Post-translational modifications in IDRs can modulate stability of the secondary structures they form and calibrate their interactions, effectively acting as molecular switches [210–212]. Sites for phosphorylation, the most common regulatory post-translational modifications in eukaryotic cells, are often located as clusters within IDRs [213]. Phosphorylation of multiple sites in an IDR of a signalling protein, sequentially or in combination, leads to precise regulation of signalling cascades [195].

1.5. The Beta Subunit of the Sec61 Channel – Sbh1

The β subunit of the Sec61 complex, Sec61β, is a small tail anchored protein peripherally associated with Sec61 [41]. Its single TM domain is conserved among species (Figure 1.15). While non-essential in mammals and yeasts, it is essential for development in *Drosophila* and conserved in *Caenorhabditis elegans* [214,215]. The Sec61β homolog in *S. cerevisiae* is called Sbh1 or Seb1, encoded by *SBH1*, and has 30% similarity to the mammalian sequence [58,216].

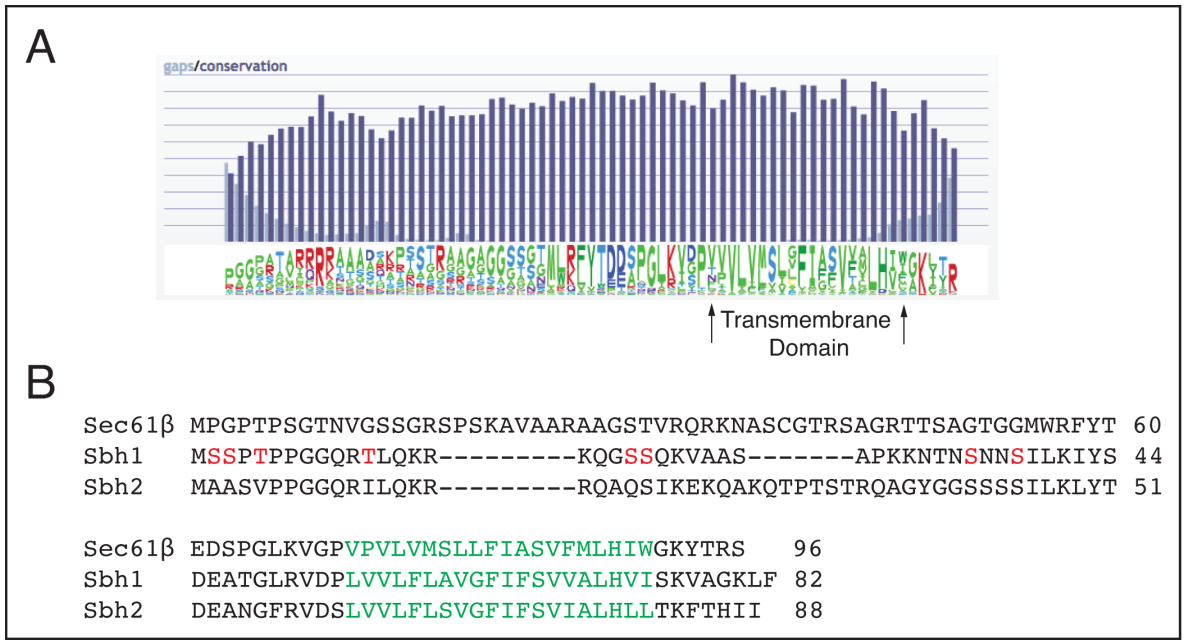

Figure 1.15 Evolutionary conservation of Sec61β/Sbh1. A) Conservation of Sec61β homologs among species generated by eVFold sequence alignment. **B)** Sequence alignment of Sec61β (human), Sbh1 and Sbh2 from *S. cerevisiae*. Residues forming the transmembrane helix are in green. Phosphorylation sites on Sbh1 are highlighted in red.

Sbh2 or Seb2, is a paralog of Sbh1 in *S. cerevisiae* originating from a whole genome duplication. Similar to *SBH1, SBH2* is also non-essential, and the protein shares about 50% of its sequence with Sbh1 [75]. Sbh2p forms the β subunit of the Sec61 complex homolog Ssh1 complex. Sbh1 and Sbh2 perform separate functions during protein translocation, as evidenced by their synthetic lethality patterns [216,217]. In the absence of Sbh1 and Ssh1, Sbh2 can associate with Sec61 as a substitution as can Sbh1 when Sbh2 and Sec61 are absent [75].

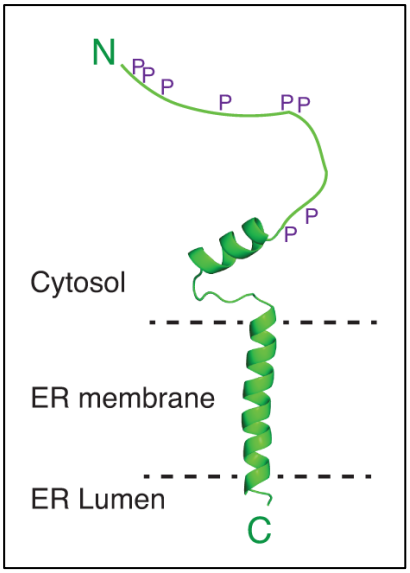

Figure 1.16 Structure of Sbh1. Cryo-EM structure of Sbh1 as a part of the Sec complex in *S. cerevisiae* (PDB code 6ND1). Unstructured cytosolic domain is not a part of the structure and is not drawn to scale. Approximate locations of phosphorylation sites are marked by purple P.

Sbh1 in *S. cerevisiae* is an 82 amino acid long, C-terminally tail anchored protein with a single, conserved, transmembrane domain (Figure 1.16). The cytosolic domain is of 54 residues, of which the 38 N-terminal residues are intrinsically disordered, and the conserved membrane proximal (CMP) domain is 16 residues long and structured [218]. The N-terminal IDR has two clusters of phosphorylation sites: S2, S3, T5, T12, S20, and S21 phosphorylation sites are close to the N-terminus, and S35 and S38 sites are close to the CMP [219]. Phosphorylation sites are also present in mammalian Sec61β, with all but one site present in

its cytosolic IDR [220]. Except for the proline-flanked T5, all other phosphorylation sites are poorly conserved [219,220]. The conserved T5 residue, however, is not found in Sbh2 and lower eukaryotes, suggesting that the residue is the result of convergent evolution and plays a potentially significant role in Sbh1 function [219]. The IDR also has a centrally located positively charged patch of Lys residues. The short C-terminal tail extends into the ER lumen [61].

Recently published cryo-EM structures revealed the interactions of Sbh1 TM domain with the components of the yeast Sec complex [63,108]. Given its central location in the Sec complex, the Sbh1p TM helix interacts with TM3 of Sec63p and makes contact with Sec71p [63]. Within the Sec61 complex, Sbh1 TM interacts with TM1 and TM4 of Sec61 [63,221].

In *S. cerevisiae*, both *SBH1* and *SBH2* are non-essential, and cells do not show a growth defect when either is absent. However, *Δsbh1 Δsbh2* cells show a synthetic growth defect at 37 ˚C [75,216,222]. The TM domain of either Sbh1 or Sbh2 is sufficient to rescue this temperature sensitivity [222]. Absence of Sbh1 in the Sec61 channel complex leads to delays in protein insertion [223]. Translocation defects observed in *Δsbh1 Δsbh2* cells so far are contradictory: Finke et al. first found moderate defects in the post-translational import of Kar2 and yeast pheromone precursor prepro-α factor (ppαF) in *Δsbh1 Δsbh2* cells at both permissive 30 ˚C and restrictive 37 ˚C and in vitro heterologous translation systems experiment the import was 2 to 5 times lower than that in wildtype [75]. Feng et al. found moderate co-and post-translational translocation defects in in vitro translocation experiments at 37 ˚C [222]. The difference in observations is attributed to different experiment systems used by the groups [222]. The levels of Gls1p and Mns1p are reduced in *Δsbh1 Δsbh2* cells even at permissive temperatures, resulting in an N-glycan trimming defect

[222]. Like temperature sensitivity, both co-translational translocation defect and N-glycan trimming defects are rescued when the cells are substituted with a truncated Sbh1 TM including 5 preceding CMP residues [222]. Sbh1 is dispensable for post-translational translocation [222].

The cytosolic domain of mammalian Sec61β interacts directly with ribosomes during co-translational translocation, likely after the ribosome has already been targeted to the ER membrane [224,225]. N-terminal targeting sequences of nascent polypeptides in the Sec61 channel vestibule interact with the cytosolic domain of Sec61β, and this interaction intensifies when the insertion of SP into the lateral gate is blocked [226,227]. As this activity is not essential for most proteins, Sec61β contributes to the recognition and insertion of specific SPs. IDR in the cytosolic domain of Sec61β also interacts with the tRNA bound RNC complex [226,227]. Sec61β thus ensures effective insertion of nascent polypeptides into the translocation complex [101].

Sbh1 plays a major role in the assembly and function of components of co-translational translocation even before nascent peptide insertion. Mammalian Sec61β was cross-linked to the signal peptidase complex, suggesting that Sec61β plays a role in recruiting the signal peptidase complex during co-translational translocation [223]. This interaction has also been reported in yeast in the absence of ribosomes [228]. The cytosolic domain of yeast Sbh1 in isolated Sec61 complex acts as a guanine nucleotide exchange factor for the β subunit of the SRP receptor and participates in the GTP switch cycle [229]. Sbh2 also plays a similar role in the Ssh1 complex [80,230]. The guanine exchange factor function of Sbh1 is inactivated when part of the post-translational Sec complex [229]. Simultaneous deletion of both Sbh1 and Sbh2 leads to abnormal gating of translocation [101].

As discussed in section 1.4, IDRs have clusters of charged residues that can transiently interact with binding partners [1]. MoRFs in IDRs often contain multiple phosphorylation sites that function as molecular switches that modulate the conformations and interactions of the IDR based on the order and combination of their phosphorylation states [208,231,232]. Phosphorylation patterns in the cellular Sbh1 pool are dynamic and potentially play a role in regulation Sbh1 function [219]. When individual Sbh1 phosphorylation sites were mutated to Ala, *S35A* mutation rendered Sbh1 incapable of complementing growth defects in *Δsbh1 Δsbh2* cells at 37 ˚C whereas the phosphomimetic *S35E* mutation could [219]. Individual *S3A* and *T5A* mutations did not affect Sbh1 function, but the *sbh1S3A/T5A* combination mutant led to a moderate growth defect at 37 ˚C and Gls1 import defect comparable to *Δsbh1 Δsbh2* which was not found in *sbh1 S3E T5E* phosphomimetic mutants [222]. Altogether, evidence suggests that interactions Sbh1 may be regulated by differential phosphorylation of its cytosolic domain.

The interdependence of microtubules that form the cytoskeleton and the ER is considered key to the spatial organisation of the ER [233,234]. Sec61β directly contacts microtubules via the basic residues in its cytosolic region interacting with the acidic tail of tubulin [215]. Sec61β likely also connects the Sec61 translocon microtubules and enhances the stability of ribosome-Sec61 complex during translocation [215].

The conserved, octameric exocyst complex tethers secretory vesicles to the plasma membrane [235]. Even though the Sec61 translocon and the exocyst are at opposite extremes of the secretory pathway, Sbh1 and Sec61β interact with exocyst complex subunits [236,237]. Sbh1 also interacts with Sec4, a Rab GTPase linked to secretory vesicles that binds to the exocyst [236]. Overexpression of *SBH1* alleviates growth defects in exocyst mutants, but Sbh1

TM domain alone could not mitigate these defects [222,236]. When not associated with the Sec61 complex, Sbh1 interacts with Rtn1 which is an ER TM protein that copurifies with the exocyst and plays a role in ER morphogenesis and ER inheritance [222,238–240]. Hence, interaction of Sec61β/Sbh1 cytosolic domain with the exocyst is crucial for its function.

Sec61β has been implicated in various pathological conditions. The expression of *SEC61B* was found to be upregulated in colorectal cancer cells, suggesting its potential contribution to tumour growth or progression [241]. Mutations in *SEC61B* have been identified as a cause of polycystic liver disease [128]. This suggests the potential Sec61β as a biomarker for these diseases.

Research so far has mainly focussed on the conserved TM domain of Sec61β/Sbh1. The Sbh1 cytosolic domain may play crucial roles beyond its interaction with microtubules and the exocyst complex. The presence of an IDR rich in phosphorylation sites at the N-terminal suggests a regulatory role, the mechanisms of which are still unclear. The role of its CMP region is unknown. These knowledge gaps highlight the need for further investigation into the functions of Sbh1, particularly its cytosolic domain, to fully understand its role in cellular processes.

1.6. Aim of the Study

The purpose of this study is to determine the role of Sec61 channel subunit Sbh1 in *S. cerevisiae*. I first studied the effect of the absence of Sbh1 in the overall structure and function of the Sec61 and Sec channels. I then focussed on the functions and interactions of the cytosolic domain of Sbh1.

The objectives of this study were as follows:

- To characterise *Δsbh1 Δsbh2* mutant.
- To investigate whether Sbh1 stabilises the Sec complex and the Sec61 complex.
- To examine the role of conserved membrane proximal (CMP) region of Sbh1 in its function.
- To identify potential interaction partners of the Sbh1 cytosolic domain.

Materials and Methods

2

2. Materials and Methods

2.1. Materials

2.1.1. Laboratory Equipment

Table 2.1 List of Laboratory Equipment used in this study.

Equipment	Manufacturer
GN 5235-20 freezer	Liebherr
4K15 Refrigerated Centrifuge	Sigma Laborzentrifugen GmbH
583 Gel Dryer	Bio-Rad Laboratories Inc.
Amersham™ Autoradiography Hypercassettes™	GE Healthcare
Amersham™ Imager 600 RGB	GE Healthcare
Amersham™ Ultrospec™ 2100 Pro UV/Vis Spectrophotometer	GE Healthcare
Analytical Balance	Sartorius AG
Avanti® J-E Highspeed Centrifuge	Beckman Coulter Inc.
Axioskop Microscope	Zeiss Microscopy Co.
Concentrator plus	Eppendorf
DX-150 Autoclave	Systec
E-BOX VX2 Gel Documantation System	Peqlab Biotechnologie GmbH
EUROSTAR Power-B Overhead Stirrer	IKA-Werke GmbH
Duomax 1030 platform shaker	Heidolph
Invitrogen™ Mini Gel Tank	Thermo Fischer Scientific
JA25.50 Rotor	Beckman Coulter Inc.
JLA-10.500 Rotor	Beckman Coulter Inc.
Biobasic 410 Refrigerator	Gram Bioline
Microcentrifuge 5415R	Eppendorf AG
MilliQ Integral Water Purification System	Merck KGaA
Mini Blot Module (Invitrogen™,	ThermoFisher Scientific
Mini-Beadbeater-24	BipSpec Products Inc.
MiniSpin® Plus	Eppendorf AG
Multitron Standard Incubation Shaker	Infors HT AG
NanoDrop™ 2000 Spectrophotometer	Thermo Scientific
Neubauer Haemocytometer	Roth GmbH & Co. KG
Optima™ L-90K Ultracentrifuge	Beckman Coulter Inc.
Optima™ MAX-XP Ultracentrifuge	Beckman Coulter Inc.
Overhead Rotator	NeoLab Migge GmbH
peqSTAR 2X Gradient Thermocycler	Peqlab Biotechnologie GmbH

Equipment	Manufacturer
PerfectBlue Gelsystem Mini S	Peqlab Biotechnologie GmbH
pipetus® pipette controller	Hirschmann™ Laborgeräte
PIPETMAN Classic Set Pipettes	Gilson Inc.
PowerPac™ 3000 Power Supply	Bio-Rad Laboratories Inc.
PowerPac™ HC Power Supply	Bio-Rad Laboratories Inc.
Quartz Cuvettes	Hellma Analytics
RCT Basic Magnetic Stirrer	IKA-Werke GmbH
Rocking Shaker	NeoLab Migge GmbH
Storage Phosphor Screens	GE Healthcare
SW60Ti Rotor	Beckman Coulter Inc.
Temperature Freezer C340	New Brunswick Scientific
ThermoMixer® C	Eppendorf AG
TLA120.1 Rotor	Beckman Coulter Inc.
Trans-Blot® Cell	Bio-Rad Laboratories Inc.
Typhoon TRIO™ Variable Mode Imager	GE Healthcare
Vortex-Genie 2	Scientific Industries Inc.
Sonorex Ultrasonic bath	Bandelin electronic GmbH & Co. KG

2.1.2. Chemicals, Reagents and Consumables

Table 2.2 List of chemicals and reagents used in this study.

Chemical	Manufacturer
1 kb DNA Ladder	New England BioLabs®
10X CutSmart® Restriction Buffer	New England BioLabs®
4-trans-(4-trans-Propylcyclohexyl)-cyclohexyl a-maltoside	GLYCON Biochemicals GmbH
Acetone	VWR® International
Adenine (>99 %)	Sigma-Aldrich®
Agar agar, Kobe I	Sigma-Aldrich®
Albumin Fraction V, Protease-free, >98% for protein analysis and molecular biology	Carl Roth GmbH
Ammonium peroxydisulfate (>98% p. a.)	Carl Roth GmbH
Ampicillin sodium salt, ≥97 %, BioScience grade	Carl Roth GmbH
BigCHAP, deoxy	Merck Millipore
Bolt™ Bis-Tris Plus Mini Protein gels, 4-12% gradient, 1 mm	Thermo Scientific™
Boric acid, BioXtra, >99.5 %	Sigma-Aldrich®
Bromophenol blue sodium salt	Sigma-Aldrich®

Chemical	Manufacturer
Calcium chloride dihydrate, >99 % p.a.	Grüssing GmbH
cOmplete™ ULTRA Tablets, Mini, EDTA-free, EASYpack Protease Inhibitor Cocktail	Roche
Con A - Sepharose™ 4B	GE Healthcare
COUNT OFF Liquid concentrate	Perkin Elmer
D-(+)-Glucose (≥99.5 %)	Sigma-Aldrich®
Digitonin-wasserlöslich	Matrix BioScience GmbH
Digitonin, High Purity	Merck Millipore
DL-Dithiothreitol, BioUltra, ≥99.0 %	Sigma-Aldrich®
DMSO, anhydrous	Sigma-Aldrich®
Drop-out -Leu	Formedium™
Drop-out -Ura	Formedium™
EasyTag™ EXPRESS 35S Protein Labelling Mix	PerkinElmer
EDTA disodium salt, dihydrate	Sigma-Aldrich®
Ethanol, 99,8% HPLC	VWR® International
Ethanol, absolute	Sigma-Aldrich®
Ethidium bromide Solution, 1 %	Carl Roth GmbH
GenElute™ PCR Clean-up Kit	Sigma-Aldrich®
GenElute™ Plasmid Miniprep Kit	Sigma-Aldrich®
Glacial acetic acid	VWR® International
Glycerol, >98 %	Carl Roth GmbH
Glycine (PUFFERAN, >99 % p. a.)	Carl Roth GmbH
GTP Solution, 100 mM	Thermo Scientific™
HEPES sodium salt ≥99.5 %	Sigma-Aldrich®
Hydrochloric acid, 37 %	Bernd Kraft GmbH
Invitrogen™ UltraPure™ Agarose	Thermo Scientific™
IPTG, dioxanfrei, 98 %	Carbolution Chemicals GmbH
L-Leucine (>98.5 %)	Sigma-Aldrich®
L-Tryptophan, >98%	Sigma-Aldrich®
Lithium acetate dihydrate, BioXtra	Sigma-Aldrich®
Magnesium acetate	Grüssing GmbH
Magnesium chloride	Grüssing GmbH
Magnesium sulfate	Applichem GmbH
Manganese chloride, 97 %	Sigma-Aldrich®
Methanol, >99.8 % Grad. - HPLC	VWR® International
MOPS, BioPerformance Certified, suitable for cell culture, ≥99.5 %	Sigma-Aldrich®

Chemical	Manufacturer
NuPAGE® MES SDS Running Buffer (20X)	Thermo Scientific™
NuPAGE® MOPS SDS Running Buffer (20X)	Thermo Scientific™
One*Taq*® 2X Master Mix	New England BioLabs®
PageRuler™ Plus Pre-stained Protein Marker	Thermo Scientific™
Peptone from casein	Carl Roth GmbH
PMSF (>99 %)	Carl Roth GmbH
Poly(ethylene glycol) 4000, BioUltra	Sigma-Aldrich®
Potassium acetate, >99% p. a.	Grüssing GmbH
Potassium chloride, >99 % p.a.	Grüssing GmbH
Potassium hydroxide, 85%	Grüssing GmbH
Protein A-Sepharose™ CL-4B	GE Healthcare
Puromycin dihydrochloride, >98 % for Biochemistry	Carl Roth GmbH
Purple 6X Gel Loading Dye	New England BioLabs®
Rotiphorese® Gel 30 (37.5:1) Acrylamide-bisacrylamide	Carl Roth GmbH
Salmon testes DNA	Sigma-Aldrich®
SDS Pellets >99%	Carl Roth GmbH
Skim milk powder	Sucofin
Sodium azide, BioUltra, >99.5 %	Sigma-Aldrich®
Sodium chloride, for molecular biology (>98 %)	Sigma-Aldrich®
Sodium hydroxide pellets	Grüssing GmbH
Sorbitol	Sigma-Aldrich®
Streptavidin-HRP	Sigma-Aldrich®
SuperSignal™ West Pico PLUS Chemiluminescent Substrate	Thermo Scientific™
T4 DNA Ligase	Thermo Scientific™
T4 DNA Ligase Buffer	Thermo Scientific™
TEMED, 99 % p. a.	Carl Roth GmbH
Trichloroacetic acid, >99 % p. a.	Carl Roth GmbH
Triton™ X-100 for molecular biology	Sigma-Aldrich®
Trizma® Base, for molecular biology, >99.8%	Sigma-Aldrich®
Tryptone, enzymatic digest from casein	Sigma-Aldrich®
Tunicamycin	Sigma-Aldrich®
Tween® 20	Sigma-Aldrich®
Uracil, >99%	Sigma-Aldrich®
Urea	Sigma-Aldrich®
Yeast Extract	Carl Roth GmbH
Yeast nitrogen base	Formedium™
Yeast nitrogen base without amino acids and ammonium sulfate	Formedium™

Chemical	Manufacturer
β-Mercaptoethanol (99%, p. a.)	Carl Roth GmbH

Table 2.3 List of consumables used in this study.

Product	Manufacturer
Graduated cylinders	DWK Life Sciences GmbH
Petri dishes, 92 x 16 mm, with vents	Greiner Bio-One
Cuvettes	SARSTEDT AG & Co. KG
Quartz cuvettes	Hellma Analytics
Reaction tubes 0.5 mL, 1.5 mL, 2 mL	SARSTEDT AG & Co. KG
Glass beads, acid washed, 1 mm	Sigma-Aldrich®
Amersham Protran® 0.2 NC Nitrocellulose Membrane (0.2 µm)	Cytiva LifeSciences
3MM Chr Chromatography Paper (Whatman™)	Cytiva LifeSciences
Conical tube, sterile, 15 mL, 50 mL	Greiner Bio-One
Phosphor Imaging plates	GE Healthcare
Open-Top Centrifuge Tubes, Polyclear, 11 x 60mm	Seton Scientific
Thickwall Polycarbonate Tube 7 x 20 mm	Thermo Scientific
Sterican hypodermic needle 0.9 x 40 mm	Braun Melsungen AG
Surgical disposible scalpel	Braun Melsungen AG
Parafilm M	Bemis
surPhob Pipette tips	Biozym Scientific GmbH
gel loading tips	Biozym Scientific GmbH
Inoculating loop, 10 µL, Sterile	SARSTEDT AG & Co. KG
Stripette™ serological pipettes 5 mL, 10 mL, 25 mL, 50 mL	Corning®
Erlenmeyer flasks	DWK Life Sciences GmbH
Beakers	DWK Life Sciences GmbH
Reagent bottles 100 mL, 250 mL, 500 mL, 1 L, 2 L	DWK Life Sciences GmbH
Amersham Hypercassette autoradiography cassette	Cytiva LifeSciences
Filtropur Sterile filtration system, PES 0.2 µm, 100 mL, 250 mL	SARSTEDT AG & Co. KG

2.1.3. Software

Table 2.4 List of software and online tools used in this study.

Software	Use
AlphaFold	Protein 3D structure prediction
BioRender	creating illustrations
Clustal X	multiple sequence alignment
eVFold	Evolutionary conservation
I-TASSER	Protein structure prediction
Illustrator	Image editing, Figure generation
ImageQuant™ TL software	Immunoblot quantification
IUPred2/ANCHOR2	Protein disorder and interaction prediction
MFSPSSMPred	MoRF prediction in protein
Microsoft Excel	Generating graphs
MoRFChiBi	Identification of MoRFs in protein sequences
MoRFPred	MoRF prediction in disordered protein
Photoshop	Image editing
PredictProtein	Protein secondary structure prediction
PSIPRED	Protein structure prediction
PyMol	Protein 3D structure visualisation
Robetta Fold	Protein 3D structure prediction
SnapGene	Primer desin, plasmid visualisation
Zotero	Bibliography and reference management

2.1.4. *Saccharomyces cerevisiae* Strains

Table 2.5 List of *S. cerevisiae* strains used used in this study.

Strain ID	Alias	Full Genotype	Source
KRY200	*sec61-32*	*MATα can1-100 leu2-3,112 his3-11,15 trp1-1 ura3-1 ade2-1 sec61::HIS3 pDQ1[sec61-32]*	Pilon et al., 1998 [242]
KRY585	*SBH1 SBH2*	*MATa leu2-3,113 ura3-52*	Toikkanen et al., 2003 [236]
KRY588	*Δsbh1 Δsbh2*	*MATa leu2-3,112 ura3-52 GAL+ seb1::KanMx seb2::hphMx*	Soromani et al., 2012 [219]
KRY869	*sec63-201*	*MATα ura3Δ99, leu2Δ1, trp1Δ99, ade2-101ochre, sec63-201*	Ng et al., 1996 [243]
KRY1015	*sbh1S3A/T5A*	*MATa seb1::KanMx seb2::hphMx leu2-3,112 ura3-52 GAL+ [pRS415 sbh1 S3A T5A]*	Römisch Lab
KRY1044	*SBH1*	*MATa leu2-3,112 ura3-52 GAL+ seb1::KanMx seb2::hphMx [pRS415 SBH1]*	Römisch Lab
KRY1045	*Δsbh1 Δsbh2*	*MATa leu2-3,112 ura3-52 GAL+ seb1::KanMx seb2::hphMx [pRS415]*	Römisch Lab
KRY1077	BY4742	*MATα his3Δ1 leu2Δ0 lys2Δ0 ura3Δ0*	Giaever et al., 2002 [244]
KRY1080	*Δire1*	*MATα his3Δ1 leu2Δ0 lys2Δ0 ura3Δ0 ire1::kanMX4*	Giaever et al., 2002 [244]
KRY1274	*sbh1D45-G49A*	*MATa leu2-3,112 ura3-52 GAL+ seb1::KanMx seb2::hphMx [pRS415 sbh1 D45-G49A]*	This work
KRY1275	*sbh1L50-V52A*	*MATa leu2-3,112 ura3-52 GAL+ seb1::KanMx seb2::hphMx [pRS415 L50-V52A]*	This work
KRY1276	*sbh1P54A*	*MATa leu2-3,112 ura3-52 GAL+ seb1::KanMx seb2::hphMx [pRS415 P54A]*	This work
KRY1279	*Δcox6*	*MATα his3Δ1 leu2Δ0 lys2Δ0 ura3Δ0 cox6::kanMX*	Morgan Lab
KRY1280	*rho0*	*MATα his3Δ1 leu2Δ0 lys2Δ0 ura3Δ0 [rho0]*	Morgan Lab

2.1.5. *Escherichia coli* Strains and Plasmids

Table 2.6 List of *E. coli* strains and plasmids used in this study.

Strain ID	Alias	Genotype	Description	Source
KRB3	-	*E. coli* (DH5α) expressing lyticase	Lyticase expression and purification	Shen et al., 1991 [245]
KRB46	DH5α	*recAF- Φ80 λ lacZ ΔM15 ΔlacZYA argF U169 deoR recA1 endA1 hsdR17 Cr-K mK+ supE44 λ- thi1 gyrA96 relA1*	Competent cells for transformation with plasmid vectors	Hanahan, 1983 [246]
KRB262	*ppαf*	p416-*ppαf-Ser* in DH5α	ppαf expression in *MATa* yeast	Römisch Lab
KRB536	pRS415	pRS415 (*CEN, LEU2, amp)* in DH5α	Empty pRS415 plasmid	Sikorski and Hieter, 1989 [247]
KRB689	*SBH1*	pRS415-*SBH1* in DH5α	*SBH1* expression in KRY588 (*Δsbh1 Δsbh2*)	Soromani et al., 2012
KRB1267	*Sbh1D45-G49A*	pRS415-*sbh1D45-G49A* in DH5α	*sbh1D45-G49A* expression (CMP mutant)	This work
KRB1268	*sbh1L50-V52A*	pRS415-*sbh1L50-V52A* in DH5α	*sbh1L50-V52A* expression (CMP mutant)	This work
KRB1269	*sbh1P54A*	pRS415-*sbh1P54A* in DH5α	*sbh1P54A* expression (CMP mutant)	This work
KRB1270	*sbh1D45-G49A/P54A*	pRS415-*sbh1D45-G49AP54A* in DH5α	*sbh1D45-G49A/P54A* expression (Combo mutant)	This work
KRB1271	*sbh1D45-V52A*	pRS415-*sbh1D45-V52A* in DH5α	*sbh1D45-V52A* (Combo mutant)	This work
KRB1272	*sbh1L50-V52A/P54A*	pRS415-*sbh1L50-V52AP54A* in DH5α	*sbh1L50-V52A/P54A* (Combo mutant)	This work
KRB1273	*Sbh1D45-V52A/P54A*	pRS415-*sbh1D45-V52AP54A* in DH5α	*Sbh1D45-V52A/P54A* (Combo mutant)	This work

2.1.6. Primers

Table 2.7 List of primers used in this study.

Name	5' → 3' Sequence	Tm (˚C)	Application
M13_Fwd	GTAAAACGACGGCCAGT	53	M13 forward primer used in MP generation
M13_Rev	CAGGAAACAGCTATGAC	47	M13 reverse primer used in MP generation
DEATG49A_Fwd	GAAGATTTATTCTGCTGCAGCTGCTGCACTAAGAGTAGATCCC	46	*sbh1D45-G49A* mutant generation, upstream
DEATG49A_Rev	GGGATCTACTCTTAGTGCAGCAGCTGCAGCAGAATAAATCTTC	46	*sbh1D45-G49A* mutant generation, downstream
LRV52A_Fwd	GAGGCTACGGGAGCAGCTGCAGATCCCTTAGTTG	52	*sbh1L50-V52A* mutant generation, upstream
LRV52A_Rev	CAACTAAGGGATCTGCAGCTGCTCCCGTAGCCTC	50	*sbh1L50-V52A* mutant generation, downstream
P54A_Fwd	GGGACTAAGAGTAGATGCTTTAGTTGTGTTG	54	*sbh1P54A* mutant generation, upstream
P54A_Rev	CAACACAACTAAAGCATCTACTCTTAGTCCC	49	*sbh1P54A* mutant generation, downstream
DP_Fwd	GAAGATTTATTCTGCTGCAGCTGCTGCACTAAGAGTAGATGCTTTAGTTGTGTTGTTTCTAGCGG	56	*sbh1D45-G49A/P54A* mutant generation, upstream
DP_Rev	CCGCTAGAAACAACACAACTAAAGCATCTACTCTTAGTGCAGCAGCTGCAGCAGAATAAATCTTC	52	*sbh1D45-G49A/P54A* mutant

Name	5’ → 3’ Sequence	Tm (˚C)	Application
			generation, downstream
DL_Fwd_2	CGATTTTGAAGATTTATTCTGCTGCAGCTGCTGCAGCAGCTGCAGATCCCTTAGTTGTGTTGTTTC	55	*sbh1D45-V52A* mutant generation, upstream
DL_Rev_2	GAAACAACACAACTAAGGGATCTGCAGCTGCTGCAGCAGCTGCAGCAGAATAAATCTTCAAAATCG	53	*sbh1D45-V52A* mutant generation, downstream
LP_Fwd	GATGAGGCTACGGGAGCAGCTGCAGATGCTTTAGTTGTGTTGTTTCTAG	55	*sbh1L50-V52A/P54A* mutant generation, upstream
LP_Rev	CTAGAAACAACACAACTAAAGCATCTGCAGCTGCTCCCGTAGCCTCATC	53	*sbh1L50-V52A/P54A* mutant generation, downstream
DLP_Fwd_2	CGATTTTGAAGATTTATTCTGCTGCAGCTGCTGCAGCAGCTGCAGATGCTTTAGTTGTGTTGTTTCTAGCGGTCG	57	*sbh1D45-V52A/P54A* mutant generation, upstream
DLP_Rev_2	CGACCGCTAGAAACAACACAACTAAAGCATCTGCAGCTGCTGCAGCAGCTGCAGCAGAATAAATCTTCAAAATCG	57	*sbh1D45-V52A/P54A* mutant generation, downstream

2.1.7. Antibodies

Table 2.8 List of antibodies and their dilutions used in this study.

Antibody	Dilution	Source
Anti-Biotin antibody HRP	Westen Blot 1:10000	Sigma-Aldrich
Anti-CPY	IP 1:100	Römisch Lab
Anti-DPAPB	IP 1:100	Pool Lab
Anti-Gls1	Western Blot 1:2000	Barlowe Lab
Anti-Kar2	Westen Blot 1:10000	Römisch Lab
Anti-Pdi1	Westen Blot 1:4000	Römisch Lab
Anti-ppαF	Westen Blot 1:2000	Römisch Lab
Anti-RpL17a	Westen Blot 1:20000	Rospert Lab
Anti-Rpn12	Westen Blot 1:5000	Römisch Lab
Anti-Sbh1$_{(1\text{-}18)}$	Westen Blot 1:2500	Römisch Lab
Anti-Sbh1$_{(39\text{-}45)}$	Westen Blot 1:2000	Römisch Lab
Anti-Sbh1$_{(Pi)}$	Westen Blot 1:2500	Römisch Lab
Anti-Sec61 C-terminal	Westen Blot 1:2000 IP 1:100	Römisch Lab
Anti-Sec62	Westen Blot 1:2500	Schekman Lab
Anti-Sec63	Westen Blot 1:2500	Schekman Lab
Anti-Sss1	Westen Blot 1:2500	Schekman Lab
Goat Anti-Rabbit IgG biotinylated secondary antibody	Westen Blot 1:10000	Sigma-Aldrich
Goat Anti-Rabbit IgG HRP-conjugated secondary antibody	Westen Blot 1:10000	Sigma-Aldrich

2.1.8. Enzymes

Table 2.9 List of enzymes used in this study.

Enzyme	Use	Source
ApaI	Restriction enzyme	New England BioLabs
BamHI	Restriction enzyme	New England BioLabs
FastAP Thermosensitive Alkaline Phosphatase	Phosphotase treatment of digested vector	Thermo Scientific
Lyticase	Microsome preperation	Römisch Lab
One*Taq*® 2X Master Mix	DNA Polymerase	New England BioLabs
PstI	Restriction enzyme	New England BioLabs
T4 DNA Ligase	Ligation of vector and DNA fragment	Thermo Scientific

2.1.9. Media and Buffers

Deionised MilliQ water was used for preparing all buffers and media in all experiments unless specified. All media were sterilised by autoclaving, unless specified. All buffer compositions are described with their corresponding methods in Section 2.2.

Table 2.10 List of *S. cerevisiae* growth media used in this study.

Medium	Composition
Yeast extract, Peptone, Dextrose (YPD)	1 % (w/v) Yeast extract / 2 % (w/v) Peptone / 2 % (w/v) D-Glucose* (For solid medium: 2 % (w/v) Agar-agar)
YPD + Tunicamycin	1 % (w/v) Yeast extract / 2 % (w/v) Peptone / 2 % (w/v) D-Glucose/ 2 % (w/v) Agar-agar / 0.5 µg/mL Tunicamycin**
Yeast extract, Peptone, Glycerol (YPG)	1 % (w/v) Yeast extract / 2 % (w/v) Peptone / 3 % (v/v) Glycerol / 2 % (w/v) Agar-agar
Selective Medium***	0.67 % (w/v) Yeast nitrogen base without amino acids / 0.13 % (w/v) Synthetic complete drop-out mixture (-Leu or -Ura) / 2 % (w/v) D-Glucose (For solid medium: 2 % (w/v) Agar-agar)

*from filtered 50% (w/v) Glucose added prior to use

**added prior to use

***Sterilised by filtration. For solid media, dissolved media components were filtered into autoclaved Agar-agar in MQ water

Table 2.11 List of *E. coli* growth media used in this study.

Medium	Composition
Lysogeny broth (LB)	0.5 % (w/v) Yeast extract / 1 % (w/v) Tryptone / 0.05 % (w/v) NaCl / 1 mM NaOH (For solid medium: 2 % (w/v) Agar-agar)
LB-Amp	0.5 % (w/v) Yeast extract / 1 % (w/v) Tryptone / 0.05 % (w/v) NaCl / 1 mM NaOH / 100 µg/mL Ampicillin* (For solid medium: 2 % (w/v) Agar-agar)

*added prior to use

2.2. Methods

2.2.1. Sterilisation

All glassware were sterilised by autoclaving at 100 kPa and 134 °C for 20 min. Media (yeast and bacterial), and all autoclavable solutions and buffers were sterilised by autoclaving at 100 kPa and 121 °C for 20 min. Synthetic media, and all other non-autoclavable solutions and buffers were sterilised by filtration through 0.2 µm PES filter.

2.2.2. Growth Cultures

2.2.2.1. Growth of *S. cerevisiae*

S. cerevisiae cells were grown in YPD (1 % (w/v) Yeast extract / 2 % (w/v) Peptone / 2 % (w/v) Glucose) or selective medium (0.67 % (w/v) Yeast nitrogen base / 2 % (w/v) Glucose / 0.13 % (w/v) Drop-out mixture) with continuous shaking at 200 rpm, or on solid media plates with agar at 30 °C unless stated otherwise. Cells were generally harvested in the early exponential phase.

2.2.2.2. Growth of *E. coli*

E. coli cells were grown in LB medium (1 % (w/v) Tryptone / 0.5 % (w/v) Yeast extract / 0.5 % (w/v) NaCl) with continuous shaking at 200 rpm or on LB-Agar plates at 37 °C. When required, the antibiotic Ampicillin (Amp) was added to a final concentration of 100 µg/mL.

2.2.3. Yeast Growth Assays

An OD_{600} of 1 of yeast grown to early exponential phase in appropriate medium was harvested, washed with sterile deionised water and serially 10-fold diluted 4 times for a total of 5 concentrations. For each dilution, 5 µL (equivalent to 10^5-10 cells) was spotted onto a media plate. Growth was documented after 3 days.

2.2.4. Protein Gel Electrophoresis and Western Blot Analysis

2.2.4.1. Preparation of Cell Extracts

Yeast cells were grown to an OD_{600} of 1 at 30 °C, 200 rpm, unless specified otherwise. Cells (2 OD_{600}) were harvested at 600 x g for 1 min (Microcentrifuge 5415R, Eppendorf) and the supernatants were discarded. Pellets were washed with 1 mL of sterile deionized water, resuspended in 100 µL 2x SDS sample buffer (100 mM Tris-HCl pH 6.8 / 4 % (w/v) SDS / 0.2 % (w/v) Bromophenol blue / 20 % (v/v) Glycerol / 200 mM DTT). Glass beads (50 µL by volume, acid washed, 1 mm) were added and the cells were disrupted in a bead beater (Mini-BeadBeater-24, BioSpec Products Inc.) at 4 ˚C for 1 min twice, with 1 min pause in between cycles. Samples were incubated at 65 ˚C for 10 min for membrane proteins, or 95 ˚C for 5 min for soluble proteins and centrifuged at 11,000 x g for 1 min. Samples were then loaded onto pre-cast 4-12% gradient Bis-Tris acrylamide gels (NuPAGE Novex, Invitrogen) for electrophoresis.

2.2.4.2. Trichloroacetic Acid (TCA) Precipitation of Protein Samples

Proteins in sample solution were precipitated with equal volume of 20 % (v/v) TCA for 30 min on ice. After centrifugation of the samples at 16,000 x g for 10 min, at 4 ˚C, the supernatant was discarded, and the pellet was washed with 1 mL of ice-cold Acetone. The pellet was air-dried and resuspended in 50 µL 2X SDS sample buffer and incubated at 65 ˚C for 10 min. Samples were then loaded onto pre-cast 4-12% gradient Bis-Tris gels for electrophoresis unless specified.

2.2.4.3. Protein Gel Electrophoresis

Proteins were resolved by sodium dodecyl sulfate polyacrylamide gel electrophoresis (SDS-PAGE). Samples were loaded onto pre-cast Bolt™ Bis-Tris Plus Mini Protein gels, 4-12% gradient (Invitrogen™, ThermoFisher Scientific) 1.0 mm thickness with 10- or 12- wells, if not stated otherwise. After loading the appropriate volume of the protein sample onto the gel, samples were run in a Mini Gel Tank (ThermoFisher Scientific) using 1X NuPAGE® MOPS SDS Running Buffer (Invitrogen™, ThermoFisher Scientific) or 1X NuPAGE® MES SDS Running Buffer (Invitrogen™, ThermoFisher Scientific), depending on the size of the protein of interest, at 80 V for 15 min and 160 V until the end of the gel run (approx. 1 h), at RT using a PowerPac™ 3000 (Bio-Rad Laboratories, Inc.) power supply. The PageRuler™ Plus Pre-stained Protein Marker (ThermoFisher Scientific) was used as the molecular weight standard as per manufacturer's instructions.

2.2.4.4. Western Blot Analysis

For transferring the proteins separated by SDS-PAGE onto a nitrocellulose membrane, a "sandwich" was assembled with the acrylamide gel and the Protran® 0.2 NC Nitrocellulose Membrane (0.2 µm pore size, Amersham™, Cytiva), 3MM Chr Chromatography Paper (Whatman™, Cytiva) and sponges soaked in Transfer Buffer (25 mM Tris / 200 mM Glycine / 20 % (v/v) Methanol / 0.2 % (w/v) SDS). The protein transfer was then conducted in Transfer Buffer for 2 hr at 100 V at 4 ˚C using a Trans-Blot® Electrophoretic Transfer Cell (Bio-Rad Laboratories, Inc.). Alternatively, Mini Blot Module (Invitrogen™, ThermoFisher Scientific) was used with a transfer time of 1 h, at 10 V and RT.

For immunoblotting, the membrane was blocked in Blocking buffer (50 mM Tris-HCl, pH 7.4 / 150 mM NaCl / 2 % (w/v) milk powder / 0.1 % (v/v) Tween20 / 5 mM NaN_3) for 1 hr while being gently shaken on a Rocking Shaker (NeoLab Migge GmbH). The membrane was then incubated with agitation with the primary antibody diluted in Blocking buffer for 2h at RT or o/n in the cold room. All antibodies used and their dilutions are mentioned in Section 2.1.7. The membrane was then washed twice (10 min each) in Blotting buffer followed by 2 washes (also of 10 min each) in 1x TBST (50 mM Tris-HCl, pH 7.4 / 150 mM NaCl / 0.1 % (v/v) Tween20 / 5 mM NaN_3). The membrane was then incubated with the Goat Anti-Rabbit IgG HRP conjugated secondary antibody (Sigma-Aldrich) diluted to 1:10000 in 1x TBST shaking for 1 hr at RT. The membrane was washed 6 times for 10 min each with 1x TBST. Immunoreactivity on the blots was visualised using the SuperSignal™ West Pico PLUS Chemiluminescent Substrate (ThermoFisher Scientific) according to the manufacturer's instructions. Signals were detected using AI600 Imager (Amersham) and quantified using ImageQuant™ TL software (GE Healthcare), when required.

2.2.4.5. Preparation of Acrylamide-Bisacrylamide Gels

When required, 15 % acrylamide-bisacrylamide gels were prepared with a 4 % Stacking gel. Components for the gel mixture are given in Table 2.12.

Table 2.12 Components of Acrylamide-Bisacrylamide Gels

Component	4 % Stacking Gel		15 % Running Gel	
	Volume	Concentration	Volume	Concentration
37:1 Acrylamide-Bisacrylamide	1.3 mL	4 % (v/v)	15 mL	15 % (v/v)
0.5 M Tris-Hcl, pH6.7	1.25 mL	62.5 mM	--	--
1.5M Tris-HCl, pH 8.7	--	--	8.1 mL	400 mM
20 % (w/v) SDS	65 µL	0.13 % (w/v)	200 µL	0.13 % (w/v)
MilliQ Water	7.23 mL	--	7.3 mL	--
10 % (w/v) APS	15 µL	--	225 µL	--
TEMED	10 µL	--	10 µL	--

2.2.5. Pulse-Labelling

For pulse-labelling with [^{35}S] isotope, yeast strains were grown in YPD or selective media at their permissive temperature (24 ˚C or 30 ˚C) to an OD_{600} of 0.5 and transferred to their respective restrictive temperature (38 ˚C or 20 ˚C) for 3 hours. Cells were harvested at 4500 x g for 5 mins, washed twice with Labelling Medium (0.67 % (w/v) Yeast nitrogen base without amino acids and ammonium sulfate / 5% (w/v) Glucose / auxotrophy supplements as required, mentioned in Table 2.13) and resuspended to OD_{600} of 6 using Labelling Medium.

Table 2.13 Concentrations of auxotrophy supplements used in labelling medium.

Compound	Concentration
Uracil	76 mg/L
L-Leucine	380 mg/L
L-Tryptophan	76 mg/L
Adenine	18 mg/L

Aliquots of 1.5 OD_{600} were made for each strain and pre-incubated at their restrictive temperatures for 10 min at 800 rpm in ThermoMixer® C (Eppendorf). Proteins were labelled for 5 mins (for soluble proteins) or 15 mins (for membrane proteins) with 30 µCi of EasyTag™ EXPRESS ^{35}S Protein Labelling Mix (PerkinElmer) per sample at their restrictive temperature. The pulse was stopped by killing the cells using ice-cold Tris-Azide Buffer (20 mM Tris-HCl, pH 7.5 / 20 mM NaN_3) and immediately transferred to ice. Cells were harvested for 1 min, 4 ˚C, at full speed in an Eppendorf 5424-R microfuge and washed once with Tris-Azide buffer. Cells were then resuspended in Resuspension Buffer (100 mM Tris-HCl, pH 9.4 / 10 mM DTT/ 20 mM NaN_3), incubated for 10 mins at room temperature, and collected at full speed for 1 min at 4 ˚C. Cells were subsequently resuspended in Lysis Buffer (20 mM Tris-HCl, pH 7.5 / 0.5 % (w/v) SDS / 1 mM DTT / 1 mM PMSF). An equal volume of glass beads was added to each sample and the cells were disrupted by bead-beating twice for 1 min, with 1 min break between intervals at room temperature. Samples were denatured at 90 ˚C (for soluble proteins) or 65 ˚C (membrane proteins). The beads were washed thrice with 250 µL Washing Buffer (150 mM NaCl / 1 % (v/v) Triton X-100 / 15 mM Tris-HCl, pH 7.5 / 2 mM NaN_3 / 1 mM PMSF). The supernatant for each sample was collected from each wash and combined.

During immunoprecipitation, non-specifically binding proteins were first cleared from each sample by incubation with 60 µL of 20% Protein A-Sepharose™ CL-4B (GE Healthcare) in IP Buffer (150 mM NaCl / 1 % (w/v) Triton X-100 / 15 mM Tris-HCl, pH 7.5 / 2 mM NaN_3 / 0.1 % (w/v) SDS) and incubated for 30 min at room temperature on a rotating wheel. Supernatants were collected by a quick spin in an Eppendorf 5424-R microfuge and incubated overnight at 4 ˚C under rotation with Protein A-Sepharose™ CL-4B in IP Buffer and 1:100 dilutions of the appropriate antibodies (Table 4). The beads were collected by a quick spin

and serially washed twice with IP Buffer and twice with Urea Wash (2 M Urea / 200 mM NaCl / 1 % (v/v) Triton X-100 / 100 mM Tris-HCl, pH 7.5 / 2 mM NaN_3). This was followed by one wash with Con A Wash (500 mM NaCl / 1 % (v/v) Triton X-100 / 20 mM Tris-HCl, pH 7.5 / 2 mM NaN_3) and once with Tris-NaCl Wash (50 mM NaCl / 10 mM Tris-HCl, pH 7.5 / 2 mM NaN_3). Beads were collected by a quick spin and resuspended in 2x SDS-PAGE sample buffer. Samples were denatured at 95 ˚C (for soluble proteins) or 65 ˚C (membrane proteins), loaded onto 4-12% pre-cast Bis-Tris gels and subjected to electrophoresis. Gels were fixed for 30 min in a Fixing Solution (10 % (v/v) Acetic acid / 40 % (v/v) Methanol), washed with deionised water, and dried for 1 hour at 80 ˚C in a gel dryer (Model 583, Bio-Rad). The dried gels were exposed to phosphorimaging plates for 72 hours. The signal was acquired using a Typhoon Trio™ Variable Mode Imager (GE Healthcare) and analysed using ImageQuant™ TL software.

2.2.6. Preparation of Rough Microsomal Membranes

2.2.6.1. Preparation of Lyticase

Lyticase was from lyticase expressing *E. coli* cells by inducing them with IPTG followed by a cold osmotic shock, according to a R. Scheckman laboratory protocol. *E. coli* strain KRB3 was grown o/n in 100 mL LB-Amp medium (1 % (w/v) Tryptone / 0.5 % (w/v) Yeast extract / 0.5 % (w/v) NaCl / 100 µg/mL Ampicillin) at 37 °C, 200 rpm. LB-Amp medium (5 L) divided into 4 flasks of 1.25 L each, was inoculated with 15 mL of the o/n KRB3 culture per flask and cells were grown at 37 °C, 200 rpm to an OD_{600} of 0.5. The cultures were induced with 0.5 mM IPTG for 5 h at 37 °C, 200 rpm. Cells were harvested at 6300 rpm for 10 min, 4°C (Avanti® J-E Centrifuge, JLA-10.500 rotor, Beckman Coulter). Pellets were resuspended in 400 mL of 25 mM Tris, pH 7.4 and centrifuged as before. The supernatant was discarded, and the pellet

was resuspended with 200 mL 25 mM Tris, pH 7.4 / 2 mM EDTA. An equal volume of 25 mM Tris pH 7.4 / 40 % (w/v) sucrose was then slowly added to the pellet and the suspension was gently stirred for 20 min at RT on a magnetic stirrer. The suspension was then centrifuged, and the supernatant was discarded. The pellet was resuspended with 75 mL of ice-cold 0.5 mM $MgSO_4$, slowly stirred at 4 °C for 20 min and centrifuged for 10 min at 6300 rpm. The supernatant containing the lyticase was aliquoted in 15 mL falcon tubes, frozen in liquid nitrogen and stored at -80 °C for future use.

The activity of the lyticase was determined using the yeast strain KRY585 cultures, which were grown in 50 mL YPD to an OD_{600} of 2. The cultures harvested by centrifugation for 5 min at 4200 rpm (4K15 Refrigerated Centrifuge, Sigma Laborzentrifugen GmbH), at RT and resuspended in 100 mM Tris-HCl pH 7.4 / 10 mM DTT to an OD_{600} of 2. Aliquots of 1 mL yeast culture (in duplicates) were incubated with different amounts of lyticase (0.01, 0.02, 0.5, 1, 2 µL). Samples were incubated at 30 °C for 30 min and the OD_{600} was immediately measured. The activity of the lyticase was calculated based on the principle that a 10% decrease of OD_{600} corresponds to 1U of lyticase activity. The two most diluted points of the curve were taken in consideration for the calculation of the activity.

2.2.6.2. Preparation of Microsomal Membranes

A yeast culture (2.5-5 L) was grown o/n either in YPD or selective medium at 30 °C (unless specified) with continuous shaking at 200 rpm to a maximum OD_{600} of 4 for YPD or OD_{600} of 2 for selective media. Cells were harvested at 5000 rpm and RT for 3 min (Avanti® J-E Centrifuge, JLA-10.500 rotor, Beckman Coulter), the pellet was resuspended in 100 mM Tris-HCl, pH 9.4 / 10 mM DTT to a concentration of 100 OD_{600}/mL and incubated for 10 min at RT to weaken

the cell walls. Cells were centrifuged at 5000 rpm and RT for 5 min and then resuspended in Lyticase Buffer (50 mM Tris-HCl, pH 7.5 / 0.75X YP / 700 mM Sorbitol / 0.5 % (w/v) Glucose / 10 mM DTT) to a concentration of 100 OD_{600}/mL. Lyticase was added to a final concentration of 40 U per OD_{600} of cells and incubated with agitation for 20 min at 30 °C, 80 rpm. Cells were then transferred onto ice for 2 min and then centrifuged for 5 min at 5000 rpm, 4 °C. The supernatant was discarded, and the pellet was washed with 2x JR Buffer (40 mM HEPES-KOH, pH 7.4 / 400 mM Sorbitol / 100 mM KOAc / 4 mM EDTA) to a concentration of 250 OD_{600}/mL and centrifuged at 10,000 rpm and 4 °C for 10 min (Avanti® J-E Centrifuge, JA25.50 rotor, Beckman Coulter). The pellet was then resuspended in 2X JR buffer to a concentration of 500 OD_{600}/mL and slowly frozen at -80 °C overnight.

The spheroplasts were thawed in an ice-cold water bath and an equal volume of cold deionised MQ water was added. After the addition of PMSF and DTT to a final concentration of 1 mM, the spheroplasts were disrupted with ten strokes of a motor-driven Potter-Elvehjem homogeniser (EUROSTAR Power-B Overhead Stirrer, IKA) at 4 °C. The lysate was centrifuged for 5 min at 3000 rpm, 4 °C (Avanti J-E Centrifuge, JA-25.50 rotor, Beckman Coulter) to sediment nuclei and undisrupted cells. The supernatant was transferred to a clean polycarbonate tube and centrifuged at 17,500 rpm and 4 °C for 15 min to pellet the membrane fraction. The sample was then transferred into ice and the pellet was resuspended in a minimum volume (0.5 mL) of B88 (20 mM HEPES-KOH, pH 6.8 / 250 mM Sorbitol / 150 mM KOAc / 5 mM $Mg(OAc)_2$), gently homogenised on ice using a small teflon pestle and carefully resuspended using a pipette. The sample was then loaded onto a 1.2 M / 1.5 M (1.5 mL of each sucrose solution previously layered into an SW60Ti tube (Beckman Coulter)) Sucrose Gradient (20 mM HEPES-KOH, pH 7.5 / 50 mM KOAc / 2 mM EDTA / 1 mM DTT / 1.2

M or 1.5 M Sucrose) and centrifuged at 44,000 rpm and 4 °C for 70 min (Optima™ L-90K Ultracentrifuge, SW60 Ti rotor, Beckman Coulter). Lysosomes at the top of the gradient were aspirated and discarded. ER-derived microsomes were collected at the interphase of the gradient and washed once with 50 mL of cold B88 followed by centrifugation at 17,500 rpm and 4°C for 15 min (Avanti® J-E Centrifuge, JA-25.50 rotor, Beckman Coulter). The pellet was carefully resuspended in a small volume of B88 (approx 0.2 mL). Membrane concentrations were measured at OD_{280} in 2 % SDS at a 1:200 dilution. The concentration was adjusted to an OD_{280} of 30 with B88 and the samples were aliquoted (25 µL or 50 µL), frozen in liquid nitrogen, and stored at -80 °C for future use.

2.2.7. Concanavalin A Binding Assay

This method was adapted from Falcone *et al.,* 2011 [248]. Microsomes (0.3 OD_{280} equivalent) were washed and resuspended in Extraction Buffer (50mM HEPES-KOH, pH 7.4 / 400mM KOAc / 5mM $Mg(OAc)_2$ / 10 % (v/v) Glycerol / 0.05 % (v/v) β-Mercaptoethanol / 1 X Protease Inhibitor Cocktail (Roche)). For solubilisation, 400 µL Extraction Buffer containing digitonin was added to a final concentration of 3 % (w/v) and incubated on ice for a total of 1 h. Alternatively Extraction Buffer containing Triton X-100 was added to a final concentration of 1% (w/v). Samples were centrifuged for 10 min at 16,000 x g (Microcentrifuge 5415R, Eppendorf), and 4 ˚C. The supernatants were diluted with Extraction Buffer (without detergent) to a digitonin concentration of 1 % (w/v) and added to 100 µL Concanavalin A (Con A)- Sepharose™ beads (Cytiva) equilibrated in Equilibration Buffer (50mM HEPES-KOH, pH 7.4 / 10 % (v/v) Glycerol / 0.05 % (v/v) β-Mercaptoethanol / 1 X Protease Inhibitor Cocktail (Roche) / 1 % (w/v) Detergent), followed by an incubation for 1 h, on a rotating wheel at 4˚C

to precipitate the complexes. Con A- Sepharose beads were collected with a short spin, washed thrice with 1 mL Equilibration Buffer, mixed with 50 µL of 2X SDS-PAGE sample buffer and denatured at 65 ˚C for 10 min. Unbound proteins in the supernatant were precipitated and prepared for SDS-PAGE by the TCA Precipitation method (Section 2.2.4.2). Proteins were separated by SDS-PAGE (Section 2.2.4.3) and analysed by Western Blotting (Section 2.2.4.4).

2.2.8. Ribosome-associated Membrane Protein (RAMP) Fractionation

This method was adapted from Pilon et al., 1998 [242]. Microsomes (2.1 OD_{280} equivalent) were washed and resuspended in Extraction Buffer (50mM HEPES-KOH, pH 7.4 / 400mM KOAc / 5mM $Mg(OAc)_2$ / 10 % (v/v) Glycerol / 0.05 % (v/v) β-Mercaptoethanol / 0.1 mM PMSF / 1 X Protease Inhibitor Cocktail (Roche)). For solubilisation, 400 µL Extraction Buffer containing digitonin was added to a final concentration of 3 % digitonin and incubated on ice for a total of 30 mins. Alternatively, Extraction Buffer containing Triton X-100 was added to a final concentration of 1%. Following incubation, the solubilised samples were centrifuged at 60,000 rpm for 30 mins at 4 ˚C in an ultracentrifuge (TLA-120.1 Rotor, Optima™ MAX-XP Ultracentrifuge, Beckman Coulter). The supernatants were diluted to have a final digitonin concentration of 1 % (w/v) with Extraction buffer (no detergent), while Triton X-100 samples were not diluted and precipitated with ConA-Sepharose as described in Section 2.2.7. The ultracentrifugation pellets were resuspended in RAMP Buffer (50 mM HEPES-KOH, pH 7.6 / 1M KOAc / 17.5 mM $Mg(OAc)_2$ / 2.5% (w/v) Digitonin or 1 % (v/v) Triton X-100 / 1 X Protease Inhibitors / 1 mM Puromycin / 0.2 mM GTP / 5 mM DTT) and incubated first on ice for 30 mins, followed by 30 mins, 300 rpm in a ThermoMixer® C (Eppendorf) set to 30 ˚C. The samples were then subjected to ultracentrifugation at 100,000 rpm for 30 mins and 4 ˚C.

Ribosome-associated membrane proteins (RAMPs) were recovered from the supernatant by TCA precipitation (Section 2.2.4.2). Samples from each fraction were resuspended in 50 µL 2 X SDS-PAGE sample buffer, denatured by incubating at 65 ˚C for 10 mins and analysed by Western Blotting (Section 2.2.4.4).

2.2.9. Native Co-IP

Microsomes (0.3 OD_{280} equivalent) were washed and resuspended in Extraction Buffer (50mM HEPES-KOH, pH 7.4 / 400mM KOAc / 5mM $Mg(OAc)_2$ / 10 % (v/v) Glycerol / 0.05 % (v/v) β-Mercaptoethanol / 1 X Protease Inhibitor Cocktail (Roche)). For solubilisation, 400 µL Extraction Buffer containing Digitonin was added to a final concentration of 3 % (w/v) and incubated on ice for 1 h. Samples were centrifuged for 10 min at 16,000 xg (Microcentrifuge 5415R, Eppendorf), and 4 ˚C. The supernatants were diluted with Extraction Buffer (without detergent) to a digitonin concentration of 1 % (w/v) and added to 100 µL of 20 % (v/v) Protein A-Sepharose™ CL-4B (GE Healthcare) equilibrated in Equilibration Buffer (50mM HEPES-KOH, pH 7.4 / 10 % (v/v) Glycerol / 0.05 % (v/v) β-Mercaptoethanol / 1 X Protease Inhibitor Cocktail (Roche) / 1 % (w/v) Digitonin), and incubated for 30 min under rotation at 4 ˚C to preclear proteins binding non-specifically to Protein A. Protein A-Sepharose beads were collected by a short spin, and the supernatant was transferred to a fresh tube. Then, 100 µL of equilibrated Protein A-Sepharose and 1:100 dilution of the appropriate antibody was added to the supernatant. The samples were then incubated on a rotating wheel at 4 ˚C for 2-4 h. The beads were collected by a short spin and washed thrice with Equilibration Buffer. The supernatant was fully aspirated and 30 µL of 2X SDS-PAGE sample buffer was added to the beads, followed by denaturing at 65 ˚C for 10 mins. The samples were analysed by Western Blotting (Section 2.2.4.4).

2.2.10. DNA Extraction

2.2.10.1. Isolation of Plasmid DNA from *E. coli*

This was the general method for isolating plasmid DNA from *E. coli* for DNA sequencing and for transforming *S. cerevisiae* using GenElute™ Plasmid Miniprep Kit (Sigma-Aldrich). *E. coli* strain containing the plasmid of interest was grown overnight and cells from 1 mL of the culture was harvested at 16,000 x g for 1 min. The supernatant was discarded, and the cells were resuspended in 200 µL Resuspension Solution, gently mixed with 200 µL of Lysis Solution and rested for 5 mins at RT. Next, 350 µL of Neutralisation Solution was added, mixed gently and the lysate was cleared by centrifuging at 16,000 x g for 10 mins at RT. Parallelly, the binding column was placed in a collection tube and activated by adding 500 µL of Column Preparation Solution and centrifuging at 16,000 x g for 1 min. The cleared lysate was then added to the binding column and the plasmid DNA was bound to the column by a short spin in the centrifuge for 1 min. The column was then washed using 750 µL of Wash Solution. The column was dried by another short spin for 1 min. The plasmid DNA bound to the column was eluted using 100 µL of Elution Solution. The thus obtained plasmid DNA was quantified using the NanoDrop™ 2000 Spectrophotometer (Thermo Scientific).

2.2.10.2. Isolation of Plasmid DNA from *E. coli* by Alkaline Lysis

This method was modified from Birnboim *et al.,* 1979 [249]. This alternative method was specifically used for isolating plasmid DNA from a large number of samples at a time during cloning and for protocols that do not require a high purity of plasmid, such as restriction analysis. A single colony of *E. coli* containing the plasmid of interest was grown overnight at 37 ˚C. Cells from 1.5 mL of this culture were harvested by centrifuging at 16,000 x g for 1 min

at RT. The supernatant was discarded, and the pellet was resuspended in 350 µL of Buffer P1 (50 mM Tris HCl, pH 8.0 / 10 mM EDTA). The cells were lysed by gently mixing 350 µL of Buffer P2 (200 mM NaOH / 1 % (w/v) SDS) and incubating at RT for 5 mins. Then, 400 µL of Buffer P3 (3 M KOAc, pH 5.5) was added and gently mixed to neutralise the reaction. Cell debris was pelleted by centrifuging at 16,000 x g for 10 mins at RT. The supernatant was transferred into a fresh tube, equal volume of ice-cold isopropanol was added and incubated on ice for 15 mins. The precipitated DNA was pelleted by centrifuging at 16,000 for 5 mins at 4 ˚C. The pellet was washed once with ice cold 75 % (v/v) ethanol and dried in a Concentrator plus (Eppendorf). The pellet was resuspended in 75 µL of sterile MQ water and quantified using NanoDrop™ 2000 spectrophotometer. Isolated plasmids were stored at -20 ˚C until further use.

2.2.11. Plasmid Insertion

2.2.11.1. Preparation of Competent *E. coli* DH5α Cells

A pre-inoculum of *E. coli* DH5α strain (KRB46) was grown overnight in LB medium at 37 ˚C with 180 rpm shaking. Fresh LB medium, 25 mL, was inoculated with 1 mL of the pre-inoculum and grown to an OD_{600} of 0.5 at 37 ˚C with 180 rpm shaking. Cells were harvested by centrifuging at 4000 rpm and 4 ˚C for 6 mins and resuspended in 8.5 mL of cold, sterile TFPI buffer (30 mM KOAc / 100 mM KCl / 10 mM $CaCl_2$ / 50 mM $MnCl_2$ / 10 % (v/v) Glycerol). Cells were incubated on ice for 10 mins and collected at 4000 rpm at 4 ˚C for 6 mins. Cells were then resuspended in 1 mL of cold, sterile TFPII buffer (10 mM KCl / 75 mM $CaCl_2$ / 10 % (v/v) Glycerol / 10 mM MOPS) and incubated on ice for 30 mins. Aliquots of 100 µL each were made, flash-frozen in liquid nitrogen and stored at -80 ˚C until further use.

2.2.11.2. Transformation of Competent *E. coli* DH5α

Competent *E. coli* DH5α cells were gently thawed on ice. Once thawed, 1 µL of isolated plasmid DNA was added, mixed gently, and incubated on ice for 30 mins. A heat shock was then given to the cells at 42 ˚C for 45 sec and immediately transferred on to ice for 2 mins. LB medium was preheated to 42 ˚C and 1 mL was added to the cells. The mixture was incubated at 37 ˚C for 1 h with 300 rpm shaking in a ThermoMixer® C (Eppendorf) and collected by centrifuging for 1 min at 10,000 x g. The supernatant was discarded, the pellet was resuspended in 100 µL LB buffer and plated on LB Agar plates containing 100 µg/mL Ampicillin.

2.2.11.3. Transformation of *S. cerevisiae* strains using heat shock

This was the general method used for transforming *S. cerevisiae* adapted from Gietz and Woods, 2002 [250]. The strain to be transformed was grown overnight and 2 mL of the culture was harvested at 3000 rpm for 2 mins. The supernatant was discarded, the pellet was washed with 1 mL of sterile LiAc-TE solution (100 mM LiAc, pH 7.5 / 10 mM Tris HCl, pH 7.5 / 1 mM EDTA) and centrifuged at 3000 rpm for 2 mins. The pellet was resuspended in 100 µL sterile LiAc-TE buffer and incubated at RT for 10 mins. To this 20 µL denatured carrier DNA (10 mg/mL Salmon testes DNA (Sigma) heated at 95 ˚C for 3 mins), 1 µg plasmid DNA and 600 µL sterile PEG buffer (100 mM LiAc, pH 7.5 / 10 mM Tris HCl, pH 7.5 / 1 mM EDTA / 400 mg/mL PEG 4000) and mixed gently. Then 50 µL of sterile 1M LiAc, pH 7.5 was added, gently mixed, and incubated at 30 ˚C for 1 h. Then 20 µL of DMSO was added, mixed gently, and incubated for 15 mins at 42 ˚C. The cells were then collected by centrifugation at 3000 rpm for 2 mins and

washed twice with 1 mL sterile TE buffer (10 mM Tris HCl, pH 7.5 / 1 mM EDTA). Cells were then resuspended in 100 µL sterile TE buffer and plated on required auxotrophic plates.

2.2.11.4. Transformation of Temperature Sensitive *S. cerevisiae* Mutant Strains

This method was used for transforming temperature sensitive *S. cerevisiae* mutant strains by avoiding heat shock. The strain to be transformed was grown to early exponential phase (OD_{600} = 1.0) and 2 mL was harvested at 3000 rpm for 2 mins. The supernatant was discarded, the pellet was washed with 1 mL of sterile LiAc-TE solution (100 mM LiAc, pH 7.5 / 10 mM Tris HCl, pH 7.5 / 1 mM EDTA) and centrifuged at 3000 rpm for 2 mins. The pellet was resuspended in 100 µL sterile LiAc-TE buffer and incubated at RT for 15 mins. To this 20 µL denatured carrier DNA (10 mg/mL Salmon testes DNA heated at 95 ˚C for 3 mins and placed on ice), 1 µg plasmid DNA and 600 µL sterile PEG buffer (100 mM LiAc, pH 7.5 / 10 mM Tris HCl, pH 7.5 / 1 mM EDTA / 400 mg/mL PEG 4000) and mixed gently. Then 50 µL of sterile 1M LiAc, pH 7.5 was added, gently mixed, and incubated at 30 ˚C for 1 h. Then 20 µL of DMSO was added, mixed gently, and incubated for 30 mins at 30 ˚C. The cells were then collected by centrifugation at 3000 rpm for 2 mins and washed twice with 1 mL sterile TE buffer (10 mM Tris HCl, pH 7.5 / 1 mM EDTA). Cells were then resuspended in 100 µL sterile TE buffer and plated on required auxotrophic plates.

2.2.11.5. Gentle Method for Transformation of Temperature Sensitive *S. cerevisiae* Mutant Strains

This method was used for transforming temperature sensitive *S. cerevisiae* mutant strains by avoiding heat shock and minimising the growth of suppressor mutants. The strain to be transformed was grown to early exponential phase (OD_{600} = 1.0) and 2 mL was harvested at 3000 rpm for 2 mins. The supernatant was discarded, the pellet was washed with 1 mL of sterile LiAc-TE solution (100 mM LiAc, pH 7.5 / 10 mM Tris HCl, pH 7.5 / 1 mM EDTA) and centrifuged at 3000 rpm for 2 mins. The pellet was resuspended in 100 µL sterile LiAc-TE buffer and incubated at RT for 15 mins. To this 20 µL denatured carrier DNA (10 mg/mL Salmon testes DNA heated at 95 ˚C for 3 mins and cooled to RT), 1 µg plasmid DNA and 600 µL sterile PEG buffer (100 mM LiAc, pH 7.5 / 10 mM Tris HCl, pH 7.5 / 1 mM EDTA / 400 mg/mL PEG 4000) and mixed gently. Then 50 µL of sterile 1M LiAc, pH 7.5 was added, gently mixed, and incubated at RT for 1 h. Then 20 µL of DMSO was added, mixed gently, and incubated for 1 h at RT. The cells were then collected by centrifugation at 3000 rpm for 2 mins and washed twice with 1 mL sterile TE buffer (10 mM Tris-HCl, pH 7.5 / 1 mM EDTA). Cells were then resuspended in 100 µL sterile TE buffer and plated on required auxotrophic plates.

2.2.12. Site Directed Mutagenesis

Mutations in the conserved membrane proximal region of Sbh1 were generated by site directed mutagenesis (SDM). Forward primers were designed by substituting specific codon in the SBH1 coding sequence with appropriate codon for the intended mutation in 5’ → 3’ direction. Reverse complement of the forward primer was used as the reverse primer. All primers were commercially synthesised by Sigma-Aldrich Custom DNA Oligos service. Lyophilised primers were reconstituted to 100 µM using sterile MQ water and stored at -20

˚C. For PCR, the primers were diluted to 10 µM as the working concentration. The strategy employed for SDM is shown in Figure 2.1.

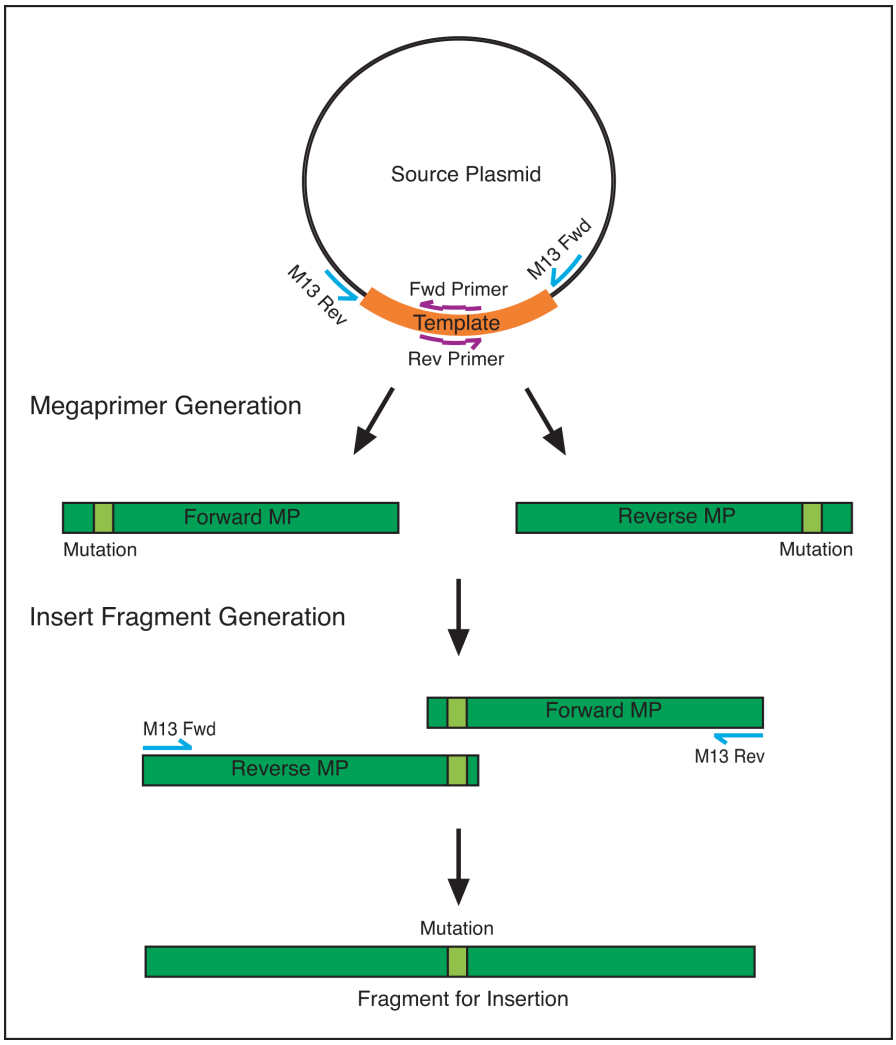

Figure 2.1 Strategy for Site Directed Mutagenesis. First, using the wildtype protein coding sequence as the template, the forward primer containing targeted mutations was amplified with the M13 reverse primer, and the reverse primer containing complement to the mutated codons was amplified with the M13 forward primer, to generate megaprimers (MP). Next, the megaprimers were used as template and amplified with M13 forward and reverse primers to generate the insert fragment comprised of the initial protein coding sequence with targeted mutations in specific codons.

Plasmid containing the SBH1 coding sequence was isolated from *E. coli* (KRB689) as described in Section 2.2.10.1. The plasmid was used as a template for generating "megaprimers" (MP) in the first polymerase chain reaction (PCR) step. The MPs were then amplified together to generate the insert fragment, which was inserted into the plasmid vector of choice after restriction digestion. The ligated plasmids were then used to transform

competent *E. coli DH5α* as described in Section 2.2.11.2. Plasmids were then isolated from selected transformants by alkaline lysis method (Section 2.2.10.2) and successful mutagenesis was confirmed by DNA sequencing. The confirmed plasmids were then used to transform *S. cerevisiae* strains (Sections 2.2.11.4 and 2.2.11.5), which were then grown on selective medium and used for characterisation experiments.

2.2.12.1. Megaprimer Generation

As the first step in SDM, the DNA template to be mutated was amplified by PCR in two separate reactions, each using a designed primer in one direction and M13 primer in the opposite direction, to generate megaprimers (MPs) which are partial fragments of the template with the targeted mutations. The template was diluted to 10 ng/µL with sterile nuclease-free water before use. The reaction was done in a total volume of 25 µL or 50 µL using One*Taq*® 2X Master Mix (New England Biolabs), which contains a blend of DNA polymerases, dNTPs and $MgCl_2$. The reaction mixture composition is detailed in Table 2.14.

Table 2.14 PCR reaction mixture composition for megaprimer generation during SDM.

Component	25 µL Vol.	50 µL Vol.
Primer 1 (Designed Fwd/Rev)	0.5 µL	1 µL
Primer 2 (M13 Rev/Fwd)	0.5 µL	1 µL
Template DNA	1 µL	2 µL
Nuclease free/Sterile MilliQ Water	10.5 µL	21 µL
2X OneTaq PCR MasterMix	12.5 µL	25 µL

A reaction mixture containing the DNA template, both M13 forward and reverse primers and no designed primers was used as the positive control, and a reaction mixture containing both the designed forward and reverse primers, no DNA template and no M13 primers was used as the negative control. All reaction mixtures were subjected to PCR in peqSTAR 2 X Gradient Thermocyler (Peqlab) using the program detailed in Table 2.15.

Table 2.15 PCR program for megaprimer generation during SDM.

Step	Temperature	Duration	
Preheat	94 ˚C	Hold	
Denaturation	94 ˚C	30 sec	
Denaturation	94 ˚C	15 sec	30 cycles
Annealing	52 ˚C	15 sec	
Elongation	68 ˚C	40 sec	
Elongation	68 ˚C	5 min	
Hold	4 ˚C	∞	

The presence of megaprimers in the PCR products was confirmed by agarose gel electrophoresis. The remaining PCR products were purified using GenElute™ PCR Clean-up Kit (Sigma-Aldrich) and stored at -20 ˚C until further use.

2.2.12.2. Agarose Gel Electrophoresis

DNA products and fragments were resolved and identified by agarose gel electrophoresis. First, 5 µL of each DNA sample was stained using 1 µL Purple 6X Gel Loading Dye (New England Biolabs) unless pre-stained using One*Taq*® 2X Master Mix (New England Biolabs) during a PCR step. The samples were loaded onto a 0.8 % (w/v) agarose gel containing 0.5 µg/mL Ethidium bromide made using TBE buffer (100 mM Tris Base / 100 mM Boric Acid / 2 mM EDTA) along with pre-stained 1 kb DNA Ladder (New England Biolabs) as the molecular weight marker. The gel was electrophoresed using TBE buffer in a Peqlab gel tank with a constant 0.1 A current until the end of the gel run. The gel was visualised under UV light and imaged using E-Box VX2 Gel Documentation System (Peqlab).

2.2.12.3. PCR Product Purification

Amplified DNA in PCR reactions was purified from the reaction mixture using GenElute™ PCR Clean-Up Kit (Sigma-Aldrich). First, the DNA binding columns were prepared by adding 0.5 mL Column Preparation Solution and centrifuged for 1 min at 16,000 x g. Samples were prepared by mixing 5 volumes of Binding Solution with 1 volume of the PCR product. The samples were then transferred to the prepared columns and centrifuged at 16,000 x g for 1 min, and then washed with 0.5 mL Wash Solution at 16,000 rpm for 1 min. The column was further centrifuged for 2 mins at 16,000 x g to remove excess wash solution. DNA bound to the column was eluted by adding 50 µL of Elution Solution and incubating it for 1 min at RT, and collected by centrifuging at 16,000 x g for 1 min. The obtained purified DNA was quantified using NanoDrop™ 2000 spectrophotometer and stored at -20 ˚C until further use.

2.2.12.4. Insert Fragment Generation

Megaprimers generated in Section 2.2.12.1 were amplified together to produce the extended insertion fragment in two PCR cycles. In cycle I, the reaction mixture containing both the megaprimers and One*Taq*® 2X Master Mix was subjected to 5 cycles of denaturation, annealing and elongation. For cycle II, M13 primers were mixed into the reaction mixture after cycle I and PCR was continued for another 30 cycles. The reaction mixture composition is detailed in Table 2.16.

Table 2.16 PCR reaction mixture composition for insert fragment generation.

Component	Volume
Megaprimer 1	1 µL
Megaprimer 2	1 µL
2X OneTaq PCR MasterMix	25 µL
Nuclease free/Sterile MilliQ Water	21 µL
Total Volume = 48 µL; PCR upto Cycle I	
M13 Fwd	1 µL
M13 Rev	1 µL

A reaction mixture containing 2 µL of template DNA used for megaprimer generation instead of megaprimers was used as positive control and reaction mixture with sterile nuclease free water instead of megaprimers acted as the negative control. The PCR program used is detailed in Table 2.17.

Table 2.17 PCR program for insert fragment generation.

Step	Temperature	Duration	
Preheat Lid	110 ˚C	--	
Preheat Block	94 ˚C	10 sec	
Pause	94 ˚C	Hold	
Denaturation	94 ˚C	30 sec	
Denaturation	94 ˚C	10 sec	5 cycles (Cycle I)
Annealing	52 ˚C	15 sec	
Elongation	68 ˚C	1 min	
Pause	8 ˚C	Hold	
Denaturation	94 ˚C	15 sec	30 cycles (Cycle II)
Annealing	52 ˚C	15 sec	
Elongation	68 ˚C	40 sec	
Elongation	68 ˚C	5 min	
End Cycle	8 ˚C	∞	

Generated insert fragment in the PCR products was confirmed by agarose gel electrophoresis (Section 2.2.12.2). The PCR products were purified before further use (Section 2.2.12.3).

2.2.12.5. Restriction Digestion of Vector and Insert

To be able to insert the DNA fragment generated in Section 2.2.12.4 into a plasmid vector, both are to be digested using the same set of restriction enzymes. The plasmid into which the generated fragment is to be inserted was isolated from *E. coli* as described in Section 2.2.10.1. Digestion mixtures containing 10X CutSmart® Restriction Buffer (New England Biolabs) and restriction enzymes were prepared as described in Table 2.18 and incubated for a minimum of 2 h or o/n at 37 ˚C. Restriction enzymes used are detailed in Section 2.1.8. Digestion was confirmed by agarose gel electrophoresis with undigested vector and cleaned, undigested insert fragments as negative controls. The digested vector was treated with alkaline phosphatase. Both the digested vector and digested insert were purified using GenElute™ PCR Clean-Up Kit, quantified using NanoDrop™ 2000 spectrophotometer and stored at -20 ˚C until further use.

Table 2.18 Digestion mixture composition for the restriction digestion of vector and insert fragment.

Component	Amount
Plasmid or Clean Insert	10 – 20 ng or ~45 µL
Restriction Enzyme	2.5 µL each
10X CutSmart® Restriction Buffer	7.5 µL
Nuclease free/Sterile MilliQ Water	Make up to 75 µL

2.2.12.6. Phosphatase Treatment of Vector

Digested plasmid from Section 2.2.12.6 was treated with alkaline phosphatase to prevent its self-ligation. To the digested vector, 1 µL of FastAP Thermosensitive Alkaline Phosphatase (Thermo Scientific) was added and incubated for 15 mins at 37 ˚C, followed by incubation for

15 mins at RT. An additional 1 µL of FastAP Thermosensitive Alkaline Phosphatase was added to the vector and incubated again at 37 ˚C for 15 mins. The digested vector was then purified using GenElute™ PCR Clean-Up Kit, quantified using NanoDrop™ 2000 spectrophotometer and stored at -20 ˚C until further use.

2.2.12.7. Ligation of Digested Fragment and Vector

T4 DNA Ligase (Thermo Scientific) was used to catalyse the formation of phosphodiester bonds between 3' hydroxyl and 5' phosphate termini of digested DNA samples in the presence of T4 DNA Ligase Buffer (Thermo Scientific) which contains ATP and $MgCl_2$ needed for ligation. The phosphatase treated vector, and the digested insert fragment were ligated together in 1:1 and 1:3 ratios. The ligation mixtures consisting of T4 DNA Ligase and T4 DNA Ligase Buffer were prepared as described in Table 2.19. A ligation mixture containing sterile, nuclease free water instead of insert fragment, i.e., 1:0 vector to insert ratio, was prepared as a control for vector self-ligation. The ligation mixture was incubated for minimum 2 h to o/n at RT.

Table 2.19 Ligation mixture composition for the ligation of digested insert fragment and vector.

Component	Amount
Digested Vector	100 ng
Digested Insert	1:1 or 1:3 ratio to vector
T4 DNA Ligase	1 µL
10X T4 DNA Ligase Buffer	1 µL
Nuclease free/Sterile MilliQ Water	Make up to 10 µL

Entire volume of ligation mixture was used to transform competent *E. coli* DH5α cells as described in Section 2.2.11.2. The 1:0 ligation control mixture was also used to transform *E. coli* and once again acts as a control.

2.2.12.8. Confirmation of Mutagenesis

To confirm the ligation of insert and vector, the plasmid was isolated from transformed *E. coli*, digested with restriction enzymes, and analysed by agarose gel electrophoresis. From the transformed *E. coli* growing on LB + Amp plates, 12 colonies with picked using sterile toothpicks and grown o/n in LB + Amp medium at 37 ˚C. Plasmid DNA was isolated from each colony by alkaline lysis method as per Section 2.2.10.2. A smaller scale digestion mixture was prepared using the isolated plasmids as described in Table 2.20. Plasmids were digested for 2 h at 37 ˚C. The digests were resolved by agarose gel electrophoresis and visualised under UV light to confirm fragment insertion (Section 2.2.12.2).

Table 2.20 Digestion mixture composition for confirmation of fragment insertion into vector.

Component	Volume
Plasmid	2 µL
10X CutSmart® Restriction Buffer	1 µL
Restriction Enzyme	0.2 µL each
Sterile MilliQ Water	Make up to 10 µL

From the isolated plasmids with successful insertion, plasmids from 3 colonies were purified as described in Section 2.2.12.3 and submitted for Sanger sequencing to Eurofins Genomics, a commercial service. Plasmids with confirmed sequence, one per mutation, were used to transform *S. cerevisiae* strains.

2.2.13. Peptide Panning Analysis

Peptide – peptide interactions were analysed by peptide panning. Peptides of Sbh1 and Sbh2 cytosolic domains were synthesised as spots on an acid-hardened cellulose membrane anchored by their C-terminus. The peptides span the length of their cytosolic domains up to the beginning their TM domains, each 20-mer in length and sliding by 2 amino acids. The Sbh1 peptide spots included combinations of N-terminal acetylation and varied phosphorylation states of each phosphorylatable residue. The peptides for interaction were synthesised with a biotinylated lysine residue at their C-terminus, and the synthesised lyophilised powder was dissolved in a 20 % (v/v) DMSO / 80 % (v/v) sterile MQ water mixture to a working concentration of 10 µM and stored at -20 ˚C.

2.2.13.1. Peptide Binding Assay

A modified version of the method described in Schäuble *et al.,* 2014 was used [251]. The acid-hardened cellulose membranes were activated using methanol and washed with deionised MQ Water. The membranes were then equilibrated with Binding Buffer (50 mM Tris-HCl pH 7.5 / 150 mM NaCl / 0.1 % (v/v) Triton-X 100) and blocked for 1 h with Binding Buffer containing 1 % (w/v) Bovine Serum Albumin. Control spots were excised from the membranes and incubated overnight with anti-phosphorylated Sbh1 antibody (1:2500 dilution) o/n at 4 ˚C with shaking. The membrane portions containing Sbh1 and Sbh2 peptides was incubated overnight with 100 mL Binding Buffer containing 2 µM biotinylated peptide of interest at 4 ˚C with shaking. After washing thrice for 10 mins each with Binding Buffer, membranes were incubated for 1 h with HRP-tagged anti-Biotin antibody (1:10,000 dilution, Sigma-Aldrich) and washed thrice again. Control spots were washed and incubated with biotinylated goat anti-rabbit antibody (1:10,000, Sigma-Aldrich) for 1 h at 4 ˚C with shaking,

followed by washing and incubation with HRP tagged anti-Biotin antibody. Peptide – peptide interactions were detected using the SuperSignal™ West Pico PLUS Chemiluminescent Substrate (Thermo Fisher Scientific) according to the manufacturer's instructions. Interactions were detected using AI600 Imager (Amersham) and analysed using ImageQuant™ TL software (GE Healthcare), when required.

2.2.13.2. Stripping of Membranes

After each assay the cellulose membranes were stripped of all bound peptides and antibodies and regenerated by incubating the membranes with approx. 100 mL Regeneration Buffer A (8 M Urea / 50 mM Tris-HCI, pH 7.0 / 1 % (w/v) SDS / 0.5 % (v/v) β-Mercaptoethanol) in an ultrasonic bath (Sonorex, Bandelin electronic GmbH) for 30 mins at RT twice, followed by three washes for 10 mins each with approx. 100 mL Regeneration Buffer B (50 % (v/v) Ethanol / 10 % (v/v) Acetic acid / 40 % (v/v) deionised MilliQ water). The membranes were then completely air dried and stored at -20 ˚C.

Results 3

3. Results

The aim of this project was to decipher the role of Sec61 channel subunit Sbh1 (homolog to Sec61β in mammals). I began with characterising the *Δsbh1 Δsbh2* mutant. I explored the contribution of Sbh1 to the stability of the Sec complex. I characterised the conserved membrane proximal region (CMP) of Sbh1 regarding its role in Sbh1 function. Further I identified the potential of Sbh1 CMP to interact not only with the N-terminal helix of Sec61 but also with the signal sequences of incoming nascent polypeptide chains.

3.1. Characterisation of the Δ*sbh1* Δ*sbh2* Mutant Strain

Yeast lacking both *SBH1* and *SBH2* have a growth defect at higher temperatures which is rescued when the strain is complemented with wildtype *SBH1* or a truncated Sbh1 consisting of the most C-terminal 5 cytosolic amino acids and the TM domain [222]. At the start of my project, the data available on the translocation defects in *Δsbh1 Δsbh2* yeast were inconsistent [75,222]. Finke *et al.* reported a moderate accumulation of post-translationally translocated α-factor precursor, prepro-α-factor (ppαF) and of co-translationally and post-translationally translocated Kar2 precursor pKar2 *in vivo* at both permissive 30 ˚C and restrictive 37 ˚C. The post-translational translocation defect was more significant in *in vitro* experiments using a heterologous translocation system in *Δsbh1 Δsbh2* cells at a restrictive temperature of 37 ˚C [75]. On the other hand, Feng *et al.* reported a moderate defect in the post-translational translocation of ppαF and a pronounced defect in co-translational translocation at 37 ˚C *in vitro* using a homologous yeast translation-translocation system [222]. Specific translocation defects of cytosolic precursors of known Sbh1 substrates Gls1 and Mns1 (pGls1 and pMns1, respectively) have been reported [75,222]. I started my project

by exploring import of several secretory precursors in *Δsbh1 Δsbh2* to better understand the effect of *SBH1* and *SBH2* deletion on protein translocation. I specifically looked at the import of precursors of Kar2, α-factor, Protein Disulfide Isomerase (PDI) and carboxypeptidase Y (CPY).

Kar2, an Hsp70 ATPase resident in the ER lumen, acts as a chaperone to promote protein folding during post-translational translocation [252]. The Kar2 precursor (pKar2, 74 kDa) is translocated both co-translationally and post-translationally into the ER, where its signal is cleaved to form the mature Kar2 (72 kDa). Accumulation of pKar2 in the cells implies a defect in co-translational or post-translational translocation, or both. I analysed the translocation into the ER of pKar2 by immunoblotting. I prepared cell extracts of wildtype *SBH1 SBH2* and the isogenic mutant *Δsbh1 Δsbh2* strains grown at 24 ˚C and shifted to restrictive 38 ˚C for 3 h. The temperature shift duration was optimised in a prior experiment by students from M.Sc. class of Infection Biology (2019) (Supplementary Figure 1). I resolved the protein content by SDS-PAGE and immunoblotted with polyclonal anti-Kar2 antibodies. As shown in Figure 3.1(A), pKar2 accumulated in the *Δsbh1 Δsbh2* mutant grown at 38 ˚C, indicating a translocation defect. This observation matches what was seen previously, and also concurrently in our lab [75,253].

Next, I looked at the translocation of the yeast mating pheromone α-factor precursor, prepro-α-factor (ppαF). Posttranslational translocation of ppαF (18 kDa) into the ER is very well characterised [114]. Upon entering the ER, the ppαF signal sequence is cleaved and pro-α-factor (~16 kDa) is triply *N*-glycosylated and transported to the Golgi where it is proteolytically cleaved to produce mature α-factor [254]. A defect in the post-translational

translocation of ppαF into the ER results in cytosolic accumulation of ppαF. A mild defect in post-translational translocation of ppαF *in vitro* was previously reported in the *Δsbh1 Δsbh2* mutant using a cell-free assay based on mutant microsomes and *in vitro* translated ppαF [75,222]. I wanted to test whether this defect is present *in vivo* as well. Since the *Δsbh1 Δsbh2* mutant strain and its isogenic wildtype that I used were of mating type a, I transformed the strains with a plasmid expressing ppαF (KRB262). I grew *SBH1 SBH2* and *Δsbh1 Δsbh2* strains at 24 ˚C and shifted to 38 ˚C for 3 hours. I used the cold-sensitive ER import mutant *sec61-32* as control grown at 30 ˚C and shifted to restrictive 20 ˚C for 3 hours. The *sec61-32* strain accumulates ppαF even at permissive temperatures [255]. Following Western blotting of cell extracts, I detected the presence of ppαF using anti-ppαF antibodies. I did not see a significant accumulation of ppαF in the *Δsbh1 Δsbh2* strain grown either at permissive or at restrictive temperature when compared to the inherent defect in *sec61-32* strain, as shown in Figure 3.1(B). This indicates that ppαF was translocated into the ER by the *Δsbh1 Δsbh2* strain. A similar observation was made concurrently in our lab [253].

Protein Disulfide Isomerase (PDI, ~65 kDa) acts as an oxidoreductase and an isomerase in the ER lumen, and plays an important role as a part of protein quality control machinery during ERAD [146]. Its cytosolic precursor, pPDI (~58 kDa), translocates post-translationally into the ER lumen where its signal sequence is cleaved, and the protein is *N*-glycosylated at 5 sites [256]. A defect in the translocation of pPDI into the ER would result in its cytosolic accumulation in cells. To test this, I prepared cell extracts of wildtype *SBH1 SBH2* and *Δsbh1 Δsbh2* strains grown at 24 ˚C and shifted to 38 ˚C for 3 h, resolved proteins by SDS-PAGE, and immunoblotted with polyclonal antibodies against PDI. Neither the *SBH1 SBH2* nor the *Δsbh1 Δsbh2* strain accumulated pPDI, as shown in Figure 3.1(C), suggesting that the import of pPDI

into the ER was not affected. The bands of lower molecular weights seen in *Δsbh1 Δsbh2* likely correspond to different *N*-glycosylation states of PDIp.

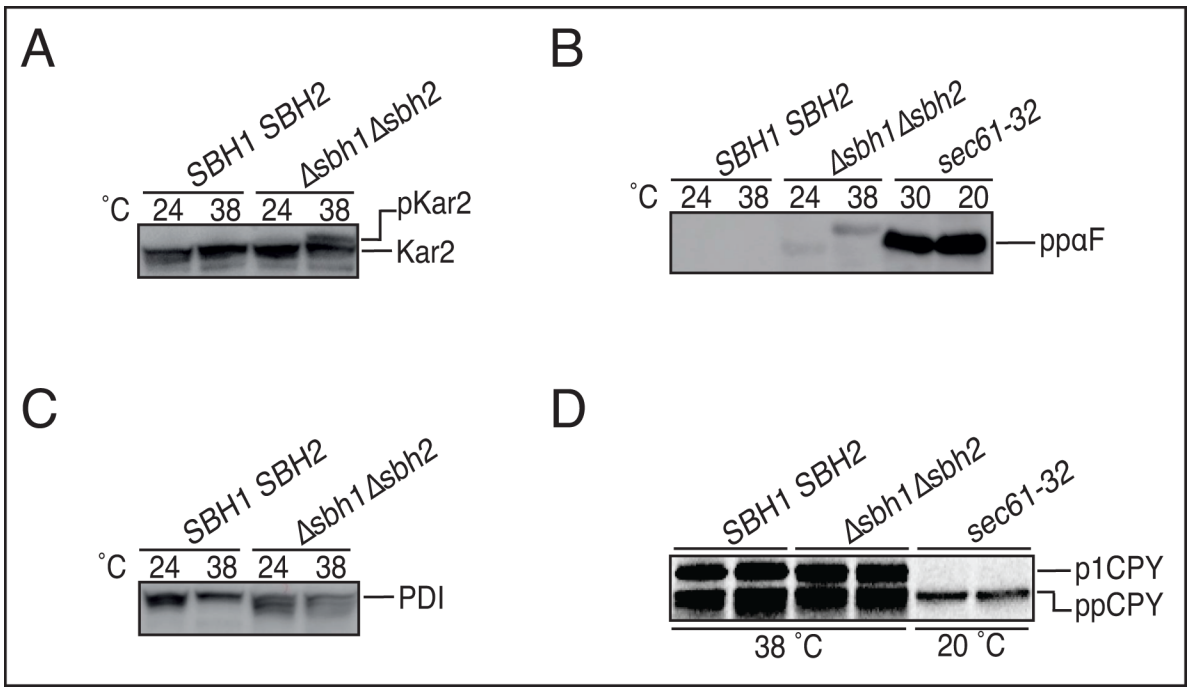

Figure 3.1 Sbh1 is required for ER import of specific substrates only. Yeast wildtype *SBH1 SBH2* and mutant *Δsbh1 Δsbh2* strains were grown at their permissive temperature (24 ˚C) to an OD_{600} of 0.5 and shifted to their restrictive temperature (38 ˚C) for 3 hours. For immunoblotting experiments, 2 OD_{600} of cells were harvested to prepare cell extracts. For each sample 0.25 OD_{600} was used to resolve by SDS-PAGE, followed by immunoblotting against specific proteins. **A)** Kar2 precursor translocation detected by immunoblotting with anti-Kar2p antibody. A band corresponding to pKar2 is seen in *Δsbh1 Δsbh2* cells grown at 38 ˚C. **B)** Alpha Factor translocation analysed by immunoblotting with anti-ppαF antibody raised against its precursor ppαF. The *sec61-32* strain was used as control, grown at permissive 30 ˚C and shifted to restrictive 20 ˚C for 3 hours. No accumulation of ppαF was seen in *SBH1 SBH2* or *Δsbh1 Δsbh2* cells. **C)** PDI precursor translocation analysed by immunoblotting with anti-PDI antibody. Accumulation of pPDI was not seen in either of the strains. **D)** CPY precursor accumulation detected by pulse-labelling of cells grown to early exponential phase with [^{35}S]-Met/Cys for 5 min. Cells were then lysed and immunoprecipitated with anti-CPY antibody. Proteins were resolved by SDS-PAGE and detected by phosphorimaging. The *sec61-32* strain was used as control. The ppCPY incorporation product p1CPY was detected in both *SBH1 SBH2* and *Δsbh1 Δsbh2* strains.

Carboxypeptidase Y (CPY) is a soluble, *N*-glycosylated vacuolar protease. The cytosolic precursor of CPY, ppCPY (~59 kDa) is post-translationally translocated into the ER, where its signal peptide is cleaved, and it is *N*-glycosylated at 4 sites to form p1CPY (67 kDa). This p1CPY is transported to the Golgi where its N-glycans are extended with mannose to p2CPY (69 kD) and then to the vacuole where it is proteolytically processed into its mature form, mCPY (59 kD) [257]. Because cytosolic ppCPY and mCPY are the same size, ppCPY translocation defects

cannot be assessed by immunoblotting on cell lysates. I analysed the ER translocation of ppCPY in *Δsbh1 Δsbh2* by pulse-labelling with [^{35}S]-Met/Cys. For this, I grew wildtype *SBH1 SBH2* and *Δsbh1 Δsbh2* at 24 ˚C and shifted to 38 ˚C for 3 hours, and the control strain *sec61-32* at 30 ˚C and shifted to 20 ˚C for 3 hours. I pulsed the cells for 5 mins and immunoprecipitated CPY from the cell lysates with polyclonal anti-CPY antibodies. I then resolved the immunoprecipitated proteins by SDS-PAGE and visualized them by phosphorimaging. The results, shown in Figure 3.1(D), show a band corresponding to p1CPY in both the wildtype and *Δsbh1 Δsbh2* whereas p1CPY was completely absent in the *sec61-32* control. This means that the translocation of ppCPY was not compromised in the absence of Sbh1.

Collectively, my precursor accumulation experiments suggest that the *Δsbh1 Δsbh2* strain does not show apparent general co-translational or post-translational translocation defects. The translocation defect in the import of pKar2 seems to be specific to the protein.

Kar2 plays an essential role in protein quality control by activating the UPR when the ER is under stress caused by an accumulation of unfolded proteins [124,258]. As the translocation of Kar2 precursor is specifically affected in the *Δsbh1 Δsbh2* strain, I investigated whether the strain also shows defects related to UPR induction. I first tested for tunicamycin hypersensitivity by performing a growth assay on YPD plates containing 0.5 µg/ml tunicamycin. Tunicamycin activates the UPR by inducing ER stress through the inhibition *N*-linked glycosylation [259]. Treatment with sublethal doses of tunicamycin leads to the accumulation of misfolded proteins in the ER because *N*-glycosylation contributes to protein folding and quality control in the ER. Cells with a proteostasis defect in the ER are

hypersensitive to tunicamycin. I performed a growth assay of wildtype *SBH1 SBH2* and *Δsbh1 Δsbh2* cells spotted on YPD plates with and without tunicamycin such that each spot contained 10^4-10 cells and documented the growth after 3 days. I used a *Δire1* strain as a control, which has a documented tunicamycin sensitivity [260]. As shown in Figure 3.2(A), the growth of *Δsbh1 Δsbh2* yeast was comparable to that of wildtype on YPD + tunicamycin medium, suggesting there is no ER proteostasis defect in *Δsbh1 Δsbh2* yeast. This independently confirmed results concurrently reported by our lab [253].

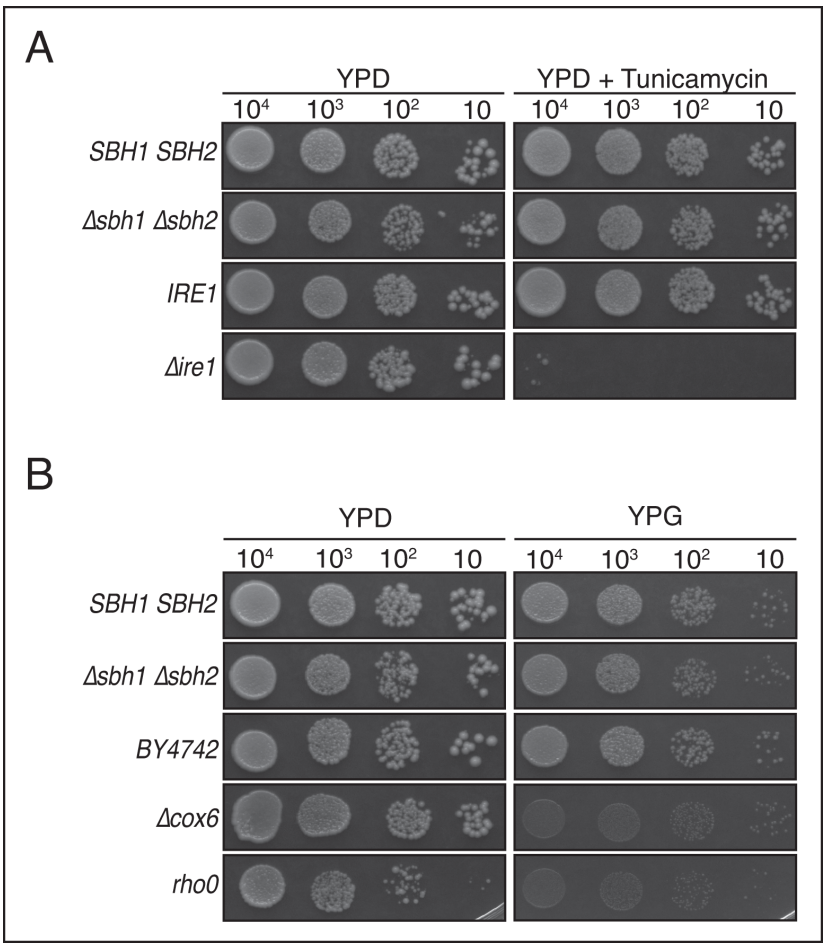

Figure 3.2 Sbh1 is not required for ER proteostasis. Yeast wildtype *SBH1 SBH2* and mutant *Δsbh1 Δsbh2* strains grown to early exponential phase were harvested, washed and diluted to 1 OD_{600}. Serial dilutions of each strain corresponding to 10^4-10 cells were grown on indicated solid media for 3 days. **A)** For Tunicamycin sensitivity, the strains were grown on YPD supplemented with 0.5 µg/mL Tunicamycin. The *Δire1* strain was used as control, and its strain background *BY4742* is indicated. Growth of *SBH1 SBH2* and *Δsbh1 Δsbh2* was unaffected in YPD+Tunicamycin plates. **B)** To test respiratory competence, the strains were grown on YP plates containing 3% Glycerol (YPG). Both *Δcox6* and *rho0* strains were used as controls, and their strain background *BY4742* is indicated. The *Δsbh1 Δsbh2* strain showed growth similar to its wildtypes *SBH1 SBH2* and *BY4742* on YPG plates.

Cheng et al. found that mutations in the Sec61 cytosolic loops caused kinetically delayed post-translational import and improper ribosome binding, resulting in co-translational translocation defects that directly correlate with the mutants losing their respiratory competence [57]. As the *Δsbh1 Δsbh2* strain showed a specific defect in importing Kar2 precursor which utilises both co-translational and post-translational translocation pathways, I wanted to test whether the strain was respiration competent. I grew the *Δsbh1 Δsbh2* strain and its isogenic wildtype on non-fermentable YPG plates (1 % Yeast Extract / 2 % Peptone / 3% Glycerol) containing glycerol as the sole carbon source. I used *Δcox6* and *rho0* strains as controls, both of which show respiration defects (Figure 3.2(B)) [261]. Respiration-competent cells can grow on non-fermentable carbon sources. The *Δsbh1 Δsbh2* cells were able to grow on the YPG medium, akin to its wildtype seen in Figure 3.2(B), suggesting that their ability for respiration was intact.

3.2. Role of Sbh1 in Complex Stability

Our lab has shown that the temperature-sensitivity of the *Δsbh1 Δsbh2* strain can be complemented with a truncated Sbh1 containing only the last 5 cytosolic amino acids and its TM domain [222]. Wu *et al.* recently solved the cryo-electron microscopy (cryo-EM) structure of the post-translational translocation complex from yeast, the Sec complex [63]. They have shown that in the Sec complex TM domain 3 (TM3) of Sec63 interacts with the TM domain of Sbh1, as well as TM1 of Sec61 [63]. The TM of Sbh1 also interacts with TM1 and TM4 of Sec61 [63,221]. Due to the central position of Sbh1 in the Sec complex and its highly conserved TM domain, I asked whether these interactions of Sec63 and Sec61 with the TM of Sbh1 stabilise the Sec complex, especially at higher temperatures. I examined the stability of the Sec complex in the absence of Sbh1 at higher temperatures and high salinity by precipitating the complex with Concanavalin A (ConA) – Sepharose. ConA is a lectin that binds to internal mannose residues in *N*- and *O*- linked glycans [262]. The only suitable glycan in the Sec complex is present on Sec71, a subunit of the Sec63 complex, and Sec61 complex subunits are not glycosylated. When the Sec complex is stable in a sample, both Sec63 and Sec61 are present in the ConA-bound fraction. If the Sec complex dissociates, Sec63 is still associated with Sec71 and is found in the ConA-bound fraction, while Sec61 complex subunits are found in the free fraction, not bound to ConA [248].

3.2.1. Selecting a Detergent for Sec Complex Isolation

I adapted the method for ConA precipitation from *Falcone et al*. (2011). Here, the starting material for the ConA precipitation of the Sec complex is yeast microsomes. If TritonX-100 (TX-100) is used to solubilise the microsomes, it dissociates the Sec61 complex from the Sec62-Sec63-Sec71-Sec72 complex. I use this as a control. In contrast, digitonin solubilisation

of microsomes leaves the Sec complex intact [248]. Since digitonin is a natural product extracted from *Digitalis purpurea,* its efficiency varies between manufacturing batches [263]. To try and avoid common problems caused variations between digitonin batches, I initially investigated alternative detergents for Sec complex solubilisation to optimise the method.

My first choice as an alternative detergent was 4-trans-(4-trans-Propylcyclohexyl)-cyclohexyl α-maltoside (PCC-α-M), a novel derivative of dodecyl-β-D-maltoside (DDM) [264]. In recent years, PCC-α-M has been increasingly adapted as the detergent of choice for stabilising membrane proteins during cryo-EM and functional studies [265]. I first compared its solubilisation efficiency with respect to the Sec complex to Digitonin. I solubilised 0.3 OD_{280} of microsomes derived from *SBH1 SBH2* grown at 24 ˚C in 3% PCC-α-M, or 3% digitonin, or 1% TX-100. I included a mock extraction with no detergent as negative control. After centrifugation at 16,000 x g, I precipitated proteins in the supernatant fraction with TCA. I analysed both the pellet and the supernatant fractions by SDS-PAGE and immunoblotted against Sec63 and Sec61 with polyclonal antibodies. Both Sec63 and Sec61 were mainly found in the solubilised fraction of PCC-α-M, with minimal amounts left in the pellet fraction. As shown in Figure 3.3(A), PCC-α-M was more efficient in solubilising Sec61 when compared to digitonin.

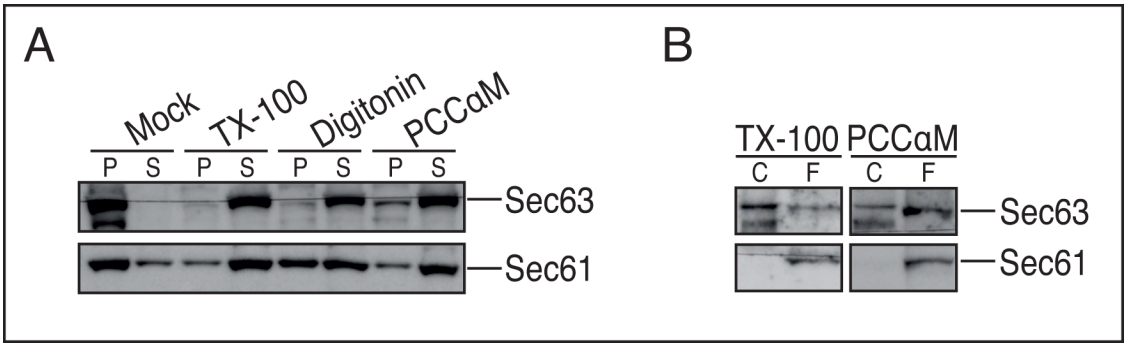

Figure 3.3 Solubilisation Efficiency and Sec complex Stability in PCC-α-M. A) A 0.3 OD_{280} of microsomes derived from *SBH1 SBH2* grown at 24 ˚C were solubilised each in Equilibration Buffer containing 1% TX-100, 3% digitonin and 3% PCC-α-M. A mock extraction without detergent was also included. Solubilised proteins were precipitated and analysed by SDS-PAGE and immunoblotting with anti-Sec63 and anti-Sec61 antibodies. Pellet containing insolubilised microsomes (P) and solubilised proteins (S) are marked. PCC-α-M could solubilise Sec63 with a small amount remaining in the P fraction, and solubilise Sec61 with greater efficiency than digitonin, smaller amount of Sec61 was left insolubilised in the P fraction as compared to that of digitonin. **B)** Microsomes from *SBH1 SBH2* strain similarly solubilised in 3% PCC-α-M, or 1% TX-100 were precipitated with equilibrated ConA-Sepharose. The free fraction was aspirated, and proteins were precipitated. The samples were resolved by SDS-PAGE and immunoblotted against Sec63 and Sec61. ConA bound fraction (C), and free, unbound fraction (F) are marked. Sec61 was found in the F fraction when solubilised in PCC-α-M, similar to TX-100.

I then used 3 % PCC-α-M in a ConA precipitation experiment with *SBH1 SBH2* microsomes from cells grown at 24 ˚C to ascertain whether the Sec complex remained stable when solubilised in PCC-α-M. I solubilised the microsomes as previously described in 3 % PCC-α-M or 1 % TX-100 and precipitated Sec complex from the samples with ConA equilibrated in buffer containing 1 % of the respective detergent. I also precipitated proteins not bound to ConA with TCA. I analysed the fractions by SDS-PAGE and immunoblotted against Sec63 and Sec61. While Sec63 was found bound to ConA, Sec61 and a significant amount of Sec63 were found in the free fraction in the sample solubilised in PCC-α-M, shown in Figure 3.3(B). I repeated the experiment two more times and found each time that the complex was unstable in PCC-α-M, thus this detergent was unsuitable for my study.

I also explored the suitability of Deoxy-BigCHAP (DBC), a non-ionic detergent that was previously used to solubilise the Sec61 complex from yeast microsomes [59]. I tested the efficiency of 3% DBC in solubilising 0.3 OD_{280} of microsomes derived from the *SBH1 SBH2* strain grown at 24 ˚C as compared to 3% digitonin using the same method as mentioned above for PCC-α-M. I found that DBC was able to solubilise the membranes but was not as efficient as digitonin under the conditions I used, shown in Figure 3.4(A). I investigated whether the Sec complex was stable when solubilised in 3% DBC by ConA precipitation as described above. The resulting immunoblot, shown in Figure 3.4(B), showed bands corresponding to both Sec63 and Sec61 in the ConA bound fraction, meaning that the Sec complex was stable. However, the intensities of the Sec61 and Sec63 bands was noticeably lower than what would be expected in the ConA-bound fraction in DBC and were considerably less than those visualized in the sample solubilised in 1% TX-100. Subsequent repeat of the experiment showed similar results. As this discrepancy could be a result of suboptimal solubilisation of the microsomes in DBC, I decided to not use DBC in my further experiments.

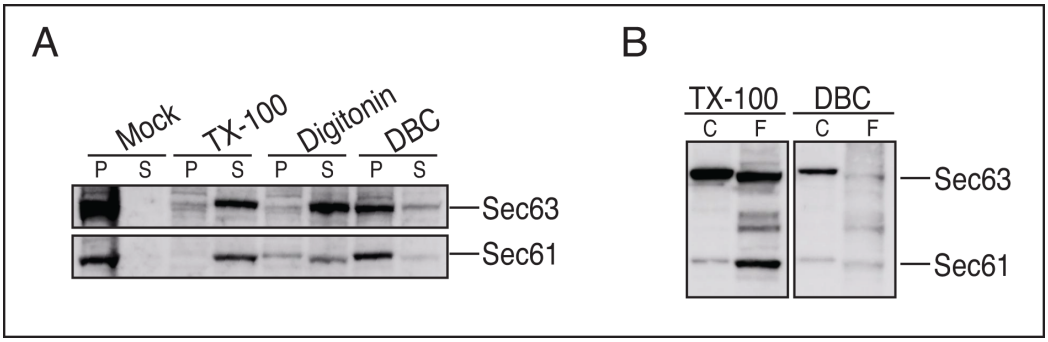

Figure 3.4 Solubilisation Efficiency and Sec complex Stability in DBC. A) A 0.3 OD_{280} of microsomes from *SBH1 SBH2* strain grown at 24 ˚C were solubilised each in Equilibration Buffer containing 3% DBC, 3% digitonin, or 1% TX-100. A mock extraction without detergent was also included. Solubilised proteins were precipitated and analysed by SDS-PAGE and immunoblotting. Pellet containing unsolubilised microsomes (P) and solubilised proteins (S) are marked. Higher amounts of Sec63 and Sec61 were present in the P fraction of DBC than in the S fraction. **B)** Microsomes similarly solubilised in 3% DBC or 1% TX-100 were precipitated with equilibrated ConA-Sepharose. Free fraction was aspirated, and proteins were precipitated. The samples were resolved by SDS-PAGE and immunoblotted against Sec63 and Sec61. ConA bound fraction (C), and free, unbound fraction (F) are marked. Both Sec63 and Sec61 were present in the C fraction of DBC.

Since my alternative detergent options proved to be unsuitable, I reverted to using digitonin to solubilise microsomal membranes. I tested the new batch of digitonin, acquired from Matrix Bioscience, to confirm that it can maintain the stability of the Sec complex in *SBH1 SBH2* microsomes (Supplementary Figure 2).

3.2.2. Determining the Influence of Sbh1 on the stability of the Sec Complex

To determine whether Sbh1 contributes to the interaction between the Sec61 complex and the Sec63 complex to form the Sec complex, I tested the stability of the Sec complex by precipitating it with ConA-Sepharose. I compared the Sec complex stability from microsomes derived from *Δsbh1 Δsbh2* cells grown at 24 ˚C and 38 ˚C with Sec complex stability from microsomes derived from *SBH1 SBH2* cells grown at 24 ˚C and 38 ˚C, which are permissive and restrictive temperatures for growth, respectively. I solubilised each batch of microsomes in Extraction Buffer containing 3% digitonin or 1% TX-100. A stable Sec complex would result in Sec63 complex and Sec61 complex subunits detected in the ConA-bound fraction when solubilised in digitonin. After precipitating the samples with ConA-Sepharose, I aspirated the unbound fraction, and TCA precipitated its constituent proteins. I resolved the samples by SDS-PAGE and transferred the proteins to nitrocellulose. I probed the membranes using primary antibodies against Sec63, Sec61, and the Sec61 complex subunit Sss1. The resulting immunoblots are shown in Figure 3.5.

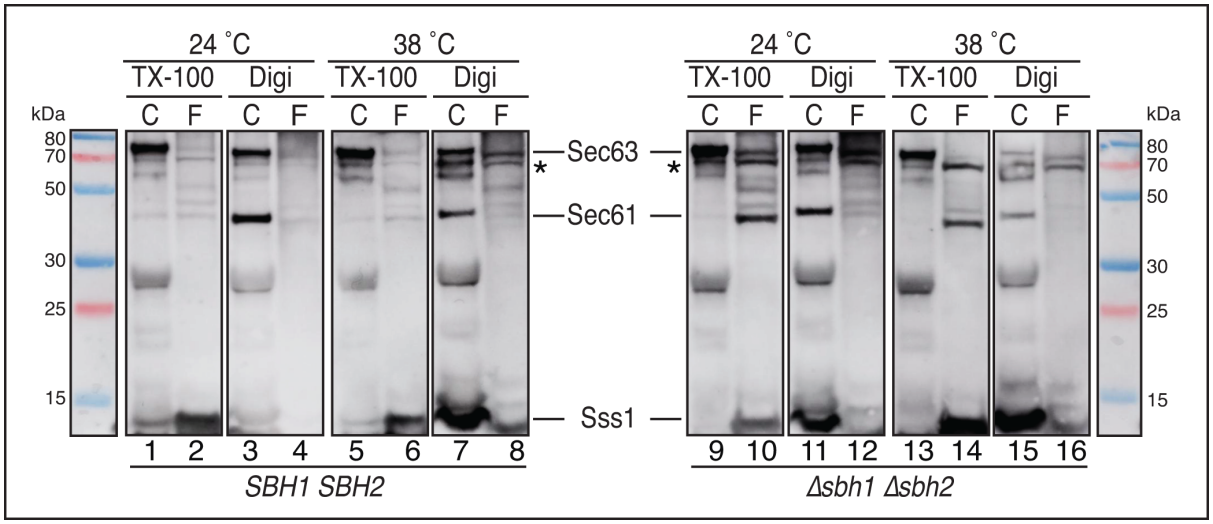

Figure 3.5 Sec complex stability in *Δsbh1 Δsbh2*. Microsomes, 0.3 OD_{280} each, obtained from *SBH1 SBH2* (left) and *Δsbh1 Δsbh2* (right) strains grown at 24 ˚C and 38 ˚C were solubilised in 3% digitonin and 1% TX-100, as control. The solubilised membranes were precipitated with ConA-Sepharose. The free, unbound proteins were precipitated from the aspirated supernatant by TCA precipitation. The proteins in the ConA-bound fraction (C) and free fraction (F) were resolved by SDS-PAGE and immunoblotting. The membranes were probed with primary antibodies against Sec63, Sec61 and Sss1. In *Δsbh1 Δsbh2* strain microsomes from 38 ˚C, Sec63, Sec61 and Sss1 were present in the C fraction when solubilised in digitonin (lane 15). The * marks a 70 kDa band reacting with Sec63 antibody.

In the samples from the wildtype *SBH1 SBH2* membranes Sec63, Sec61 and Sss1 were all present in the ConA-bound fraction in digitonin solubilised samples both at 24 ˚C and 38 ˚C (Figure 3.5, lanes 3 and 7). The presence of ConA also seems to affect the run of lower molecular weight proteins, causing a curve in Sss1 band. In the samples from the *Δsbh1 Δsbh2* mutant grown at 24 ˚C, Sec63, Sec61, and Sss1 were seen in the ConA-bound fraction in the digitonin-solubilised sample (Figure 3.5, lane 11). I saw a similar result for the *Δsbh1 Δsbh2* mutant membranes when the cells had been grown at 38 ˚C (Figure 3.5, lane 15), indicating that the Sec complex remains stable in the *Δsbh1 Δsbh2* mutant at both permissive and restrictive temperature. The experiment was repeated twice, and the same results were obtained each time. My data suggests that Sbh1 is not essential for the stability of the Sec complex.

Molecular dynamics (MD) simulations based on the cryo-EM structure of the Sec complex which gave insight into the interaction sites between Sec63 and Sec61. They observed four interaction sites between Sec63 and Sec61 in the simulations, of which two interaction sites in the ER membrane were located close to their interaction sites with the Sbh1 TM domain [266]. If Sbh1 indeed contributes to the Sec complex stability as I hypothesised, its absence alone would not destabilise the Sec complex as the other two interactions would suffice to maintain stability. The results of a ConA precipitation experiment in such a scenario would match what I saw in Figure 3.5. Taking into consideration these new insights, I wanted to re-examine Sec complex stability in the absence of Sbh1 and determine if Sbh1 stabilises the interactions between Sec63 and Sec61 TM domains in the presence of high salt, which would disrupt the interaction at the Sbh1-independent contact sites. Since the cytosolic interaction was likely electrostatic and the ER luminal interaction was polar, these interactions can be destabilised by increasing the salt concentration [266].

I first optimised the salt concentrations in a pilot experiment (Supplementary Figure 3). I used 0.3 OD_{280} of microsomes from *Δsbh1 Δsbh2* and *SBH1 SBH2* strains both grown at 24 ˚C and 38 ˚C. I solubilised the microsomes in Extraction buffer containing 3% digitonin and 400 mM Potassium acetate (KOAc), in duplicates. Before precipitation with ConA-Sepharose, I added Extraction Buffer containing 1 M KOAc and no detergent to the samples to raise the salt concentration to 800 mM and dilute the digitonin concentration to 1%. After precipitation, I aspirated the free fraction and TCA-precipitated the unbound proteins. I analysed the samples by Western Blot and probed for Sec63 complex subunits Sec62 and Sec63, and Sec61 complex subunits Sec61 and Sss1 with polyclonal antibodies as before. Precipitations from solubilised *SBH1 SBH2* microsomes were used as control for the stability

of the Sec complex under high salt conditions. In the resulting immunoblot shown in Figure 3.6, Sec63, Sec62, Sec61, and Sss1 were all found bound to ConA in *Δsbh1 Δsbh2* microsomes from cells grown at 24 ˚C and 38 ˚C (Figure 3.6, lanes 9 and 10, and 13 and 14). Equivalent results were seen in immunoblots with *SBH1 SBH2* microsomes from cells grown at 24 ˚C and 38 ˚C (Figure 3.6, lanes 1 and 2, and 5 and 6). My experiments confirm that the Sec complex remains stable in the absence of Sbh1, at restrictive temperature and under elevated salt concentrations.

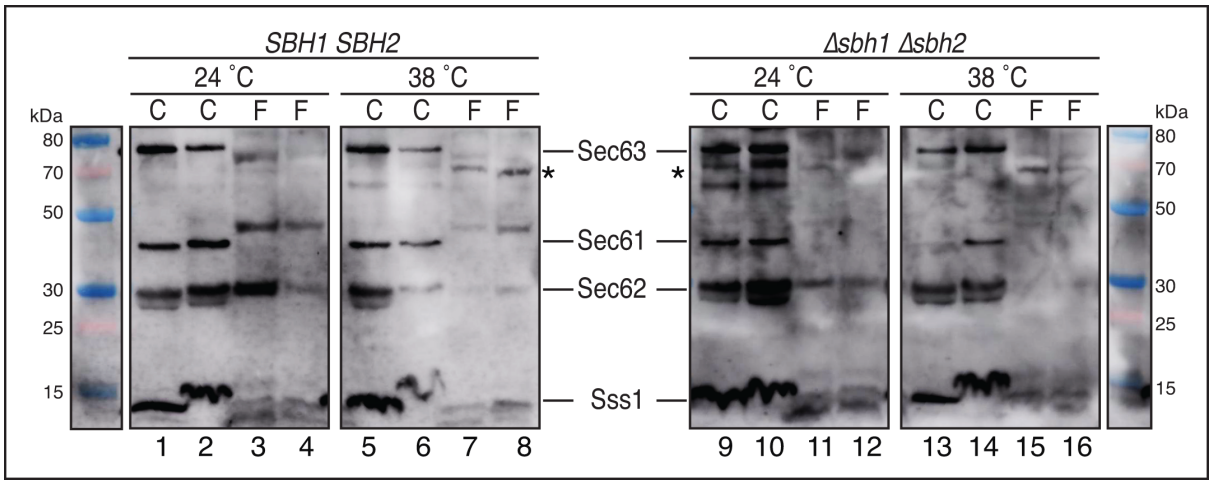

Figure 3.6 Sec complex stability in Δsbh1 Δsbh2 in elevated salt concentration. Microsomes from *SBH1 SBH2* and *Δsbh1 Δsbh2* strains grown at 24 ˚C and 38 ˚C, 0.3 OD_{280} each, were solubilised in 3% digitonin and then diluted to 1% digitonin in duplicates while raising salt concentration to 800 mM KOAc using Extraction Buffer containing 1 mM KOAc and no detergent. Samples were then precipitated with ConA-Sepharose, free fraction was aspirated, and unbound proteins were precipitated using TCA precipitation method. The samples were analysed by Western Blotting and probed for Sec63, Sec62, Sec61 and Sss1. The *SBH1 SBH2* strain acts as control. Sec63, Sec62, Sec61 and Sss1 were all present in the C fractions of *Δsbh1 Δsbh2*, at both temperatures (lanes 9 and 10, and 13 and 14). The * marks a 70 kDa band cross-reacting with Sec63 antibody.

In the ConA-precipitation experiments, I noticed a 70 kDa protein band close to Sec63 in its molecular weight appearing in the free, unbound fraction. This band is marked with an * in Figures 3.5 and 3.6, was developed when probed with the Sec63 antibody. To clarify whether the 70 kDa band is a protein cross-reacting with the Sec63 antibody, I used 0.075 OD_{280} of microsomes from *SBH1 SBH2* and *Δsbh1 Δsbh2* cells grown at 24 ˚C and 38 ˚C and washed them with Equilibration Buffer, containing protease inhibitors. I used the *sec63-201*

mutant strain, which has a truncated form of Sec63 that lacks C-terminal 27 amino acid residues, as a control [267]. I grew *sec63-201* strain at permissive 30 ˚C and shifted to restrictive 37 ˚C for 3 hours and isolated microsomes. I subjected the samples to SDS-PAGE transferred the proteins to nitrocellulose and probed the membranes with polyclonal anti-Sec63 antibodies. As shown in Figure 3.7(A) none of the strains showed the cross-reactive 70 kDa band. This suggested that the 70 kDa protein was not present in the initial microsomal samples.

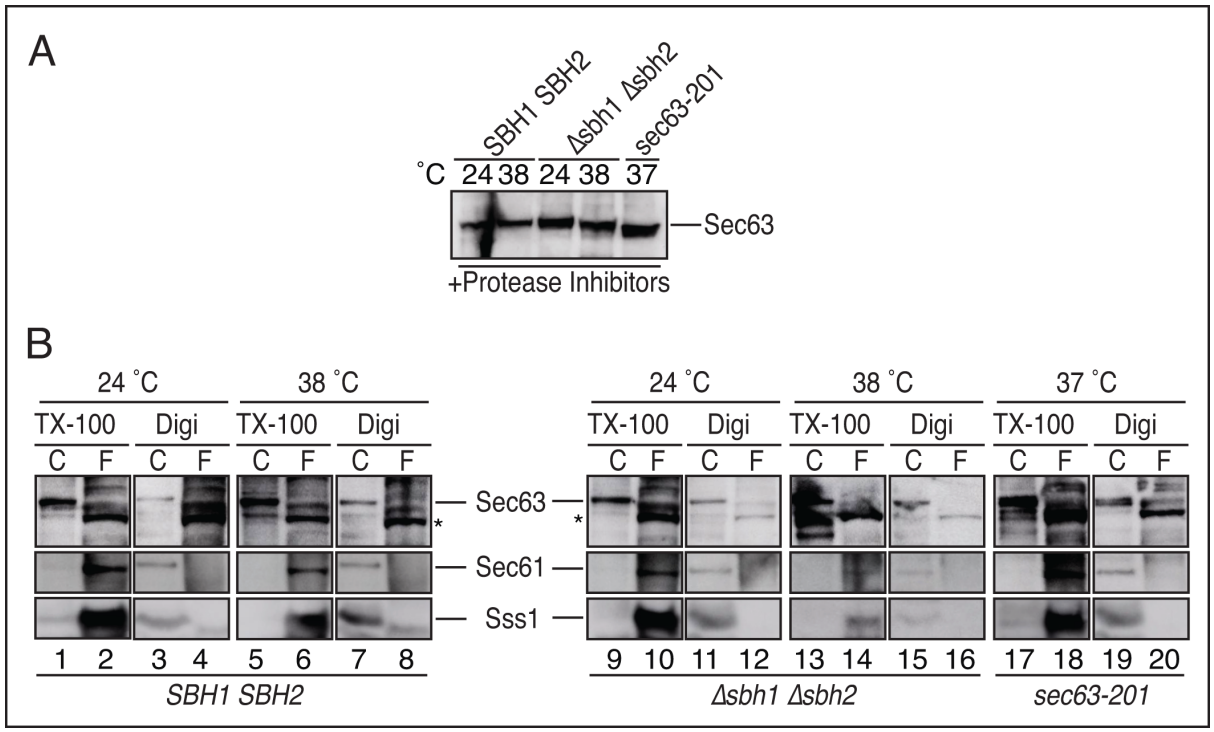

Figure 3.7 Identifying a Cross-reacting Band. A) Microsomes, 0.075 OD_{280} each, from *SBH1 SBH2* and *Δsbh1 Δsbh2* strains grown at 24 ˚C and 38 ˚C and *sec63-201* strain grown at 37 ˚C were washed with Equilibration Buffer containing protease inhibitors. They were then analysed by Western Blot and probed for Sec63. **B)** A 0.3 OD_{280} each of microsomes from *SBH1 SBH2* and *Δsbh1 Δsbh2* strains grown at 24 ˚C and 38 ˚C and *sec63-201* strain grown at 37 ˚C were solubilised in 3 % digitonin or 1 % TX-100 and precipitated with ConA-Sepharose. The unbound proteins in the free fractions were precipitated by TCA precipitation. The samples were analysed by Western Blot and probed for Sec63, and later for Sec61 and Sss1 after stripping. The * marks the reappearing cross-reacting protein band seen in the F fractions (even numbered lanes).

To determine whether the 70 kDa protein band is developed during a ConA precipitation experiment, I performed another ConA precipitation experiment with solubilised *SBH1 SBH2* and *Δsbh1 Δsbh2* microsomes from cells grown at 24 ˚C and 38 ˚C, and sec63-201 microsomes,

grown at 37 ˚C. I first probed the immunoblots for Sec63. In the results, shown in Figure 3.7(B), the 70 kDa band appears again in the free fractions of not only *SBH1 SBH2* and *Δsbh1 Δsbh2* lysates, but also in the free fractions corresponding to *sec63-201* lysate. To confirm that the Sec complex was stable in this experiment, I again probed the blots for Sec61 and Sss1. I found that the Sec complex remained stable in all the microsomes solubilised in digitonin (Figure 3.7 (B). Altogether, my results suggest that the protein band 70 kDa is likely a degradation product of Sec63 formed in the course of the ConA precipitation experiment.

Taken together, my results suggest that Sbh1 does not stabilise the TM domain interactions between Sec63 and Sec61 and does not contribute to the overall stability of the Sec complex.

3.2.3. Investigating the Contribution of Sbh1 to the Co-translational Translocation Complex Stability

During co-translational translocation, the cytosolic domain of mammalian Sec61β directly interacts with the RNC bound to the Sec61 channel, as well as with the incoming SPs within the Sec61 channel vestibule [224,225,227]. My next step was to investigate if Sbh1, through a similar interaction, contributes to the stability of the Sec61-ribosome co-translational translocation complex. I wanted to investigate the complex stability by ribosome-associated membrane protein (RAMP) fractionation (detailed in Section 2.2.8). In this method, microsomes are first solubilised in an extraction buffer containing 3 % digitonin and ultracentrifuged to pellet ribosomes and RAMPs. The supernatant is subjected to ConA precipitation (Section 2.2.7). The pellet is resuspended in RAMP buffer containing puromycin

to dissociate bound proteins from ribosomes and subjected to another round of ultracentrifugation to pellet ribosomes. The freed proteins are precipitated by TCA method (Section 2.2.4.2) and all the samples are analysed by SDS-PAGE (Section 2.2.4.3) and immunoblotting (Section 2.2.4.4). If the Sec61-ribosome complex is stable, Sec61 channel components should be present in the RAMP fraction as well as in the ConA-bound fraction as a part of the Sec complex.

I first wanted to optimise the method for RAMP fractionation using microsomes derived from wildtype *SBH1 SBH2* strain grown at 24 ˚C, as in Section 2.2.8. I solubilised the microsomes in 3 % digitonin or 1 % TX-100 as control. After ultracentrifugation to sediment ribosomes, I precipitated the non-RAMPs in the ultracentrifugation supernatant with ConA-Sepharose to obtain the ConA-bound (C) fraction and the unbound free (F) fraction. I resuspended the pellet containing ribosomes and RAMPs in RAMP buffer containing 1 mM puromycin. Puromycin causes premature termination of translation and dissociation of the RNC from the Sec61 translocon. Then I subjected the ribosome/RAMP fraction to a second ultracentrifugation to sediment the dissociated ribosomes from RAMPs. I precipitated the proteins in the supernatant by TCA precipitation to obtain the RAMP (R) fraction and directly resuspended the ribosome containing final pellet (P) in SDS-PAGE sample buffer. I resolved the proteins by SDS-PAGE and analysed them by immunoblotting against Sec63, Sec62, Sec61 and Sss1.

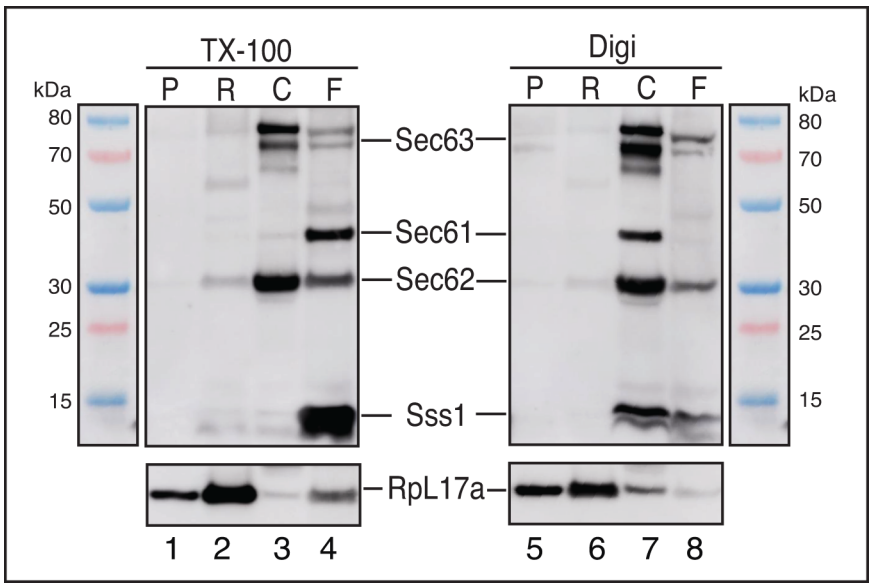

Figure 3.8 Ultracentrifugation was insufficient to fully fractionate ribosomes. A 0.84 OD_{280} of microsomes derived from *SBH1 SBH2* strain grown at 24 ˚C were solubilised in 3% digitonin (right) or 1 % TX-100 (left) and subjected to ultracentrifugation to sediment ribosomes and RAMPs. The supernatant was used for ConA precipitation to obtain ConA-bound (C) and free, unbound (F) fractions. The pellet was resuspended in RAMP buffer containing puromycin to dissociate RAMPs from ribosomes and ribosomes were sedimented by a second ultracentrifugation step to obtain the ribosomal pellet (P) fraction and the RAMP (R) fraction. The samples were analysed by Western blotting and probed for Sec63, Sec62, Sec61 and Sss1. Sec63 and Sec62 were detected in C fractions (Lanes 3 and 7) and partially in the F fractions (Lanes 4 and 8). Sec61 and Sss1 were only found in the F fraction of TX-100 solubilised microsomes (Lane 4) and C fraction of digitonin solubilised microsomes (Lane 7). The immunoblot was reprobed for the ribosomal protein RpL17a, which was detected in all fractions.

In the resulting immunoblot, shown in Figure 3.8, I detected Sec61 and Sss1 in the F fraction of microsomes solubilised in TX-100 (Lane 4) and the C fraction of digitonin solubilised sample (Lane 7) as is expected. I did not detect Sec61 and Sss1 in the final P fraction (Lanes 1 and 5), implying that the RAMPs fully dissociated from the ribosomes. However, I did not detect Sec61 or Sss1 in the R fraction of either detergent solubilised sample (Lanes 2 and 6), which should be present in an optimal method. To detect whether the ribosomes were properly sedimented, I decorated the immunoblot with antibodies against the ribosomal protein RpL17a. I detected RpL17a in every fraction of both the samples (Figure 3.8, lower blot), suggesting that ribosomes were only partially sedimented by the ultracentrifugation steps, with significant amounts of ribosomes/RAMPs still present in the supernatants aspirated and used for further fractionation. Presence of RpL17a in the R fractions (Lanes 2

and 7) suggests that protein content present after TCA precipitation, and that Sec61 and Sss1 were likely present at too low of a concentration to be detected by immunoblotting.

In the next experiment, I increased the starting concentration of *SBH1 SBH2* microsomes (derived from cells grown at 24 ˚C) by 2.5 times, to 2.1 OD_{280} to improve the concentration of proteins across all fractions. I increased speed and time of the first ultracentrifugation step to 90,000 rpm for 1 h at 4 ˚C and the second ultracentrifugation to 100,000 rpm for 2 h at 4 ˚C (TLA-120.1 Rotor, Optima^{TM} MAX-XP Ultracentrifuge, Beckman Coulter) to match the conditions used by Kalies *et al.* in a similar study [224]. After the first ultracentrifugation, I resuspended the pellet in RAMP buffer not containing puromycin and added puromycin to a final concentration of 2 mM after the pellet was fully resuspended to avoid its degradation in the buffer. I followed all other steps for RAMP fractionation as described in Section 2.2.8. After SDS-PAGE, I transferred the entire gel with the stacking gel intact to detect any protein aggregates.

I first probed the blot with anti-Sec61 antibody and detected Sec61 only in F fraction of TX-100 solubilised sample and C fraction of digitonin solubilised sample (Figure 3.9, Lanes 4 and 7 respectively). I also detected a high molecular weight band in P and R fractions in the stacking gel with the Sec61 antibody, suggesting its dissociation from ribosomes and subsequent aggregation (Lanes 2, 5 and 6, marked with an arrow). I further probed the blot with antibodies against Sec63, Sec62 and Sss1. I detected Sec63 in the C fraction (Lanes 3 and 7), Sec62 in both C and F fractions (Lanes 3, 4, 7 and 8), and Sss1 only in the F fraction of TX-100 solubilised sample (Lane 4) and the C fraction of digitonin solubilised sample (Lane 7). I stripped the blot and probed with anti-RpL17a antibodies and detected RpL17a in both the P

and R fractions (Lanes 1, 2, 5 and 6). Together, my results suggest that the first ultracentrifugation step was sufficient to pellet ribosomes/RAMPs, while the second ultracentrifugation step could either not fully sediment the ribosomes or I was inadvertently aspirating the ultracentrifugation pellet while separating the supernatant. As Sec61 is known to aggregate when solubilised, prolonged incubation time in the RAMP buffer likely resulted in the Sec61 aggregates detected in the R fraction.

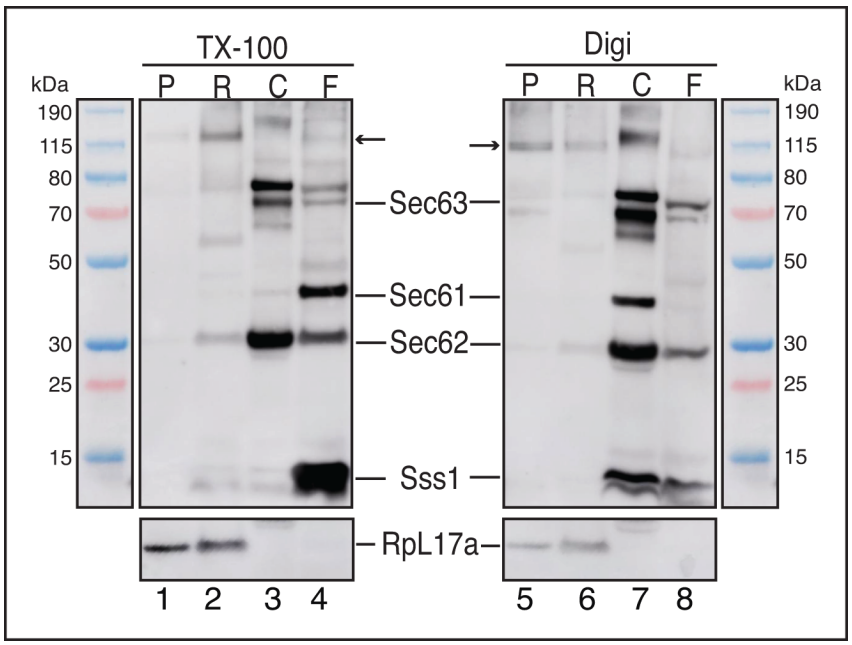

Figure 3.9 Changes in ultracentrifugation parameters were insufficient to sediment ribosomes. A 2.1 OD_{280} of microsomes derived from *SBH1 SBH2* strain grown at 24 ˚C were solubilised in 3% digitonin (right) or 1 % TX-100 (left) and subjected to ultracentrifugation at 90,000 rpm to sediment ribosomes and RAMPs. The supernatant was used for ConA precipitation to obtain ConA-bound (C) and free, unbound (F) fractions. The pellet was resuspended in RAMP buffer containing 2 mM puromycin to dissociate RAMPs from ribosomes and ribosomes were sedimented by a second ultracentrifugation at 100,000 rpm to obtain the ribosomal pellet (P) fraction and the RAMP (R) fraction. The samples were analysed by Western blotting and probed for Sec63, Sec62, Sec61 and Sss1. Sec63 and Sec62 were detected in C fractions (Lanes 3 and 7) and Sec62 was also detected partially in the F fractions (Lanes 4 and 8). Sec61 and Sss1 were only found in the F fraction of TX-100 solubilised microsomes (Lane 4) and C fraction of digitonin solubilised microsomes (Lane 7). Aggregated Sec61 was also detected in P fraction (Lane 5) and R fractions (Lanes 2 and 6). The immunoblot was reprobed for the ribosomal protein RpL17a, which was detected in P and R fractions (Lanes 1, 2, 5 and 6).

In the next optimisation experiment I solubilised 2.1 OD_{280} each of microsomes derived from *SBH1 SBH2* and *Δsbh1 Δsbh2* strains (grown at permissive temperature) in Extraction Buffer containing 3 % digitonin. Like in the previous experiment, I ultracentrifuged the solubilised microsomes first at 90,000 rpm for 1 h at 4 ˚C (TLA-120.1 Rotor, Optima™ MAX-XP Ultracentrifuge, Beckman Coulter) to sediment ribosomes/RAMPs with a 100 µL sucrose cushion (200 mM sucrose in Extraction Buffer) to separate the pellet from the supernatant. After resuspending and incubating the first pellet with RAMP buffer containing 2 mM puromycin, I separated the ribosomes from the dissociated RAMPs by ultracentrifugation at 100,000 rpm for 2 h at 4 ˚C including a 100 µL sucrose cushion (200 mM sucrose in RAMP buffer).

I resolved the proteins by SDS-PAGE in one set of the duplicates using pre-cast Bolt™ Bis-Tris Plus Mini Protein gels, 4-12% gradient (Invitrogen™, ThermoFisher Scientific) and analysed by Western blotting probed for Sec63, Sec61 and Sss1. For better resolution of lower molecular weight proteins, the other set of samples were resolved by SDS-PAGE using 15 % acrylamide-bisacrylamide gel (Section 2.2.4.5) using electrophoresis as described in Section 2.2.4.3, following Western blotting were probed for Sbh1 and RpL17a. I probed for Sbh1 to detect the location of all Sec61 complex subunits in the various fractions. I detected Sec63, Sec61 and Sss1 in the ConA-bound fraction of both strains (Figure 3.10, Lanes 3 and 7), as well as partially in the free fraction (Lanes 4 and 8). I detected Sbh1 only in the ConA-bound fraction of *SBH1 SBH2* (Lane 3). I detected RpL17a in P, C and F fractions of both strains (Lanes 1, 3, 4, 5, 7 and 8). I did not detect any of the proteins in the R fraction of either strain (Lanes 2 and 6). These results indicate that neither of the ultracentrifugation steps could sufficiently sediment ribosomes.

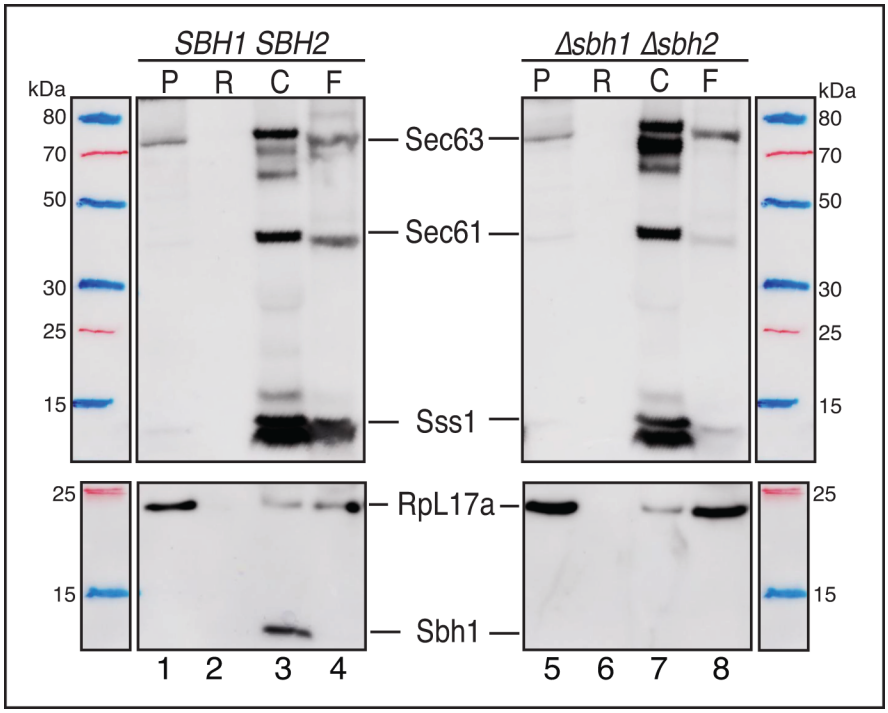

Figure 3.10 Inconsistent sedimentation of ribosomes points to a technical error. A 2.1 OD_{280} of microsomes derived from *SBH1 SBH2* and *Δsbh1 Δsbh2* strains grown at 24 ˚C were solubilised in 3% digitonin and subjected to ultracentrifugation with a sucrose cushion at 90,000 rpm to sediment ribosomes and RAMPs. The supernatant was used for ConA precipitation to obtain ConA-bound (C) and free, unbound (F) fractions. The pellet was resuspended in RAMP buffer containing 2 mM puromycin to dissociate RAMPs from ribosomes and ribosomes were sedimented by a second ultracentrifugation with a sucrose cushion at 100,000 rpm to obtain the ribosomal pellet (P) fraction and the RAMP (R) fraction. The samples were analysed by SDS-PAGE and Western blotting using a 4-12% Bis-Tris gel and a 15% arylamide-bisacryamide gel. The blot from the 4-12% gel was probed for Sec63, , Sec61 and Sss1 (top) and the blot from the 15% gel was probed for Sbh1 and RpL17a. Sec63, Sec61 and Sss1 were detected mainly in the C fractions (Lanes 3 and 7) and also detected partially in the F fractions (Lanes 4 and 8). Sbh1 was only detected in the C fraction of *SBH1 SBH2* (Lane 3). RpL17a was detected in P, C and F fractions (Lanes 1, 3, 4, 5 , 7 and 8).

Taken together, my inconsistent results point to a technical error with the ultracentrifuge used (Optima™ MAX-XP Ultracentrifuge, Beckman Coulter). Due to the unavailability of a suitable ultracentrifuge in Saarbrücken campus, I could not continue with this study.

3.2.4. Sec61-Sbh1 interaction with native Co-IP

The TM of Sbh1 interacts with TM1 and TM4 of Sec61 and TM3 of Sec63 within the Sec complex [63,221]. The deletion of *SBH1* and *SBH2* leads to temperature sensitivity at 38 ˚C [75,222]. As an alternative method to investigate the Sec complex at 38 ˚C, I wanted to study the interaction between Sec61 and Sec63 by native co-immunoprecipitation (Co-IP) in the presence and absence of Sbh1, i.e., in *SBH1 SBH2* and *Δsbh1 Δsbh2* strains grown at 38 ˚C. In this method, microsomes are solubilised in Extraction buffer containing 3 % digitonin and the samples are incubated with anti-Sec61 antibody and Protein A-Sepharose (ProtA), which binds to immunoglobulin, to co-precipitate Sec61. The Sepharose beads are then collected, and the co-precipitated proteins are analysed by Western blotting. Probing the blot with anti-Sec63 antibodies would detect the presence of Sec61-bound Sec63.

I performed an experiment to optimise the order and time of incubation of ProtA and the anti-Sec61 antibody with the solubilised microsomes. I solubilised microsomes derived from *SBH1 SBH2* cells grown at 24 ˚C in Extraction Buffer containing 3 % digitonin and incubated the samples with ProtA-Sepharose to pre-clear non-specific ProtA binding proteins. I prepared 4 sets of samples, each with different conditions in duplicate. Set I was pre-cleared sample precipitated by TCA method (Section 2.2.4.2) to detect the proteins present after the pre-clear step. Set II was incubated first with anti-Sec61 antibody for 1 h and then incubated with ProtA for 1 h. Set III was incubated with both Anti-Sec61 antibody and ProtA together for 2 h. Set IV was incubated only with ProtA. I collected the Sepharose beads after incubation and analysed the precipitated proteins by Western blotting, probing for Sec61. I probed one of the two blots also for Sss1 and the other blot for Sbh1. Due to Sec61 having the same molecular weight as a non-specific band, it could not be detected reliably. Sss1 was detected

in Sets I, II and III (Figure 3.11 (A), Lanes 1 - 6). Sbh1 was detected in Sets II and III (Figure 3.11 (B), Lanes 11 - 14). Molecular weight difference in Sbh1 and Sss1 in Sets II and III was likely caused by the uneven movement of the buffer front due to the presence of ProtA in the samples. My results imply that Sec61 does not non-specifically bind to ProtA and Sec61-associated proteins can be co-precipitated efficiently irrespective of the order of antibody and ProtA addition. Sharper proteins bands in Set III (Figure 3.11 (A) lanes 5 and 6, (B) lanes 13 and 14) suggest that it is preferable to incubate the sample with anti-Sec61 antibody and ProtA together for 2 h. Sec61 could not be detected in the blots due to the presence of antibody heavy chains which run at approximately similar molecular weights and are detected by the secondary antibody. Unfortunately, due to inherent time constraints and competing priorities, I could not continue with this project.

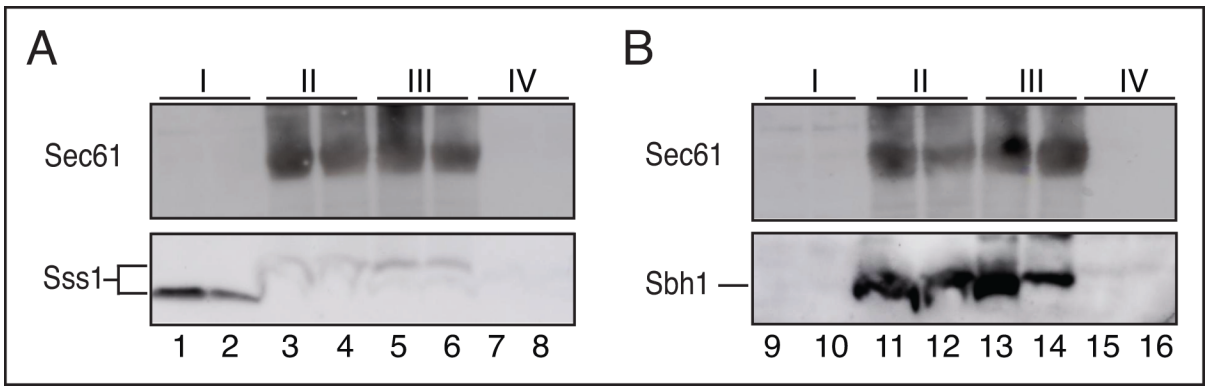

Figure 3.11 Optimising incubation conditions for Native Co-IP. A 0.3 OD_{280} of *SBH1 SBH2* microsomes derived from strains grown at 24 ˚C were solubilised in 3 % digitonin and pre-cleared with ProtA to remove non-specifically binding proteins. Proteins in Set I were TCA precipitated. Set II was incubated first with anti-Sec61 antibody, followed by ProtA. Set III was simultaneously incubated with anti-Sec61 antibody and ProtA. Set IV was only incubated with ProtA. The samples were analysed by Western blotting. **A)** Immunoblot probed for Sec61 and Sss1. Sss1 was detected in all samples, except Set IV. **B)** Immunoblot probed for Sec61 and Sbh1. Sbh1 was detected in Sets II and III. Sec61 could not be reliably detected due to the presence of cross-reactive bands at similar molecular weights.

3.3. Deciphering the role of Sbh1 CMP region

The amphipathic N-terminal helix of Sec61 is deeply embedded in the ER membrane [64]. The Sbh1 TM and Sec61 TM1 and TM4 interact, the presence of a positive patch of Lys residues in the Sbh1 IDR, and a negative patch of Asp and Glu residues on the Sec61 N-terminal helix, together with their proximity makes it likely for the Sec61 N-terminal helix and Sbh1 cytosolic IDR to interact. Pratiti Bhadra modelled MD simulations for such an interaction. She saw that a segment ^{19}EVIAPERK^{26} of Sec61 was always in close contact with ^{45}DEATG^{49} of Sbh1, shown in Figure 3.13 (A). An extended conformation also suggested an interaction with ^{45}DEATGLRV^{52} residues of Sbh1 [268]. The ^{45}DEATGLRV^{52} residues are a part of the conserved membrane proximal (CMP) region of Sbh1. The CMP region of Sbh1 is 16 residues long situated between its cytosolic IDR and TM domain, extending from I39 to P54 residues and is structured [218].

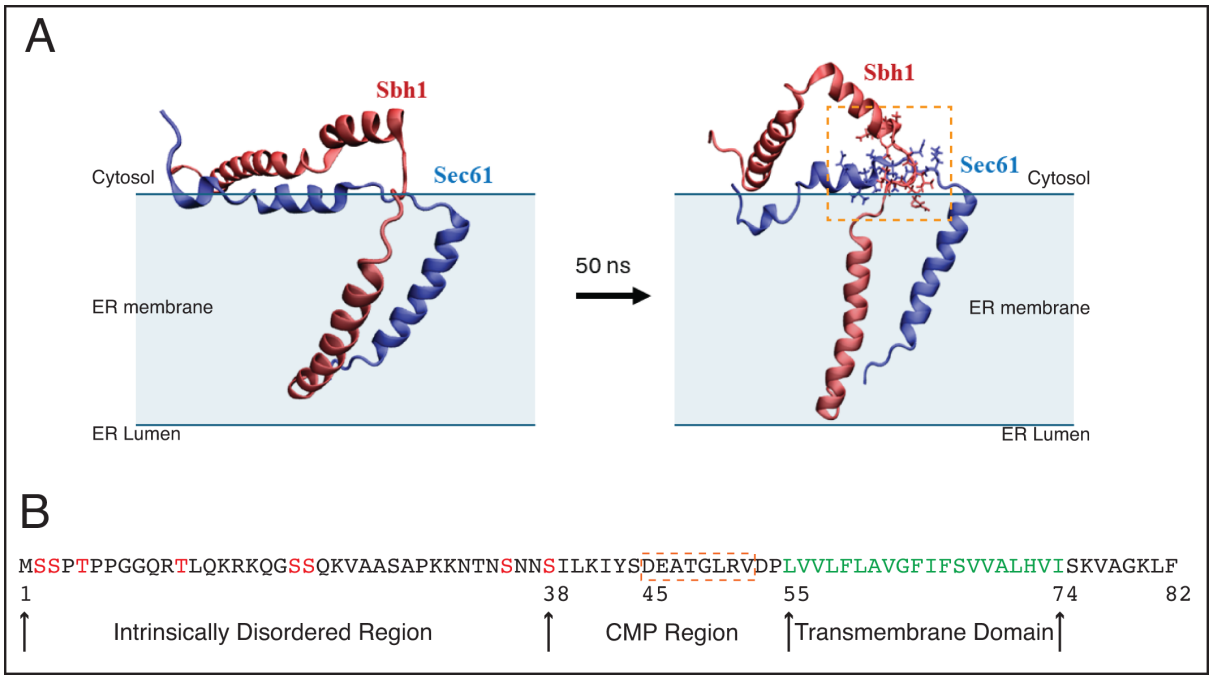

Figure 3.12 MD simulation of Sbh1 and Sec61 N-terminal region revealed putative contact sites. A) Final snapshot of 50 ns MD simulation between Sec61 N-terminus and Sbh1 showing close contact berween ^{19}EVIAPERK^{26} of Sec61 and ^{45}DEATG^{49} of Sbh1. The sidechains in contact are highlighted with an orange box. Modified figure from Yadhanapudi *et al.*, 2024. **B)** Amino acid sequence of Sbh1. Phosphorylation sites are in red and the TM residues are in green. Sec61 contact site is highlighted with an orange box.

Previously Feng *et al.* had reported that the growth defect of *Δsbh1 Δsbh2* strain at 38 ˚C is rescued when the cells are supplemented with the truncated TM domain of Sbh1 [222]. The truncated Sbh1 supplemented included 5 residues preceding the TM domain, namely, ^{50}LRVDP^{54} residues of the CMP region. Given the apparent relevance of this region as indicated by published data and MD simulations, I studied the Sbh1 CMP region. I generated mutations in this region and characterised the resulting mutant strains for translocation defects.

3.3.1. Generation of mutants in Sbh1 CMP region by site directed mutagenesis

The extended MD simulation revealed that the ^{45}DEATGLRV^{52} sequence in the Sbh1 CMP region interacted with Sec61. The P54 residue of Sbh1 is critical for the Sbh1 TM interaction with Sec61 TM1 and TM4 and is suggested to function as a hinge to direct the Sbh1 cytosolic domain away from the Sec61 lateral gate [64,221]. This led me to mutate D45-V52 and P54 residues in Sbh1 CMP region to Ala for my study. For logistical simplicity, I broke down the mutation sites into 3 stretches: D45-G49, L50-V52 and P54 and exchanged them to Ala by site directed mutagenesis (referred to as “CMP mutants”). I then mutated the CMP mutants to create combinations of the mutation sites: *sbh1D45-G49A/P54A, sbh1D45-V52A, sbh1L50-V52A/P54A* and *sbh1D45-V52A/P54A.* The mutation sites are indicated in Figure 3.13. Table 3.1 lists all the mutants generated, and their mutation sites.

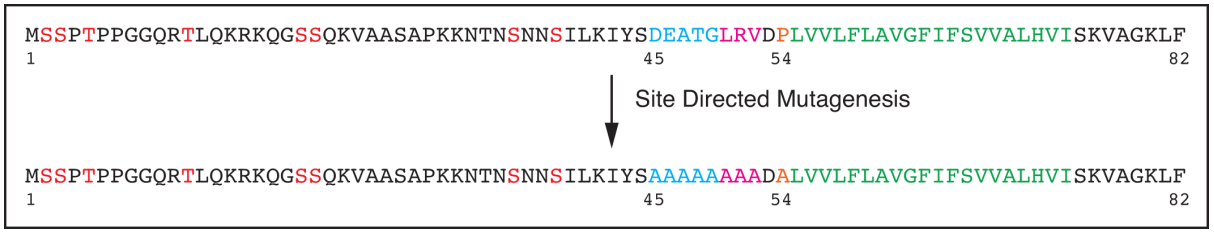

Figure 3.13 mutation sites in Sbh1 CMP region targeted by site directed mutagenesis. In the Sbh1 protein sequence, phosphorylation sites are highlighted in red and the TM domain is highlighted in green. Within its CMP region, D45-G49 mutation sites are highlighted in blue, L50-V52 mutation sites in magenta and the P54 mutation site in orange. These sites were mutated to Ala by site-directed mutagenesis.

Table 3.1 List of mutants and their mutations generated by site directed mutagenesis**.**

Strain	**Mutation**	
sbh1D45-G49A	D45-G49A	CMP mutants
sbh1L50-V52A	L50-V52A	
sbh1P54A	P54A	
sbh1D45-G49A/P54A	D45-G49A, P54A	Combo mutants
sbh1D45-V52A	D45-V52A	
sbh1L50-V52A/P54A	L50-V52A, P54A	
sbh1D45-V52A/P54A	D45-V52A, P54A	

I designed the forward primers for site directed mutagenesis by substituting specific codons in the *SBH1* coding sequence with Ala codon in 5' → 3' direction and included 12 bases upstream and downstream of the mutation site. I used the reverse complement of the forward primer as the reverse primer. Supplementary Figure 4 shows the primers aligned with mutation sites in *SBH1* coding sequence. All the designed primers are listed in Section 2.1.6.

I used *SBH1* coding sequence in a pRS415 plasmid (KRB689) to generate the mutations as described in Section 2.2.12. I inserted the mutated *sbh1* fragments into the yeast centromeric vector pRS415. The plasmid map for pRS415 is shown in Supplementary Figure 5, for KRB 689 in Supplementary Figure 6, CMP mutants in Supplementary Figure 7 and for combo mutants

in Supplementary Figure 8. Once the mutations were confirmed by DNA sequencing, I transformed the plasmids into the *Δsbh1 Δsbh2* strain (KRY 588) for my experiments. I also transformed the KRY 588 strain with an empty pRS415 plasmid (as Δ*sbh1 Δsbh2* strain) and with pRS415-*SBH1* plasmid from KRB 689 (as *SBH1* strain) to use as controls for further experiments.

3.3.2. Characterisation of CMP and combo mutants

I used the *Δsbh1 Δsbh2* strain transformed with pRS415 plasmid containing mutant *sbh1* to functionally characterise the Sbh1 CMP region. I subjected mutants to growth assays at different temperatures, quantified the levels of Sbh1 and the Sbh1 dependent substrate Gls1 produced by the mutants, and evaluated them for translocation defects.

I transformed the 3 CMP mutant plasmids into KRY 588 strain: *sbh1D45-G49A, sbh1L50-V52A* and *sbh1P54A*. When 5 randomly picked colonies showed similar growth behaviour in a preliminary test, I used one of the colonies for growth assay at 20˚, 30˚ and 38 ˚C as described in Section 2.2.3. I used KRY 588 strain transformed with *SBH1*-pRS415 as positive control (*SBH1*). I also used KRY 588 transformed with empty pRS415 (*Δsbh1 Δsbh2*) as control for severe temperature sensitivity at 38 ˚C and *sbh1S3A/T5A* mutant as a control for moderate temperature sensitivity at 38 ˚C [253].

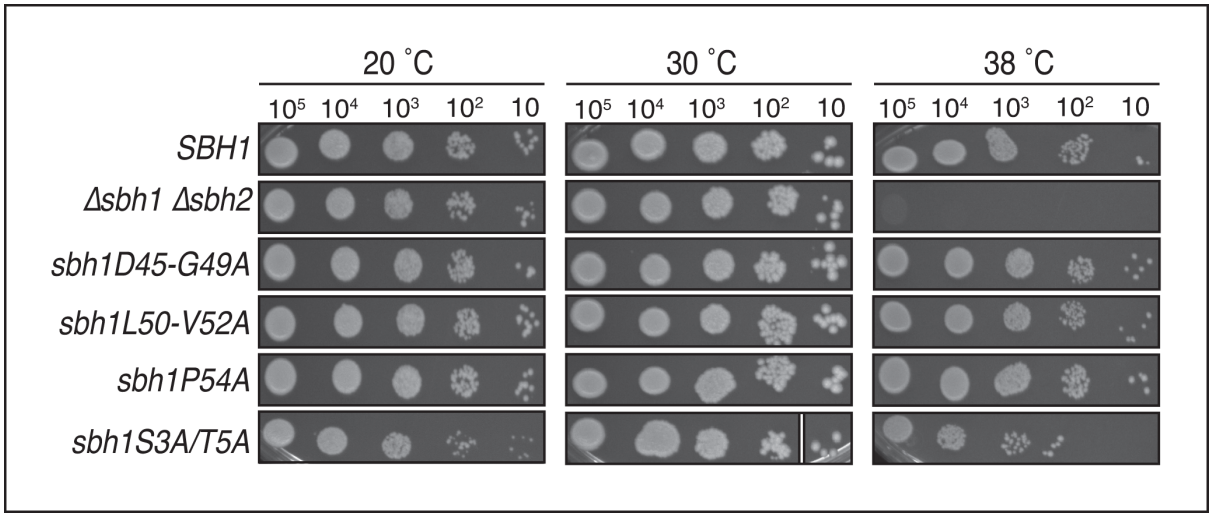

Figure 3.14 CMP mutants do not show temperature sensitivity. Transformed yeast strains grown to early exponential phase were harvested, washed and diluted to 1 OD_{600}. Serial dilutions of each strain corresponding to 10^5-10 cells were grown on -Leu media for 3 days at lower 20 ˚C, permissive 30 ˚C and restrictive 38 ˚C. The growth of the three CMP mutants, *sbh1 D45-G49A, sbh1 L50-V52A* and *sbh1 P54A,* was similar to the *SBH1* positive control strain. The negative control strain *Δsbh1 Δsbh2* strain showed severe growth defect and *sbh1S3A/T5A* strain showed moderate growth defect at 38 ˚C. All strains used were generated by transforming KRY 588 strain with mutated *SBH1* coding sequence, or wildtype *SBH1* sequence in the case of *SBH1* strain. The 10-cell spot in *sbh1S3A/T5A* strain grown at 30 ˚C was misaligned on the agar plate and spliced in to fit in the figure.

All three CMP mutants that were assayed showed growth similar to *SBH1* strain at the three temperatures tested (Figure 3.14). As expected, *Δsbh1 Δsbh2* strain showed a severe growth defect at 38 ˚C and *sbh1S3A/T5A* strain showed a moderate defect at 38 ˚C. My results imply that the Sbh1 CMP mutants *sbh1D45-G49A, sbh1L50-V52A* and *sbh1P54A* do not show growth defects as compared to *SBH1* strain, suggesting that CMP mutations do not interfere with the function of Sbh1p.

Next, I transformed the combo mutant plasmids into KRY 588 strain: *sbh1D45-G49A/P54A, sbh1D49-V52A, sbh1L50-V52A/P54A* and *sbh1D49-V52A/P54A*. For a preliminary growth test, I randomly picked 5 colonies each and resuspended them in 100 µL of -Leu medium. I used 50 µL of the resuspension to inoculate 5 mL of -Leu medium and measured the growth of these colonies in real-time by growing them at 30 ˚C and periodically measuring

their OD_{600}. I observed that the different colonies of each mutant were not growing at the same rate. I streaked 10 µL of each colony on -Leu plates along with the transformed *SBH1* and *Δsbh1 Δsbh2* strains. Suspicious of a growth defect even at 30 ˚C, I included 25 ˚C as a potential alternative for permissive temperature along with 20 ˚C, 30˚C and 38 ˚C.

I documented the results after 3 days, shown in Figure 3.15. While most colonies from the same strain showed growth comparable to each other and to *SBH1* strain, I saw variations in growth phenotypes of certain colonies of the same mutant. Colony 3 of *sbh1D45-G49A/P54A* strain showed a growth defect at 20 ˚C while the other colonies showed growth comparable to *SBH1* strain at all temperatures tested. Among *sbh1D45-V52A* strain colonies, colonies 1 and 2 showed lower growth than *SBH1* strain and other colonies at 20 and 25 ˚C, and colony 2 also showed growth defect at 38 ˚C. Colonies 1 and 2 of *sbh1L50-V52A/P54A* strain showed mild defects at 38 ˚C as compared to *SBH1*. In *sbh1D45-V52A/P54A,* colony 1 appears to show a mild growth defect at 20 ˚C as compared to *SBH1*. I retransformed the strains and performed growth assays two more times but could not achieve consistent growth between picked colonies. I decided to not proceed with characterising the combo mutants as the strains appeared to adapt rapidly and unpredictably to compensate for their phenotype.

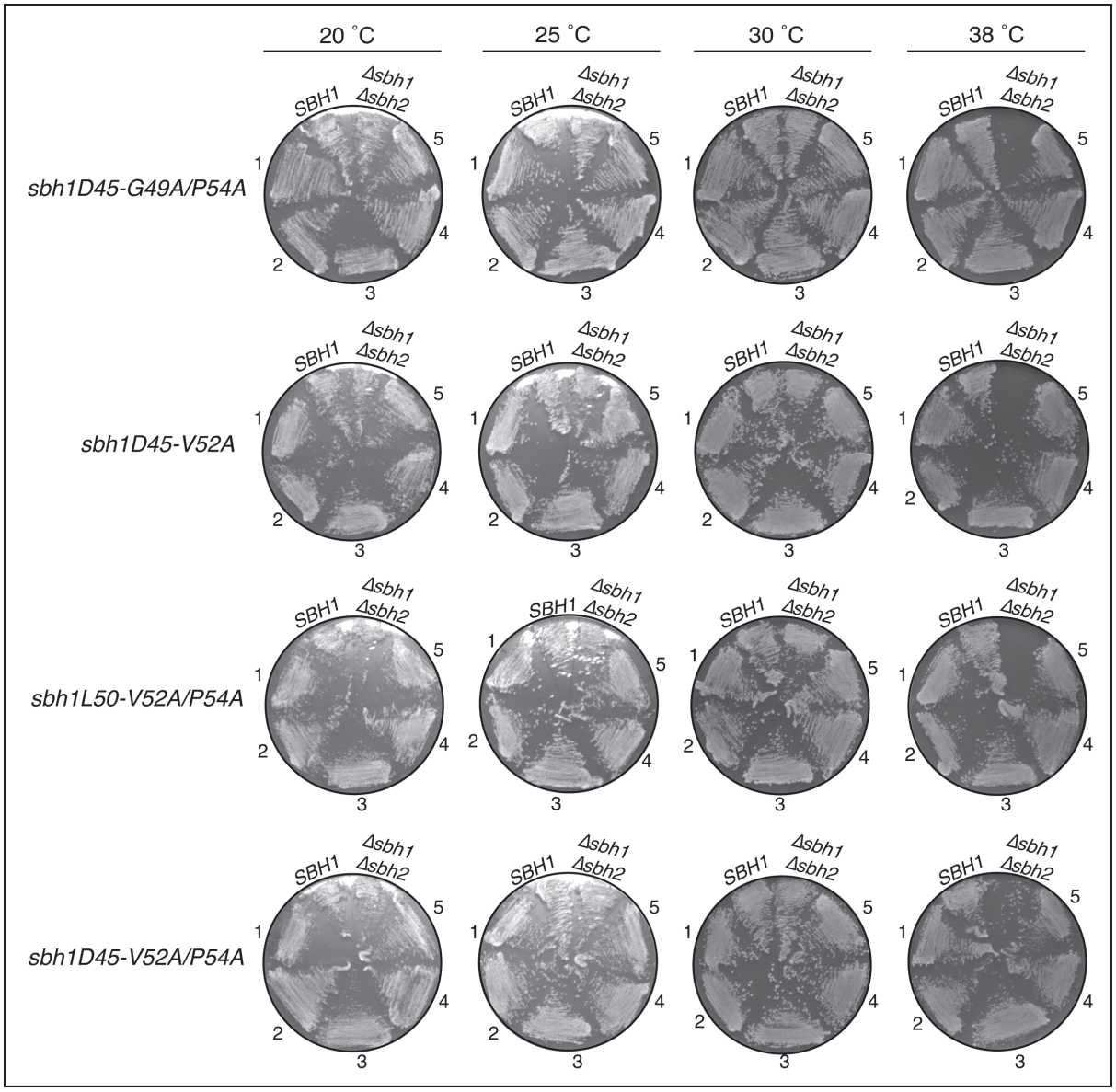

Figure 3.15 Combo mutants show variations in growth of different colonies even at the same temperature. Five colonies were randomly picked from transformed *sbh1* mutant strains grown on -Leu selective media plates at 20˚, 25˚, 30˚ and 38 ˚C for 3 days. KRY 588 strain transformed with *SBH1*-pRS415 plasmid (*SBH1* strain) and with empty pRS415 plasmid (*Δsbh1 Δsbh2* strain) were used as controls. Specific colonies from each mutant strain did not show a growth phenotype that matched the rest of the colonies or the control *SBH1* strain: *sbh1D45-G49A/P54A* colony 3 appears sensitive to 20 ˚C; *sbh1D45-V52A* colonies 1 and 2 appear to be sensitive to 20˚ and 25 ˚C and colony 2 is additionally also sensitive to 38 ˚C; *sbh1L50-V52A/P54A* show mild defects at 38 ˚C; *sbh1D45-V52A/P54A* colony 1 appears to be sensitive to 20 ˚C.

I moved forward with characterising the CMP mutants *sbh1D45-G49A, sbh1L50-V52A* and *sbh1P54A*. I determined the steady-state levels of Sbh1 produced by each of these mutants at 30 ˚C using whole cell extracts. I also determined the steady-state levels of Gls1 in CMP mutants at 30 ˚C, as *Δsbh1 Δsbh2* strain was previously shown to have reduced Gls1 levels

even at permissive temperature [222]. Gls1 is dependent on the phosphorylation of S3 and T5 residues of Sbh1 [253]. I used KRY 588 strain transformed with *SBH1*-pRS415 as positive control (*SBH1*) and KRY 588 transformed with empty pRS415 (*Δsbh1 Δsbh2*) as negative control. I analysed the cell extracts by Western blotting (Section 2.2.4), probing for Sbh1 or Gls1 and Rpn12 as a loading control. I quantified the immunoblots using ImageQuant™ TL software (GE Healthcare). The results are presented in Figure 3.16 (A). I found that *sbh1D45-G49A* strain produced 165% of Sbh1 in the control *SBH1* strain, *sbh1L50-V52A* strain produced only 22% of Sbh1 in *SBH1* strain and *sbh1P54A* strain produced 72% (Figure 3.16 (A), left). Among the Gls1 levels, *sbh1D45-G49A* strain had closest to *SBH1* strain with 130%, *sbh1L50-V52A* had 170% of *SBH1* strain level, and *sbh1P54A* produced 230% Gls1 of *SBH1* strain (Figure 3.16 (A), right). While Sbh1 levels vary greatly from *SBH1* strain, Gls1 levels produced by the CMP mutant appears to be higher than *SBH1* strain as a general trend.

When I repeated this experiment, saw very different results. Sbh1 levels for *sbh1D45-G49A* strain reduced to 88% of *SBH1* strain, Sbh1 level in *sbh1L50-V52A* strain stayed within a similar range at 26% and *sbh1P54A* strain Sbh1 level increased to 140% of *SBH1* strain (Figure 3.16 (B), left). On the other hand, Gls1 levels in all the CMP mutants changed to be closer to *SBH1* strain level, with both *sbh1D45-G49A* and *sbh1L50-V52A* strains producing 128% of *SBH1* strain Gls1 and *sbh1P54A* strain producing 110% (Figure 3.16 (B), right).

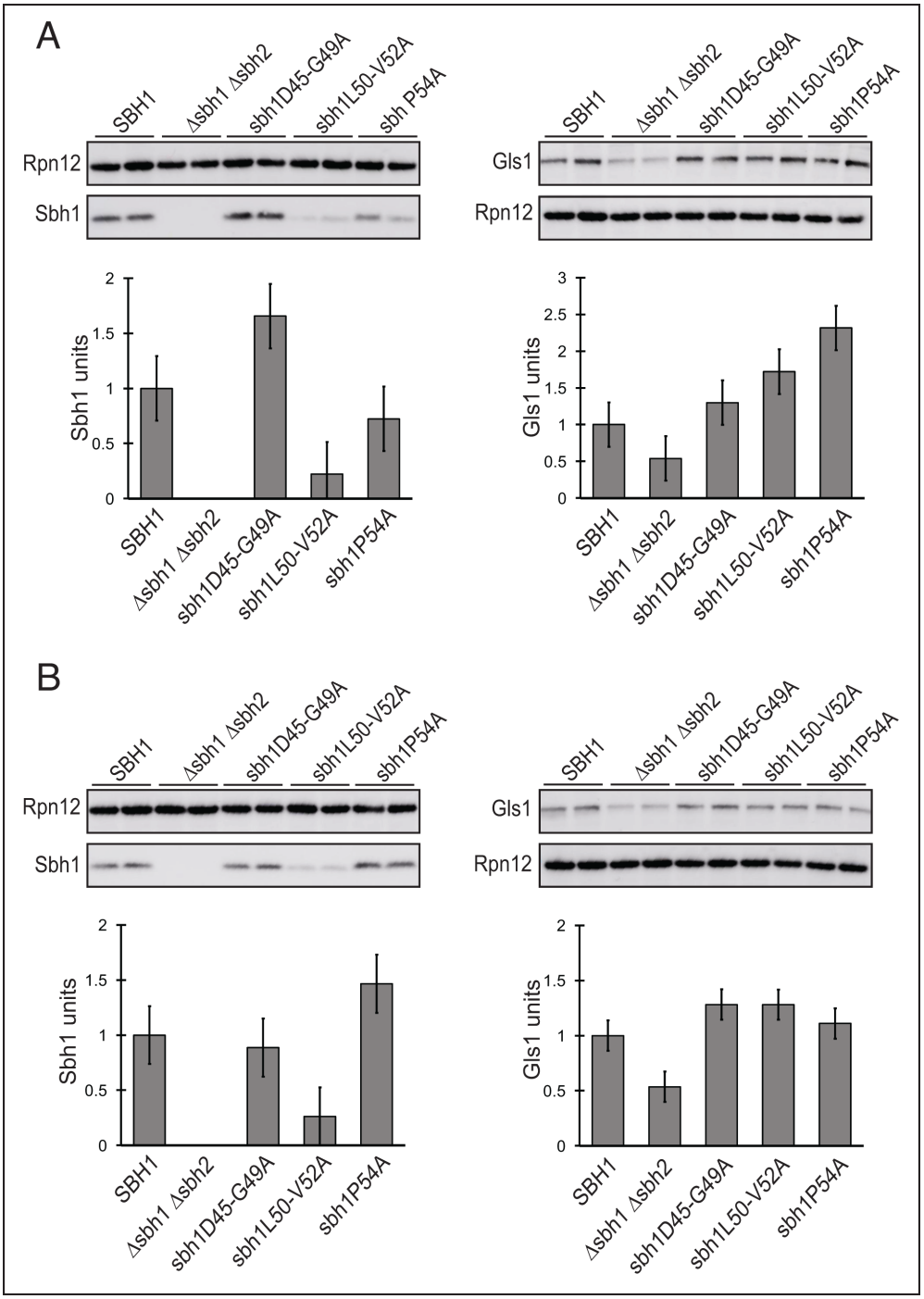

Figure 3.16 Sbh1 and Gls1 levels in CMP mutants vary with time. Cells extracts were prepared from 1 OD_{600} of CMP mutant strains grown to early exponential phase at 30 ˚C. KRY 588 strain transformed with pRS415- *SBH1* plasmid (*SBH1* strain) and with empty pRS415 plasmid (*Δsbh1 Δsbh2* strain) were used as positive and negative controls, respectively. The extracts were analysed by Western blotting and probed for Sbh1 or Gls1, and Rpn12 as loading control. The amount of Sbh1/Gls1 detected in the immunoblot was quantified and plotted in a chart given below each immunoblot. **A)** Sbh1 (left) and Gls1 (right) levels in CMP mutants 1 week after transformation. When compared to the levels in *SBH1* strain, *sbh1D45-G49A* strain produced 168 % of Sbh1 but 130 % of Gls1, *sbh1L50-V52A* strain produced 22 % of Sbh1 and 170 % of Gls1, and *sbh1P54A* strain produced 72 % of Sbh1 but 230 % of Gls1, more than twice the amount of Gls1 seen in *SBH1* strain. **B)** Sbh1 (left) and Gls1 (right) levels in CMP mutants 3 weeks after transformation. The *sbh1D45-G49A* strain reduced the amount of Sbh1 produced to 88 % of *SBH1* strain level, *sbh1L50-V52A* strain produced nearly the same amount of Sbh1 at 26 %, and *sbh1P54A* strain increased the amount of Sbh1 produced to 140%, nearly twice the Sbh1 seen in new transformants. The amount of Gls1 produced by each strain altered closer that in *SBH1* strain, with *sbh1D45-G49A* and *sbh1L50-V52A* strains both producing 128 % and *sbh1P54A* strain producing 110%.

I used the same transformants of the CMP mutant strains for both experiments. The strains were 1 week old at the time of the first experiment, and 3 weeks old at the time of the second. I retransformed the CMP mutant strains and repeated the experiment within one week of their transformation. I determined the levels of Sbh1 and Gls1 in 5 randomly picked colonies of each mutant (Supplementary Figure 9). I found the amount of both Sbh1 and Gls1 matched those seen in Figure 3.16 (A).

Taken together, my results show that with time, the CMP mutants adapt to compensate for their phenotype in uncertain ways, similar to what I had seen in the previous section when characterising growth defects in combo mutants. To minimise any variation in results, I retransformed the CMP mutants, picked one colony from each mutant and cryopreserved it within 4 days of transformation. I confirmed that they show similar growth as in Figure 3.15 by repeating the growth assay. I revived these newly transformed CMP mutant strains at the beginning of each week and ensured to use strains that were no older than 10 days from transformation for each experiment in the following sections.

I assessed the Sbh1 and Gls1 levels in the newly transformed CMP mutant strains grown to early exponential phase at 30 ˚C, in duplicates, by Western blot analysis of their cell extracts. I probed the blots for Sbh1 or Gls1 and for the loading control Rpn12. I quantified the immunoblots using ImageQuant™ TL software (GE Healthcare). I found the Sbh1 level in *sbh1D45-G49A* is 158% of that in *SBH1* strain, in *sbh1L50-V52A* it is 48% and in *sbh1P54A* it is 83% (Figure 3.17, left). Gls1 level in *sbh1D45-G49A* is 108% of that in *SBH1* strain, in *sbh1L50-V52A* it is 145% and in *sbh1P54A* it is 140% (Figure 3.17, right).

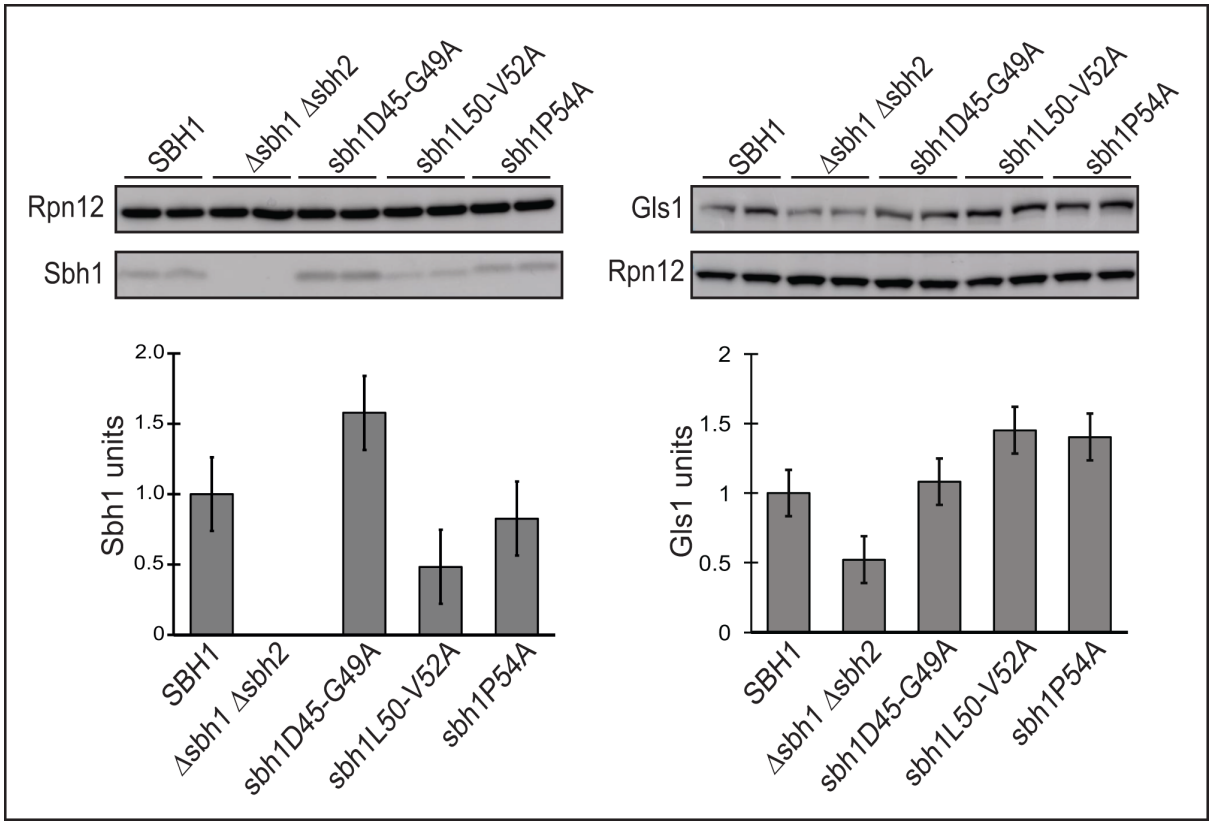

Figure 3.17 CMP mutants have impaired Sbh1 production and Gls1 import. Cells extracts were prepared from 1 OD_{600} of newly transformed CMP mutant strains grown to early exponential phase at 30 ˚C. KRY 588 strain transformed with *SBH1*-pRS415 plasmid (*SBH1* strain) and with empty pRS415 plasmid (*Δsbh1 Δsbh2* strain) were used as positive and negative controls, respectively. The extracts were analysed by Western blotting and probed for Sbh1 or Gls1, and Rpn12 as loading control. The amount of Sbh1/Gls1 detected in the immunoblot was quantified and plotted in a chart below each immunoblot. When compared to the levels in *SBH1* strain, *sbh1D45-G49A* strain produced 158 % of Sbh1 but 108 % of Gls1, *sbh1L50-V52A* strain produced 48 % of Sbh1 and 145 % of Gls1, and *sbh1P54A* strain produced 83 % of Sbh1 but 140 % of Gls1.

My results show that mutations in Sbh1 CMP residues alters the production of Sbh1. The amount of Gls1, a Sbh1 phosphorylation-dependent substrate, produced in CMP mutants is also affected. As the amount of Gls1 produced by the CMP mutants alters with time to be closer to that produced by *SBH1* strain, the ER import function of Sbh1 is likely affected by the CMP mutations.

Next, I investigated the general translocation efficiency of CMP mutants. For these experiments, I looked at the ER import of specific precursors at restrictive temperatures, namely, the precursors of Kar2, DPAPB, PDI and CPY. I grew the CMP mutant strains at

permissive 24 ˚C until they reach 0.5 OD_{600} and transferred the strains to restrictive 38 ˚C for 3 hours. I used KRY 588 strain transformed with pRS415-*SBH1* as positive control (*SBH1*) and depending on the substrate being investigated, KRY 588 transformed with empty pRS415 (*Δsbh1 Δsbh2*) or *sec61-32* strain as the negative controls. The *sec61-32* strain is cold sensitive, I grew the strain at permissive 30 ˚C and shifted to restrictive 20 ˚C when used [242].

First, I checked the import of Kar2 precursor pKar2, which is translocated both co-translationally and post-translationally into the ER. Kar2 is an ER resident Hsp70 ATPase. As demonstrated in Section 3.1, Kar2 depends on Sbh1 for its import at 38 ˚C. I analysed whole cell extracts of CMP mutants, *SBH1* and Δ*sbh1 Δsbh2* strains by Western blotting and probed the blot with anti-Kar2 antibodies. I did not detect accumulation of pKar2 in the CMP mutants, indicating that its import was unaffected (Figure 3.18(A)).

To test for the presence of general co-translational translocation defects, I analysed the import of DPAPB precursor. DPAPB (120 kDa) is an integral membrane protein. Its cytosolic precursor pDPAPB (96 kDa) is imported co-translationally into the ER where it is glycosylated to form mature protein [269]. I investigated the accumulation of pDPAPB in the CMP mutants, *SBH1* and *sec61-32* strains grown at their restrictive temperatures by pulse-labelling cells with [^{35}S]-Met/Cys, immunoprecipitation with DPAPB antibody and detecting by autoradiography. The *sec61-32* strain acts as the positive control here. I did not detect pDPAPB in the CMP mutants, shown in Figure 3.18(B), implying that it was imported into the ER.

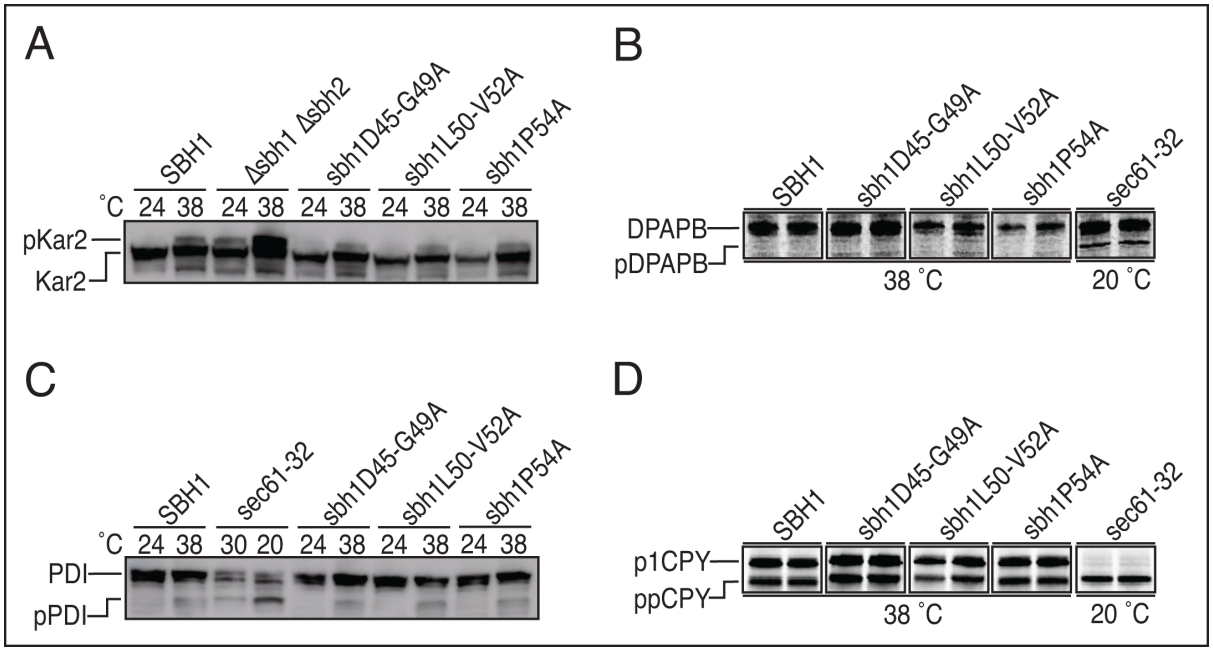

Figure 3.18 CMP mutants do not show general protein translocation defects. Accumulation of co-translationally and post-translationally imported protein cytosolic precursors in CMP mutant strains. CMP mutants, *SBH1, Δsbh1 Δsbh2* and *sec61-32* strains were grown at their permissive temperature (24˚ or 30 ˚C) to 0.5 OD_{600} and shifted to their restrictive temperature (38˚ or 20 ˚C) for 3 h. For Western blotting, cell extracts were prepared from 2 OD_{600} of cells grown at both permissive and restrictive temperatures and sample corresponding to 0.25 OD_{600} of cells was resolved by SDS-PAGE, followed by immunoblotting against specific proteins. In pulse-labelling experiments, 1.5 OD_{600} duplicates of each strain grown at their restricted temperature for 3 h were pulse-labelled with [^{35}S]-Met/Cys and extracted, immunoprecipitated with specific antibodies, and detected by autoradiography. In all experiments *SBH1* strain acts as the negative control, and *Δsbh1 Δsbh2* or *sec61-32* strain acts as the positive control. **A)** Kar2 precursor accumulation analysed by Western blotting. **B)** DPAPB precursor accumulation by pulse-labelling the cells with [^{35}S]-Met/Cys for 15 mins and immunoprecipitated with anti-DPAPB antibody.. **C)** PDI precursor accumulation analysed by Western blotting. **D)** CPY precursor incorporation analysed by pulse labelling the cells with [^{35}S]-Met/Cys for 5 mins and immunoprecipitated with anti-CPY antibody.

Next, I tested the import of post-translationally translocated PDI precursor, pPDI. PDI is an ER resident chaperone. I analysed the accumulation of pPDI in cell extracts of CMP mutants, *SBH1* and *sec61-32* strains grown at their permissive and restrictive temperatures by Western blotting of cell extracts and probed the blot with antibodies against PDI. The CMP mutants did not accumulate pPDI, as shown in Figure 3.18(C), suggesting that its import into the ER was not affected.

I investigated the post-translational import of the cytosolic precursor of CPY vacuolar protease, ppCPY. Upon its import into the ER, ppCPY is glycosylated to p1CPY. I pulse labelled CMP mutants, *SBH1* and *sec61-32* strains grown at their restrictive temperatures with [^{35}S]-Met/Cys, immunoprecipitated the proteins with anti-CPY antibodies and detected the presence of CPY precursors by autoradiography. I saw that the CMP mutants were not defective in ppCPY import, implied by the presence of the ER incorporation product p1CPY in Figure 3.18(D).

My results suggest that CMP mutants do not have general defects in co-translational or post-translational translocation of proteins. While the import of Kar2 is dependent on Sbh1, it is independent of its phosphorylation [253]. The import of Gls1, which was defective even at 30 ˚C (Figure 3.17), depends on phosphorylation of S3 and T5 residues of Sbh1 [253].

Altogether, my results imply that the CMP region of Sbh1 plays a specific role in the import of S3/T5 phosphorylation dependent Sbh1 substrate, Gls1. Mutations in CMP region affect the ability of Sbh1 to import Gls1 into the ER and CMP mutant strains can compensate for this defect by adjusting the amount of Sbh1 produced.

3.4. Identifying interactions of Sbh1 cytosolic domain

Structural versatility of IDRs enables them to interact with various binding partners [199]. These disorder-to-order transitions are often modulated by post-translational modifications such as phosphorylation [195]. The cytosolic domain of Sbh1 includes an N-terminal IDR which has 7 phosphorylation sites and the CMP region. The cytosolic domain of mammalian Sec61β interacts with the ribosome [224,225], nascent polypeptide in the Sec61 channel vestibule [226,227] and helps effectively insert the nascent polypeptide chain [101]. Several proteins have been identified as dependent on Sbh1, and Sbh1 phosphorylation for their insertion in yeast [253]. My data indicates the involvement of Sbh1 CMP region in the insertion of S3/T5 phosphorylation dependent substrates. Given this context and the broader implications of regulation of the structural configuration of Sbh1 IDR, I wanted to investigate the protein-protein interactions of Sbh1 cytosolic domain and identify the specific residues involved in these interactions.

3.4.1. Predicting molecular recognition features in Sbh1

IDRs can adopt a structure suitable for an interaction with their target protein. Molecular recognition features (MoRFs) are short binding sites within the IDR that interact with the binding partner and contribute to the function of the IDR [198]. MoRFs are typically islands of conserved aromatic and hydrophobic residues [199]. As Sbh1 IDR has such residues, I wanted to assess the possibility of them being MoRF(s).

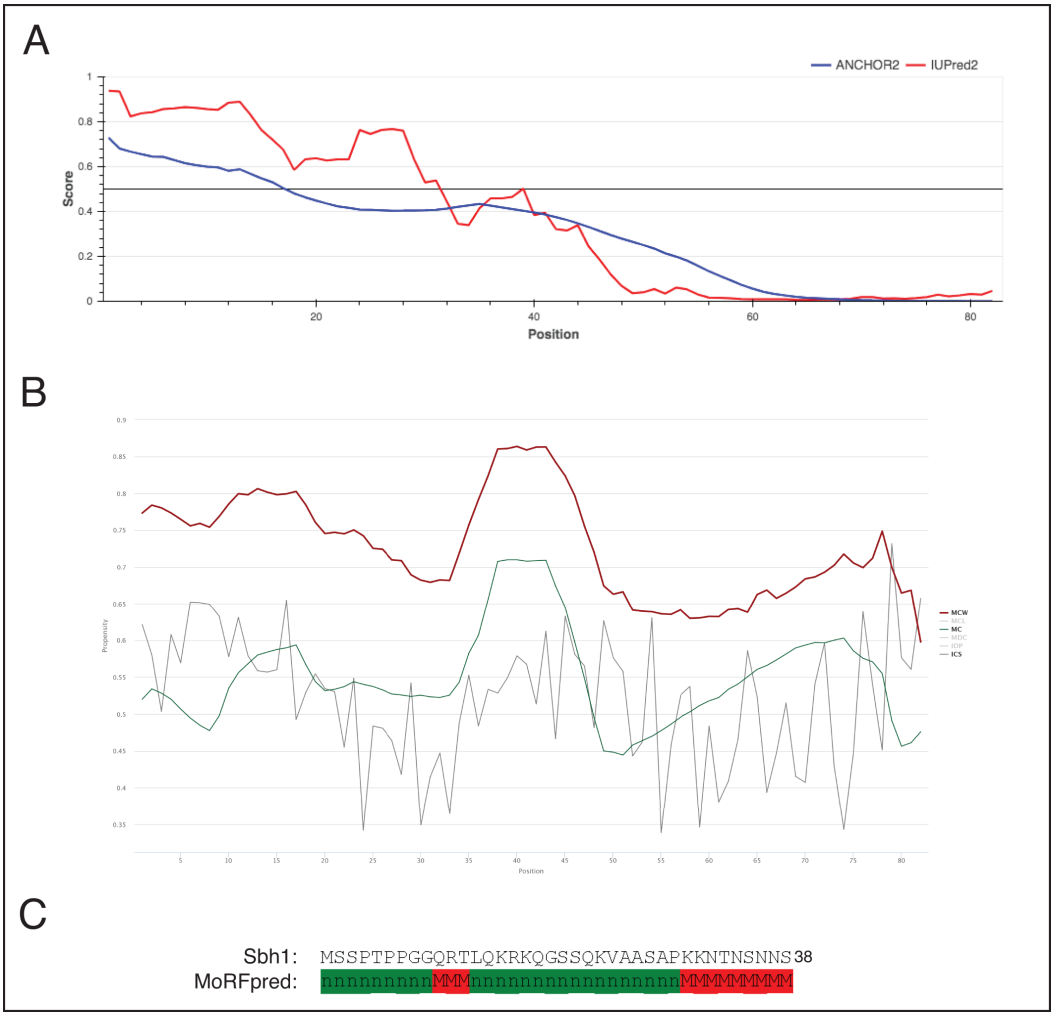

Figure 3.19 Sbh1 IDR has two potential MoRFs. A) Tendency for disorder and protein binding in Sbh1. IUPred2 plot (red) shows M1 to S35 residues have a propensity score >0.5 and tend to be disordered. ANCHOR2 plot (blue) shows M1 to K17 residues have a propensity score >0.5 and are protentially protein binding. **B)** MoRF predictions using $MoRF_{CHiBi\_Web}$. Conservation based propensity score ICS (gray) was >0.5 for M1 to R16. MC propensity score (green) based on physicochemical properties of residues was >0.5 for the Sbh1 IDR, except for residues T5 to Q10. Overall MoRF propensity score MCW (brown) was >0.65 for the Sbh1 IDR, with M1 to Q18 being >0.75. **C)** MoRFs in the Sbh1 IDR as predicted by MoRFpred. Potential MoRFs are highlighted with a red M, non-MoRFs are identified with a green n.

Various computational algorithms have been developed to predict MoRFs. I ran the full Sbh1 sequence through one such tool, IUPred2/ANCHOR2 [270]. IUPred2 identifies disordered regions and the disorder tendency of residues. ANCHOR2 identifies disordered binding regions and the probability of the residues being part of a binding region. The prediction in Figure 3.19(A), IUPred2A plot showed Sbh1 N-terminal residues M1 to S35 have a score > 0.5 and have a greater probability of being disordered, and an ANCHOR2 plot shows residues M1to K17 have a > 0.5 score and have a higher probability of protein binding.

I used MoRFChiBi system as another way to predict MoRFs in Sbh1. This method assesses physicochemical properties of the sequence, and its conservation generates propensity scores using Bayes rule [271]. Figure 3.19(B). The MC score based on physiochemical properties showed a > 0.5 propensity score for all residues except T5 to Q10. The conservation score ICS was > 0.5 for M1 to R16 residues. MoRFCHiBi_Web showed an overall propensity score (MCW) > 0.75 for M1 to Q18 residues and > 0.65 for the rest. The S35 to A47 residues, which include the C-terminal of IDR and the first 9 residues of the CMP region, showed high scores despite mostly not being in the IDR.

I also used MoRFPred and MFSPSSMPred which showed MoRFs in similar regions, one close to N-terminal including at least the T12 phosphorylation site, one towards the C-end of the IDR and extending into CMP (Supplementary Figure 10) [272].

To focus only on the Sbh1 IDR, I ran more predictions using Sbh1 M1 to S38. MoRFPred uses sequence alignment, residue properties, disorder prediction, solvent accessibility and B-factor [273]. It identified two MoRFs: Q10 to T12 and K30 to S38 (Figure 3.19(C)). I used the Sbh1 IDR in Disopred3 and MoRFChiBi tools and saw the same MoRFs (Supplementary Figure 11).

Taken together, the predictions imply the presence of at least 2 MoRFs in Sbh1 cytosolic domain, one between Q10 to T12 phosphorylation site and another encompassing the C-terminal end of the disordered region including S35 and S38 phosphorylation sites. ANCHOR2 and MoRFChiBi tools also predict a high propensity of the N-terminal residues M1 to R16 to be protein binding. This region has 4 phosphorylation sites, including S3 and T5, which could

potentially participate in the disorder-to-order transition of the IDR, thereby regulating Sbh1 function.

3.4.2. Peptide Panning Strategy and pilot experiments

Sbh1 is required for translocation of specific proteins. Recent results identified proteins that specifically depended on phosphorylation of Sbh1 [253]. Phosphorylation can induce disorder-to-order transitions in IDRs [195]. Sbh1 IDR has residues that can potentially act as a MoRF and has 7 phosphorylation sites possibly regulate the IDR structure and function. In Section 3.2 I identified a potential interaction between Sbh1 CMP region and Sec61 N-terminal helix and demonstrated its importance for the import of specific Sbh1 S3/T5 phosphorylation dependent substrates. Sec61β was crosslinked to incoming polypeptides in the vestibule of Sec61 channel [226,227]. This motivated me to explore the interactions of Sbh1 cytosolic domain.

I wanted to identify specific residues of the of Sbh1 cytosolic domain that can directly interact with other proteins. To achieve this, I used a peptide panning technique, summarised in Figure 3.20. In this method, an array of Sbh1 peptides is synthesised on an acid-hardened membrane and is probed with biotinylated peptides of potential interaction partners. The peptide-peptide interaction is then detected using anti-biotin antibodies, similar to an immunoblot.

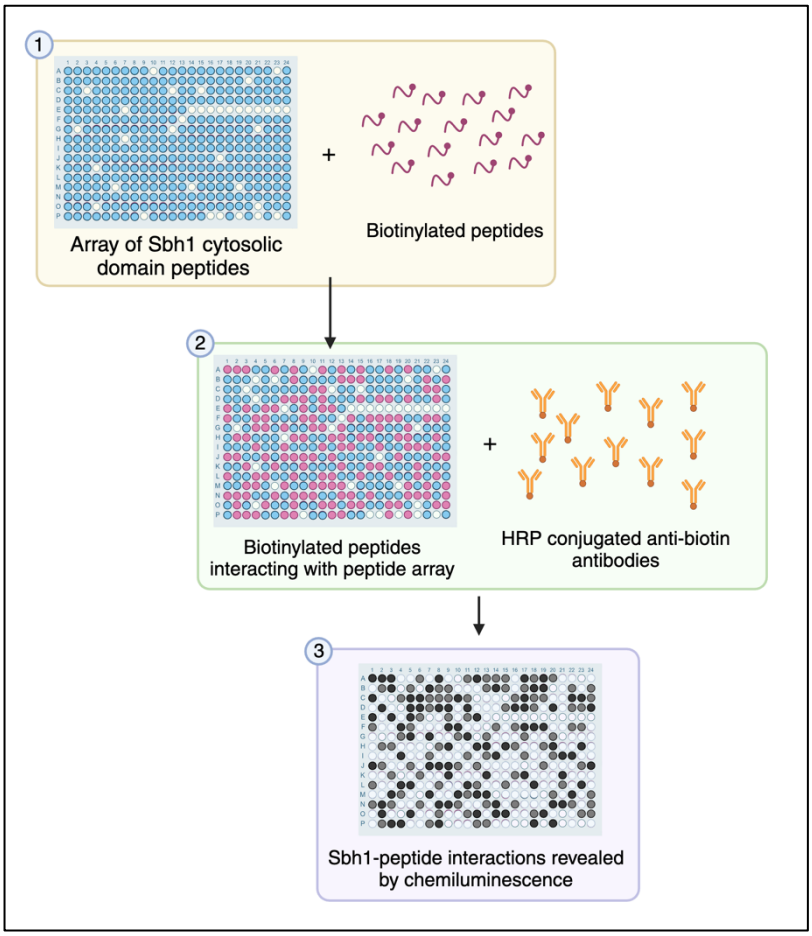

Figure 3.20 Overview of Peptide Panning Analysis. Step 1. Peptides panning the length of Sbh1 cytosolic domain are C-terminally anchored to an acid-hardened cellulose membrane in a pre-designed array. The peptide array is probed with C-terminally biotinylated peptides to investigate their interaction with Sbh1. **Step 2.** The membrane is probed with HRP conjugated anti-biotin antibodies to detect Sbh1-peptide interactions. **Step 3.** Sbh1-peptide interactions are revealed by chemiluminiscence. Detection spots may appear lighter or darker depending on the strngth of the interaction with the peptide at that spot. Here, the array design and interactions are for representation only. Created with BioRender.com.

Sbh1 peptides panning the cytosolic domain from M1 to L55 were synthesised onto an acid-hardened cellulose membrane, each 20 residues in length and moving with a 2-residue sliding window (Figure 3.21(A)). Peptides were anchored to the membrane at their C-terminal end to mimic their orientation in the intact protein in the ER membrane. To reflect the effect of Sbh1 phosphorylation on interactions, phosphorylated state of each S and T residue and all combinations of these residues were included. For the N-terminal peptide, combinations of N-terminal phosphorylation, which is seen physiologically, was also included [274]. Cytosolic domain peptides of Sbh1 paralog Sbh2 from M1 to L62 were analogously synthesised. Sbh2 is

a part of Ssh1 complex and was previously shown to rescue cells from temperature sensitivity in the absence of Sbh1 [222]. Phosphorylation of Sbh2 has not yet been shown, hence not included in this study.

The layout of the peptide panning array is shown in Figure 3.21(C). The array starts with N-terminally acetylated Sbh1 S2 to S21 residues at position A01. The next set is Sbh1 M1 to S20 residues starting at spot A17, followed by P4 to K23 residues, and so on and ends with combinations of N36 to L55 residues at position I22. A spot was left empty between two peptide sets to help with orientation. Sbh2 peptides are from spot I24 to J15. Spots K01 to T15 are a duplicate of spots A01 to J15. Thus, each experiment is inherently run as duplicates. Spots T20 and T24 are positive controls, containing a peptide of phosphorylated Sbh1. Spots T22 and T26 are negative controls, containing a peptide which does not show similarity with Sbh1. Complete index of spots is provided in Appendix B.

For the experiments, I spliced the control spots from the membrane and incubated them with anti-phosphorylated Sbh1 instead of biotinylated peptide, then with biotinylated secondary antibody and finally detected using HRP conjugated anti-biotin antibody (Figure 3.21 (B)). I imaged the membranes in AI600 Imager (Amersham) with a 2 sec exposure time. After each experiment I stripped and reused the blots.

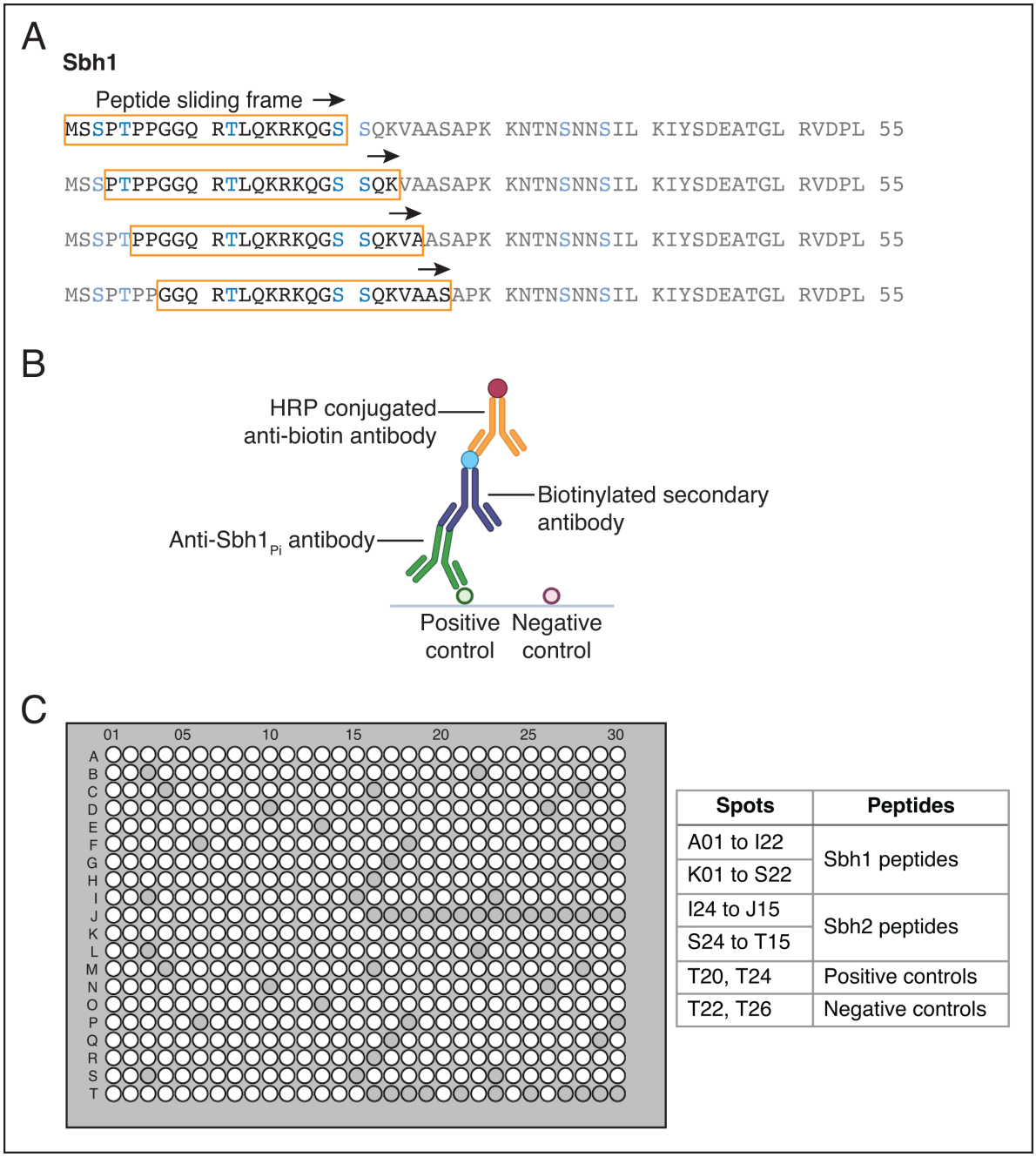

Spots	Peptides
A01 to I22	Sbh1 peptides
K01 to S22	
I24 to J15	Sbh2 peptides
S24 to T15	
T20, T24	Positive controls
T22, T26	Negative controls

Figure 3.21 Design of peptide panning membrane. A) Selection of peptides for peptide panning. Sbh1 20-mer peptides were synthesised from M1 to L55 panning the entire cytosolic domain with a 2 residue sliding frame, indicated by an orange box. Peptides with combination of Ser/Thr phosphorylation states and N-terminal acetylation were included. Sbh2 cytosolic domain peptides panning M1 to L62 were also synthesised (not pictured). **B)** Detection of control peptides. A short phosphorylated Sbh1 peptide was used as positive control and a non-Sbh1 peptide was used as negative control. During experiments, the control spots were spliced out of the peptide panning membrane and separately probed with anti-Sbh1$_{Pi}$ antibody. The membrane was further probed with biotinylated secondary antibody, followed by HRP conjugated anti-biotin antibody to detect the control peptides. **C)** Layout of the peptide panning membrane. Each stretch of white spots corresponding to a Sbh1 20-mer and its variations is separated by a blank spot (gray). Spots K01 to T30 are a duplicate set of the spots from A01 to J30. Table gives the legend for the peptide array.

Potential Sbh1 interaction partners to test were chosen based on previously reported associations. Additionally, the peptides needed to be synthesised in soluble form to be usable in the experimental setup. Since MD simulations identified an interaction between Sbh1 CMP region and Sec61 N-terminal helix (Figure 3.13), Sec61 N-terminal helix was a potential interaction partner to investigate [268]. SPs of two Sbh1 dependent proteins, Gls1 and Irc22, and two Sbh1-independent proteins, ppCPY and ppαF, were also selected to investigate for their interaction with Sbh1 cytosolic domain. These SPs do not depend on Sbh2 for their import. The sequences of the biotinylated peptides used are listed in Table 3.2.

Table 3.2 List of biotinylated peptides used in this study.

Peptide	Sequence
Gls1 Peptide (first 24 aa-Biotin)	MLISKSKMFKTFWILTSIVLLASAK-Biotin
Irc22 Peptide (first 21aa-Biotin)	MRFSMLIGFNLLTALSSFCAAK-Biotin
Prepro-CPY Peptide (first 20 aa-Biotin)	MKAFTSLLCGLGLSTTLAKAK-Biotin
ppαF (first 20 aa-Biotin)	MRFPSIFTAVLFAASSALAK-Biotin
Sec61 N-terminal Helix	acSSNRVLDLFKPFESFLPEVIAPERK-Biotin

I began my investigation by running pilot experiments to optimise the method. Initially, I planned to detect protein interactions using HRP conjugated streptavidin. Streptavidin has a high affinity for biotin and binds to it non-covalently. To rule out any cross-reactions in the experiment system, I activated an intact membrane (control spots were not spliced out), blocked it with BSA, and incubated it with streptavidin-HRP. I visualised the membrane using chemiluminescence. Unexpectedly, I saw interactions with Sbh1 N-terminal peptides corresponding to the N-terminus (Figure 3.22). Various positions between spots A01 and C29, corresponding to Sbh1 M1 to T33 residues, including acetylated N-terminus. Among these,

strongest interactions were observed with peptides ranging from M1 to K23 residues. Comparable Sbh2 residues also showed interactions in row I24 to J01, covering M1 to T32 residues. Same interactions were seen in the duplicate spots as well.

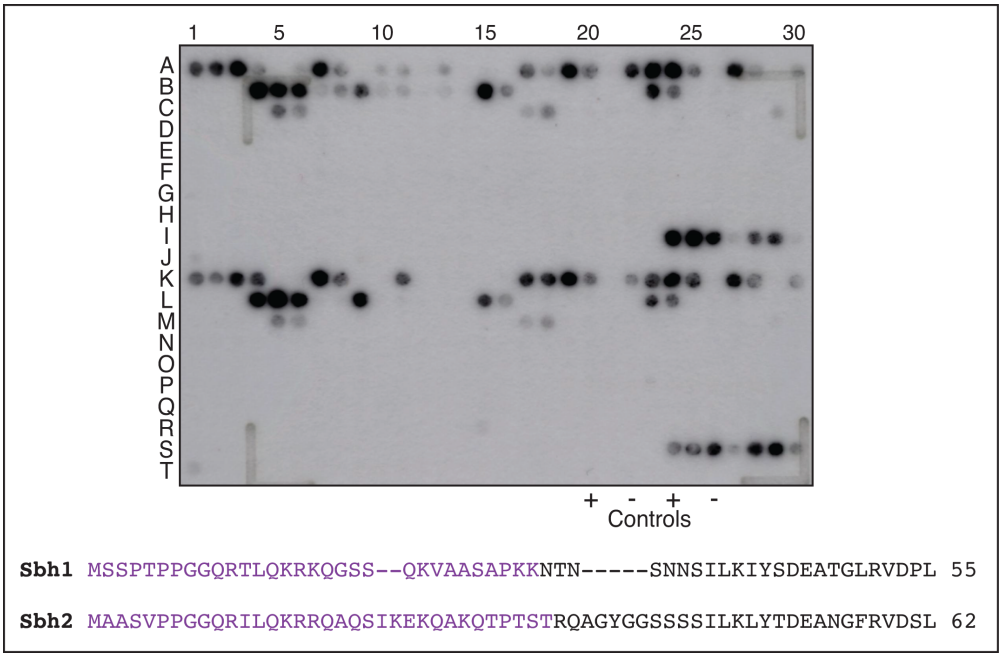

Figure 3.22 N-terminal peptides cross-react with streptavidin. The peptide panning membrane was activated with methanol, blocked with 1 % BSA, washed with binding buffer and probed with streptavidin-HRP. Interactions were revealed by chemiluminiscence. Interactions were revealed with various Sbh1 peptide spots between A01 and C29 corresponding to M1 to T33 residues. Sbh2 peptide spots I24 to J01 corresponding to M1 to T32 residues also showed interactions. The interacting residues of Sbh1 and Sbh2 are highlighted in purple.

I repeated the experiment in an unused membrane by activating it with methanol, equilibrating it in binding buffer and probing it with streptavidin-HRP. I saw the exact same interaction spots again, implying that streptavidin was cross-reacting with Sbh1 and Sbh2 N-terminal peptides. I decided to avoid using streptavidin further experiments and switched to HRP conjugated anti-biotin antibody instead. Upon repeating the experiment, I observed cross-reactivity with the anti-biotin antibody as well, shown in Supplementary Figure 12. However, it was easier to strip the antibody from the membrane than streptavidin, which requires harsher stripping protocol that would degrade the peptide array faster. Bearing

practicality in mind, I decided to use anti-biotin-HRP antibody to reveal the peptide-peptide interactions.

3.4.3. Interactions of Sbh1 cytosolic domain

I first wanted to study the interactions between Sbh1 cytosolic domain and Sec61 N-terminal helix. I probed the activated and blocked peptide panning membrane with biotinylated Sec61 N-terminal peptide. Surprisingly, I saw interactions only with cross-reacting spots (Figure 3.23). The Sec61 N-terminal helix is amphipathic and is embedded into the lipid bilayer. Incompatibility of the isolated residues with the aqueous buffer system used could lead to the lack of interactions that may occur in physiological conditions.

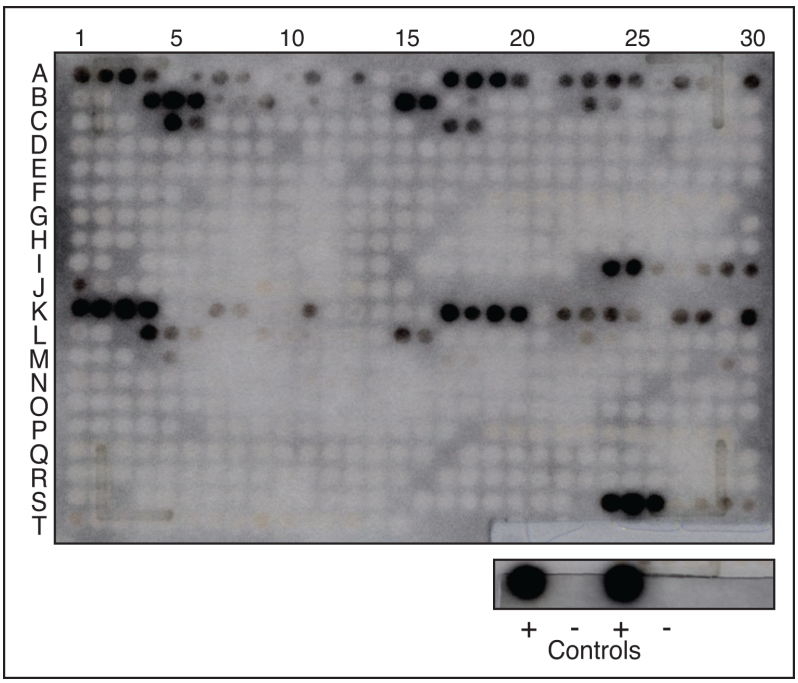

Figure 3.23 Sec61 N-terminal helix does not interact with Sbh1 cytosolic domain peptides. Peptide panning membrane was activated with methanol, blocked with 1 % BSA, probed with 2 µM biotinylated Sec61 N-terminal peptideand visualised using anti-biotin HRP antibody. The interactions seen with Sbh1 and Sbh2 N-terminal peptides correspond to the cross-reacting peptides seen previously. The spliced control spots were imaged separately.

Next, I investigated the interactions of Sbh1 cytosolic domain with SPs. I wanted to study the interactions of Sbh1 cytosolic domain with the SPs of proteins that depend on Sbh1 for their translocation. The first SP I analysed was that of Gls1, which depends on S3 T5 phosphorylated Sbh1 for its import. I probed the activated and blocked membrane with biotinylated Gls1 SP. I visualised the interactions using anti-biotin HRP antibody, shown in Figure 3.24(A). I saw strong interactions in positions A01 to F17, corresponding to Sbh1 M1 to K41 residues, including N-terminally acetylated residues. This was followed by a stretch of spots showing no interaction, from F19 to F29 corresponding to V24 to Y43 residues. Interactions picked up again from G01 to I22 spots where Sbh1 peptides end, i.e., A26 to L55 residues with varying intensities. Intensity of interactions seem to increase as the sliding frame moves towards the C-terminal end as it is including more CMP domain residues, from G30 to I22. In Sbh2, I saw strong interaction from I24 to J03 spots corresponding to N-terminal peptides M1 to G38 and interaction of varying intensities from J10 to J15 which corresponds to Sbh2 CMP region, with little to no interaction between J04 to J09. My results imply Gls1 SP shows strong interactions with Sbh1 N-terminal peptides and CMP peptides, and with Sbh2 N-terminal peptides.

I examined Sbh1 cytosolic domain interactions with the SP of another Sbh1 phosphorylation dependent substrate Irc22. I probed blocked peptide panning membrane with 2 µM biotinylated Irc22 SP and visualised their interactions, shown in Figure 3.24(B). I saw strong interactions with Sbh1 N-terminal peptides in spots A01 to F17, corresponding to M1 to K41 residues and no interaction with a stretch of spots from F19 to F29, corresponding to V24 to Y43 residues. Interactions picked up again from spots G01 to I22, starting weak but get stronger as they move towards Sbh1 CMP region. Similarly, for Sbh2, strong I24 to J03

interactions corresponding to N-terminal peptides M1 to G38, strong interactions from J10 to J15 spots corresponding to Sbh2 CMP region and weak to no interaction from J04 to J09 spots. Both Gls1 and Irc22 interactions are very similar, showing strong interactions with Sbh1 N-terminal peptides and CMP peptides, and with Sbh2 N-terminal peptides. This could be indicative of a pattern of interaction.

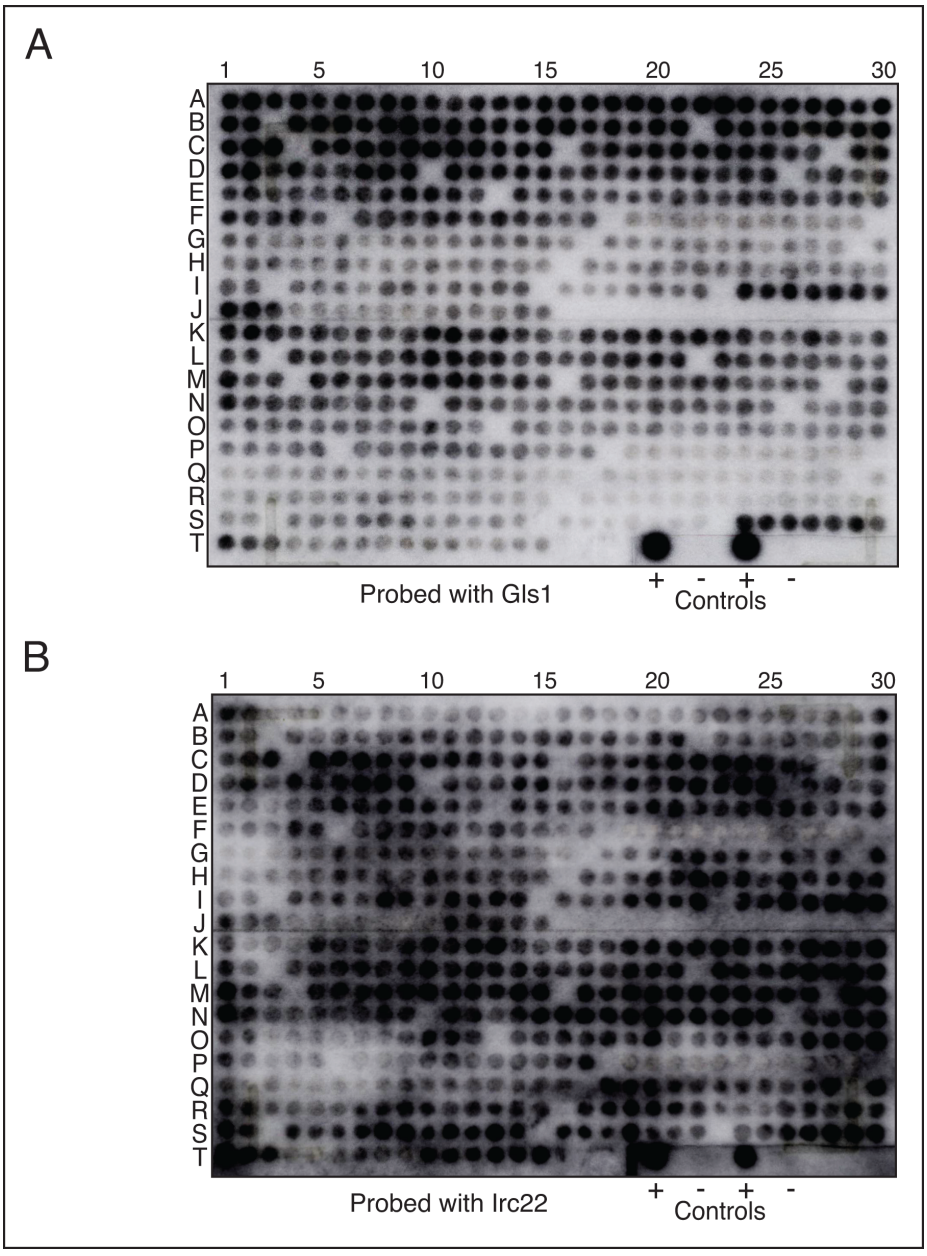

Figure 3.24 Sbh1 dependent signal peptides interact with Sbh1 N-terminal and CMP peptides. Peptide panning membrane was activated, blocked with 1 % BSA and probed with 2 µM biotinylated SPs. The interactions were detected by chemiluminiscence using anti-Biotin HRP antibody. Strong interactions were detected with Sbh1 N-terminal peptides in spots A01 to F17, F19 to F29 spots do not show any interaction, and interactions are seen again with Sbh1 CMP peptides in spots G01 to I22. Sbh2 N-terminal peptides in spots I24 to J03 and CMP peptides in spots J10 to J15 also interact with the SPs. **A)** Interactions with biotinylated Gls1 SP. **B)** Interactions with biotinylated Irc22 SP.

I further investigated Sbh1 cytosolic domain interactions with SPs of proteins not dependent of Sbh1 for their import into the ER. First, I probed the blocked peptide panning membrane with biotinylated ppCPY SP. I revealed interactions using anti-biotin HRP antibody, shown in Figure 3.25(A). I saw interactions of varying intensities between A01 to F17, corresponding to Sbh1 N-terminal peptides of M1 to K41 residues. I saw no further interactions with Sbh1 peptides. For Sbh2, I saw interactions between I24 to J03 spots corresponding to Sbh2 N-terminal M1 to G38 residues and with J11 to J15 spots corresponding to Sbh2 CMP region residues R35 to L62. My results imply the Sbh1 and Sbh2 N-terminal peptides, and Sbh2 CMP peptides interact generally with peptides.

Next, I looked at the interactions of ppαF SP, which is also not dependent on Sbh1 for its import, shown in Figure 3.25(B). I saw interactions of varying intensity between A01 to F17 spots of Sbh1 N-terminal M1 to K41 residues and no interaction with peptides between F19 to F29 spots. I further occasional interactions with spots H19 to H26 and I04 to I09 corresponding to Sbh1 N32 to D53. The peptides of the interacting spots include phosphorylation of T33, S44 and T48 residues which are not seen physiologically in Sbh1. For Sbh2, strong interactions seen between I24 and J03 corresponding to N-terminal, and weak interactions with J09 to J15 spots corresponding to Sbh2 P31 to L52 residues. N-terminal interactions of Sbh1 and the interactions of Sbh2 with ppαF SP match with the interactions with ppCPY SP. Sbh2 CMP peptides appear to interact with SPs in general.

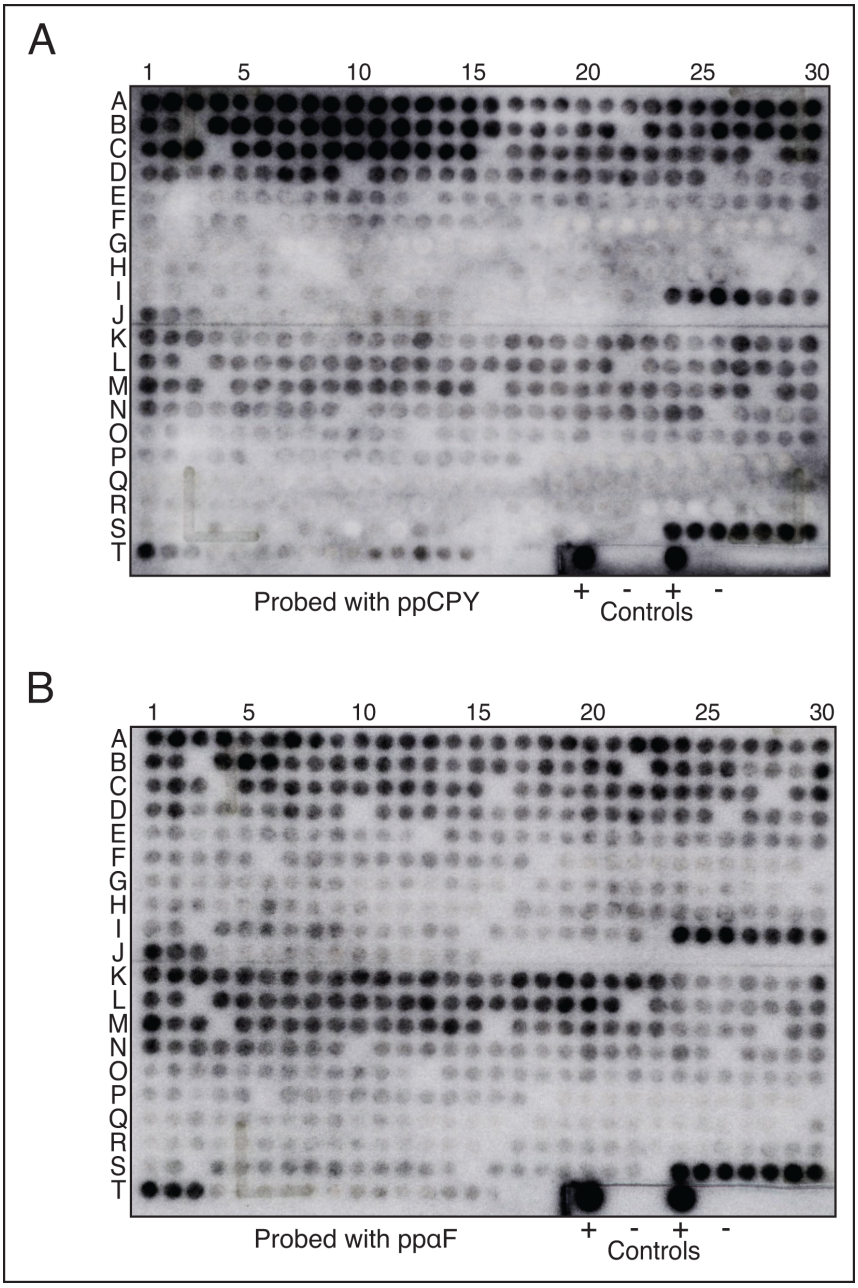

Figure 3.25 Sbh1 independent SPs do not interact with Sbh1 CMP peptides. Peptide panning membrane was activated, blocked with 1 % BSA and probed with 2 µM biotinylated SPs. The interactions were detected by chemiluminiscence using anti-Biotin HRP antibody. Strong interactions were detected with Sbh1 N-terminal peptides in spots A01 to F17. Sbh2 N-terminal peptides in spots I24 to J03 and CMP peptides in spots J11 to J15 also interact with the SPs. **A)** Interactions with biotinylated ppCPY SP. **B)** Interactions with biotinylated ppαF SP. Strong interactions are seen in spots H19 to 26 and I04 to I09 corresponding to Sbh1 CMP peptides with non-physiological phosphorylation states.

I observed that the peptide panning membranes often showed high background around the spots at the outer corners of the membrane, i.e., rows A and T and columns 01 and 30. This was likely due to the accumulation of proteins and peptides in the corners during the long incubation times with shaking. I tried to offset this with shaking in different angles and

rigorous washing. With each successive use of the membrane, there was a noticeable increase in the background noise. I analysed the imaged membranes using ImageQuant software to subtract background and normalised spot intensities using positive control spots as 100%. I only considered spots that were detected by the software as interactions.

Taken together, my results demonstrate that the Sbh1 N-terminal M1 to K23 residues tend to interact generally with SPs. Sbh1 V24 to I42 do not interact with any SPs. Residues Y43 to L55 interact specifically with Sbh1 dependent SPs. The interactions seem to be independent of Sbh1 S35 S38 phosphorylation. Sbh2 N-terminal M1 to G38 residues and CMP L49 to L62 residues also interact with SPs in general. Additionally, Sbh1 M1 to K23 and Sbh1 M1 to G38 also cross-react with streptavidin and anti-biotin HRP antibody. A peptide panning experiment with a randomised peptide needs to be performed to determine if these N-terminal interactions are SP and streptavidin/anti-biotin HRP antibody specific or if these residues interact non-specifically with proteins. The results of peptide panning analysis are summarised in Figure 3.26.

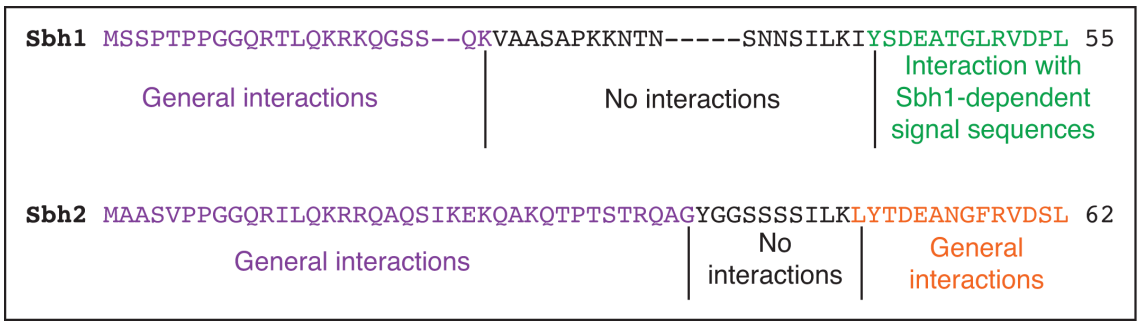

Figure 3.26 Summary of interactions between SPs and Sbh1/Sbh2. Sbh1 N-terminal M1 to K23 residues and Sbh2 N-terminal M1 to G38 residues show general interactions with SPs, streptavidin and anti-biotin HRP antibody and are highlighted in purple. Sbh1 CMP Y43 to L55 residues interact specifically with Sbh1 dependent SPs and are highlighted in green. Sbh2 CMP L49 to L62 residues interacts generally with SPs and are highlighted in orange.

Discussion 4

4. Discussion

My objective in this study was to better understand the function of Sbh1/Sec61β in ER protein translocation. For this purpose, I characterised the *S. cerevisiae Δsbh1 Δsbh2* mutant for defects in protein translocation, UPR, and respiratory competence. I evaluated the effect of Sbh1 in stabilising the Sec complex. Subsequently, I studied the functions of Sbh1 CMP domain and examined the interactions of the Sbh1 cytosolic domain with signal peptides and the Sec61 N-terminus.

Sbh1/Sec61β is the only non-essential subunit of the Sec61 complex. An estimated 12 % of signal peptides in *S. cerevisiae* depend on Sbh1 for their translocation into the ER [253]. Our lab had additionally identified a small number of proteins (2% of the secretome library) that are dependent on S3/T5 phosphorylation of Sbh1 for their transport into the ER [253]. Sec61β expedites co-translational translocation by directly interacting with the translating ribosome and aiding the insertion of nascent polypeptides into the Sec61 channel [223–225]. The cytosolic domain of Sec61β directly interacts with the signal peptides or N-terminal sequences of nascent polypeptides, likely contributing to their recognition [226,227].

In *S. cerevisiae*, the absence of Sbh1 combined with the absence of its paralog Sbh2 causes temperature-sensitivity at higher temperatures [75,222]. Supplementing the said *Δsbh1 Δsbh2* strain with truncated Sbh1 consisting of its TM domain and 5 cytosolic amino acids was sufficient to rescue the temperature-sensitive growth defect [222]. Sbh1 has previously been shown to be required for ER translocation of specific substrates [75,222]. The data available on translocation defects in *Δsbh1 Δsbh2,* however, was contradictory. The Sbh1 TM domain interacts with TM1 and TM4 of Sec61, as well as with TM3 of Sec63 in the Sec

complex. Whether these interactions within the TM domains stabilise the Sec complex was unknown.

The Sbh1 CMP region is 16 amino acid long and universally conserved, suggesting its functional importance (Figure 1.15) [218]. The truncated Sbh1 TM domain that could complement the temperature sensitivity defect in the *Δsbh1 Δsbh2* strain included 5 CMP residues that precede the TM helix [222]. The role of the Sbh1 CMP region was unknown prior to my work.

The N-terminal IDR of Sbh1 includes the first 38 amino acids and contains at least 7 phosphorylation sites [219]. These phosphorylation sites can potentially regulate the functions and interactions of Sbh1 by controlling the disorder-to-order transition of the cytosolic IDR into a stable structure that can interact with specific interaction partners [275,276]. The cytosolic IDR of mammalian Sec61β has been directly crosslinked to signal sequences of nascent polypeptide chains, but interactions of the Sbh1 unstructured cytosolic domain have not yet been explored [226,227].

Deletion of Sbh1 homolog MoSec61β in the rice blast fungus *Magnaporthe oryzae* leads to reduction in its pathogenicity and increases susceptibility to plant immunity [277]. Sbh1 is essential for virulence *Cryptococcus neoformans* where it regulates the biogenesis of virulence factors [278]. Mutations in the gene encoding human Sec61β, *SEC61B*, have been linked to polycystic liver disease [128]. Upregulation of *SEC61B* has been suggested as a biomarker for early detection of colorectal cancer [241]. Investigating the function of

Sec61β/Sbh1 could provide crucial insights into the underlying mechanisms of these pathologies, potentially leading to the development of novel therapeutic approaches.

In this work, I started with characterising *Δsbh1 Δsbh2* for defects in protein translocation, UPR, and respiration. I then explored the stability of Sec complex in the absence of Sbh1 at permissive and restrictive temperatures, and under high salt conditions. Based on a MD simulation by Pratiti Bhadra that identified a potential site for interacting with Sec61 N-helix in the Sbh1 CMP region, I created CMP mutants using site-directed mutagenesis and assessed their ER import efficiency. Finally, to explore the interactions of the Sbh1 cytosolic domain, I used peptides representing the Sbh1 cytosolic domain synthesised onto an acid-hardened cellulose membrane and probed these with the Sec61 N-terminal helix and Sbh1-dependent and Sbh1 independent synthetic biotinylated signal peptides. I discovered that signal peptides dependent on Sbh1 for their import into the ER specifically interacted with the Sbh1 CMP domain. Based on my data, I hypothesised that Sbh1 acts as a gatekeeper for ER import and aids specific signal peptides for insertion.

4.1. Characteristics of the Δ*sbh1* Δ*sbh2* Mutant Strain

As the first step in deducing the role of Sbh1 in yeast, I characterised the *Δsbh1 Δsbh2* mutant (Section 3.1). It was previously shown that deletion of both *SBH1* and its paralog *SBH2* leads to a growth defect at 37 ˚C, while the deletion of only one of either genes does not result in a growth phenotype [75,216,222]. The *Δsbh1 Δsbh2* strain showed reduced levels of mannosidase 1 (Mns1) and glucosidase 1 (Gls1) even at permissive 30 ˚C, leading to an N-glycan trimming defect [222]. The temperature-sensitivity and the N-glycan trimming defects

were rescued when the *Δsbh1 Δsbh2* cells were complemented with only the Sbh1 TM domain and five preceding CMP residues (residues 50 – 75 of Sbh1p) [222]. The TM domain of Sbh2 alone can also salvage Sbh1 TM domain function in the Sec61 complex [222].

Reports on the translocation dynamics of the *Δsbh1 Δsbh2* strain, however, were contradictory. In intact yeast cells, Finke *et al.* found moderate defects in the post-translational translocation of α factor precursor ppαF and in the transport of co-translationally and post-translationally translocated Kar2 precursor pKar2 in *Δsbh1 Δsbh2* cells at both permissive 30 ˚C and restrictive 37 ˚C [75]. In *in vitro* translocation experiments in a heterologous translocation system consisting of yeast microsomes and reticulocyte lysate, they found a 2- to 5- fold reduction in the rate of transportation of ppαF and bacterial proOmpA into the mutant membranes as compared to wildtype membranes [75]. In contrast, the *in vitro* translocation experiments using homologous yeast translation-translocation system with microsomes and yeast cell extract, resulted in moderate post-translational and co-translational transportation defects into *Δsbh1 Δsbh2* membranes at 37 ˚C [222]. The difference in the defects seen can be attributed to the different in vitro translocation systems used or different strain backgrounds. To obtain a clearer picture of protein translocation in the absence of *SBH1* and *SBH2*, I looked at the import of precursors of Kar2, α factor, PDI, and CPY in intact yeast cells.

Accumulation of Kar2 precursor pKar2 in *Δsbh1 Δsbh2* mutants had previously been reported at even at permissive 30 ˚C [75]. Since 24 ˚C was shown to be permissive to the grown of *Δsbh1 Δsbh2* before, I chose 24 ˚C as the permissive temperature and 38 ˚C as the restrictive temperature for my protein translocation experiments [222]. I planned to grow the

strains at the permissive temperature, shift them to the restrictive temperature for a fixed period of time to induce translocation defects and analyse proteins in the cell extracts by Western blotting. To optimise the shift period, I analysed the pKar2 in *Δsbh1 Δsbh2* strain grown at 24 ˚C, shifted to 38 ˚C for 2 h, 3 h, 4 h and 5 h. The *Δsbh1 Δsbh2* cells grown only at 24 ˚C did not show pKar2 accumulation, confirming that 24 ˚C functions as permissive temperature (Supplementary Figure 1(B)). Accumulation of pKar2 was seen in *Δsbh1 Δsbh2* cells after each shift period, while the resolution between the pKar2 and Kar2 bands decreased from the 4 h mark possibly as the cells began to upregulate Kar2 due to ER stress (Supplementary Figure 1(B)) [124]. This experiment was performed by students of M.Sc. class of Infection Biology in 2019 under my supervision. These results led me to choose 3 h as the optimal shifting period for my experiments as the corresponding cell extract showed distinct bands for pKar2 and Kar2. This optimisation experiment also established that precursor accumulation in *Δsbh1 Δsbh2* could also be analysed by the less sensitive Western blotting method instead of pulse-labelling method using [^{35}S]-Met as in previously published experiments [75,222]. I repeated the experiment and found accumulation of pKar2 only in *Δsbh1 Δsbh2* cells grown at restrictive temperature (Figure 3.1(A)). Guido Barbieri concurrently found accumulation of pKar2 in *Δsbh1 Δsbh2* using [^{35}S]-Met/Cys pulse-labelling of cell extracts [75,253].

As Kar2 is translocated both co-translationally and post-translationally into the ER, either or both transport pathways could have been affected. I first looked for defects in post-translational translocation of α factor precursor ppαF, which was previously found to be defective in *Δsbh1 Δsbh2* mutants [75,222]. As the *SBH1 SBH2* and *Δsbh1 Δsbh2* strains I was using for my experiments were of mating type a, I transformed the strains with p416 plasmid

expressing wildtype *MFalpha1*. In contrast to previous reports, I did not find a defect in ppαF translocation at 38 ˚C in the *Δsbh1 Δsbh2* strain, while the control *sec61-32* strain showed a distinct defect at its restrictive temperature (Figure 3.1 (B)). Similar conclusion was derived from a parallel experiment performed by Guido Barbieri in our lab [253]. I also investigated the translocation of two additional post-translationally translocated proteins, PDI and CPY. I analysed cell extracts for the PDI by Western blotting and did not detect the presence of its precursor pPDI, suggesting that its import is not affected in the absence of Sbh1 (Figure 3.1 (C)). I investigated the incorporation of CPY precursor ppCPY into the ER by pulse-labelling *Δsbh1 Δsbh2* cells grown at 38 ˚C with [^{35}S]-Met/Cys and detected the presence of its ER glycosylation product p1CPY, implying efficient import into the ER and processing of ppCPY (Figure 3.1 (D)). Combined, my results imply an absence of post-translational translocation defects.

No translocation defect was detected in the co-translational translocation of DPAPB in *Δsbh1 Δsbh2* strain in contemporaneous experiments performed at our lab [253]. Altogether, my results support the observation that the absence of general translocation defects in the *Δsbh1 Δsbh2* strain. The translocation defect in the import of Kar2 precursor appears to be specific for the protein. Two other substrates that were known dependent on Sbh1 for their import into the ER, Gls1 and Mns1, were found to be dependent on phosphorylation of Sbh1 at S3/T5 residues [222,253]. Recent studies at our lab showed that while the import of pKar2 into the ER is dependent on Sbh1, it is independent of its S3/T5 phosphorylation and the exact mechanism of its translocation is not yet known.[253]. Kar2 plays several roles in protein processing: it participates in ER import of newly synthesised proteins, acts as a chaperone during protein folding, and maintains proteostasis through the UPR. Due to its critical

functions, Kar2 biosynthesis is likely regulated by multiple mechanisms and not wholly dependent on Sbh1. My results, and concurrent observations made in our lab, indicate that pKar2 relies on Sbh1 for its import into the ER under specific physiological conditions [253].

At times of ER stress the UPR is induced, causing a substantial upregulation of Kar2 [124,258]. Kar2 binds to precursors of secretory and TM proteins in the ER lumen to prevent misfolding. In the absence of folding intermediates, Kar2 is bound to Ire1 to inactivate it [173]. During the UPR, Kar2 dissociates from Ire1 to bind to excess unfolded proteins and Ire1 is in turn activated which starts a signalling cascade to increase levels of Hac1p by HAC1-mRNA splicing, another component of UPR [258]. As the *Δsbh1 Δsbh2* strain exhibits defective Kar2 precursor translocation into the ER, I was prompted to check if the strain also has UPR defects. I performed a growth assay of *Δsbh1 Δsbh2* on YPD plates containing tunicamycin, a known UPR inducer [259]. The *Δsbh1 Δsbh2* strain, in the presence of tunicamycin, showed growth comparable to that of *SBH1 SBH2* (Figure 3.2 (A)). My result shows that even with translocation defect, Kar2 function and UPR are not affected when Sbh1 and Sbh2 are absent. This observation was confirmed in a parallel experiment by Guido Barbieri in our lab [253].

I also examined *Δsbh1 Δsbh2* for respiratory competence. *S. cerevisiae* is a facultative anaerobe [279]. A previous study showed that Sec61 loop mutants that lost respiratory competence had low growth rates and this correlated with their co-translational ER import defects and delayed post-translational ER import [57]. Since the *Δsbh1 Δsbh2* strain has a specific defect in the import of co-translationally and post-translationally translocated Kar2 precursor, I assayed its growth on non-fermentable YPGlycerol medium. I found that the growth of *Δsbh1 Δsbh2* was unaffected, similar to its wildtype *SBH1 SBH2*, unlike the controls

rho0 and *Δcox6* (Figure 3.2 (B)). A recent study by Phuong *et al.* suggested that UPR upregulation by *HAC1*-mRNA splicing is aggravated in hypoxic conditions and this ER stress is alleviated by both mitochondrial respiration and Ero1-mediated oxidative protein folding [280]. The lack of UPR defects and the retention of respiratory competence in *Δsbh1 Δsbh2* seen in my results imply that Sbh1 is not vital for ER proteostasis.

4.2. Sbh1 does not Contribute to Sec complex Stability

In the recently published cryo-EM structure of the Sec complex in yeast, the TM3 of Sec63 interacts with the TM of Sbh1, as well as TM1 of Sec61 [63]. The TM of Sbh1 also interacts with TM1 and TM4 of Sec61 [63,221]. The complementation of *Δsbh1 Δsbh2* cells with Sbh1 TM including 5 preceding cytosolic residues is sufficient for alleviation of its translocation defects and temperature-sensitivity [222]. These observations motivated me to investigate whether the interactions of Sec63 and Sec61 with the TM of Sbh1 stabilise the Sec complex, especially at higher temperatures, as described in Section 3.2.

I planned to study the Sec complex stability in the absence of Sbh1 by precipitating the Sec complex with ConA-Sepharose, which binds to the internal mannose residues of the only *N*-glycosylated subunit of the Sec62-Sec63 complex, Sec71. The established method for ConA precipitation of the Sec complex utilises digitonin as the detergent to solubilise microsomal membranes in native conditions [248]. Digitonin, however, is a natural product with limited availability, and shows high inter-batch and intra-batch variations in efficiency, requiring titration for each batch prior to use [263]. In the interest of time and resources, I sought cost-effective alternatives to digitonin to use in my experiments (Section 3.2.1). The first detergent

I tested was PCC-α-M, a novel derivative of DDM often used to stabilise membrane proteins in functional studies [265]. PCC-α-M could effectively solubilize the Sec complex but could not keep it stable during ConA precipitation (Figure 3.3). Another detergent I tested was DBC, which was previously used to solubilise the Sec61 complex from yeast microsomes [59]. DBC could solubilise the Sec complex but was not effective enough in stabilising it during a ConA experiment, as the complex subunits could be found in the unbound, free fraction (Figure 3.4). As the alternative detergents were ineffective, I chose to continue using digitonin for my experiments. To avoid problems associated with batch-to-batch variation, I acquired a substantial quantity of digitonin which Prof. Römisch was able to finance through an 'Anschubfinanzierungs-Grant' from the Forschungsausschuss of the UdS. I tested this batch of digitonin first, and confirmed it as appropriate for ConA precipitation experiments. The new batch of digitonin, acquired from Matrix Bioscience, efficiently solubilised the Sec complex while maintaining its integrity, see Supplementary Figure 3.

In Section 3.2.2, I investigated whether Sbh1 contributes to the interaction between Sec61 and Sec63 in the Sec complex by determining the stability of the Sec complex in microsomes derived from *Δsbh1 Δsbh2* cells grown at the permissive temperature of 24 ˚C. Since Sbh1 is essential for growth at elevated temperatures, I also determined Sec complex stability in microsomes derived from *Δsbh1 Δsbh2* grown at 38 ˚C to evaluate of Sbh1 is necessary for this interaction at the restrictive temperature. I compared the Sec complex stability to that in *Δsbh1 Δsbh2* microsomes to its stability in microsomes derived from wildtype *SBH1 SBH2* strain grown at 24 ˚C and 38 ˚C. As a control, I also solubilised microsomes in TX-100 at each condition. TX-100 dissociates the Sec62-Sec63 complex from the Sec61 complex. I saw that the Sec complex in the wildtype membranes was stable at both 24 ˚C and 38 ˚C, as expected.

The Sec complex in *Δsbh1 Δsbh2* remained stable at both 24 ˚C and 38 ˚C as well (Figure 3.5). I repeated this experiment twice with different batches of microsomal preparations and made the same observations. My results imply Sbh1 is not essential for the stability of the Sec complex, under my experimental conditions. This result was later published in collaboration with Pratiti Bhadra [266].

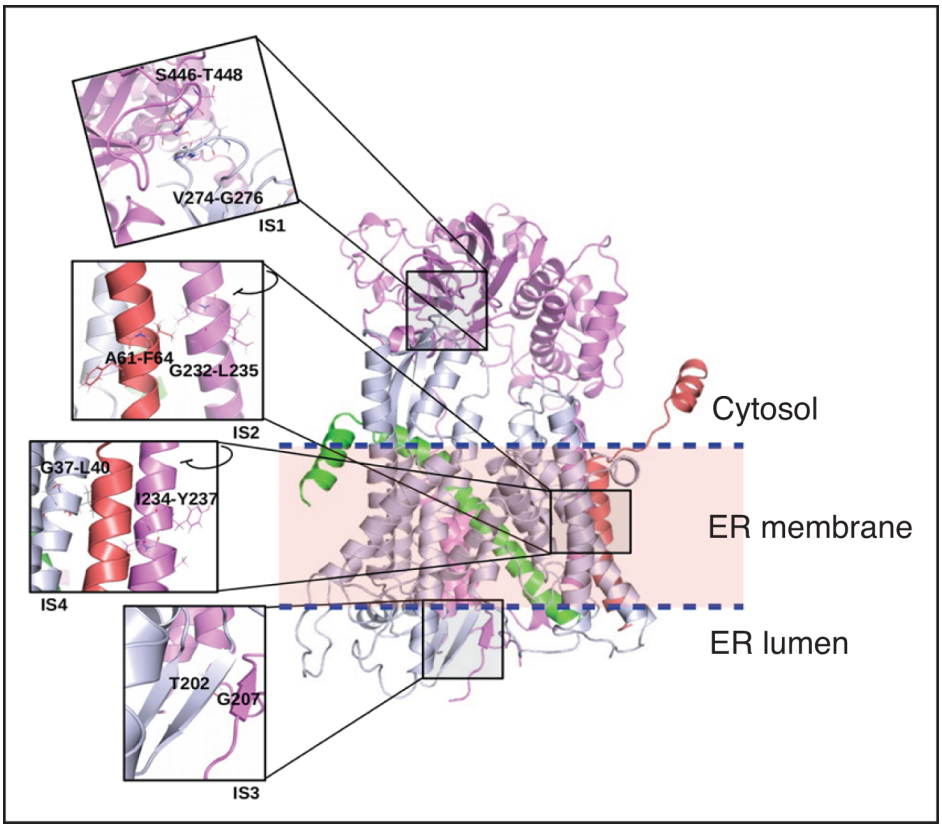

Figure 4.1 Interaction sites between Sec63 and Sec61 complex subunits. Sec63 is coloured in pink, Sec61 in grey, Sbh1 in red and Sss1 in green. The four interaction sites (IS) seen in cryo-EM structure are magnified. Interacting residues are as follows: IS1) V274-G276 of Sec61 and S446 to T448 of Sec63. IS2) A61-F63 of Sbh1 and G232-L235 of Sec63. IS3) T202 of Sec61 and G207 of Sec63. IS4) G37-L40 of Sec 61 and I234 to Y237 of Sec63. *Figure from Bhadra et al., 2021.*

Subsequent to my initial Sec complex stability experiments, Pratiti Bhadra had shown that Sec63 and Sec61 stably interact at 4 sites, two of which, IS2 and IS4, are in the ER membrane and close to where they individually interact with Sbh1 [266] (Figure 4.1). Given this new perspective about the Sec63-Sec61 interactions in the Sec complex, it is likely the Sec complex is stabilised by several interactions. Although Sbh1 contributes to the Sec61-Sec63 TM domain

interactions, in its absence the other two interactions, IS1 and IS3, seem to be sufficient to stabilise the Sec complex. This could explain the stability of the Sec complex that I saw in my experiment in Figure 3.5.

In Figure 4.1, the interaction at IS1 is likely electrostatic and the interaction at IS3 is polar [266]. I therefore tested the stability of the Sec complex again by ConA precipitation, this time in the presence of high salt to destabilise the polar/electrostatic interactions between Sec61 and Sec63. Through a pilot experiment, I optimised 800 mM as the salt concentration to use as this was the highest concentration I could realistically achieve without compromising the total volume of each sample or the quality of the final Western blot (Supplementary Figure 3). I first solubilised the microsomes in digitonin and destabilised the polar/hydrophobic interactions by raising the salt concentration to 800 mM, twice the concentration in the previous experiment, followed by ConA precipitation. I found that the Sec complex stability in *Δsbh1 Δsbh2* was unaffected by the increase in salt concentration both in microsomes derived at 24 ˚C and at 38 ˚C (Figure 3.6). This result reaffirms that Sbh1 does not contribute to the Sec61-Sec63 TM domain interactions.

Throughout my ConA precipitation experiments, I noticed a recurring 70 kDa band close to Sec63 in its molecular weight cross-reacting with the Sec63 antibody, marked by an * in Figures 3.5 and 3.6. A band at the same location was also observed by Falcone *et al.* in their ConA precipitation experiments, whose method I used as reference [248]. To determine whether this band can be attributed to a protein cross-reacting with the Sec61 antibody, I treated microsomes derived from *Δsbh1 Δsbh2* and *SBH1 SBH2* strains grown at 24 ˚C and 38 ˚C with protease inhibitors and probed them with Sec63 antibody after Western blotting.

These microsomes were from the same preparation that I had previously used for testing the stability of the Sec complex, shown in Figure 3.5. I also analysed microsomes derived from *sec63-201* strain grown at restrictive 37 ˚C as a control for this experiment. The *sec63-201* strain expresses a truncated form of Sec63 in which C-terminal 27 residues are deleted [89]. I did not observe the 70 kDa band in any of the microsomes tested (Figure 3.7 (A)), indicating that the protein in question was not present in the microsomes used. This could be the case if the 70 kDa band was a product formed during a ConA experiment, either due to protein degradation or protein aggregation. I performed a ConA precipitation experiment using *Δsbh1 Δsbh2* and *SBH1 SBH2* microsomes from strains grown at 24 ˚C and 38 ˚C and *sec63-201* microsomes from the strain grown at restrictive 37 ˚C as control. I first probed the resulting immunoblot with only anti-Sec63 antibody and detected the 70 kDa band in all unbound (F) fractions (Figure 3.7 (B)). I further probed the blots for Sec61 and Sss1 and found that the Sec complex remained stable in this experiment (Figure 3.7 (B)), and the result was comparable to the previous experiment (Figure 3.5). The Extraction Buffers and the Equilibration Buffers used in the method for ConA precipitation contain protease inhibitors. Since the 70 kDa band was present only in immunoblots from ConA experiments and could be detected when probed only with anti-Sec63 antibody, I concluded that the 70 kDa band was likely a degradation product of Sec63 that formed during the long incubation times during a ConA precipitation. This partial degradation of Sec63 did not affect the ability of the cells to form a stable Sec complex. The truncated Sec63 expressed by *sec63-201* strain was previously shown to have an impaired interaction with Sec62, while still being functional [89,267]. The stability of the Sec complex in *sec63-201* strain seen in my results (Figure 3.7 (B), Lanes 19 & 20) confirm the previous observation made by *Young et al.* that the role of Sec63 in stabilising the Sec complex is independent of its interaction with Sec62 [267].

I planned to use Blue Native PAGE as an alternative method to evaluate Sec complex stability. A pilot experiment to optimise the method showed promising results. Due to technical difficulties faced during the establishment of a Native PAGE setup I decided not to pursue the experiment further.

Taking all my results from the ConA precipitation experiments together, I conclude that Sbh1 does not contribute to the interactions between Sec63 and Sec61 TM domains under my experimental conditions and is not essential for the stability of the Sec complex even at higher temperatures. The Sec complex stability is effectively maintained even when the polar and electrostatic interactions between the subcomplexes are disrupted. Recent studies on the Sec channel revealed several interaction sites between the Sec61 complex and the Sec62-Sec63 complex with varied physiochemical properties [63,108,281]. The Brl domain of Sec63 is essential for the assembly of the Sec complex and interacts with Sec61 at TM6-TM7 and TM8-TM9 cytosolic loops to form a static anchor point [63,282]. TM3 of Sec63 also interacts with the TM of Sss1, and the N-terminus of Sec63 wedges between Sss1 and TM5-TM6 loop of Sec61 in the ER luminal [63,108]. The TM1 of Sec62 interacts with the N-terminal and TM3 of Sec61 [283]. These diverse interactions likely contribute to the robustness of the Sec complex, keeping it stable and functional.

The cytosolic domain of mammalian Sec61β has previously been crosslinked directly to ER targeting sequences, suggesting that it extends into the large ribosomal subunit channel [226]. Sec61β was also shown to directly interact with ribosomes during co-translational translocation [224,225]. I wanted to investigate whether such an interaction between Sbh1 cytosolic domain and the ribosome in yeast stabilises the Sec61 – ribosome complex, and

whether Sbh1 plays a role in Sec61-ribosome complex stability at elevated temperatures (Section 3.2.3). I intended to examine the Sec61-ribosome complex stability in the absence of Sbh1 by fractionating ribosome associated membrane proteins (RAMPs) and precipitating from the non-ribosome bound fractions with ConA starting with microsomes from the *Δsbh1 Δsbh2* strain grown at 24 ˚C and 38 ˚C. I wanted to compare the amount of Sec61 complex in the RAMP fraction to that in microsomes from the wildtype *SBH1 SBH2* strain grown at 24 ˚C and 38 ˚C. I began with optimising the experiment using *SBH1 SBH2* microsomes from cells grown at 24 ˚C.

In my first experiment I probed for Sec61, Sec62, Sec63 and Sss1. I did not observe any bands in the RAMP fraction, which should at least show a band correlating to Sec61 (Figure 3.8). I probed the immunoblot again for the ribosomal protein RpL17a to determine whether the ribosomes had been sufficiently pelleted and removed during ultracentrifugation. I found RpL17a bands in every fraction (Figure 3.8), implying that ribosomes had not been fully dissociated from associated membrane proteins, the dissociated ribosomes were not fully pelleted by ultracentrifugation and contaminated the supernatants that were next used for ConA precipitation. In subsequent experiments, I optimised the puromycin concentration in the RAMP buffer (Figure 3.9) and rectified ribosome contamination in the supernatants by using a sucrose cushion to prevent accidental re-uptake of ribosomes from the pellet during removal of the supernatant (Figure 3.10). Yet, I was unable to fully sediment ribosomes during ultracentrifugation. In my second experiment, I increased the speed and duration of the two ultracentrifugation steps, from 60,000 rpm for 30 mins and 100,000 rpm for 30 mins to 90,000 rpm for 1 h and 100,000 rpm for 2 h (TLA-120.1 Rotor, Beckman Coulter), respectively. This resulted in the aggregation of significant amounts Sec61 in the solution due to the prolonged

duration of the run and the second ultracentrifugation step was still insufficient to completely pellet the ribosomes (Figure 3.9). I tried to increase the g force of the second ultracentrifugation, but this began to test the technical limits of the tabletop centrifuge I was using (Optima^{TM} MAX-XP Ultracentrifuge, Beckman Coulter). Considering multiple equipment failures disrupting my experiment, I decided to discontinue this study.

During the RAMP fractionation optimisation experiments, I faced multiple technical issues while running the ultracentrifugation steps in the instrument I used. The alternative ultracentrifuge available to me in Saarbrücken (Optima^{TM} TL 100 Ultracentrifuge, Beckman Coulter) was unable to function at the speeds I was using, and prematurely terminated the runs. Lower speeds only increased the aggregation of Sec61 in solution. Due to delays in purchasing a new ultracentrifuge and delays in its delivery due to the COVID-19 pandemic, I was unable to continue with investigating the contribution of Sbh1 to the Sec61 channel-RNC complex stability.

The interaction between Sec61 TM1 and Sec63 TM3 within the Sec complex prompted my interest in examining whether this interaction undergoes any changes at restrictive temperatures [63,283]. As a different approach to study the Sec complex at elevated temperature, I planned to co-precipitate Sec61 with its complex subunits Sbh1 and Sss1 in *SBH1 SBH2* microsomes obtained from the strain grown at 38 ˚C (Section 3.2.4). I first wanted to optimise the method using *SBH1 SBH2* microsomes from cells grown at 24 ˚C (Figure 3.12). Regrettably, absence of a functioning ultracentrifuge in our lab or the neighbouring labs in Saarbrücken prevented me from conducting the experiment as planned. It would be

advantageous for another researcher to pursue this idea, given the potential importance of the findings.

4.3. Sbh1 CMP Domain Plays a Role in Import of Specific Substrates into the ER

The cryo-EM structure of the Sec complex shows that the Sec61 N-terminal amphipathic helix is deeply embedded in the ER membrane and its TM1 and TM4 interact with the TM of Sbh1 in the Sec complex [63]. The N-terminal helix of Sec61 is critical for protein import into the ER [274]. Given the interaction between their TM domains and their close proximity in the ER membrane, there is a possibility of an interaction between the patch of positively charged amino acids in the Sbh1 cytosolic domain and the negatively charged amino acids in the amphipathic Sec61 N-terminal helix. Pratiti Bhadra simulated this interaction by molecular dynamics (MD) modelling and observed that the segment ^{19}EVIAPERK^{26} of Sec61 makes contact with ^{45}DEATGLRV^{52} of Sbh1, of which ^{45}DEATG^{49} remained in persistent close contact (less than 5 Å) (Figure 3.12) [268]. This contact site in Sbh1 is a part of its CMP region. Previous experiments that showed the growth defect in *Δsbh1 Δsbh2* cells at 38 ˚C was restored when the cells are compensated with truncated Sbh1 TM domain which included a part of its CMP preceding the TM domain, ^{50}LRVDP^{54} (Figure 3.12) [222]. Its potential significance in the interactions of Sbh1 compelled me to study the Sbh1 CMP domain, which I detailed in Section 3.3.

The Sbh1 P54 and V57 residues had been shown previously to be critical for the interactions with Sec61 TM1 and TM4 domains (Figure 1.15) [221]. Zhao & Jäntti also hypothesised that the rigid P54 residue at the start of the Sbh1 TM domain acts as a hinge,

likely orienting the Sbh1 cytosolic domain towards away from the Sec61 lateral gate during channel opening [64,221]. I wanted to investigate the effect P54 on Sbh1 function and included it in my CMP mutant study.

I explored the function of the Sbh1 CMP domain within Sbh1 by mutating the CMP domain and characterising the resulting phenotypes. I generated mutations in *SBH1* using site directed mutagenesis method, by substituting the targeted residues with A (Figure 3.13). I first generated mutations in D45-G49, L50-V52 and P54 residues and later combined the mutations in various combinations, including a full CMP mutation to A (referred to as "combo mutants") (Table 3.1). After confirming mutagenesis by DNA sequencing, I inserted the mutated *sbh1* sequence in yeast centromeric vector pRS415 and transformed the *Δsbh1 Δsbh2* strain (KRY 588) with the plasmid for my experiments. As controls, I transformed the KRY 588 strain with pRS415 containing wildtype SBH1 coding sequence as the wildtype *SBH1* strain and KRY 588 strain transformed with empty pRS415 as *Δsbh1 Δsbh2* strain for reference. Using *SBH1* expressed from the same plasmid as control instead of using chromosomally expressed *SBH1* is critical because the amounts of Sbh1 in the cell are higher when *SBH1* is expressed from a plasmid, even if it is a CEN plasmid (Römisch lab, unpublished).

I characterised the individual *sbh1* CMP mutants I had generated, *sbh1D45-G49A, sbh1L50-V52A,* and *sbh1P54A* had no growth defects at low or high temperatures (20 ˚C and 38 ˚C) as compared to the wildtype strain (Figure 3.14). While growing combo mutants, *sbh1D45-G49A/P54A, sbh1D49-V52A, sbh1L50-V52A/P54A* and *sbh1D49-V52A/P54A,* for determining their growth rate at 30 ˚C, I noticed inter-colony variations in growth rate within each combo mutant. Suspecting a temperature sensitivity defect at even 30 ˚C, I performed a

qualitative growth test for each of the combo mutants using 5 different colonies from newly transformed strains. I found variations in growth among the 5 colonies of each mutant even at 25 ˚C, which I had used as permissive temperature (Figure 3.15). I repeated the experiment using newly transformed mutants and did not see consistent growth among colonies. It appeared that mutating the Sbh1 CMP region impaired its function, but the cells appear to adapt to these changes to achieve growth comparable to the wildtype. As the combo mutants proved impractical to work with due to their variations in growth and fast adaptations, I decided to not characterise these strains further.

I continued with the characterisation of *sbh1D45-G49A, sbh1L50-V52A* and *sbh1P54A* strains (referred to as "CMP mutants"). When I repeated the Western blotting experiments to determine the levels of Sbh1 and the Sbh1-dependent translocation substrate, Gls1, in the CMP mutants 2 weeks after the first experiment, I noticed that the strains had adapted by adjusting their Sbh1 levels such that their Gls1 levels were closer to that expressed by wildtype cells (Figure 3.16). The CMP mutants can potentially achieve this by reducing their rate of protein translation to allow for efficient protein import, as is the case for yeast SRP mutant strains [284]. In the case of *sbh1L50-V52A,* the decrease in Gls1 level from 170 % to 128 % after two weeks could also be caused by the elimination of excess Gls1 from the cells. I transformed the *Δsbh1 Δsbh2* strain again with Sbh1 CMP mutant plasmids and analysed the Sbh1 and Gls1 levels in 5 colonies of each CMP mutant within one week of transformation. The Sbh1 and Gls1 levels in these new transformants matched those seen in my first experiment with freshly transformed CMP mutants (Supplementary Figure 9). This proved mutations in the Sbh1 CMP region raised more complications than deleting it entirely, and with time CMP mutants adapt to efficiently compensate for the defects in their mutant Sbh1

function. To avoid discrepancies in results, I ensured to always use fresh transformants, no older than 10 days since transformation, for all further experiments. I cryo-preserved the colonies used for the experiment shown in Figure 3.17 4 days after their transformation and used these to repeat experiments as needed.

The *sbh1* CMP mutants had altered levels of Sbh1 protein (Figure 3.17). I detected elevated Sbh1 levels in the *sbh1D45-G49A* mutant, a near 50% reduction in *sbh1L50-V52A* while *sbh1P54A* showed a normal amount of Sbh1 as compared to the wildtype (Figure 3.17, left). The import of Sbh1-dependent substrate Gls1 was close to wildtype levels in *sbh1D45-G49A* and had increased in *sbh1L50-V52A* and *sbh1P54A* (Figure 3.17, right). Next, I analysed the mutants for defects in general protein import into the ER. I did not detect the presence of cytosolic precursors of co-translationally translocated DPAPB, post-translationally translocated PDI and CPY, or co-translationally and post-translationally translocated Kar2 in the mutants in any of the CMP mutants (Figure 3.18), indicating the absence of general protein translocation defects. While the import of pKar2 is dependent on Sbh1, it is independent of Sbh1 S3/T5 phosphorylation [253]. The import of Gls1 is dependent Sbh1 S3/T5 phosphorylation [253]. These results collectively imply that Sbh1 CMP domain plays a role in the import of specific proteins dependent on Sbh1 N-terminal S3/T5 phosphorylation for their efficient import. The levels of other Sbh1 S3/T5-phosphorylation-dependent substrates such as Mns1 need to be investigated for a definitive conclusion.

S3/T5 phosphorylation dependent Sbh1 substrates Gls1 and Mns1 are involved in glycan processing in the ER [253]. A reduced amount of Gls1 and Mns1 in the ER leads to *N*-glycan trimming defects in *Δsbh1 Δsbh2* cells even at permissive temperature [222]. *N*-glycan

trimming is critical for targeting misfolded proteins for ERAD [285,286]. However, *Δsbh1 Δsbh2* strain are not defective in ERAD or the UPR (Figure 3.2) [222,287]. Complementing *Δsbh1 Δsbh2* cells with truncated Sbh1(50-75), which includes 5 residues of the CMP domain, rescues the *N*-glycan trimming defect [222]. The variation in the amount of Sbh1 available in CMP mutants and its efficiency in importing Gls1 suggests that Sbh1 possibly acts as a "gatekeeper" for the import of Sec61 channel specific proteins that are critical for ER function. The Sbh1 CMP possibly aids insertion of these proteins through direct interaction or through its potential interaction with Sec61 N-terminal helix suggested by molecular dynamics simulation (Figure 3.12). The adaptation in CMP mutants to maintain wildtype equivalent Gls1 levels with time implies that the gatekeeping function is impaired, but not fully lost. Studying translation kinetics of Gls1 in CMP mutants could reveal if this adaptation occurs through modifying the rate of protein translation.

The "gatekeeper" function of Sec61β/Sbh1 has been implied in virulence of pathogenic fungi and to polycystic liver disease. Deletion of *MoSEC61β* in rice blast fungus, *Magnaporthe oryzae,* results in abnormal secretion and localisation of its apoplastic factors leading to a reduction of its virulence [277]. Sbh1 in *Cryptococcus neoformans* regulates the biosynthesis and secretion of virulence factors and is thereby essential for its virulence. In polycystic liver disease caused by the inactivation of Sec61β, the biogenesis of cyst determinant protein Polycystin-1 is impaired, and the reduction in its dosage leads to cyst formation in biliary epithelium of the liver [128].

Truncated Sbh1(50-75) that includes CMP residues could interact with other Sec61 complex subunits Sec61 and Sss1 [222]. As Sbh1 CMP mutants affect protein translocation,

they likely associate with other Sec61 complex and Sec complex proteins. Their presence in Sec61 complex can be verified by crosslinking Sbh1 CMP mutant with Sec61 complex subunits. Its presence in the Sec complex can be determined by ConA precipitation.

To gain insight into the structure-function relationship of Sbh1 CMP mutant proteins, I used PSIPRED Protein Analysis Workbench to predict the 2D structure of the protein [288]. The program predicted an α-helix that included 6 residues between the C-terminal end of the unstructured cytosolic domain and the CMP region in wildtype Sbh1, the length of which shortened to three residues in Sbh1L50-V52A and increased to 7 residues in Sbh1P54A (Supplementary Figure 13). Recent advances in protein structure prediction tools made it possible to visualise 3D structures of proteins with intrinsically disordered regions (IDR) with high accuracy. I predicted the possible 3D structures of sbh1 CMP mutants using AlphaFold ColabFold. The structures predicted by ColabFold showed a longer membrane proximal α helix in all three mutants than the wildtype Sbh1 in the AlphaFold database (Figure 4.2). Robetta predictions, shown in Supplementary Figure 14, show a close to wildtype structure for Sbh1D45-G49A and reoriented cytosolic domains in the structures for Sbh1L50-V52A and Sbh1P54A. The cytosolic domain of Sbh1L50-V52A is oriented up and away from where the Sec61 channel would be located (Supplementary Figure 14 (C)) and Sbh1P54A cytosolic domain is oriented in the opposite direction (Supplementary Figure 14 (D)). While the Robetta predictions seem to account for the gatekeeping phenotype seen in the mutants, the structural predictions are still speculative [268]. The structural predictions are based on a combination of *ab initio* folding and multiple sequence alignment algorithms and reflect the steady state structure of the protein [289,291]. The predictions do not account for the physiological environment of the protein, its molecular dynamics, post-translational

modifications such as phosphorylation and N-terminal acetylation, or the effect of its interaction partners, which play a crucial role in the disorder-to-order transition of an IDR [275,292]. Molecular Dynamics simulations of Sbh1 mutant proteins within the Sec61 complex in the ER membrane may be able to predict their structures more accurately and CryoEM studies are required to definitively prove the structures.

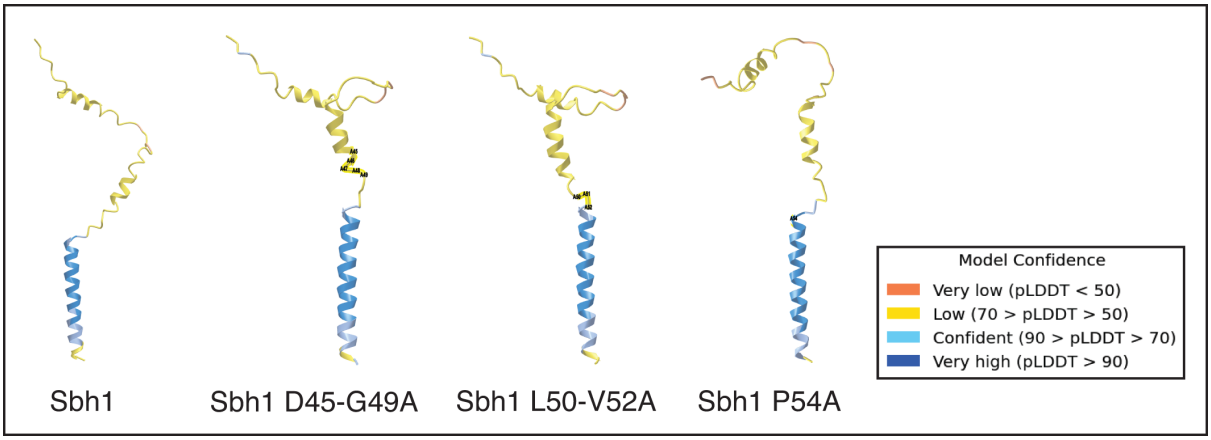

Figure 4.2 Structures of Sbh1 CMP mutants predicted by ColabFold. Structure of Sbh1 was imported from AlphaFold database (Accession number P52870). Structures of Sbh1 CMP mutants were generated using ColabFold. Residues mutated to A are highlighted.

4.4. Interactions of the Sbh1 cytosolic domain

IDRs in stable proteins can fold into a stable tertiary structure by binding to their interaction partners [292]. Phosphorylation often regulates these structural transitions and protein interactions [275,276]. MoRFs are specific motifs within the IDR that tend to interact with proteins and initiate disorder-to-order transitions [198]. A MoRF in the disordered linker domain of the mammalian SRP facilitates its interaction with the SRP receptor during SRP-mediated co-translational protein import [209]. The IDR of the mammalian Sec61β was crosslinked to the ER targeting sequences in nascent chains, and also to tRNA bound ribosome – nascent polypeptide complexes [226,227]. Recognising the potential of the

phosphorylatable unstructured Sbh1 cytosolic domain, I became interested in exploring its interactions (Section 3.4).

Using various computational methods, I was able to identify two potential MoRFs in the Sbh1 cytosolic domain, one MoRF that includes the phosphorylatable T12 residue, from Q10 to T12, and a second MoRF encompassing the C-terminal end of the cytosolic domain, K30 to S38 (Figure 3.19). The C-terminal MoRF extended up to A47 in the CMP region when the full sequence of Sbh1 was used as the query. The structure prediction tool DisoPred3 also showed Q10 to T12 residues as a part of a helix, the location of which corresponded to the decrease in disorder predicted by IUPred2A. This helix was also seen in the predicted Sbh1 structure in the AlphaFold database (accession number P52870). The existing cryo-EM structures for Sbh1 show N36 to E47 as a part of a helix (PDB code 6ND1).

I wanted to pinpoint the specific residues of the Sbh1 cytosolic domain that can interact with other proteins experimentally. The Sbh1 S3 and T5 residues, when phosphorylated, had been previously reported to be involved in Sbh1-dependent protein translocation [253]. My results from the characterisation of CMP mutants implied that Sbh1 CMP region is also involved in translocating Sbh1-dependent proteins. Following this line of thought, I decided to examine protein interactions along the entire Sbh1 cytosolic domain, including its CMP domain, from M1 to L55 (Section 3.4.2). A peptide array was synthesised by Martin Jung's lab (UKS Homburg), with each spot corresponding to a 20mer of the Sbh1 cytosolic domain moving with a 2 amino acid sliding frame, including phosphorylation of every S and T residue individually and in combinations, as well as combination with *N*-terminal acetylation (Figure 3.21). Sbh2 cytosolic domain peptides M1 to L62 were also synthesised and included as Sbh2

can compensate for the lack of Sbh1 in *Δsbh1 Δsbh2* cells [75,222]. The complete list of peptides synthesised onto the cellulose membrane can be found in Appendix B.

As the MD simulations identified an interaction between Sbh1 CMP region and Sec61 N-terminal helix (Figure 3.12), Sec61 N-terminal helix was selected as an interaction partner to investigate [268]. Signal peptides were either dependent on Sbh1 like Gls1 and Irc22 signal peptides were selected because an interaction between these signal peptides with S3/T5 phosphorylated Sbh1 was implied during the ER import of these proteins [253]. Two signal peptides of Sbh1-independent proteins, ppCPY and ppαF, were also synthesised. Mns1 and Pdi1 signal peptides, though planned, could not be synthesised in usable quality as the synthesis of these peptides was limited by the solubility of the signal peptide. The peptides of interest were C-terminally tagged with a biotinylated K residue and are listed in Table 3.2.

The membranes were stripped after each experiment and reused. At this point, peptide panning method was relatively new and needed to be optimised for detecting peptide-peptide interactions. My initial strategy was to probe the peptide panning membrane with biotinylated peptides and detect interactions using streptavidin (Figure 3.22). During method optimisation experiments, I unfortunately detected interactions between Sbh1 M1 to T33 peptides and streptavidin. Equivalent Sbh2 peptides ranging from M1 to T32 also interacted with streptavidin. Moreover, the membranes were designed to be stripped and reused after each experiment. The stripping method mentioned in Section 2.2.13.2 could not sufficiently disrupt the Sbh1 peptide – streptavidin interaction, and an alternative method for stripping using dimethylformamide (DMF) had to be employed. The DMF stripping method, while efficient, led to faster deterioration of the peptide panning membrane. The combination of

these two factors led me to reconsider and ultimately modify my approach for detecting specific interactions with my biotinylated probes.

I switched to detecting Sbh1 – peptide interactions with anti-Biotin-HRP followed by chemiluminescence. I observed a gradual rise in background noise after each use. To ensure consistent identification of interaction signals, I imaged each membrane using a fixed exposure time of 2 sec. The membranes were reused multiple times until the background noise made it harder to identify interactions. As membrane quality control I always imaged the membrane after stripping to ensure all the interacting proteins and peptides were dissociated. I additionally imaged the membrane prior to each experiment (after activation, before blocking) to make note of any residual interactions.

I probed the peptide panning membrane with biotinylated signal peptides of Sbh1-dependent (Gls1 and Irc22) and Sbh1-independent (ppCPY and ppαF) proteins, and the biotinylated Sec61 N-terminal helix (Sec61N) (Section 3.4.3). I found that all four signal peptides I tested interacted with the N-terminal region of Sbh1 cytosolic domain from residues M1 to K23, independently of its acetylation (Figure 3.26). The residues spanning the C-terminal end of the Sbh1 unstructured section of the cytosolic domain up to the beginning of its CMP region, i.e., V24 to Y43, did not interact with any of the biotinylated peptides used (Figure 3.24 and 3.25). The Sbh1 CMP region peptides S44 to L55 interacted only with the signal peptides of Sbh1-dependent substrates (Figures 3.24). The interactions were independent of phosphorylation of the Sbh1 derived peptides. Similar to the interactions with Sbh1, Sbh2 N-terminal peptides M1 to Q20 also interacted with all peptides. Peptides encompassing C-terminal of Sbh2 unstructured cytosolic domain to the beginning of its CMP

region, S21 to Y50, did not interact with any peptides, while its CMP residues T51 to L62 interacted with all signal peptides (Figure 3.26).

I did not find any evidence for a specific interaction between the Sec61 N-terminal helix and the Sbh1 CMP as had been suggested by MD modelling (Figures 3.12 and 3.23). The Sec61 N – Sbh1 cytosolic domain interactions in the peptide panning experiment shown in Figure 3.12 coincide with cross-reaction of streptavidin and anti-biotin antibody with Sbh1 that I saw in an earlier experiment (Figure 3.11 and Supplementary Figure 12). In the ER membrane, TM1 of Sec61 that is connected directly to the N-terminal amphipathic helix interacts with the Sbh1 TM [63]. It is possible that the Sec61 N-terminal helix needs these TM interactions in the ER membrane for it to be positioned such that it is able to interact with the Sbh1 CMP as simulated in the molecular dynamics modelling. This could explain the lack of specific interaction seen in my peptide panning experiments.

The Sbh1 cytosolic domain N-terminal region M1 to K23 appears to interact indiscriminately with all biotinylated peptides used as probes, irrespective of its N-terminal acetylation. The Sbh1 M1 to K23 residues and corresponding Sbh2 M1 to Q20 residues also cross-reacted with streptavidin (Figure 3.22) and anti-biotin-HRP antibody (Supplementary Figure 13). To confirm whether these residues interact with proteins in general additional experiments using “scrambled” peptides that do not resemble a signal peptide are required. The intensity of the N-terminal interactions began to weaken as the peptide sliding frame moved towards the C-terminal of the unstructured part of the cytosolic domain, non-specific interactions began to weaken and eventually disappeared in the peptide spots correlating to V24 to Y43 residues (Figure 3.24, Spots F19 to F29). This matches the decline in binding

propensity scores of Sbh1 unstructured cytosolic domain residues seen in ANCHOR2 and $MoRF_{CHiBi\_Web}$ predictions (Figure 3.19 (B) and (C)). Sbh1-dependent signal peptides start to interact specifically with when the peptide sliding frame begins to include CMP residues (Figure 3.24, Spots G01 to I22). These specific interactions intensify as more CMP residues are incorporated. A summary of the interactions of Sbh1 cytosolic domain is presented in Figure 3.26.

Phosphorylation of S3, T5, T12, S20 and S21 in the peptides did not make interaction of Sbh1-derived phosphorylated peptides with signal peptides specific for those whose ER import is dependent on Sbh1 (Figure 3.24). This was surprising as we already knew that S3/T5 phosphorylation specifically enhances ER import of Gls1 and Irc22 [253]. It suggests that Sbh1 phosphorylation in the N-terminal half of the cytosolic domain is not a direct binding site for Sbh1-phosphorylation-dependent substrates. While S35 and S38 were present in the CMP peptides specifically interacting with Sbh1-dependent signal peptides, the variation in their phosphorylation state did not influence their interaction. It is possible that the phosphorylation of S3/T5 residues causes a large conformational change in the Sbh1 cytosolic domain which generates, or exposes, the binding site for Sbh1-phosphorylation-dependent substrates. Due to the short length of the Sbh1 peptides generated (20mers), such a change cannot be reproduced in the peptide panning membrane and limits the interactions that can be studied.

The N-terminal region of the Sbh2 cytosolic domain that interacted with all biotinylated peptides is slightly shorter than that of Sbh1, extending from M1 to Q20 while the non-interacting region is longer, extending from S21 to Y50 (Figures 3.24 and 3.25). The Sbh2 CMP

region, despite interacting only with signal peptides, did not demonstrate any specificity in its binding preferences. Interactions of Sbh2 are also summarised in Figure 3.26.

The peptide panning method I used in this study has obvious limitations. I investigated peptide-peptide interactions in isolation, outside of their physiological context. Full lengths of Sbh1 and proteins of interest, native conditions, and the presence of Sec61 complex and other components protein translocation machinery could impact their interaction capabilities. Lastly, while the results I obtained in this study provide insights into potential interactions based on physicochemical properties of the peptides in the buffer used (50 mM Tris-HCl pH 7.5 / 150 mM NaCl / 0.1 % (v/v) Triton-X 100), they do not definitively confirm that these interactions occur in vivo. Further studies in more biologically relevant settings will be necessary to validate the observations. Cross-linking Sbh1 and signal sequences together would show the existence of an interaction between them. Repeating the experiment with CMP mutant Sbh1 could help determine the specific site of the interaction if there is any.

I also tried to visualise the interactions between the Sbh1 cytosolic domain and signal peptides using AlphaFold Colab [290,291]. In these interactions shown in Figure 4.3, the C-terminal end of the unstructured cytosolic domain of Sbh1 and the CMP region appears to have an α-helical structure from N36 to G45, 2 residues longer than what is seen in the cryo-EM structure of Sbh1 in the Sec complex. The Sbh1-dependent signal peptides (Figure 4.3 (A) & (B)) seem to interact parallelly with the Sbh1 CMP helix, with their N-terminal helix oriented towards the C-terminal end of the Sbh1 cytosolic domain where the vestibule of the Sec61 complex would be in the intact Sec61 complex (Figure 1.4). The Sbh1-independent signal peptides (Figure 4.3 (C) & (D)) appear perpendicular to the Sbh1 CMP helix. The relatively

closer orientation of ppαF to the Sbh1 CMP helix could be due to its physicochemical properties and would also explain the occasional weak interactions with the N32 to D53 peptides in peptide panning (Figure 3.37). The visualisation of the interactions depicted here, however, are purely illustrative and necessitates validation from biological studies. The distances between Sbh1 cytosolic domain and the signal peptides are too large (>5 Å) to be considered physiological. I also noticed minor variations in the structures due to updates to the algorithm used.

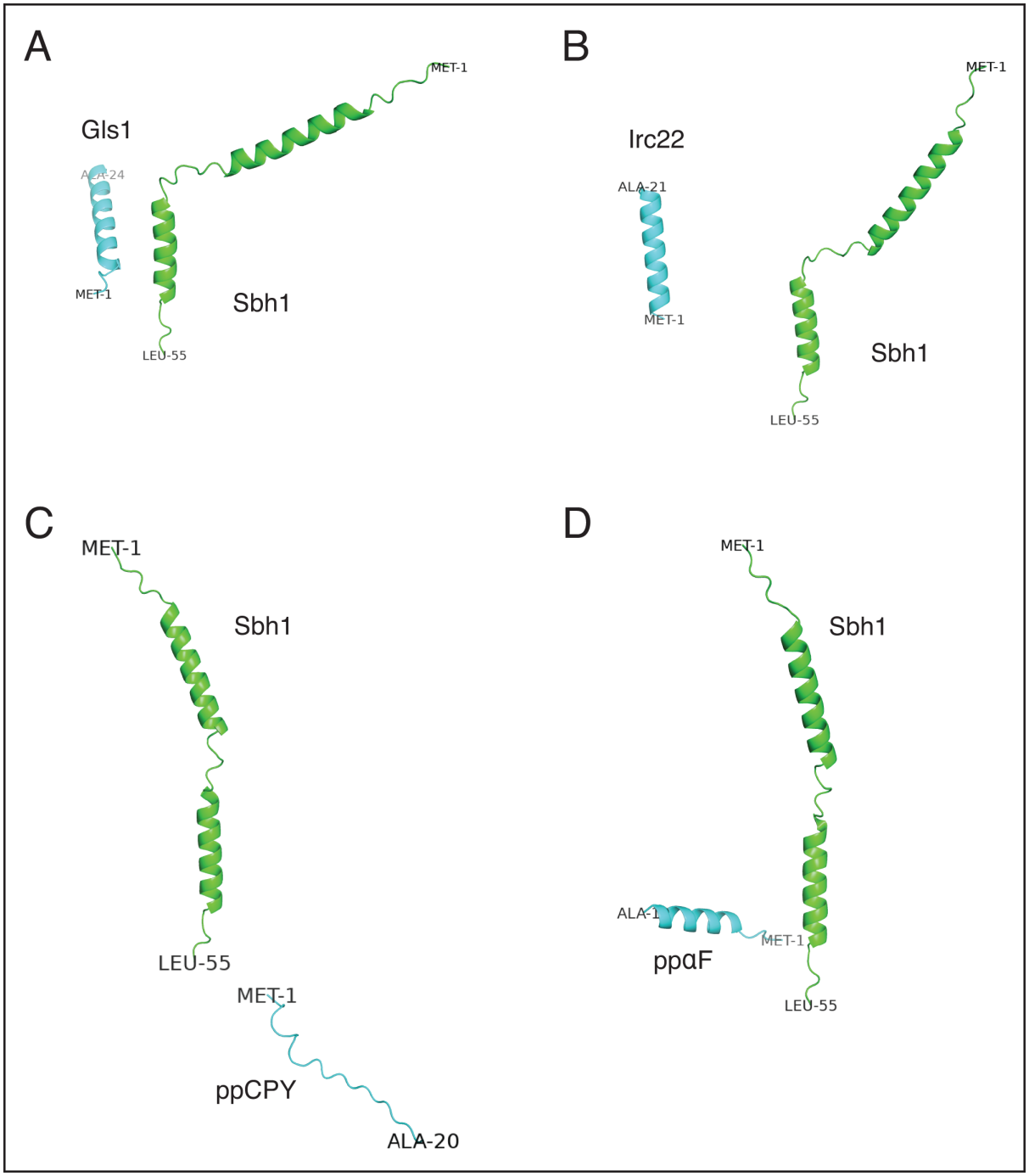

Figure 4.3 Illustration of interactions between Sbh1 cytosolic domain and signal peptides. Interactions between Sbh1 1-55 and signal peptides used in peptide panning generated using AlphaFold ColabFold. **A)** Gls1 signal peptide **B)** Irc22 signal peptide **C)** ppCPY signal peptide **D)** ppαF signal peptide.

Irc22 was recently identified to be dependent on Sbh1 and S3/T5 phosphorylation of Sbh1 for their import [253]. The same study also found that Sbh1-dependent signal peptides, in general, have low hydrophobicity and an inverse or no charge bias [253]. My results from the Sbh1 CMP mutant characterisation imply that the Sbh1 CMP region is involved in efficient

import of Sbh1 S3/T5 phosphorylation-dependent proteins. While the specific interaction of these signal peptides with S3/T5 phosphorylated Sbh1 peptides could not be assessed by peptide panning, it is possible that the regulation of Sbh1 S3/T5 phosphorylation-dependent protein import contributes to the orientation of signal peptides in the Sec61 channel with the N-terminus towards the cytosol. I hypothesise that S3/T5 phosphorylation instead causes a conformational change in the Sbh1 cytosolic domain that makes the signal peptide binding site in the CMP region accessible or contributes to signal peptide orientation.

Phosphorylation-induced conformational change in IDPs is well documented [276]. Phosphorylation of Sbh1 at S3/T5 residues would lend a net negative charge to the N-terminus. This could induce an interaction with the positive patch of K15-K17 residues in the middle of the unstructured Sbh1 cytosolic domain, causing a conformational change that obscures the interacting N-terminal residues. Recent results from our lab support the existence of such a conformational change. Antibodies raised against two unphosphorylated epitopes in the N-terminal region of Sbh1 could not recognise S3/T5 phosphorylated Sbh1 but could recognise mutant Sbh1 S3A/T5A protein, implying that the epitopes were occluded in the S3/T5-phosphorylated Sbh1 and hence unavailable for antibody binding [268].

Combining my data and recent studies from other lab members, I propose a hypothetical model to explain the interaction and function of Sbh1 CMP region in Figure 4.4: Signal peptides not dependent on Sbh1 can insert into the Sec61 channel without interacting with the CMP domain of the unphosphorylated Sbh1 (Figure 4.4 (A)). Phosphorylation of Sbh1 at S3 and T5 residues would cause the N-terminus to fold over, allowing the negatively charged phosphate groups to interact with the positively charged K15 and K17 residues in the within

the unstructured part of the Sbh1 cytosolic domain (Figure 4.4 (B)). Signal sequences reliant on this phosphorylation would then freely interact with the Sbh1 CMP residues and aided by this interaction, orient towards the Sec61 channel for their subsequent insertion. While this model explains the "gatekeeper" activity of Sbh1, detailed structural and biochemical evidence would be required to establish this mechanism.

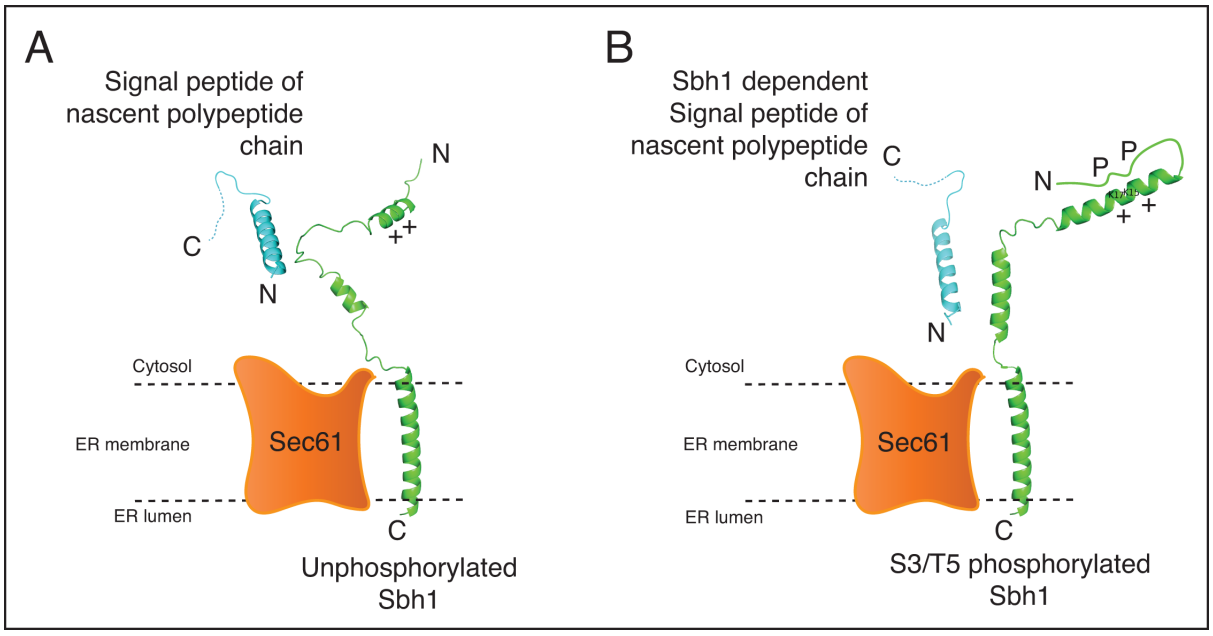

Figure 4.4 Hypothetical model for the CMP guided insertion of Sbh1 dependent import substrates. A) Insertion of Sbh1-independent signal peptides. Structure of Sbh1 was taken from AlphaFold database and Sbh1 independent signal peptide (ppCPY) modelled in PyMOL. Interaction shown here is hypothetical. **B)** Specific interaction of Sbh1 dependent signal peptide of a nascent polypeptide chain with the CMP region of phosphorylated Sbh1. Phosphorylated S3/T5 (PP) residues interact with the positively charged K15-K17 (++) residues of Sbh1 causing a conformational change that masks the non-specific interaction site at the Sbh1 N-terminus. Sbh1 dependent signal peptides can now freely interact with Sbh1 CMP residues. This interaction orients the N-terminus of suboptimal signal peptides towards the Sec61 channel vestibule and guides its insertion. Here, the Sbh1 TM structure was taken from AlphaFold database and the Sbh1 cytosolic domain interaction with Sbh1 dependent signal peptide (Gls1) was generated using AlphaFold ColabFold.

4.5. Conclusion

In this work I studied the role of Sec61 complex subunit Sbh1 in *S. cerevisiae*, I showed that Sbh1 does not contribute to the Sec complex stability despite its central location in the structure, and I discovered that the Sbh1 SMP domain interacts specifically with Sbh1-dependent signal peptides.

My results from the ER translocation experiments in *Δsbh1 Δsbh2* suggest that the simultaneous deletion of Sbh1 and its paralog Sbh2 does not result in general defects in ER protein translocation. Additionally, results from growth assays show that Sbh1 is not essential for ER proteostasis or for maintaining their respiratory competence. These findings accord with the observations made by previously at our lab [253].

I investigated whether the TM domain of Sbh1 stabilises the interaction between TM domains of Sec61 and Sec63, consequently stabilising the Sec complex and found that Sbh1 does not contribute to the stability of the Sec complex.

I generated mutations in the CMP region of Sbh1, which was identified by MD simulations as a potential site for interaction with the Sec61 N-terminal helix. I found that the Sbh1 CMP mutants show impaired Sbh1 production, which causes a specific impact on the import of S3/T5 phosphorylation dependent Sbh1 substrates. Through peptide panning, I demonstrated that the Sbh1 CMP region engages in a direct and specific interaction with Sbh1 dependent signal peptides, while the N-terminal region interacts non-selectively with most proteins and all signal peptides.

Based on the evidence presented, I proposed a hypothetical mechanism for phosphorylation-mediated insertion of specific proteins into the ER, guided by interaction with Sbh1 CMP domain, shown in Figure 4.3.

REFERENCES

1. Theillet FX, Binolfi A, Frembgen-Kesner T, Hingorani K, Sarkar M, Kyne C, et al. Physicochemical properties of cells and their effects on intrinsically disordered proteins (IDPs). Chemical Reviews. American Chemical Society; 2014. pp. 6661–6714. doi:10.1021/cr400695p

2. Diekmann Y, Pereira-Leal JB. Evolution of intracellular compartmentalization. Biochemical Journal. 2012;449: 319–331. doi:10.1042/BJ20120957

3. Feyder S, De Craene J-O, Bär S, Bertazzi DL, Friant S. Membrane Trafficking in the Yeast Saccharomyces cerevisiae Model. International Journal of Molecular Sciences. 2015;16: 1509–1525. doi:10.3390/ijms16011509

4. Zimmermann R, Eyrisch S, Ahmad M, Helms V. Protein translocation across the ER membrane. Biochimica et Biophysica Acta (BBA) - Biomembranes. 2011;1808: 912–924. doi:10.1016/j.bbamem.2010.06.015

5. Simon SM, Blobel G. Signal peptides open protein-conducting channels in E. coli. Cell. 1992;69: 677–684. doi:10.1016/0092-8674(92)90231-z

6. Hatahet F, Ruddock LW. Modulating proteostasis: peptidomimetic inhibitors and activators of protein folding. Curr Pharm Des. 2009;15: 2488–2507. doi:10.2174/138161209788682343

7. Goto M. Protein O-glycosylation in fungi: diverse structures and multiple functions. Biosci Biotechnol Biochem. 2007;71: 1415–1427. doi:10.1271/bbb.70080

8. Delic M, Valli M, Graf AB, Pfeffer M, Mattanovich D, Gasser B. The secretory pathway: exploring yeast diversity. FEMS Microbiology Reviews. 2013;37: 872–914. doi:10.1111/1574-6976.12020

9. Dobson CM. The structural basis of protein folding and its links with human disease. Philos Trans R Soc Lond B Biol Sci. 2001;356: 133–145. doi:10.1098/rstb.2000.0758

10. Kabani M, Kelley SS, Morrow MW, Montgomery DL, Sivendran R, Rose MD, et al. Dependence of Endoplasmic Reticulum-associated Degradation on the Peptide Binding Domain and Concentration of BiP. Mol Biol Cell. 2003;14: 3437–3448. doi:10.1091/mbc.E02-12-0847

11. Gardner BM, Pincus D, Gotthardt K, Gallagher CM, Walter P. Endoplasmic reticulum stress sensing in the unfolded protein response. Cold Spring Harb Perspect Biol. 2013;5: a013169. doi:10.1101/cshperspect.a013169

12. Ruggiano A, Foresti O, Carvalho P. Quality control: ER-associated degradation: protein quality control and beyond. J Cell Biol. 2014;204: 869–879. doi:10.1083/jcb.201312042

13. Brandizzi F, Barlowe C. Organization of the ER–Golgi interface for membrane traffic control. Nat Rev Mol Cell Biol. 2013;14: 382–392. doi:10.1038/nrm3588

14. Lewis MJ, Pelham HR. SNARE-mediated retrograde traffic from the Golgi complex to the endoplasmic reticulum. Cell. 1996;85: 205–215. doi:10.1016/s0092-8674(00)81097-1

15. Pelham HR, Munro S. Sorting of membrane proteins in the secretory pathway. Cell. 1993;75: 603–605. doi:10.1016/0092-8674(93)90479-a

16. Rossanese OW, Soderholm J, Bevis BJ, Sears IB, O'Connor J, Williamson EK, et al. Golgi Structure Correlates with Transitional Endoplasmic Reticulum Organization in Pichia pastoris and Saccharomyces cerevisiae. J Cell Biol. 1999;145: 69–81.

17. Castillon GA, Watanabe R, Taylor M, Schwabe TME, Riezman H. Concentration of GPI-anchored proteins upon ER exit in yeast. Traffic. 2009;10: 186–200. doi:10.1111/j.1600-0854.2008.00857.x

18. Barlowe C, Orci L, Yeung T, Hosobuchi M, Hamamoto S, Salama N, et al. COPII: a membrane coat formed by Sec proteins that drive vesicle budding from the endoplasmic reticulum. Cell. 1994;77: 895–907. doi:10.1016/0092-8674(94)90138-4

19. Barlowe CK, Miller EA. Secretory protein biogenesis and traffic in the early secretory pathway. Genetics. 2013;193: 383–410. doi:10.1534/genetics.112.142810

20. Dancourt J, Barlowe C. Protein sorting receptors in the early secretory pathway. Annu Rev Biochem. 2010;79: 777–802. doi:10.1146/annurev-biochem-061608-091319

21. Lee MCS, Miller EA, Goldberg J, Orci L, Schekman R. Bi-directional protein transport between the ER and Golgi. Annu Rev Cell Dev Biol. 2004;20: 87–123. doi:10.1146/annurev.cellbio.20.010403.105307

22. Miller EA, Beilharz TH, Malkus PN, Lee MCS, Hamamoto S, Orci L, et al. Multiple cargo binding sites on the COPII subunit Sec24p ensure capture of diverse membrane proteins into transport vesicles. Cell. 2003;114: 497–509. doi:10.1016/s0092-8674(03)00609-3

23. Hughes H, Stephens DJ. Assembly, organization, and function of the COPII coat. Histochem Cell Biol. 2008;129: 129–151. doi:10.1007/s00418-007-0363-x

24. Viotti C. ER to Golgi-Dependent Protein Secretion: The Conventional Pathway. Methods Mol Biol. 2016;1459: 3–29. doi:10.1007/978-1-4939-3804-9_1

25. Ferro-Novick S, Brose N. Nobel 2013 Physiology or medicine: Traffic control system within cells. Nature. 2013;504: 98. doi:10.1038/504098a

26. Jahn R, Scheller RH. SNAREs — engines for membrane fusion. Nat Rev Mol Cell Biol. 2006;7: 631–643. doi:10.1038/nrm2002

27. Preuss D, Mulholland J, Franzusoff A, Segev N, Botstein D. Characterization of the Saccharomyces Golgi complex through the cell cycle by immunoelectron microscopy. Mol Biol Cell. 1992;3: 789–803. doi:10.1091/mbc.3.7.789

28. Rossanese OW, Reinke CA, Bevis BJ, Hammond AT, Sears IB, O'Connor J, et al. A Role for Actin, Cdc1p, and Myo2p in the Inheritance of Late Golgi Elements in Saccharomyces cerevisiae. Journal of Cell Biology. 2001;153: 47–62. doi:10.1083/jcb.153.1.47

29. Lowe M. Structural organization of the Golgi apparatus. Curr Opin Cell Biol. 2011;23: 85–93. doi:10.1016/j.ceb.2010.10.004

30. Shorter J, Warren G. Golgi architecture and inheritance. Annu Rev Cell Dev Biol. 2002;18: 379–420. doi:10.1146/annurev.cellbio.18.030602.133733

31. Hara-Kuge S, Kuge O, Orci L, Amherdt M, Ravazzola M, Wieland F, et al. En bloc incorporation of coatomer subunits during the assembly of COP-coated vesicles. Journal of Cell Biology. 1994;124: 883–892. doi:10.1083/jcb.124.6.883

32. Emr S, Glick BS, Linstedt AD, Lippincott-Schwartz J, Luini A, Malhotra V, et al. Journeys through the Golgi--taking stock in a new era. J Cell Biol. 2009;187: 449–453. doi:10.1083/jcb.200909011

33. Gomez-Navarro N, Miller E. Protein sorting at the ER-Golgi interface. J Cell Biol. 2016;215: 769–778. doi:10.1083/jcb.201610031

34. Chen Y, Zhang Y, Yin Y, Gao G, Li S, Jiang Y, et al. SPD--a web-based secreted protein database. Nucleic Acids Res. 2005;33: D169-173. doi:10.1093/nar/gki093

35. Dubnikov T, Cohen E. The Emerging Roles of Early Protein Folding Events in the Secretory Pathway in the Development of Neurodegenerative Maladies. Front Neurosci. 2017;11. doi:10.3389/fnins.2017.00048

36. Klaips CL, Jayaraj GG, Hartl FU. Pathways of cellular proteostasis in aging and disease. Journal of Cell Biology. 2017;217: 51–63. doi:10.1083/jcb.201709072

37. Huang Y, Arora K, Mun KS, Yang F, Moon C, Yarlagadda S, et al. Targeting DNAJB9, a novel ER luminal co-chaperone, to rescue ΔF508-CFTR. Sci Rep. 2019;9: 9808. doi:10.1038/s41598-019-46161-4

38. Carter S, Kelly S, Caples E, Grogan B, Doyle J, Gallagher CG, et al. Ivacaftor as salvage therapy in a patient with cystic fibrosis genotype F508del/R117H/IVS8-5T. Journal of Cystic Fibrosis. 2015;14: e4–e5. doi:10.1016/j.jcf.2015.01.010

39. Kramer G, Shiber A, Bukau B. Mechanisms of Cotranslational Maturation of Newly Synthesized Proteins. Annual Review of Biochemistry. 2019;88: 337–364. doi:10.1146/annurev-biochem-013118-111717

40. Hegde RS, Bernstein HD. The surprising complexity of signal sequences. Trends Biochem Sci. 2006;31: 563–571. doi:10.1016/j.tibs.2006.08.004

41. Park E, Rapoport TA. Mechanisms of Sec61/SecY-Mediated Protein Translocation Across Membranes. Annual Review of Biophysics. 2012;41: 21–40. doi:10.1146/annurev-biophys-050511-102312

42. Owji H, Nezafat N, Negahdaripour M, Hajiebrahimi A, Ghasemi Y. A comprehensive review of signal peptides: Structure, roles, and applications. European Journal of Cell Biology. 2018;97: 422–441. doi:10.1016/j.ejcb.2018.06.003

43. Mandon EC, Trueman SF, Gilmore R. Protein Translocation across the Rough Endoplasmic Reticulum. Cold Spring Harb Perspect Biol. 2013;5: a013342. doi:10.1101/cshperspect.a013342

44. von Heijne G. The signal peptide. J Membrain Biol. 1990;115: 195–201. doi:10.1007/BF01868635

45. Hiss JA, Schneider G. Architecture, function and prediction of long signal peptides. Briefings in Bioinformatics. 2009;10: 569–578. doi:10.1093/bib/bbp030

46. von Heijne G. Net N-C charge imbalance may be important for signal sequence function in bacteria. Journal of Molecular Biology. 1986;192: 287–290. doi:10.1016/0022-2836(86)90365-7

47. Zheng N, Gierasch LM. Signal Sequences: The Same Yet Different. Cell. 1996;86: 849–852. doi:10.1016/S0092-8674(00)80159-2

48. von Heijne G. A new method for predicting signal sequence cleavage sites. Nucleic Acids Res. 1986;14: 4683–4690. doi:10.1093/nar/14.11.4683

49. Chen X, VanValkenburgh C, Liang H, Fang H, Green N. Signal peptidase and oligosaccharyltransferase interact in a sequential and dependent manner within the endoplasmic reticulum. J Biol Chem. 2001;276: 2411–2416. doi:10.1074/jbc.M007723200

50. Shaffer KL, Sharma A, Snapp EL, Hegde RS. Regulation of protein compartmentalization expands the diversity of protein function. Developmental Cell. 2005;9: 545–554. doi:10.1016/j.devcel.2005.09.001

51. Kim SJ, Hegde RS. Cotranslational Partitioning of Nascent Prion Protein into Multiple Populations at the Translocation Channel. Mol Biol Cell. 2002;13: 3775–3786. doi:10.1091/mbc.E02-05-0293

52. Spiess M, Junne T, Janoschke M. Membrane Protein Integration and Topogenesis at the ER. Protein Journal. 2019;38: 306–316. doi:10.1007/s10930-019-09827-6

53. Nguyen D, Stutz R, Schorr S, Lang S, Pfeffer S, Freeze HH, et al. Proteomics reveals signal peptide features determining the client specificity in human TRAP-dependent ER protein import. Nat Commun. 2018;9: 3765. doi:10.1038/s41467-018-06188-z

54. Yim C, Jung S jun, Kim JEH, Jung Y, Jeong SD, Kim H. Profiling of signal sequence characteristics and requirement of different translocation components. Biochimica et Biophysica Acta - Molecular Cell Research. 2018;1865: 1640–1648. doi:10.1016/j.bbamcr.2018.08.018

55. Beckmann R, Spahn CM, Eswar N, Helmers J, Penczek PA, Sali A, et al. Architecture of the protein-conducting channel associated with the translating 80S ribosome. Cell. 2001;107: 361–372. doi:10.1016/s0092-8674(01)00541-4

56. Beckmann R, Bubeck D, Grassucci R, Penczek P, Verschoor A, Blobel G, et al. Alignment of conduits for the nascent polypeptide chain in the ribosome-Sec61 complex. Science. 1997;278: 2123–2126. doi:10.1126/science.278.5346.2123

57. Cheng Z, Jiang Y, Mandon EC, Gilmore R. Identification of cytoplasmic residues of Sec61p involved in ribosome binding and cotranslational translocation. Journal of Cell Biology. 2005;168: 67–77. doi:10.1083/jcb.200408188

58. Panzner S, Dreier L, Hartmann E, Kostka S, Rapoport TA. Posttranslational protein transport in yeast reconstituted with a purified complex of Sec proteins and Kar2p. Cell. 1995;81: 561–570. doi:10.1016/0092-8674(95)90077-2

59. Kalies K, Allan S, Sergeyenko T, Kröger H, Römisch K. The protein translocation channel binds proteasomes to the endoplasmic reticulum membrane. The EMBO Journal. 2005;24: 2284–2293. doi:10.1038/sj.emboj.7600731

60. Römisch K. ENDOPLASMIC RETICULUM–ASSOCIATED DEGRADATION. Annual Review of Cell and Developmental Biology. 2005;21: 435–456. doi:10.1146/annurev.cellbio.21.012704.133250

61. van den Berg B, Clemons WM, Collinson I, Modis Y, Hartmann E, Harrison SC, et al. X-ray structure of a protein-conducting channel. Nature. 2004;427: 36–44. doi:10.1038/nature02218

62. Tsirigotaki A, De Geyter J, Šoštaric N, Economou A, Karamanou S. Protein export through the bacterial Sec pathway. Nat Rev Microbiol. 2017;15: 21–36. doi:10.1038/nrmicro.2016.161

63. Wu X, Cabanos C, Rapoport TA. Structure of the post-translational protein translocation machinery of the ER membrane. Nature. 2019;566: 136–139. doi:10.1038/s41586-018-0856-x

64. Voorhees RM, Hegde RS. Structure of the Sec61 channel opened by a signal sequence. Science. 2016;351: 88–89. doi:10.1126/science.aad4992

65. Reithinger JH, Yim C, Kim S, Lee H, Kim H. Structural and Functional Profiling of the Lateral Gate of the Sec61 Translocon. J Biol Chem. 2014;289: 15845–15855. doi:10.1074/jbc.M113.533794

66. Gogala M, Becker T, Beatrix B, Armache J-P, Barrio-Garcia C, Berninghausen O, et al. Structures of the Sec61 complex engaged in nascent peptide translocation or membrane insertion. Nature. 2014;506: 107–110. doi:10.1038/nature12950

67. Egea PF, Stroud RM. Lateral opening of a translocon upon entry of protein suggests the mechanism of insertion into membranes. Proceedings of the National Academy of Sciences. 2010;107: 17182–17187. doi:10.1073/pnas.1012556107

68. Esnault Y, Feldheim D, Blondel MO, Schekman R, Képès F. SSS1 encodes a stabilizing component of the Sec61 subcomplex of the yeast protein translocation apparatus. Journal of Biological Chemistry. 1994;269: 27478–27485. doi:10.1016/S0021-9258(18)47010-X

69. Voorhees RM, Fernández IS, Scheres SHW, Hegde RS. Structure of the Mammalian Ribosome-Sec61 Complex to 3.4 Å Resolution. Cell. 2014;157: 1632–1643. doi:10.1016/j.cell.2014.05.024

70. Voorhees RM, Hegde RS. Toward a structural understanding of co-translational protein translocation. Current Opinion in Cell Biology. 2016;41: 91–99. doi:10.1016/j.ceb.2016.04.009

71. Allen WJ, Corey RA, Oatley P, Sessions RB, Baldwin SA, Radford SE, et al. Two-way communication between SecY and SecA suggests a Brownian ratchet mechanism for protein translocation. Hegde RS, editor. eLife. 2016;5: e15598. doi:10.7554/eLife.15598

72. Bischoff L, Wickles S, Berninghausen O, van der Sluis EO, Beckmann R. Visualization of a polytopic membrane protein during SecY-mediated membrane insertion. Nat Commun. 2014;5: 4103. doi:10.1038/ncomms5103

73. Li L, Park E, Ling J, Ingram J, Ploegh H, Rapoport TA. Crystal structure of a substrate-engaged SecY protein-translocation channel. Nature. 2016;531: 395–399. doi:10.1038/nature17163

74. Rapoport TA, Li L, Park E. Structural and Mechanistic Insights into Protein Translocation. Annual Review of Cell and Developmental Biology. 2017;33: 369–390. doi:10.1146/annurev-cellbio-100616-060439

75. Finke K, Plath K, Panzner S, Prehn S, Rapoport TA, Hartmann E, et al. A second trimeric complex containing homologs of the Sec61p complex functions in protein transport across the ER membrane of S. cerevisiae. EMBO J. 1996;15: 1482–1494.

76. Jan CH, Williams CC, Weissman JS. Principles of ER cotranslational translocation revealed by proximity-specific ribosome profiling. Science. 2014;346: 1257521. doi:10.1126/science.1257521

77. Osborne AR, Rapoport TA, van den Berg B. Protein translocation by the Sec61/SecY channel. Annu Rev Cell Dev Biol. 2005;21: 529–550. doi:10.1146/annurev.cellbio.21.012704.133214

78. Prinz WA, Grzyb L, Veenhuis M, Kahana JA, Silver PA, Rapoport TA. Mutants Affecting the Structure of the Cortical Endoplasmic Reticulum in Saccharomyces cerevisiae. J Cell Biol. 2000;150: 461–474.

79. Becker T, Bhushan S, Jarasch A, Armache J-P, Funes S, Jossinet F, et al. Structure of monomeric yeast and mammalian Sec61 complexes interacting with the translating ribosome. Science. 2009;326: 1369–1373. doi:10.1126/science.1178535

80. Wittke S, Dünnwald M, Albertsen M, Johnsson N. Recognition of a Subset of Signal Sequences by Ssh1p, a Sec61p-related Protein in the Membrane of Endoplasmic Reticulum of Yeast Saccharomyces cerevisiae. Mol Biol Cell. 2002;13: 2223–2232. doi:10.1091/mbc.01-10-0518

81. Driessen AJM, Nouwen N. Protein translocation across the bacterial cytoplasmic membrane. Annu Rev Biochem. 2008;77: 643–667. doi:10.1146/annurev.biochem.77.061606.160747

82. Brown JD, Hann BC, Medzihradszky KF, Niwa M, Burlingame AL, Walter P. Subunits of the Saccharomyces cerevisiae signal recognition particle required for its functional expression. The EMBO Journal. 1994;13: 4390–4400. doi:10.1002/j.1460-2075.1994.tb06759.x

83. Chartron JW, Hunt KCL, Frydman J. Cotranslational signal-independent SRP preloading during membrane targeting. Nature. 2016;536: 224–228. doi:10.1038/nature19309

84. Voorhees RM, Hegde RS. Structures of the scanning and engaged states of the mammalian SRP-ribosome complex. Kuriyan J, editor. eLife. 2015;4: e07975. doi:10.7554/eLife.07975

85. Voss NR, Gerstein M, Steitz TA, Moore PB. The geometry of the ribosomal polypeptide exit tunnel. J Mol Biol. 2006;360: 893–906. doi:10.1016/j.jmb.2006.05.023

86. Seidelt B, Innis CA, Wilson DN, Gartmann M, Armache J-P, Villa E, et al. Structural insight into nascent polypeptide chain-mediated translational stalling. Science. 2009;326: 1412–1415. doi:10.1126/science.1177662

87. Cross BCS, Sinning I, Luirink J, High S. Delivering proteins for export from the cytosol. Nat Rev Mol Cell Biol. 2009;10: 255–264. doi:10.1038/nrm2657

88. Halic M, Beckmann R. The signal recognition particle and its interactions during protein targeting. Curr Opin Struct Biol. 2005;15: 116–125. doi:10.1016/j.sbi.2005.01.013

89. Ng DTW, Walter P. ER Membrane Protein Complex Required for Nuclear Fusion. The Journal of Cell Biology. 1996;132.

90. Walter P, Blobel G. Translocation of proteins across the endoplasmic reticulum. II. Signal recognition protein (SRP) mediates the selective binding to microsomal membranes of in-vitro-assembled polysomes synthesizing secretory protein. J Cell Biol. 1981;91: 551–556. doi:10.1083/jcb.91.2.551

91. Keenan RJ, Freymann DM, Walter P, Stroud RM. Crystal structure of the signal sequence binding subunit of the signal recognition particle. Cell. 1998;94: 181–191. doi:10.1016/s0092-8674(00)81418-x

92. Zhang Y, Berndt U, Gölz H, Tais A, Oellerer S, Wölfle T, et al. NAC functions as a modulator of SRP during the early steps of protein targeting to the endoplasmic reticulum. Mol Biol Cell. 2012;23: 3027–3040. doi:10.1091/mbc.E12-02-0112

93. del Alamo M, Hogan DJ, Pechmann S, Albanese V, Brown PO, Frydman J. Defining the specificity of cotranslationally acting chaperones by systematic analysis of mRNAs associated with ribosome-nascent chain complexes. PLoS Biol. 2011;9: e1001100. doi:10.1371/journal.pbio.1001100

94. Wolin SL, Walter P. Signal recognition particle mediates a transient elongation arrest of preprolactin in reticulocyte lysate. J Cell Biol. 1989;109: 2617–2622. doi:10.1083/jcb.109.6.2617

95. Ciryam P, Morimoto RI, Vendruscolo M, Dobson CM, O'Brien EP. In vivo translation rates can substantially delay the cotranslational folding of the Escherichia coli cytosolic proteome. Proc Natl Acad Sci U S A. 2013;110: E132-140. doi:10.1073/pnas.1213624110

96. Halic M, Becker T, Pool MR, Spahn CMT, Grassucci RA, Frank J, et al. Structure of the signal recognition particle interacting with the elongation-arrested ribosome. Nature. 2004;427: 808–814. doi:10.1038/nature02342

97. Zhang G, Ignatova Z. Folding at the birth of the nascent chain: coordinating translation with co-translational folding. Curr Opin Struct Biol. 2011;21: 25–31. doi:10.1016/j.sbi.2010.10.008

98. Gilmore R, Walter P, Blobel G. Protein translocation across the endoplasmic reticulum. II. Isolation and characterization of the signal recognition particle receptor. J Cell Biol. 1982;95: 470–477. doi:10.1083/jcb.95.2.470

99. Meyer DI, Krause E, Dobberstein B. Secretory protein translocation across membranes-the role of the "docking protein'. Nature. 1982;297: 647–650. doi:10.1038/297647a0

100. Wild K, Halic M, Sinning I, Beckmann R. SRP meets the ribosome. Nat Struct Mol Biol. 2004;11: 1049–1053. doi:10.1038/nsmb853

101. Jiang Y, Cheng Z, Mandon EC, Gilmore R. An interaction between the SRP receptor and the translocon is critical during cotranslational protein translocation. Journal of Cell Biology. 2008;180: 1149–1161. doi:10.1083/jcb.200707196

102. Ast T, Cohen G, Schuldiner M. A Network of Cytosolic Factors Targets SRP-Independent Proteins to the Endoplasmic Reticulum. Cell. 2013;152: 1134–1145. doi:10.1016/j.cell.2013.02.003

103. Deshaies RJ, Sanders SL, Feldheim DA, Schekman R. Assembly of yeast Sec proteins involved in translocation into the endoplasmic reticulum into a membrane-bound multisubunit complex. Nature. 1991;349: 806–808. doi:10.1038/349806a0

104. Aviram N, Schuldiner M. Targeting and translocation of proteins to the endoplasmic reticulum at a glance. Journal of Cell Science. 2017;130: 4079–4085. doi:10.1242/jcs.204396

105. Feldheim D, Yoshimura K, Admon A, Schekman R. Structural and functional characterization of Sec66p, a new subunit of the polypeptide translocation apparatus in the yeast endoplasmic reticulum. MBoC. 1993;4: 931–939. doi:10.1091/mbc.4.9.931

106. Deshaies RJ, Schekman R. Structural and functional dissection of Sec62p, a membrane-bound component of the yeast endoplasmic reticulum protein import machinery. Mol Cell Biol. 1990;10: 6024–6035. doi:10.1128/mcb.10.11.6024-6035.1990

107. Wittke S, Dünnwald M, Johnsson N. Sec62p, A Component of the Endoplasmic Reticulum Protein Translocation Machinery, Contains Multiple Binding Sites for the Sec-Complex. Mol Biol Cell. 2000;11: 3859–3871.

108. Itskanov S, Park E. Structure of the posttranslational Sec protein-translocation channel complex from yeast. Science. 2018;363: 84–87. doi:10.1126/science.aav6740

109. Feldheim D, Rothblatt J, Schekman R. Topology and functional domains of Sec63p, an endoplasmic reticulum membrane protein required for secretory protein translocation. Mol Cell Biol. 1992;12: 3288–3296. doi:10.1128/mcb.12.7.3288-3296.1992

110. Plath K, Rapoport TA. Spontaneous release of cytosolic proteins from posttranslational substrates before their transport into the endoplasmic reticulum. J Cell Biol. 2000;151: 167–178. doi:10.1083/jcb.151.1.167

111. Deshaies RJ, Koch BD, Werner-Washburne M, Craig EA, Schekman R. A subfamily of stress proteins facilitates translocation of secretory and mitochondrial precursor polypeptides. Nature. 1988;332: 800–805. doi:10.1038/332800a0

112. Tripathi A, Mandon EC, Gilmore R, Rapoport TA. Two alternative binding mechanisms connect the protein translocation Sec71-Sec72 complex with heat shock proteins. J Biol Chem. 2017;292: 8007–8018. doi:10.1074/jbc.M116.761122

113. Shao S, Hegde RS. A calmodulin-dependent translocation pathway for small secretory proteins. Cell. 2011;147: 1576–1588. doi:10.1016/j.cell.2011.11.048

114. Plath K, Wilkinson BM, Stirling CJ, Rapoport TA. Interactions between Sec Complex and Prepro-α-Factor during Posttranslational Protein Transport into the Endoplasmic Reticulum. MBoC. 2004;15: 1–10. doi:10.1091/mbc.e03-06-0390

115. Matlack KES, Misselwitz B, Plath K, Rapoport TA. BIP acts as a molecular ratchet during posttranslational transport of prepro-α factor across the ER membrane. Cell. 1999;97: 553–564. doi:10.1016/S0092-8674(00)80767-9

116. Rapoport TA. Protein translocation across the eukaryotic endoplasmic reticulum and bacterial plasma membranes. Nature. 2007;450: 663–669. doi:10.1038/nature06384

117. Cymer F, von Heijne G, White SH. Mechanisms of Integral Membrane Protein Insertion and Folding. Journal of Molecular Biology. 2015;427: 999–1022. doi:10.1016/j.jmb.2014.09.014

118. Hizlan D, Robson A, Whitehouse S, Gold VA, Vonck J, Mills D, et al. Structure of the SecY Complex Unlocked by a Preprotein Mimic. Cell Rep. 2012;1: 21–28. doi:10.1016/j.celrep.2011.11.003

119. von Heijne G, Gavel Y. Topogenic signals in integral membrane proteins. Eur J Biochem. 1988;174: 671–678. doi:10.1111/j.1432-1033.1988.tb14150.x

120. Briggs MS, Cornell DG, Dluhy RA, Gierasch LM. Conformations of signal peptides induced by lipids suggest initial steps in protein export. Science. 1986;233: 206–208. doi:10.1126/science.2941862

121. McKnight CJ, Stradley SJ, Jones JD, Gierasch LM. Conformational and membrane-binding properties of a signal sequence are largely unaltered by its adjacent mature region. Proc Natl Acad Sci U S A. 1991;88: 5799–5803. doi:10.1073/pnas.88.13.5799

122. Lyko F, Martoglio B, Jungnickel B, Rapoport TA, Dobberstein B. Signal Sequence Processing in Rough Microsomes (∗). Journal of Biological Chemistry. 1995;270: 19873–19878. doi:10.1074/jbc.270.34.19873

123. Beuret N, Rutishauser J, Bider MD, Spiess M. Mechanism of endoplasmic reticulum retention of mutant vasopressin precursor caused by a signal peptide truncation associated with diabetes insipidus. J Biol Chem. 1999;274: 18965–18972. doi:10.1074/jbc.274.27.18965

124. Kang SW, Rane NS, Kim SJ, Garrison JL, Taunton J, Hegde RS. Substrate-Specific Translocational Attenuation during ER Stress Defines a Pre-Emptive Quality Control Pathway. Cell. 2006;127: 999–1013. doi:10.1016/j.cell.2006.10.032

125. Liu M, Lara-Lemus R, Shan S, Wright J, Haataja L, Barbetti F, et al. Impaired Cleavage of Preproinsulin Signal Peptide Linked to Autosomal-Dominant Diabetes. Diabetes. 2012;61: 828–837. doi:10.2337/db11-0878

126. Lang S, Pfeffer S, Lee PH, Cavalié A, Helms V, Förster F, et al. An update on Sec 61 channel functions, mechanisms, and related diseases. Frontiers in Physiology. 2017;8: 887. doi:10.3389/FPHYS.2017.00887/BIBTEX

127. Heaton NS, Moshkina N, Fenouil R, Gardner TJ, Aguirre S, Shah PS, et al. Targeting Viral Proteostasis Limits Influenza Virus, HIV, and Dengue Virus Infection. Immunity. 2016;44: 46–58. doi:10.1016/j.immuni.2015.12.017

128. Besse W, Dong K, Choi J, Punia S, Fedeles SV, Choi M, et al. Isolated polycystic liver disease genes define effectors of polycystin-1 function. American Society for Clinical Investigation; 1 May 2017 [cited 22 Dec 2023]. doi:10.1172/JCI90129

129. Lu Z, Zhou L, Killela P, Rasheed AB, Di C, Poe WE, et al. Glioblastoma Proto-oncogene SEC61γ Is Required for Tumor Cell Survival and Response to Endoplasmic Reticulum Stress. Cancer Research. 2009;69: 9105–9111. doi:10.1158/0008-5472.CAN-09-2775

130. Linxweiler M, Schick B, Zimmermann R. Let's talk about Secs: Sec61, Sec62 and Sec63 in signal transduction, oncology and personalized medicine. Signal Transduction and Targeted Therapy 2017 2:1. 2017;2: 1–10. doi:10.1038/sigtrans.2017.2

131. Saibil H. Molecular chaperones: containers and surfaces for folding, stabilising or unfolding proteins. Curr Opin Struct Biol. 2000;10: 251–258. doi:10.1016/s0959-440x(00)00074-9

132. Bukau B, Weissman J, Horwich A. Molecular chaperones and protein quality control. Cell. 2006;125: 443–451. doi:10.1016/j.cell.2006.04.014

133. Young CL, Robinson AS. Protein Folding and Secretion: Mechanistic Insights Advancing Recombinant Protein Production in S. cerevisiae. Curr Opin Biotechnol. 2014;0: 168–177. doi:10.1016/j.copbio.2014.06.018

134. Ellgaard L, Helenius A. Quality control in the endoplasmic reticulum. Nat Rev Mol Cell Biol. 2003;4: 181–191. doi:10.1038/nrm1052

135. Mayer MP, Bukau B. Hsp70 chaperones: cellular functions and molecular mechanism. Cell Mol Life Sci. 2005;62: 670–684. doi:10.1007/s00018-004-4464-6

136. Vembar SS, Jonikas MC, Hendershot LM, Weissman JS, Brodsky JL. J domain co-chaperone specificity defines the role of BiP during protein translocation. The Journal of biological chemistry. 2010;285: 22484–22494. doi:10.1074/jbc.M110.102186

137. Bukau B, Horwich AL. The Hsp70 and Hsp60 chaperone machines. Cell. 1998;92: 351–366. doi:10.1016/s0092-8674(00)80928-9

138. Craig EA, Huang P, Aron R, Andrew A. The diverse roles of J-proteins, the obligate Hsp70 co-chaperone. Rev Physiol Biochem Pharmacol. 2006;156: 1–21. doi:10.1007/s10254-005-0001-0

139. Hennessy F, Nicoll W, Zimmermann R, Cheetham M, Blatch G. Hennessy F, Nicoll WS, Zimmermann R, Cheetham ME, Blatch GL.. Not all J domains are created equal: implications for the specificity of Hsp40-Hsp70 interactions. Protein Sci 14: 1697-1709. Protein science : a publication of the Protein Society. 2005;14: 1697–709. doi:10.1110/ps.051406805

140. Brodsky JL. Post-translational protein translocation: not all hsc70s are created equal. Trends in Biochemical Sciences. 1996;21: 122–126. doi:10.1016/S0968-0004(96)80163-0

141. McCaffrey K, Braakman I. Protein quality control at the endoplasmic reticulum. Essays Biochem. 2016;60: 227–235. doi:10.1042/EBC20160003

142. Nishikawa S, Endo T. The yeast JEM1p is a DnaJ-like protein of the endoplasmic reticulum membrane required for nuclear fusion. J Biol Chem. 1997;272: 12889–12892. doi:10.1074/jbc.272.20.12889

143. Schlenstedt G, Harris S, Risse B, Lill R, Silver PA. A yeast DnaJ homologue, Scj1p, can function in the endoplasmic reticulum with BiP/Kar2p via a conserved domain that specifies interactions with Hsp70s. J Cell Biol. 1995;129: 979–988. doi:10.1083/jcb.129.4.979

144. Gilbert HF. Protein disulfide isomerase. Methods Enzymol. 1998;290: 26–50. doi:10.1016/s0076-6879(98)90005-2

145. Gauss R, Kanehara K, Carvalho P, Ng DTW, Aebi M. A Complex of Pdi1p and the Mannosidase Htm1p Initiates Clearance of Unfolded Glycoproteins from the Endoplasmic Reticulum. Molecular Cell. 2011;42: 782–793. doi:10.1016/j.molcel.2011.04.027

146. Gillece P, Luz JM, Lennarz WJ, de la Cruz FJ, Römisch K. Export of a Cysteine-Free Misfolded Secretory Protein from the Endoplasmic Reticulum for Degradation Requires Interaction with Protein Disulfide Isomerase. J Cell Biol. 1999;147: 1443–1456.

147. Kimura T, Hosoda Y, Sato Y, Kitamura Y, Ikeda T, Horibe T, et al. Interactions among yeast protein-disulfide isomerase proteins and endoplasmic reticulum chaperone proteins influence their activities. J Biol Chem. 2005;280: 31438–31441. doi:10.1074/jbc.M503377200

148. Nørgaard P, Westphal V, Tachibana C, Alsøe L, Holst B, Winther JR. Functional differences in yeast protein disulfide isomerases. J Cell Biol. 2001;152: 553–562. doi:10.1083/jcb.152.3.553

149. Puig A, Gilbert HF. Protein disulfide isomerase exhibits chaperone and anti-chaperone activity in the oxidative refolding of lysozyme. J Biol Chem. 1994;269: 7764–7771.

150. Cai H, Wang CC, Tsou CL. Chaperone-like activity of protein disulfide isomerase in the refolding of a protein with no disulfide bonds. Journal of Biological Chemistry. 1994;269: 24550–24552. doi:10.1016/S0021-9258(17)31426-6

151. Katiyar S, Till EA, Lennarz WJ. Studies on the function of yeast protein disulfide isomerase in renaturation of proteins. Biochim Biophys Acta. 2001;1548: 47–56. doi:10.1016/s0167-4838(01)00214-x

152. Wang CC, Tsou CL. Protein disulfide isomerase is both an enzyme and a chaperone. FASEB J. 1993;7: 1515–1517. doi:10.1096/fasebj.7.15.7903263

153. Wang Q, Groenendyk J, Michalak M. Glycoprotein Quality Control and Endoplasmic Reticulum Stress. Molecules. 2015;20: 13689–13704. doi:10.3390/molecules200813689

154. Xu C, Ng DTW. Glycosylation-directed quality control of protein folding. Nat Rev Mol Cell Biol. 2015;16: 742–752. doi:10.1038/nrm4073

155. Zielinska DF, Gnad F, Wiśniewski JR, Mann M. Precision mapping of an in vivo N-glycoproteome reveals rigid topological and sequence constraints. Cell. 2010;141: 897–907. doi:10.1016/j.cell.2010.04.012

156. Kelleher DJ, Gilmore R. An evolving view of the eukaryotic oligosaccharyltransferase. Glycobiology. 2006;16: 47R-62R. doi:10.1093/glycob/cwj066

157. Scheper W, Thaminy S, Kais S, Stagljar I, Römisch K. Coordination of *N*-Glycosylation and Protein Translocation across the Endoplasmic Reticulum Membrane by Sss1 Protein*. Journal of Biological Chemistry. 2003;278: 37998–38003. doi:10.1074/jbc.M300176200

158. Loibl M, Wunderle L, Hutzler J, Schulz BL, Aebi M, Strahl S. Protein *O*-Mannosyltransferases Associate with the Translocon to Modify Translocating Polypeptide Chains*. Journal of Biological Chemistry. 2014;289: 8599–8611. doi:10.1074/jbc.M113.543116

159. Shahheydari H, Ragagnin A, Walker AK, Toth RP, Vidal M, Jagaraj CJ, et al. Protein Quality Control and the Amyotrophic Lateral Sclerosis/Frontotemporal Dementia Continuum. Front Mol Neurosci. 2017;10. doi:10.3389/fnmol.2017.00119

160. Bett JS. Proteostasis regulation by the ubiquitin system. Essays Biochem. 2016;60: 143–151. doi:10.1042/EBC20160001

161. Amm I, Sommer T, Wolf DH. Protein quality control and elimination of protein waste: The role of the ubiquitin–proteasome system. Biochimica et Biophysica Acta (BBA) - Molecular Cell Research. 2014;1843: 182–196. doi:10.1016/j.bbamcr.2013.06.031

162. Mezzacasa A, Helenius A. The transitional ER defines a boundary for quality control in the secretion of tsO45 VSV glycoprotein. Traffic. 2002;3: 833–849. doi:10.1034/j.1600-0854.2002.31108.x

163. Stevenson J, Huang EY, Olzmann JA. Endoplasmic Reticulum-Associated Degradation and Lipid Homeostasis. Annu Rev Nutr. 2016;36: 511–542. doi:10.1146/annurev-nutr-071715-051030

164. Tannous A, Pisoni GB, Hebert DN, Molinari M. N-linked sugar-regulated protein folding and quality control in the ER. Semin Cell Dev Biol. 2015;41: 79–89. doi:10.1016/j.semcdb.2014.12.001

165. Helenius A, Aebi M. Roles of N-linked glycans in the endoplasmic reticulum. Annu Rev Biochem. 2004;73: 1019–1049. doi:10.1146/annurev.biochem.73.011303.073752

166. Hammond C, Braakman I, Helenius A. Role of N-linked oligosaccharide recognition, glucose trimming, and calnexin in glycoprotein folding and quality control. Proc Natl Acad Sci U S A. 1994;91: 913–917. doi:10.1073/pnas.91.3.913

167. Jakob CA, Burda P, Roth J, Aebi M. Degradation of Misfolded Endoplasmic Reticulum Glycoproteins in Saccharomyces cerevisiae Is Determined by a Specific Oligosaccharide Structure. J Cell Biol. 1998;142: 1223–1233.

168. Carvalho P, Goder V, Rapoport TA. Distinct ubiquitin-ligase complexes define convergent pathways for the degradation of ER proteins. Cell. 2006;126: 361–373. doi:10.1016/j.cell.2006.05.043

169. Denic V, Quan EM, Weissman JS. A luminal surveillance complex that selects misfolded glycoproteins for ER-associated degradation. Cell. 2006;126: 349–359. doi:10.1016/j.cell.2006.05.045

170. Vembar SS, Brodsky JL. One step at a time: endoplasmic reticulum-associated degradation. Nat Rev Mol Cell Biol. 2008;9: 944–957. doi:10.1038/nrm2546

171. Xu X, Azakami H, Kato A. P-domain and lectin site are involved in the chaperone function of Saccharomyces cerevisiae calnexin homologue. FEBS Letters. 2004;570: 155–160. doi:10.1016/j.febslet.2004.06.039

172. Travers KJ, Patil CK, Wodicka L, Lockhart DJ, Weissman JS, Walter P. Functional and genomic analyses reveal an essential coordination between the unfolded protein response and ER-associated degradation. Cell. 2000;101: 249–258. doi:10.1016/s0092-8674(00)80835-1

173. Bertolotti A, Zhang Y, Hendershot LM, Harding HP, Ron D. Dynamic interaction of BiP and ER stress transducers in the unfolded-protein response. Nat Cell Biol. 2000;2: 326–332. doi:10.1038/35014014

174. Gardner BM, Walter P. Unfolded proteins are Ire1-activating ligands that directly induce the unfolded protein response. Science. 2011;333: 1891–1894. doi:10.1126/science.1209126

175. Pincus D, Chevalier MW, Aragón T, Anken E van, Vidal SE, El-Samad H, et al. BiP Binding to the ER-Stress Sensor Ire1 Tunes the Homeostatic Behavior of the Unfolded Protein Response. PLOS Biology. 2010;8: e1000415. doi:10.1371/journal.pbio.1000415

176. Sidrauski C, Walter P. The transmembrane kinase Ire1p is a site-specific endonuclease that initiates mRNA splicing in the unfolded protein response. Cell. 1997;90: 1031–1039. doi:10.1016/s0092-8674(00)80369-4

177. Cox JS, Walter P. A novel mechanism for regulating activity of a transcription factor that controls the unfolded protein response. Cell. 1996;87: 391–404. doi:10.1016/s0092-8674(00)81360-4

178. Smith MH, Ploegh HL, Weissman JS. Road to Ruin: Targeting Proteins for Degradation in the Endoplasmic Reticulum. Science. 2011;334: 1086–1090. doi:10.1126/science.1209235

179. Lemus L, Goder V. Regulation of Endoplasmic Reticulum-Associated Protein Degradation (ERAD) by Ubiquitin. Cells. 2014;3: 824–847. doi:10.3390/cells3030824

180. Huyer G, Piluek WF, Fansler Z, Kreft SG, Hochstrasser M, Brodsky JL, et al. Distinct Machinery Is Required in *Saccharomyces cerevisiae* for the Endoplasmic Reticulum-associated Degradation of a Multispanning Membrane Protein and a Soluble Luminal Protein*. Journal of Biological Chemistry. 2004;279: 38369–38378. doi:10.1074/jbc.M402468200

181. Feldman M, van der Goot FG. Novel ubiquitin-dependent quality control in the endoplasmic reticulum. Trends Cell Biol. 2009;19: 357–363. doi:10.1016/j.tcb.2009.05.005

182. Wu Y, Swulius MT, Moremen KW, Sifers RN. Elucidation of the molecular logic by which misfolded alpha 1-antitrypsin is preferentially selected for degradation. Proc Natl Acad Sci U S A. 2003;100: 8229–8234. doi:10.1073/pnas.1430537100

183. Xie W, Ng DTW. ERAD substrate recognition in budding yeast. Semin Cell Dev Biol. 2010;21: 533–539. doi:10.1016/j.semcdb.2010.02.007

184. Jakob CA, Bodmer D, Spirig U, Battig P, Marcil A, Dignard D, et al. Htm1p, a mannosidase-like protein, is involved in glycoprotein degradation in yeast. EMBO Rep. 2001;2: 423–430. doi:10.1093/embo-reports/kve089

185. Molinari M, Calanca V, Galli C, Lucca P, Paganetti P. Role of EDEM in the release of misfolded glycoproteins from the calnexin cycle. Science. 2003;299: 1397–1400. doi:10.1126/science.1079474

186. Gauss R, Jarosch E, Sommer T, Hirsch C. A complex of Yos9p and the HRD ligase integrates endoplasmic reticulum quality control into the degradation machinery. Nat Cell Biol. 2006;8: 849–854. doi:10.1038/ncb1445

187. Carvalho P, Stanley AM, Rapoport TA. Retrotranslocation of a misfolded luminal ER protein by the ubiquitin-ligase Hrd1p. Cell. 2010;143: 579–591. doi:10.1016/j.cell.2010.10.028

188. Lilley BN, Ploegh HL. A membrane protein required for dislocation of misfolded proteins from the ER. Nature. 2004;429: 834–840. doi:10.1038/nature02592

189. Wiertz EJ, Tortorella D, Bogyo M, Yu J, Mothes W, Jones TR, et al. Sec61-mediated transfer of a membrane protein from the endoplasmic reticulum to the proteasome for destruction. Nature. 1996;384: 432–438. doi:10.1038/384432a0

190. Glickman MH, Ciechanover A. The ubiquitin-proteasome proteolytic pathway: destruction for the sake of construction. Physiol Rev. 2002;82: 373–428. doi:10.1152/physrev.00027.2001

191. Nakatsukasa K, Huyer G, Michaelis S, Brodsky JL. Dissecting the ER-associated degradation of a misfolded polytopic membrane protein. Cell. 2008;132: 101–112. doi:10.1016/j.cell.2007.11.023

192. Richly H, Rape M, Braun S, Rumpf S, Hoege C, Jentsch S. A series of ubiquitin binding factors connects CDC48/p97 to substrate multiubiquitylation and proteasomal targeting. Cell. 2005;120: 73–84. doi:10.1016/j.cell.2004.11.013

193. Comyn SA, Chan GT, Mayor T. False start: cotranslational protein ubiquitination and cytosolic protein quality control. J Proteomics. 2014;100: 92–101. doi:10.1016/j.jprot.2013.08.005

194. Xue B, Dunker AK, Uversky VN. Orderly order in protein intrinsic disorder distribution: disorder in 3500 proteomes from viruses and the three domains of life. J Biomol Struct Dyn. 2012;30: 137–149. doi:10.1080/07391102.2012.675145

195. Wright PE, Dyson HJ. Intrinsically disordered proteins in cellular signalling and regulation. Nat Rev Mol Cell Biol. 2015;16: 18–29. doi:10.1038/nrm3920

196. Uversky VN, Gillespie JR, Fink AL. Why are “natively unfolded” proteins unstructured under physiologic conditions? Proteins. 2000;41: 415–427. doi:10.1002/1097-0134(20001115)41:3<415::aid-prot130>3.0.co;2-7

197. Dunker AK, Lawson JD, Brown CJ, Williams RM, Romero P, Oh JS, et al. Intrinsically disordered protein. J Mol Graph Model. 2001;19: 26–59. doi:10.1016/s1093-3263(00)00138-8

198. Vacic V, Oldfield CJ, Mohan A, Radivojac P, Cortese MS, Uversky VN, et al. Characterization of Molecular Recognition Features, MoRFs, and Their Binding Partners. J Proteome Res. 2007;6: 2351–2366. doi:10.1021/pr0701411

199. Oldfield CJ, Cheng Y, Cortese MS, Romero P, Uversky VN, Dunker AK. Coupled folding and binding with alpha-helix-forming molecular recognition elements. Biochemistry. 2005;44: 12454–12470. doi:10.1021/bi050736e

200. Mohan A, Oldfield CJ, Radivojac P, Vacic V, Cortese MS, Dunker AK, et al. Analysis of molecular recognition features (MoRFs). J Mol Biol. 2006;362: 1043–1059. doi:10.1016/j.jmb.2006.07.087

201. Uversky VN, Dunker AK. Understanding protein non-folding. Biochim Biophys Acta. 2010;1804: 1231–1264. doi:10.1016/j.bbapap.2010.01.017

202. Kovacs D, Szabo B, Pancsa R, Tompa P. Intrinsically disordered proteins undergo and assist folding transitions in the proteome. Arch Biochem Biophys. 2013;531: 80–89. doi:10.1016/j.abb.2012.09.010

203. Sugase K, Dyson HJ, Wright PE. Mechanism of coupled folding and binding of an intrinsically disordered protein. Nature. 2007;447: 1021–1025. doi:10.1038/nature05858

204. Espinoza-Fonseca LM. Reconciling binding mechanisms of intrinsically disordered proteins. Biochemical and Biophysical Research Communications. 2009;382: 479–482. doi:10.1016/j.bbrc.2009.02.151

205. Wright PE, Dyson HJ. Intrinsically unstructured proteins: re-assessing the protein structure-function paradigm. J Mol Biol. 1999;293: 321–331. doi:10.1006/jmbi.1999.3110

206. Dyson HJ, Wright PE. Intrinsically unstructured proteins and their functions. Nat Rev Mol Cell Biol. 2005;6: 197–208. doi:10.1038/nrm1589

207. Pontius BW. Close encounters: why unstructured, polymeric domains can increase rates of specific macromolecular association. Trends Biochem Sci. 1993;18: 181–186. doi:10.1016/0968-0004(93)90111-y

208. Bah A, Vernon RM, Siddiqui Z, Krzeminski M, Muhandiram R, Zhao C, et al. Folding of an intrinsically disordered protein by phosphorylation as a regulatory switch. Nature. 2015;519: 106–109. doi:10.1038/nature13999

209. Hwang Fu YH, Chandrasekar S, Lee JH, Shan SO. A molecular recognition feature mediates ribosome-induced SRP-receptor assembly during protein targeting. The Journal of cell biology. 2019;218: 3307–3319. doi:10.1083/jcb.201901001

210. Lee CW, Ferreon JC, Ferreon ACM, Arai M, Wright PE. Graded enhancement of p53 binding to CREB-binding protein (CBP) by multisite phosphorylation. Proc Natl Acad Sci U S A. 2010;107: 19290–19295. doi:10.1073/pnas.1013078107

211. Pufall MA, Lee GM, Nelson ML, Kang H-S, Velyvis A, Kay LE, et al. Variable control of Ets-1 DNA binding by multiple phosphates in an unstructured region. Science. 2005;309: 142–145. doi:10.1126/science.1111915

212. Van Roey K, Gibson TJ, Davey NE. Motif switches: decision-making in cell regulation. Curr Opin Struct Biol. 2012;22: 378–385. doi:10.1016/j.sbi.2012.03.004

213. Iakoucheva LM, Radivojac P, Brown CJ, O'Connor TR, Sikes JG, Obradovic Z, et al. The importance of intrinsic disorder for protein phosphorylation. Nucleic Acids Res. 2004;32: 1037–1049. doi:10.1093/nar/gkh253

214. Valcárcel R, Weber U, Jackson DB, Benes V, Ansorge W, Bohmann D, et al. Sec61beta, a subunit of the protein translocation channel, is required during Drosophila development. J Cell Sci. 1999;112 (Pt 23): 4389–4396. doi:10.1242/jcs.112.23.4389

215. Zhu Y, Zhang G, Lin S, Shi J, Zhang H, Hu J. Sec61β facilitates the maintenance of endoplasmic reticulum homeostasis by associating microtubules. Protein Cell. 2018;9: 616–628. doi:10.1007/s13238-017-0492-5

216. Toikkanen J, Gattis E, Takeis K, Saloheimo M. Yeast Protein Translocation Comdex : Isolation of Two Genes SEBl and SEB2 Encoding ' Proteins Homologous to the SecGlp subunit. Yeast. 1996;12: 425–438.

217. Jonikas MC, Collins SR, Denic V, Oh E, Quan EM, Schmid V, et al. Comprehensive characterization of genes required for protein folding in the endoplasmic reticulum. Science. 2009;323: 1693–1697. doi:10.1126/science.1167983

218. Kinch LN, Saier, Jr MH, Grishin NV. Sec61β – a component of the archaeal protein secretory system. Trends in Biochemical Sciences. 2002;27: 170–171. doi:10.1016/S0968-0004(01)02055-2

219. Soromani C, Zeng N, Hollemeyer K, Heinzle E, Klein MC, Tretter T, et al. N-acetylation and phosphorylation of Sec complex subunits in the ER membrane. BMC Cell Biology. 2012;13: 34. doi:10.1186/1471-2121-13-34

220. Gruss OJ, Feick P, Frank R, Dobberstein B. Phosphorylation of components of the ER translocation site. European Journal of Biochemistry. 1999;260: 785–793. doi:10.1046/j.1432-1327.1999.00215.x

221. Zhao X, Jäntti J. Functional characterization of the trans-membrane domain interactions of the Sec61 protein translocation complex beta-subunit. BMC Cell Biology. 2009;10: 76. doi:10.1186/1471-2121-10-76

222. Feng D, Zhao X, Soromani C, Toikkanen J, Römisch K, Vembar SS, et al. The Transmembrane Domain Is Sufficient for Sbh1p Function, Its Association with the Sec61 Complex, and Interaction with Rtn1p *. Journal of Biological Chemistry. 2007;282: 30618–30628. doi:10.1074/jbc.M701840200

223. Kalies K-U, Rapoport TA, Hartmann E. The β Subunit of the Sec61 Complex Facilitates Cotranslational Protein Transport and Interacts with the Signal Peptidase during Translocation. Journal of Cell Biology. 1998;141: 887–894. doi:10.1083/jcb.141.4.887

224. Kalies KU, Görlich D, Rapoport TA. Binding of ribosomes to the rough endoplasmic reticulum mediated by the Sec61p-complex. Journal of Cell Biology. 1994;126: 925–934. doi:10.1083/jcb.126.4.925

225. Levy R, Wiedmann M, Kreibich G. In Vitro Binding of Ribosomes to the β Subunit of the Sec61p Protein Translocation Complex*. Journal of Biological Chemistry. 2001;276: 2340–2346. doi:10.1074/jbc.M004867200

226. Laird V, High S. Discrete Cross-linking Products Identified during Membrane Protein Biosynthesis*. Journal of Biological Chemistry. 1997;272: 1983–1989. doi:10.1074/jbc.272.3.1983

227. MacKinnon AL, Paavilainen VO, Sharma A, Hegde RS, Taunton J. An allosteric Sec61 inhibitor traps nascent transmembrane helices at the lateral gate. Schekman R, editor. eLife. 2014;3: e01483. doi:10.7554/eLife.01483

228. Antonin W, Meyer H-A, Hartmann E. Interactions between Spc2p and Other Components of the Endoplasmic Reticulum Translocation Sites of the YeastSaccharomyces cerevisiae *. Journal of Biological Chemistry. 2000;275: 34068–34072. doi:10.1074/jbc.M006126200

229. Helmers J, Schmidt D, Glavy JS, Blobel G, Schwartz T. The beta-subunit of the protein-conducting channel of the endoplasmic reticulum functions as the guanine nucleotide exchange factor for the beta-subunit of the signal recognition particle receptor. J Biol Chem. 2003;278: 23686–23690. doi:10.1074/jbc.C300180200

230. Schwartz T, Blobel G. Structural basis for the function of the beta subunit of the eukaryotic signal recognition particle receptor. Cell. 2003;112: 793–803. doi:10.1016/s0092-8674(03)00161-2

231. Valk E, Venta R, Örd M, Faustova I, Kõivomägi M, Loog M. Multistep phosphorylation systems: Tunable components of biological signaling circuits. Molecular Biology of the Cell. 2014;25: 3456–3460. doi:10.1091/mbc.E14-02-0774

232. Bah A, Forman-Kay JD. Modulation of intrinsically disordered protein function by post-translational modifications. Journal of Biological Chemistry. 2016;291: 6696–6705. doi:wu

233. Goyal U, Blackstone C. Untangling the web: mechanisms underlying ER network formation. Biochim Biophys Acta. 2013;1833: 2492–2498. doi:10.1016/j.bbamcr.2013.04.009

234. Terasaki M, Chen LB, Fujiwara K. Microtubules and the endoplasmic reticulum are highly interdependent structures. J Cell Biol. 1986;103: 1557–1568. doi:10.1083/jcb.103.4.1557

235. Guo W, Novick P. The exocyst meets the translocon: a regulatory circuit for secretion and protein synthesis? Trends Cell Biol. 2004;14: 61–63. doi:10.1016/j.tcb.2003.12.008

236. Toikkanen JH, Miller KJ, Söderlund H, Jäntti J, Keränen S. The β Subunit of the Sec61p Endoplasmic Reticulum Translocon Interacts with the Exocyst Complex in Saccharomyces cerevisiae*. Journal of Biological Chemistry. 2003;278: 20946–20953. doi:10.1074/jbc.M213111200

237. Lipschutz JH, Lingappa VR, Mostov KE. The exocyst affects protein synthesis by acting on the translocation machinery of the endoplasmic reticulum. J Biol Chem. 2003;278: 20954–20960. doi:10.1074/jbc.M213210200

238. De Craene J-O, Coleman J, Estrada de Martin P, Pypaert M, Anderson S, Yates JR, et al. Rtn1p Is Involved in Structuring the Cortical Endoplasmic Reticulum. Mol Biol Cell. 2006;17: 3009–3020. doi:10.1091/mbc.E06-01-0080

239. Voeltz GK, Prinz WA, Shibata Y, Rist JM, Rapoport TA. A class of membrane proteins shaping the tubular endoplasmic reticulum. Cell. 2006;124: 573–586. doi:10.1016/j.cell.2005.11.047

240. Piña FJ, Fleming T, Pogliano K, Niwa M. Reticulons regulate the ER inheritance block during ER Stress. Dev Cell. 2016;37: 279–288. doi:10.1016/j.devcel.2016.03.025

241. Fan C-W, Chan C-C, Chen K-T, Twu J, Huang Y-S, Han C-L, et al. Identification of SEC61β and its autoantibody as biomarkers for colorectal cancer. Clinica Chimica Acta. 2011;412: 887–893. doi:10.1016/j.cca.2011.01.012

242. Pilon M, Römisch K, Quach D, Schekman R. Sec61p serves multiple roles in secretory precursor binding and translocation into the endoplasmic reticulum membrane. Kaiser C, editor. Molecular Biology of the Cell. 1998;9: 3455–3473. doi:10.1091/mbc.9.12.3455

243. Ng DTW, Brown JD, Walter P. Signal sequences specify the targeting route to the endoplasmic reticulum membrane. Journal of Cell Biology. 1996;134: 269–278. doi:10.1083/jcb.134.2.269

244. Giaever G, Chu AM, Ni L, Connelly C, Riles L, Véronneau S, et al. Functional profiling of the Saccharomyces cerevisiae genome. Nature. 2002;418: 387–391. doi:10.1038/nature00935

245. Shen SH, Chrétien P, Bastien L, Slilaty SN. Primary sequence of the glucanase gene from Oerskovia xanthineolytica. Expression and purification of the enzyme from Escherichia coli. J Biol Chem. 1991;266: 1058–1063.

246. D H. Studies on transformation of Escherichia coli with plasmids. Journal of molecular biology. 1983;166. doi:10.1016/s0022-2836(83)80284-8

247. Sikorski RS, Hieter P. A system of shuttle vectors and yeast host strains designed for efficient manipulation of DNA in Saccharomyces cerevisiae. Genetics. 1989;122: 19–27. doi:10.1093/genetics/122.1.19

248. Falcone D, Henderson MP, Nieuwland H, Coughlan CM, Brodsky JL, Andrews DW. Stability and Function of the Sec61 Translocation Complex Depends on the Sss1p Tail-Anchor Sequence Domina. Biochemical Journal. 2011;436: 291–303. doi:10.1042/BJ20101865.Stability

249. Birnboim HC, Doly J. A rapid alkaline extraction procedure for screening recombinant plasmid DNA. Nucleic Acids Research. 1979;7: 1513–1523. doi:10.1093/nar/7.6.1513

250. Gietz RD, Woods RA. Transformation of yeast by lithium acetate/single-stranded carrier DNA/polyethylene glycol method. Methods Enzymol. 2002;350: 87–96. doi:10.1016/s0076-6879(02)50957-5

251. Schäuble N, Cavalié A, Zimmermann R, Jung M. Interaction of Pseudomonas aeruginosa Exotoxin A with the human Sec61 complex suppresses passive calcium efflux from the endoplasmic reticulum. Channels (Austin). 2014;8: 76–83. doi:10.4161/chan.26526

252. Allen WJ, Collinson I, Römisch K. Post-translational protein transport by the Sec complex. Trends in Biochemical Sciences. 2019;44: 1–7. doi:10.1016/j.tibs.2019.03.003

253. Barbieri G, Simon J, Lupusella CR, Pereira F, Elia F, Meyer H, et al. Sec61 channel subunit Sbh1/Sec61β promotes ER translocation of proteins with suboptimal targeting sequences and is fine-tuned by phosphorylation. Journal of Biological Chemistry. 2023;299: 102895. doi:10.1016/j.jbc.2023.102895

254. Waters MG, Evans EA, Blobel G. Prepro-alpha-factor has a cleavable signal sequence. Journal of Biological Chemistry. 1988;263: 6209–6214. doi:10.1016/S0021-9258(18)68773-3

255. Pilon M, Schekman R, Römisch K. Sec61p mediates export of a misfolded secretory protein from the endoplasmic reticulum to the cytosol for degradation. The EMBO Journal. 1997;16: 4540–4548. doi:10.1093/emboj/16.15.4540

256. Mizunaga T, Katakura Y, Miura T, Maruyama Y. Purification and Characterization of Yeast Protein Disulfide Isomerase. The Journal of Biochemistry. 1990;108: 846–851. doi:10.1093/oxfordjournals.jbchem.a123291

257. Valls LA, Hunter CP, Rothman JH, Stevens TH. Protein sorting in yeast: The localization determinant of yeast vacuolar carboxypeptidase Y resides in the propeptide. Cell. 1987;48: 887–897. doi:10.1016/0092-8674(87)90085-7

258. Kimata Y, Kimata YI, Shimizu Y, Abe H, Farcasanu IC, Takeuchi M, et al. Genetic Evidence for a Role of BiP/Kar2 That Regulates Ire1 in Response to Accumulation of Unfolded Proteins. MBoC. 2003;14: 2559–2569. doi:10.1091/mbc.e02-11-0708

259. Tran JR, Tomsic LR, Brodsky JL. A Cdc48p-associated Factor Modulates Endoplasmic Reticulum-associated Degradation, Cell Stress, and Ubiquitinated Protein Homeostasis*. Journal of Biological Chemistry. 2011;286: 5744–5755. doi:10.1074/jbc.M110.179259

260. Nikawa J, Akiyoshi M, Hirata S, Fukuda T. Saccharomyces cerevisiae IRE2/HAC1 is involved in IRE1-mediated KAR2 expression. Nucleic Acids Res. 1996;24: 4222–4226. doi:10.1093/nar/24.21.4222

261. Woo DK, Poyton RO. The absence of a mitochondrial genome in rho0 yeast cells extends lifespan independently of retrograde regulation. Experimental Gerontology. 2009;44: 390–397. doi:10.1016/j.exger.2009.03.001

262. Gabel CA, Bergmann JE. Processing of the asparagine-linked oligosaccharides of secreted and intracellular forms of the vesicular stomatitis virus G protein: in vivo evidence of Golgi apparatus compartmentalization. Journal of Cell Biology. 1985;101: 460–469. doi:10.1083/jcb.101.2.460

263. Autzen HE, Julius D, Cheng Y. Membrane mimetic systems in CryoEM: keeping membrane proteins in their native environment. Current Opinion in Structural Biology. 2019;58: 259–268. doi:10.1016/j.sbi.2019.05.022

264. Hovers J, Potschies M, Polidori A, Pucci B, Raynal S, Bonneté F, et al. A class of mild surfactants that keep integral membrane proteins water-soluble for functional studies and crystallization. Molecular Membrane Biology. 2011;28: 171–181. doi:10.3109/09687688.2011.552440

265. Missel JW, Salustros N, Becares ER, Steffen JH, Laursen AG, Garcia AS, et al. Cyclohexyl-α maltoside as a highly efficient tool for membrane protein studies. Current Research in Structural Biology. 2021;3: 85–94. doi:10.1016/j.crstbi.2021.03.002

266. Bhadra P, Yadhanapudi L, Römisch K, Helms V. How does Sec63 affect the conformation of Sec61 in yeast? PLOS Computational Biology. 2021;17: e1008855. doi:10.1371/journal.pcbi.1008855

267. Young BP, Craven RA, Reid PJ, Willer M, Stirling CJ. Sec63p and Kar2p are required for the translocation of SRP-dependent precursors into the yeast endoplasmic reticulum in vivo. The EMBO Journal. 2001;20: 262–271. doi:10.1093/emboj/20.1.262

268. Yadhanapudi L, Bhadra P, Barbieri G, Jung M, Lommel M, Helms V, et al. The conserved membrane-proximal domain of Sbh1/ Sec61β guides signal peptides into the Sec61 channel. bioRxiv; 2024. p. 2024.03.12.584615. doi:10.1101/2024.03.12.584615

269. Roberts CJ, Pohlig G, Rothman JH, Stevens TH. Structure, biosynthesis, and localization of dipeptidyl aminopeptidase B, an integral membrane glycoprotein of the yeast vacuole. J Cell Biol. 1989;108: 1363–1373. doi:10.1083/jcb.108.4.1363

270. Mészáros B, Erdős G, Dosztányi Z. IUPred2A: context-dependent prediction of protein disorder as a function of redox state and protein binding. Nucleic Acids Research. 2018;46: W329–W337. doi:10.1093/nar/gky384

271. Malhis N, Jacobson M, Gsponer J. MoRFchibi SYSTEM: software tools for the identification of MoRFs in protein sequences. Nucleic Acids Research. 2016;44: W488–W493. doi:10.1093/nar/gkw409

272. Fang C, Noguchi T, Tominaga D, Yamana H. MFSPSSMpred: identifying short disorder-to-order binding regions in disordered proteins based on contextual local evolutionary conservation. BMC Bioinformatics. 2013;14: 300. doi:10.1186/1471-2105-14-300

273. Disfani FM, Hsu W-L, Mizianty MJ, Oldfield CJ, Xue B, Dunker AK, et al. MoRFpred, a computational tool for sequence-based prediction and characterization of short disorder-to-order transitioning binding regions in proteins. Bioinformatics. 2012;28: i75–i83. doi:10.1093/bioinformatics/bts209

274. Elia F, Yadhanapudi L, Tretter T, Römisch K. The N-terminus of Sec61p plays key roles in ER protein import and ERAD. PLOS ONE. 2019;14: e0215950. doi:10.1371/journal.pone.0215950

275. Mészáros B, Dobson L, Fichó E, Tusnády GE, Dosztányi Z, Simon I. Sequential, Structural and Functional Properties of Protein Complexes Are Defined by How Folding and Binding Intertwine. Journal of Molecular Biology. 2019;431: 4408–4428. doi:10.1016/j.jmb.2019.07.034

276. Newcombe EA, Delaforge E, Hartmann-Petersen R, Skriver K, Kragelund BB. How phosphorylation impacts intrinsically disordered proteins and their function. Mukhopadhyay S, editor. Essays in Biochemistry. 2022;66: 901–913. doi:10.1042/EBC20220060

277. Wei Y-Y, Liang S, Zhang Y-R, Lu J-P, Lin F-C, Liu X-H. MoSec61β, the beta subunit of Sec61, is involved in fungal development and pathogenicity, plant immunity, and ER-phagy in *Magnaporthe oryzae*. Virulence. 2020; 21505594.2020.1848983. doi:10.1080/21505594.2020.1848983

278. Santiago-Tirado FH, Hurtaux T, Geddes-McAlister J, Nguyen D, Helms V, Doering TL, et al. The ER Protein Translocation Channel Subunit Sbh1 Controls Virulence of Cryptococcus neoformans. Idnurm A, editor. mBio. 2023; e03384-22. doi:10.1128/mbio.03384-22

279. Diaz-Ruiz R, Rigoulet M, Devin A. The Warburg and Crabtree effects: On the origin of cancer cell energy metabolism and of yeast glucose repression. Biochimica et Biophysica Acta (BBA) - Bioenergetics. 2011;1807: 568–576. doi:10.1016/j.bbabio.2010.08.010

280. Phuong HT, Ishiwata-Kimata Y, Nishi Y, Oguchi N, Takagi H, Kimata Y. Aeration mitigates endoplasmic reticulum stress in Saccharomyces cerevisiae even without mitochondrial respiration. Microbial Cell. 2021;8: 77–86. doi:10.15698/MIC2021.04.746

281. Weng T, Steinchen W, Beatrix B, Berninghausen O, Becker T, Bange G, et al. Architecture of the active post-translational Sec translocon. The EMBO Journal. 2020; 1–12. doi:10.15252/embj.2020105643

282. Jermy AJ, Willer M, Davis E, Wilkinson BM, Stirling CJ. The Brl domain in Sec63p is required for assembly of functional endoplasmic reticulum translocons. Journal of Biological Chemistry. 2006;281: 7899–7906. doi:10.1074/jbc.M511402200

283. Itskanov S, Kuo KM, Gumbart JC, Park E. Stepwise gating of the Sec61 protein-conducting channel by Sec63 and Sec62. Nature Structural and Molecular Biology. 2021. doi:10.1038/s41594-020-00541-x

284. Mutka SC, Walter P. Multifaceted Physiological Response Allows Yeast to Adapt to the Loss of the Signal Recognition Particle-dependent Protein-targeting Pathway. Mol Biol Cell. 2001;12: 577–588.

285. Hosokawa N, Tremblay LO, You Z, Herscovics A, Wada I, Nagata K. Enhancement of Endoplasmic Reticulum (ER) Degradation of Misfolded Null Hong Kong α1-Antitrypsin by

Human ER Mannosidase I*. Journal of Biological Chemistry. 2003;278: 26287–26294. doi:10.1074/jbc.M303395200

286. Hosokawa N, Wada I, Hasegawa K, Yorihuzi T, Tremblay LO, Herscovics A, et al. A novel ER α-mannosidase-like protein accelerates ER-associated degradation. EMBO reports. 2001;2: 415–422. doi:10.1093/embo-reports/kve084

287. Barbieri G. Regulation of protein transport into the ER by phosphorylation of Sbh1/Sec61β. 2022 [cited 6 May 2024]. doi:10.22028/D291-38985

288. Buchan DWA, Minneci F, Nugent TCO, Bryson K, Jones DT. Scalable web services for the PSIPRED Protein Analysis Workbench. Nucleic Acids Research. 2013;41: W349–W357. doi:10.1093/nar/gkt381

289. Baek M, DiMaio F, Anishchenko I, Dauparas J, Ovchinnikov S, Lee GR, et al. Accurate prediction of protein structures and interactions using a three-track neural network. Science. 2021;373: 871–876. doi:10.1126/science.abj8754

290. Jumper J, Evans R, Pritzel A, Green T, Figurnov M, Ronneberger O, et al. Highly accurate protein structure prediction with AlphaFold | Nature. Nature. 2021;596: 583–589. doi:10.1038/s41586-021-03819-2

291. Mirdita M, Schütze K, Moriwaki Y, Heo L, Ovchinnikov S, Steinegger M. ColabFold: making protein folding accessible to all. Nat Methods. 2022;19: 679–682. doi:10.1038/s41592-022-01488-1

292. Chakrabarti P, Chakravarty D. Intrinsically disordered proteins/regions and insight into their biomolecular interactions. Biophysical Chemistry. 2022;283: 106769. doi:10.1016/j.bpc.2022.106769

PUBLICATIONS

Yadhanapudi, L., Bhadra, P., Barbieri, G., Jung, M., Lommel, M., Helms, V. and Romisch, K., 2024. The conserved membrane-proximal domain of Sbh1/Sec61β guides signal peptides into the Sec61 channel. *bioRxiv*, pp.2024-03. (In preparation)

Bhadra, P., **Yadhanapudi, L.**, Römisch, K. and Helms, V., 2021. How does Sec63 affect the conformation of Sec61 in yeast?. *PLOS Computational Biology*, *17*(3), p.e1008855.

Yadhanapudi, L. and Römisch, K. (2019) Role of Sbh1 in the Sec channel. EMBO Workshop: Tools for Structural Biology of Membrane Proteins, Hamburg (Germany) (POSTER)

Yadhanapudi, L., Bhadra, P., Jung, J., Helms, V. and Römisch, K. (2022) The intrinsically disordered cytosolic domain of Sbh1 and its interactions. EMBO Workshop: Protein termini – from mechanisms to biological impact, Bergen (Norway) (POSTER)

ACKNOWLEDGEMENTS

My deepest gratitude and appreciation go to my supervisor Prof. Dr. Karin Römisch for her support and guidance during my PhD journey. Her vast expertise and ease of navigating challenges in research have been truly inspiring. Working with you has shaped me into a confident, independent scientist. Thank you for giving me this opportunity, for your patience and encouragement every step of the way.

I would like to thank my second supervisor Prof. Dr. Martin van der Laan for his interest in my work and his suggestions, especially in the early days of my research.

I thank Prof. Dr. Volkhard Helms and Dr. Pratiti Bhadra for their collaboration and contributions to this work. The distinct viewpoints you both would bring to our discussions has broadened my perspectives immeasurably.

I would like to thank Dr. Martin Jung for synthesising the peptide panning membranes and peptide probes that I used in my study, and for the help with troubleshooting when I was optimising the method.

I would also like to thank Prof. Dr. Schmitt group for kindly sharing their equipment, especially Steffi, Ruth, Hasib and Achim for being friendly and always ready to help.

I also thank Prof. Dr. Kathrin Philippar for allowing me to use their ultracentrifuge. My special thanks to Dr. Jens Neunzig for helping me out many times with the instrument and the isotope lab.

I thank Dr. Martin Pool (University of Manchester, UK) for contributing anti-DPAPB antibodies, Prof. Charles Barlowe (Dartmouth University, USA) for gifting the anti-Gls1 antibodies, and Prof. Dr. Sabine Rospert (University of Freiburg, Germany) for kindly providing anti-RpL17a antibodies. I also thank Prof. Bruce Morgan and Gurleen for kindly providing *rho*^{0} and *Δcox6* strains.

Now to my dear lab mates. Guido, thank you for being such a great companion throughout this adventure. We have been through a crazy rollercoaster together in these past few years, thank you for being a great friend. To Richa, your arrival transformed our shared workspace. Thank you for the lively discussions, for the laughter and turning our shared struggles into fond memories. Thank you, Aline for being such a bright spark during the Pandemic days. Vanessa and Yassaman, you have become such great friends to me within a short span of time, your energy is infectious. I want to thank all the students who did their lab rotations with us, especially Paula, Lea, Janine and Leon, for bringing in their fresh minds, asking oh so many questions and keeping me on my toes.

My gratitude to Dr. Mark Lommel, your insights and friendship have been invaluable to me. Thank you for your help with setting up SDM and for designing the peptide panning membrane. I will miss our conversations about research, life and everything in between.

I thank Juncal Z. González, for helping with everything inside and outside the university. It was so easy to navigate in this new country with an unknown language, I would have been lost without you. Thank you for making me feel safe and welcome.

I would like to thank Prof. Dr. Gert-Wieland Kohring for handing down the technical know-how of everything in the lab. I also thank Carmen Clemens her technical assistance during the initial days of my PhD and introducing me to German culture.

I thank Nina Dhonau for helping me out with administrative issues and making my last few days in the lab a breeze.

Last but not the least, I would like to thank my family. I thank my parents for always believing in me, trusting my judgement and encouraging me to grab every opportunity. The person I am today is because of your love, support, and sacrifices. To Kashyap, thank you for being the best brother in the world, my anchor. I thank my cousins for being the unwavering support system that I can always rely on, no matter where we are or what time it is. And my dear husband. You are my best friend and my biggest cheerleader, always motivating me and holding my hand when things get rough. Thank you for always being there for me, no matter what.

Appendix A

Supplementary Data

APPENDIX A SUPPLEMENTARY DATA

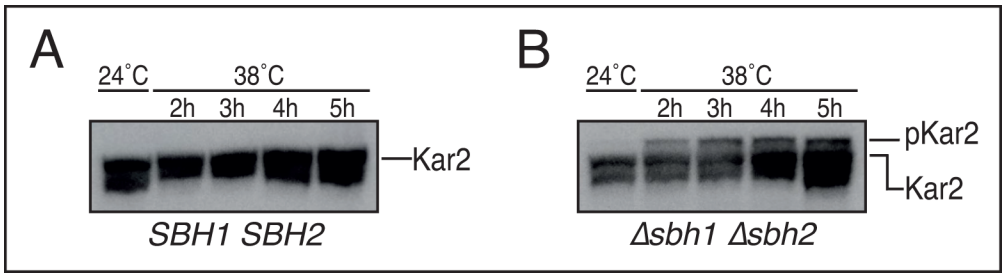

Supplementary Figure 1 Accumulation of pKar2 with time in *Δsbh1 sbh2* cells. Yeast wildtype *SBH1 SBH2* and mutant *Δsbh1 Δsbh2* strains were grown at their permissive 24 ˚C to an OD_{600} of 0.5 and shifted to their restrictive 38 ˚C. A 2 OD_{600} of cells were harvested after 2h, 3h, 4, and 5h to prepare cell extracts. For each sample 0.25 OD_{600} was used to resolve by SDS-PAGE, followed by immunoblotting against Kar2. **A)** Kar2 in *SBH1 SBH2* cells grown at permissive 24 ˚C to 1 OD_{600} and at restrictive temperature for 2-5h. No pKar2 accumulation was seen in the cells at 38 ˚C. **B)** Kar2 in *Δsbh1 Δsbh2* cells grown at permissive 24 ˚C to 1 OD_{600} and at restrictive temperature for 2-5h. Accumulation of pKar2 increased with time at 38 ˚C. However, resolution between Kar2 and pKar2 bands decreased considerably from 4h. This experiment was performed by M.Sc. students from class of Infection Biology in 2019 under my supervision.

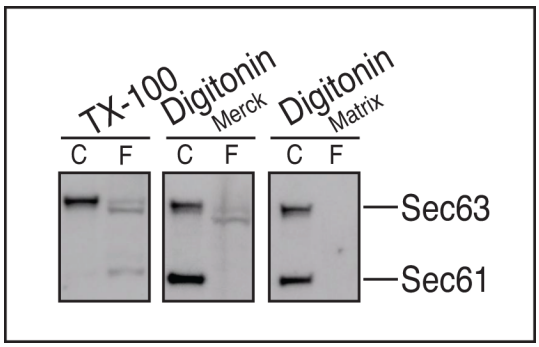

Supplementary Figure 2 Solubilisation Efficiency and Sec complex Stability in newly acquired Digitonin. A 0.3 OD_{280} of *SBH1 SBH2* microsomes derived from cells grown at 24 ˚C were solubilised in 3% Digitonin (Merck, existing), 3% Digitonin (Matrix Bioscience, newly acquired) or 1% TX-100 were precipitated with equilibrated ConA-Sepharose. Proteins were precipitated from aspirated free fractions. The samples were resolved by SDS-PAGE and immunoblotted against Sec63 and Sec61. ConA bound fraction (C), and free, unbound fraction (F) are marked. Both Sec63 and Sec61 were found in the C fraction of digitonin (Matrix Bioscience), like digitonin (Merck).

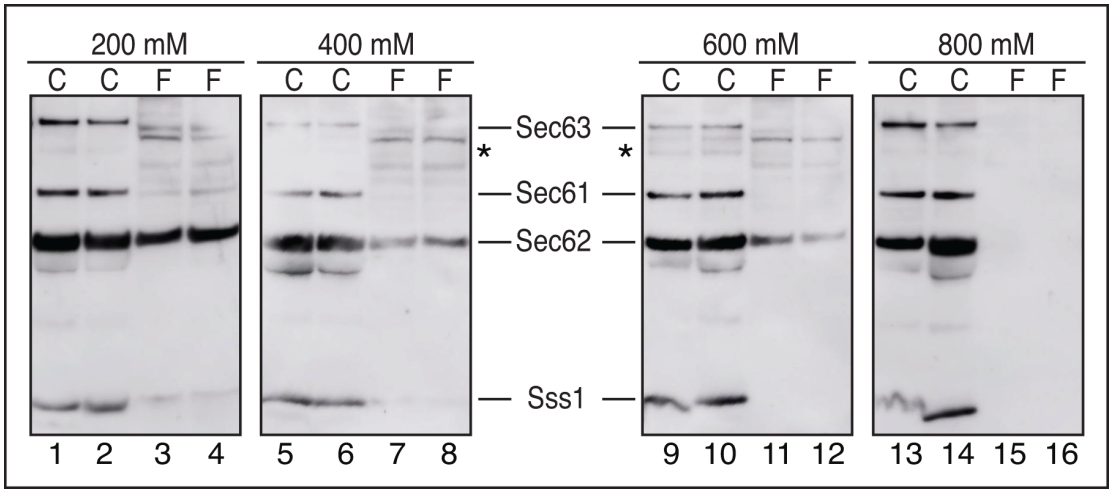

Supplementary Figure 4 Optimising salt concentration to test Sec complex stability. Microsomes from *SBH1 SBH2* strain grown at 24 ˚C, 0.3 OD_{280} each, were solubilised in 3% digitonin and then diluted to 1% digitonin in duplicates while raising KOAc concentration to 600 mM or 800 mM KOAc using Extraction Buffer containing 1 mM KOAc and no detergent, reducing to 200 mM using Extraction Buffer containing no KOAc and no detergent or keeping the KOAc concentration at 400 mM using Extraction Buffer containing 400 mM KOAc and no detergent. Samples were then precipitated with ConA-Sepharose, free fraction was aspirated, and unbound proteins were precipitated using TCA precipitation method. The samples were analysed by Western Blotting and probed for Sec63, Sec62, Sec61 and Sss1. The sample with 400 mM KOAc acts as control (lanes 5 to 8). Sec63, Sec62, Sec61 and Sss1 were all present in all C fractions (lanes 1 and 2, 5 and 6, 9 and 10, and 13 and 14). The * marks a 70 kDa protein cross-reacting with Sec63 antibody.

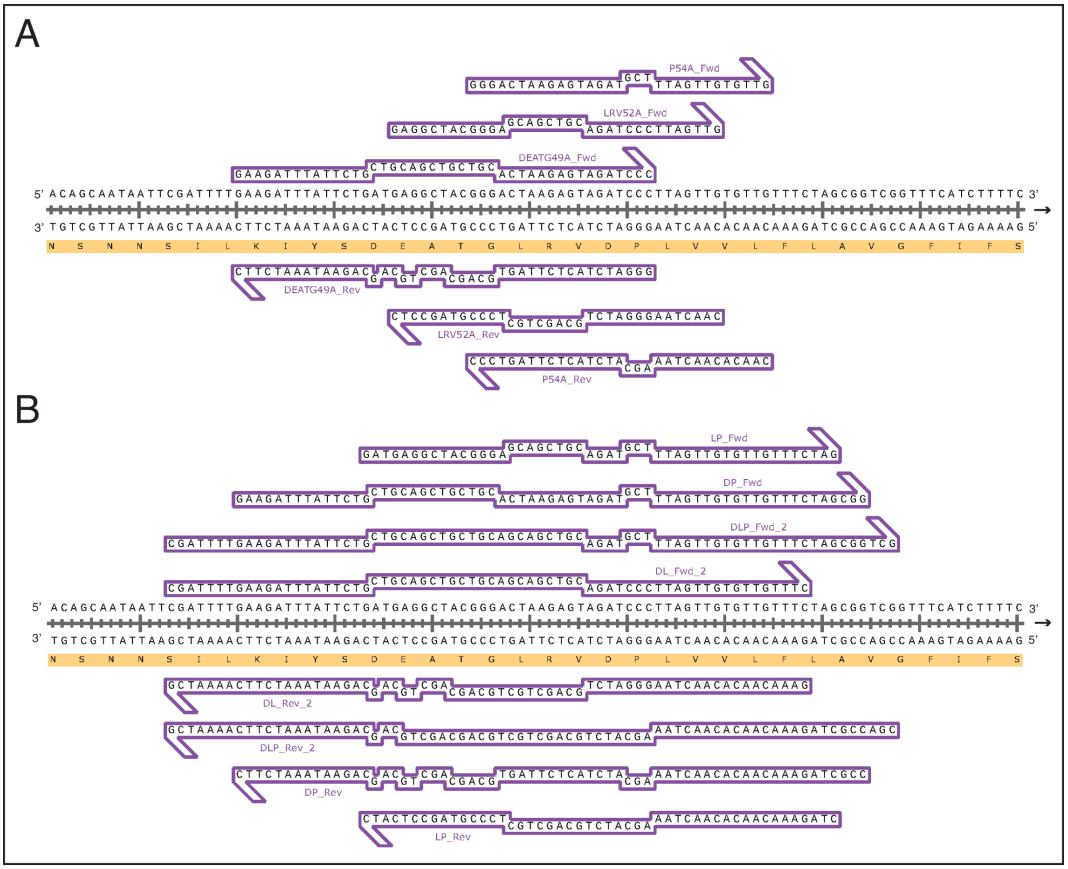

Supplementary Figure 3 Primers used for site directed mutagenesis of *SBH1*. A) Primers used to generate CMP mutants aligned with *SBH1* coding sequence. **B)** Primers used to generate combo mutants aligned with *SBH1* coding sequence.

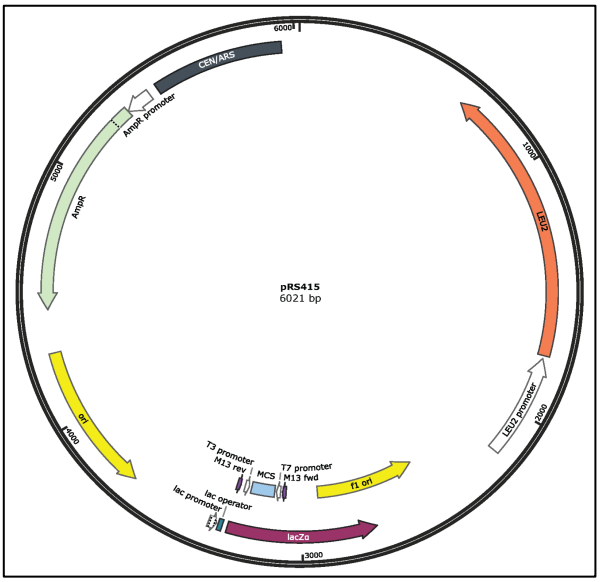

Supplementary Figure 5 Map of pRS415 plasmid. Yeast centromeric plasmid pRS415 used as the vector for generation of Sbh1 CMP and combo mutants.

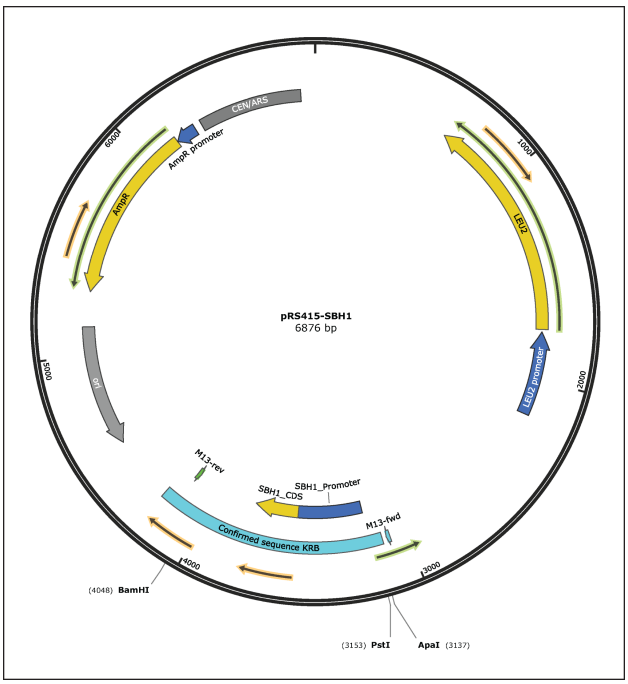

Supplementary Figure 6 Map of pRS415-*SBH1*. The *SBH1* coding sequence was used as the template for site directed mutagenesis of the CMP region.

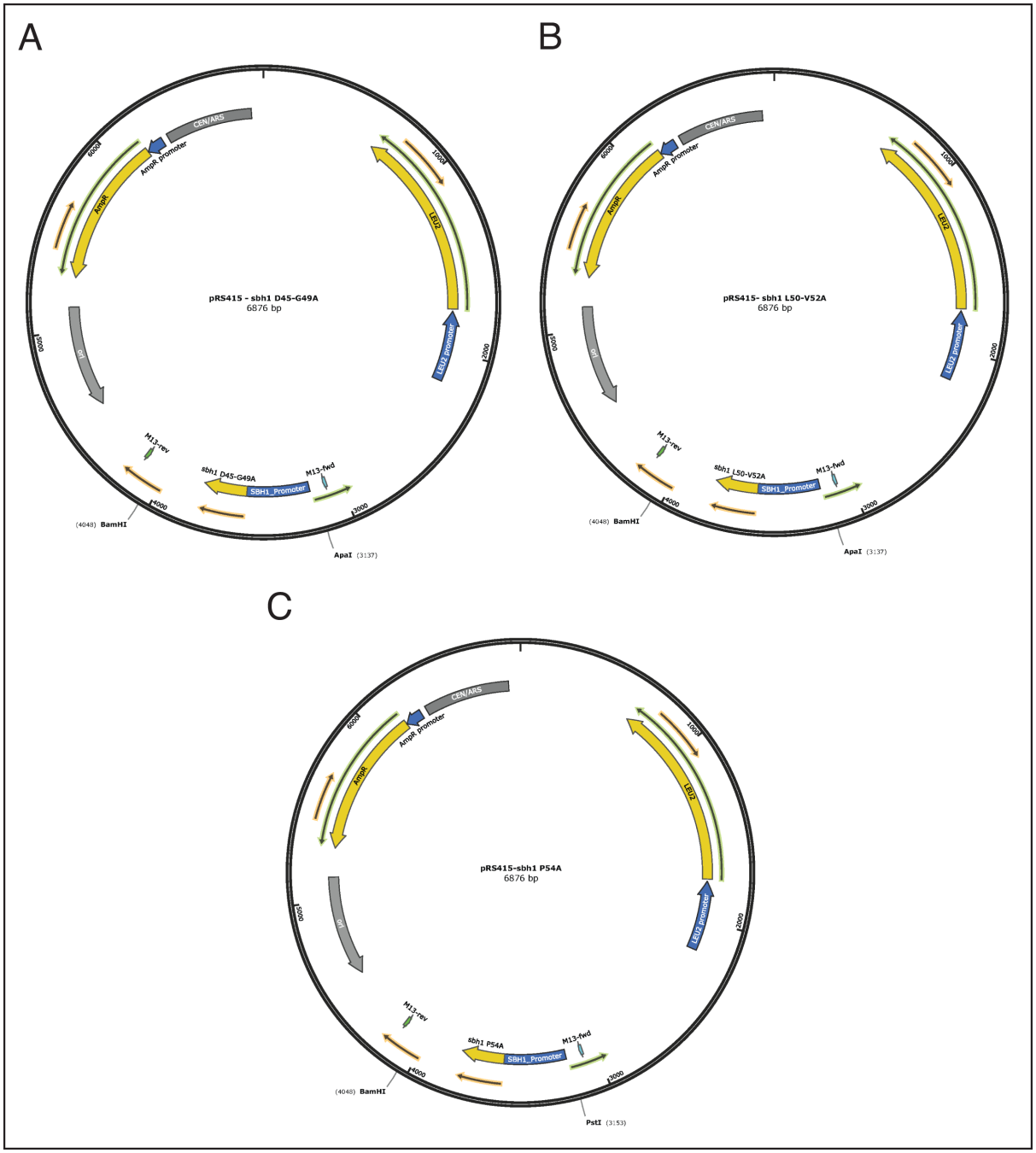

Supplementary Figure 7 Plasmids for CMP mutants. A) Map of pRS415-*sbh1D45-G49A* plasmid. **B)** Map of pRS415-*sbh1L50-V52A* plasmid. **C)** Map of pRS415-*sbh1P54A* plasmid.

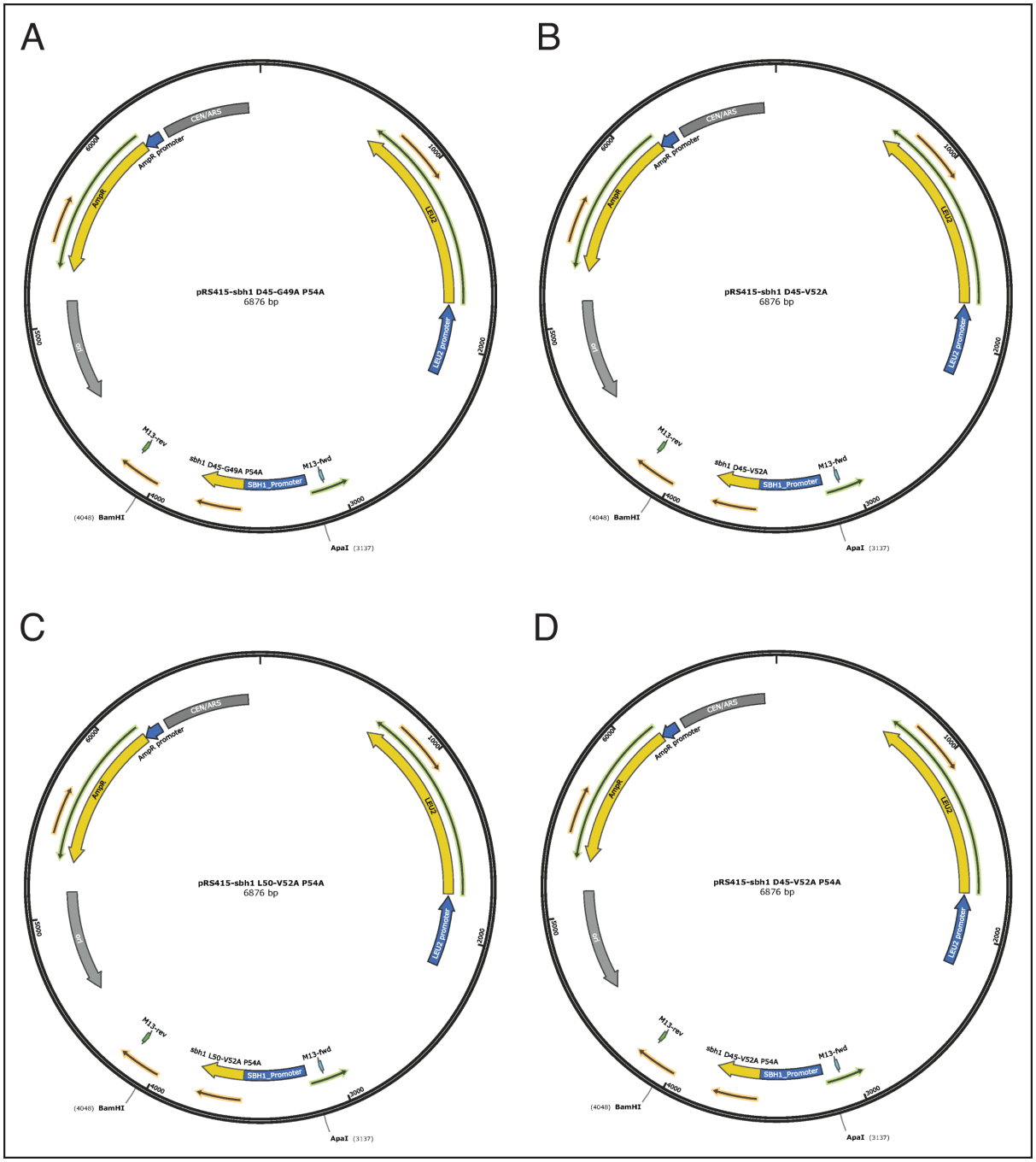

Supplementary Figure 8 Plasmids for Combo mutants. A) Map of pRS415-*sbh1D45-G49A/P54A* plasmid. **B)** Map of pRS415-*sbh1D45-V54A* plasmid. **C)** Map of pRS415-*sbh1L50-V52A/P54A* plasmid. **D)** Map of pRS415-*sbh1D45-V52A/P54A* plasmid.

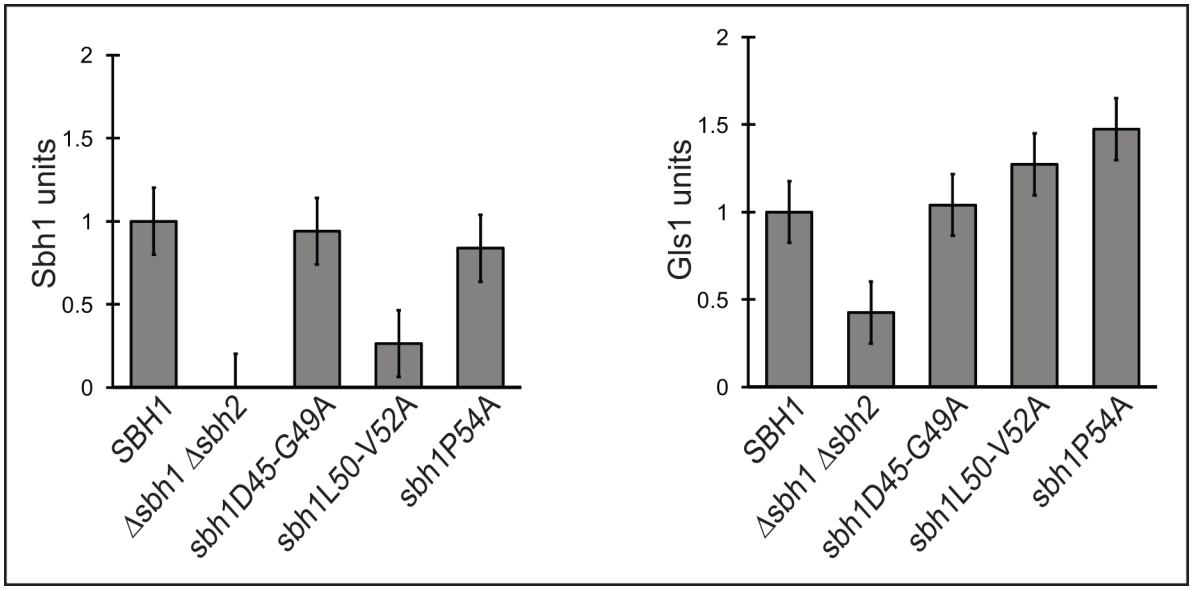

Supplementary Figure 9 Average Sbh1 and Gls1 levels in 5 colonies of CMP mutants. Cells extracts were prepared from 1 OD_{600} of CMP mutant strains grown to early exponential phase at 30 ˚C. KRY 588 strain transformed with pRS415-*SBH1* plasmid (*SBH1* strain) and with empty pRS415 plasmid (*Δsbh1 Δsbh2* strain) were used as positive and negative controls, respectively. The extracts were analysed by Western blotting and probed for Sbh1 or Gls1, and Rpn12 as loading control. The amount of Sbh1/Gls1 detected in the immunoblot was quantified and plotted in a chart given below each immunoblot. Average Sbh1 (left) and Gls1 (right) levels in 5 randomly picked colonies of each CMP mutant 1 week after transformation. When compared to the levels in *SBH1* strain, *sbh1D45-G49A* strain produced an average of 94 % of Sbh1 and 104 % of Gls1, *sbh1L50-V52A* strain produced average of 26 % of Sbh1 and 127 % of Gls1, and *sbh1P54A* strain produced 84 % of Sbh1 but 147 % of Gls1 on average.

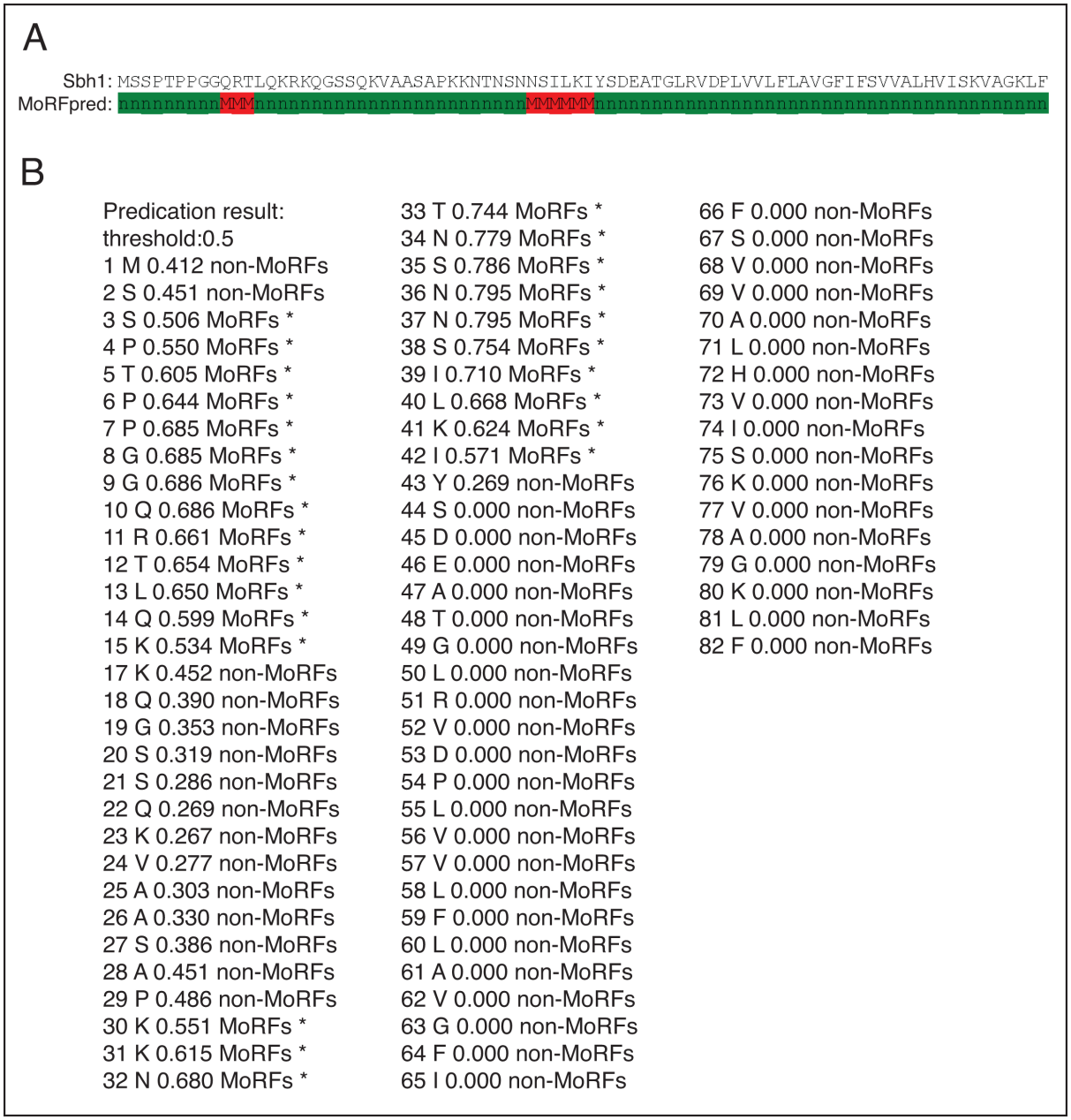

Supplementary Figure 10 Additional MoRF predictions for Sbh1. A) MoRF prediction by MoRFPred using full Sbh1 sequence. **B)** MoRF prediction by MFSPSSMPred using full Sbh1 sequence.

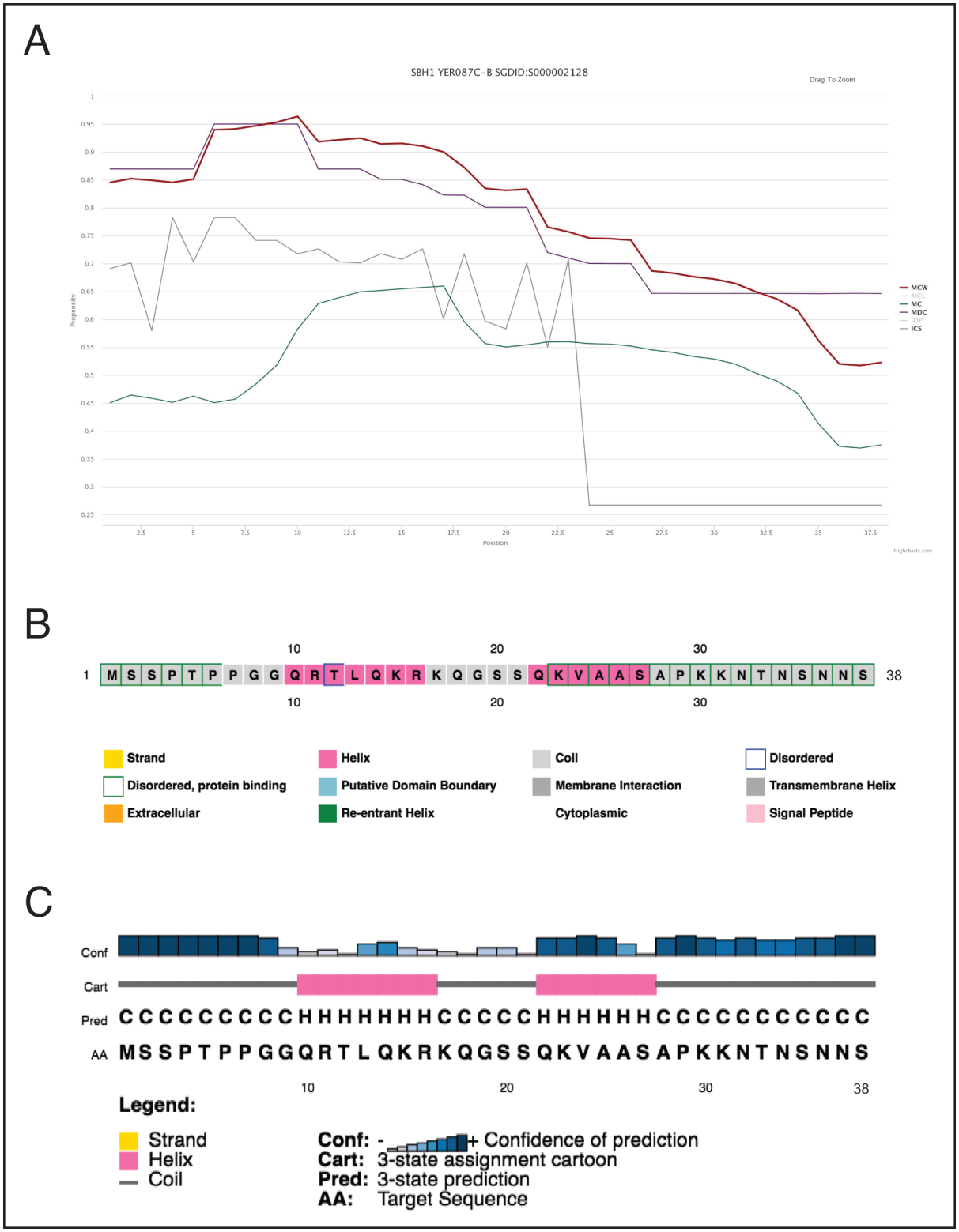

Supplementary Figure 11 Additional MoRF predictions for Sbh1 IDR. A) Prediction by MoRF$_{ChiBi.}$ **B)** Prediction by DisoPred3. **C)** Structural prediction by DisoPred3.

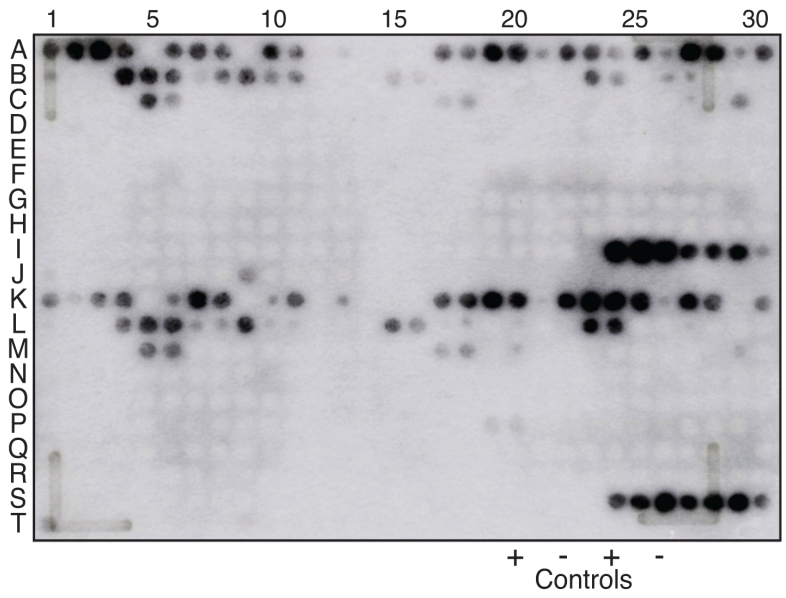

Sbh1 MSSPTPPGGQRTLQKRKQGSS--QKVAASAPKKNTN-----SNNSILKIYSDEATGLRVDPL 55

Sbh2 MAASVPPGGQRILQKRRQAQSIKEKQAKQTPTSTRQAGYGGSSSSILKLYTDEANGFRVDSL 62

Supplementary Figure 12 Sbh1 and Sbh2 N-terminal peptides cross-react with HRP conjugated anti-biotin antibody. The peptide panning membrane was activated with methanol, equilibrated with binding buffer and probed with anti-biotin-HRP antibody. Interactions were revealed by chemiluminiscence. Interactions were revealed with various Sbh1 peptide spots between A01 and C29 corresponding to M1 to T33 residues. Sbh2 peptide spots I24 to J01 corresponding to M1 to T32 residues also showed interactions. The interacting residues of Sbh1 and Sbh2 are highlighted in purple.

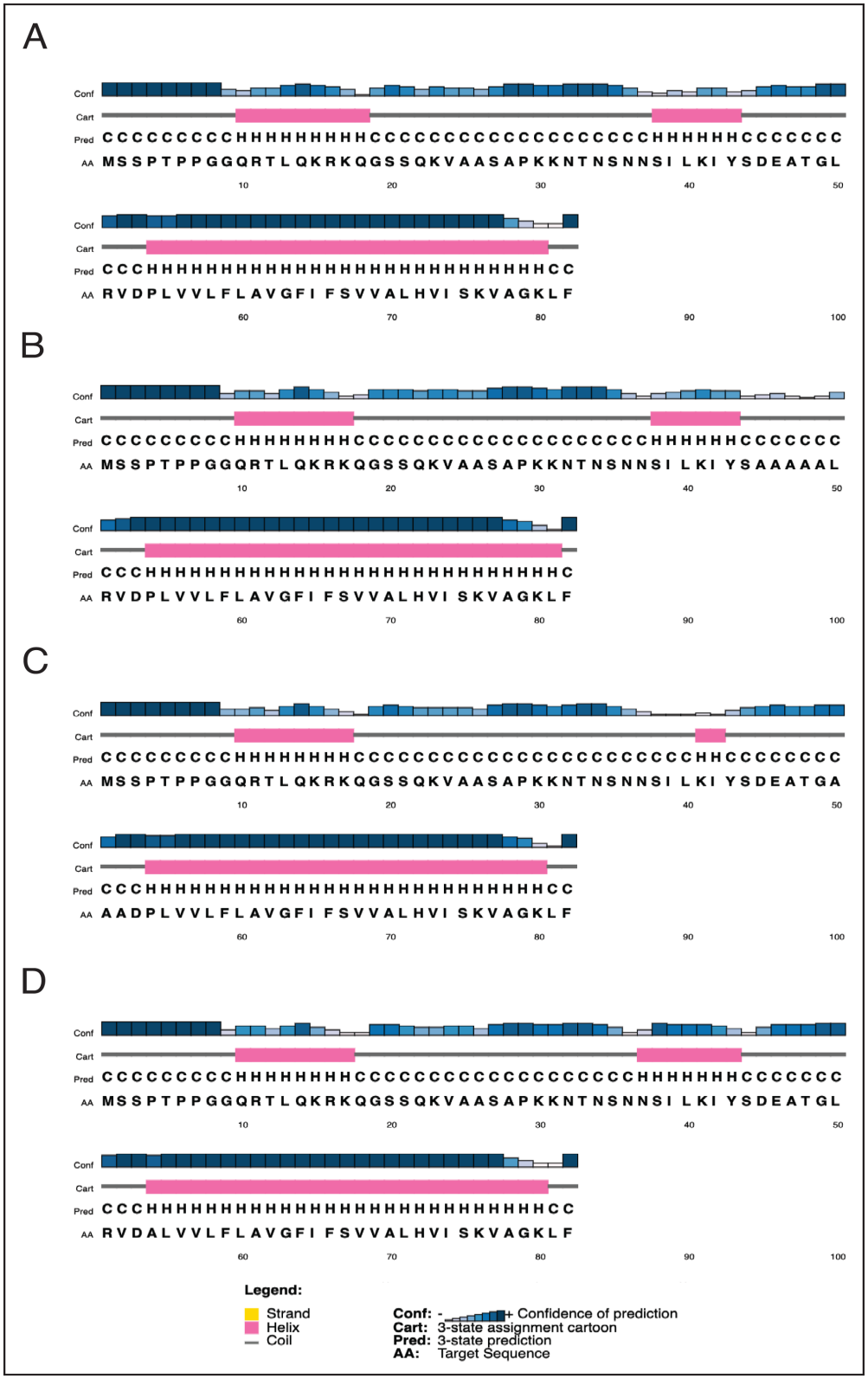

Supplementary Figure 13 Structures for CMP mutants predicted by PSIPRED. A) Structure of wildtype Sbh1 suggesting a helix in the IDR from Q10 to Q18, including the previously predicted MoRF between Q10 to T12 and the T12 phosphorylation site, and a second helix from S38 to Y33 including the last residue of the IDR and the first 5 residues of the CMP region. **B)** Structure of sbh1D45-G49A suggesting a slightly shorter helix in the IDR from Q10 to K17, and a second helix from S38 to Y33. **C)** Structure of sbh1L50-V52A suggesting a slightly helix in the IDR from Q10 to K17, and a shortened second helix of K41 and I42. **D)** Structure of sbh1P54A suggesting a slightly helix in the IDR from Q10 to K17, a longer second helix from N37 to Y33, and an elongated TM helic to include A54.

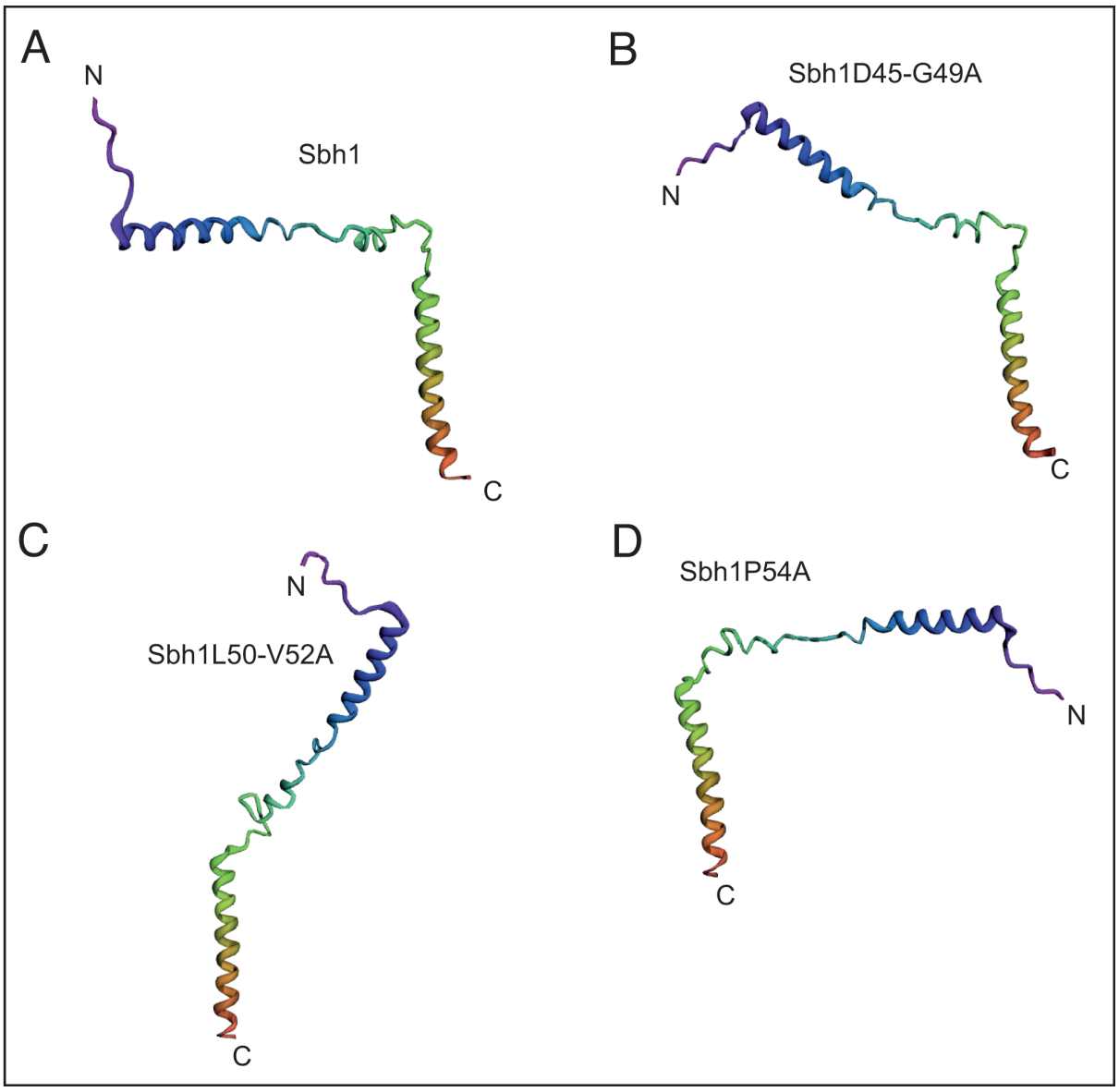

Supplementary Figure 14 Structures of CMP mutants predicted by Robetta. Structure of wildtype Sbh1 and Sbh1 CMP mutant proteins as predicted by Robetta *ab initio* modelling. Figure adapted from Yadhanapudi *et al.,* 2024.

Appendix B

Peptide Panning Membrane Legend

APPENDIX B PEPTIDE PANNING MEMBRANE LEGEND

Supplementary Table 1 Legend for peptide panning membrane.

Location	Peptide
A01	acS-S-P-T-P-P-G-G-Q-R-T-L-Q-K-R-K-Q-G-S-S
A02	acS-pS-P-T-P-P-G-G-Q-R-T-L-Q-K-R-K-Q-G-S-S
A03	acS-S-P-pT-P-P-G-G-Q-R-T-L-Q-K-R-K-Q-G-S-S
A04	acS-S-P-T-P-P-G-G-Q-R-pT-L-Q-K-R-K-Q-G-S-S
A05	acS-S-P-T-P-P-G-G-Q-R-T-L-Q-K-R-K-Q-G-pS-S
A06	acS-S-P-T-P-P-G-G-Q-R-T-L-Q-K-R-K-Q-G-S-pS
A07	acS-pS-P-pT-P-P-G-G-Q-R-T-L-Q-K-R-K-Q-G-S-S
A08	acS-pS-P-T-P-P-G-G-Q-R-pT-L-Q-K-R-K-Q-G-S-S
A09	acS-pS-P-T-P-P-G-G-Q-R-T-L-Q-K-R-K-Q-G-pS-S
A10	acS-pS-P-T-P-P-G-G-Q-R-T-L-Q-K-R-K-Q-G-S-pS
A11	acS-S-P-pT-P-P-G-G-Q-R-pT-L-Q-K-R-K-Q-G-S-S
A12	acS-S-P-pT-P-P-G-G-Q-R-T-L-Q-K-R-K-Q-G-pS-S
A13	acS-S-P-pT-P-P-G-G-Q-R-T-L-Q-K-R-K-Q-G-S-pS
A14	acS-S-P-T-P-P-G-G-Q-R-pT-L-Q-K-R-K-Q-G-pS-S
A15	acS-S-P-T-P-P-G-G-Q-R-pT-L-Q-K-R-K-Q-G-S-pS
A16	acS-S-P-T-P-P-G-G-Q-R-T-L-Q-K-R-K-Q-G-pS-E
A17	M-pS-S-P-T-P-P-G-G-Q-R-T-L-Q-K-R-K-Q-G-S
A18	M-pS-E-P-T-P-P-G-G-Q-R-T-L-Q-K-R-K-Q-G-S
A19	M-pS-S-P-pT-P-P-G-G-Q-R-T-L-Q-K-R-K-Q-G-S
A20	M-pS-S-P-T-P-P-G-G-Q-R-pT-L-Q-K-R-K-Q-G-S
A21	M-pS-S-P-T-P-P-G-G-Q-R-T-L-Q-K-R-K-Q-G-pS
A22	M-S-S-P-T-P-P-G-G-Q-R-T-L-Q-K-R-K-Q-G-S
A23	M-S-pS-P-T-P-P-G-G-Q-R-T-L-Q-K-R-K-Q-G-S
A24	M-S-S-P-pT-P-P-G-G-Q-R-T-L-Q-K-R-K-Q-G-S
A25	M-S-S-P-T-P-P-G-G-Q-R-pT-L-Q-K-R-K-Q-G-S
A26	M-S-S-P-T-P-P-G-G-Q-R-T-L-Q-K-R-K-Q-G-pS
A27	M-S-pS-P-pT-P-P-G-G-Q-R-T-L-Q-K-R-K-Q-G-S
A28	M-S-pS-P-T-P-P-G-G-Q-R-pT-L-Q-K-R-K-Q-G-S
A29	M-S-pS-P-T-P-P-G-G-Q-R-T-L-Q-K-R-K-Q-G-pS
A30	M-S-S-P-pT-P-P-G-G-Q-R-pT-L-Q-K-R-K-Q-G-S
B01	M-S-S-P-pT-P-P-G-G-Q-R-T-L-Q-K-R-K-Q-G-pS
B02	M-S-S-P-T-P-P-G-G-Q-R-pT-L-Q-K-R-K-Q-G-pS
B03	(space)
B04	P-T-P-P-G-G-Q-R-T-L-Q-K-R-K-Q-G-S-S-Q-K
B05	P-pT-P-P-G-G-Q-R-T-L-Q-K-R-K-Q-G-S-S-Q-K
B06	P-T-P-P-G-G-Q-R-pT-L-Q-K-R-K-Q-G-S-S-Q-K
B07	P-T-P-P-G-G-Q-R-T-L-Q-K-R-K-Q-G-pS-S-Q-K
B08	P-T-P-P-G-G-Q-R-T-L-Q-K-R-K-Q-G-S-pS-Q-K
B09	P-pT-P-P-G-G-Q-R-pT-L-Q-K-R-K-Q-G-S-S-Q-K
B10	P-pT-P-P-G-G-Q-R-T-L-Q-K-R-K-Q-G-pS-S-Q-K

Location	Peptide
B11	P-pT-P-P-G-G-Q-R-T-L-Q-K-R-K-Q-G-S-pS-Q-K
B12	P-T-P-P-G-G-Q-R-pT-L-Q-K-R-K-Q-G-pS-S-Q-K
B13	P-T-P-P-G-G-Q-R-pT-L-Q-K-R-K-Q-G-S-pS-Q-K
B14	P-T-P-P-G-G-Q-R-T-L-Q-K-R-K-Q-G-pS-E-Q-K
B15	P-P-G-G-Q-R-T-L-Q-K-R-K-Q-G-S-S-Q-K-V-A
B16	P-P-G-G-Q-R-pT-L-Q-K-R-K-Q-G-S-S-Q-K-V-A
B17	P-P-G-G-Q-R-T-L-Q-K-R-K-Q-G-pS-S-Q-K-V-A
B18	P-P-G-G-Q-R-T-L-Q-K-R-K-Q-G-S-pS-Q-K-V-A
B19	P-P-G-G-Q-R-pT-L-Q-K-R-K-Q-G-pS-S-Q-K-V-A
B20	P-P-G-G-Q-R-pT-L-Q-K-R-K-Q-G-S-pS-Q-K-V-A
B21	P-P-G-G-Q-R-T-L-Q-K-R-K-Q-G-pS-E-Q-K-V-A
B22	(space)
B23	G-G-Q-R-T-L-Q-K-R-K-Q-G-S-S-Q-K-V-A-A-S
B24	G-G-Q-R-pT-L-Q-K-R-K-Q-G-S-S-Q-K-V-A-A-S
B25	G-G-Q-R-T-L-Q-K-R-K-Q-G-pS-S-Q-K-V-A-A-S
B26	G-G-Q-R-T-L-Q-K-R-K-Q-G-S-pS-Q-K-V-A-A-S
B27	G-G-Q-R-T-L-Q-K-R-K-Q-G-S-S-Q-K-V-A-A-pS
B28	G-G-Q-R-pT-L-Q-K-R-K-Q-G-pS-S-Q-K-V-A-A-S
B29	G-G-Q-R-pT-L-Q-K-R-K-Q-G-S-pS-Q-K-V-A-A-S
B30	G-G-Q-R-pT-L-Q-K-R-K-Q-G-S-S-Q-K-V-A-A-pS
C01	G-G-Q-R-T-L-Q-K-R-K-Q-G-pS-E-Q-K-V-A-A-S
C02	G-G-Q-R-T-L-Q-K-R-K-Q-G-pS-S-Q-K-V-A-A-pS
C03	G-G-Q-R-T-L-Q-K-R-K-Q-G-S-pS-Q-K-V-A-A-pS
C04	(space)
C05	Q-R-T-L-Q-K-R-K-Q-G-S-S-Q-K-V-A-A-S-A-P
C06	Q-R-pT-L-Q-K-R-K-Q-G-S-S-Q-K-V-A-A-S-A-P
C07	Q-R-T-L-Q-K-R-K-Q-G-pS-S-Q-K-V-A-A-S-A-P
C08	Q-R-T-L-Q-K-R-K-Q-G-S-pS-Q-K-V-A-A-S-A-P
C09	Q-R-T-L-Q-K-R-K-Q-G-S-S-Q-K-V-A-A-pS-A-P
C10	Q-R-pT-L-Q-K-R-K-Q-G-pS-S-Q-K-V-A-A-S-A-P
C11	Q-R-pT-L-Q-K-R-K-Q-G-S-pS-Q-K-V-A-A-S-A-P
C12	Q-R-pT-L-Q-K-R-K-Q-G-S-S-Q-K-V-A-A-pS-A-P
C13	Q-R-T-L-Q-K-R-K-Q-G-pS-E-Q-K-V-A-A-S-A-P
C14	Q-R-T-L-Q-K-R-K-Q-G-pS-S-Q-K-V-A-A-pS-A-P
C15	Q-R-T-L-Q-K-R-K-Q-G-S-pS-Q-K-V-A-A-pS-A-P
C16	(space)
C17	T-L-Q-K-R-K-Q-G-S-S-Q-K-V-A-A-S-A-P-K-K
C18	pT-L-Q-K-R-K-Q-G-S-S-Q-K-V-A-A-S-A-P-K-K
C19	T-L-Q-K-R-K-Q-G-pS-S-Q-K-V-A-A-S-A-P-K-K
C20	T-L-Q-K-R-K-Q-G-S-pS-Q-K-V-A-A-S-A-P-K-K
C21	T-L-Q-K-R-K-Q-G-S-S-Q-K-V-A-A-pS-A-P-K-K
C22	pT-L-Q-K-R-K-Q-G-pS-S-Q-K-V-A-A-S-A-P-K-K
C23	pT-L-Q-K-R-K-Q-G-S-pS-Q-K-V-A-A-S-A-P-K-K

Location	Peptide
C24	pT-L-Q-K-R-K-Q-G-S-S-Q-K-V-A-A-pS-A-P-K-K
C25	T-L-Q-K-R-K-Q-G-pS-E-Q-K-V-A-A-S-A-P-K-K
C26	T-L-Q-K-R-K-Q-G-pS-S-Q-K-V-A-A-pS-A-P-K-K
C27	T-L-Q-K-R-K-Q-G-S-pS-Q-K-V-A-A-pS-A-P-K-K
C28	(space)
C29	Q-K-R-K-Q-G-S-S-Q-K-V-A-A-S-A-P-K-K-N-T
C30	Q-K-R-K-Q-G-pS-S-Q-K-V-A-A-S-A-P-K-K-N-T
D01	Q-K-R-K-Q-G-S-pS-Q-K-V-A-A-S-A-P-K-K-N-T
D02	Q-K-R-K-Q-G-S-S-Q-K-V-A-A-pS-A-P-K-K-N-T
D03	Q-K-R-K-Q-G-S-S-Q-K-V-A-A-S-A-P-K-K-N-pT
D04	Q-K-R-K-Q-G-pS-E-Q-K-V-A-A-S-A-P-K-K-N-T
D05	Q-K-R-K-Q-G-pS-S-Q-K-V-A-A-pS-A-P-K-K-N-T
D06	Q-K-R-K-Q-G-pS-S-Q-K-V-A-A-S-A-P-K-K-N-pT
D07	Q-K-R-K-Q-G-S-pS-Q-K-V-A-A-pS-A-P-K-K-N-T
D08	Q-K-R-K-Q-G-S-pS-Q-K-V-A-A-S-A-P-K-K-N-pT
D09	Q-K-R-K-Q-G-S-S-Q-K-V-A-A-pS-A-P-K-K-N-pT
D10	(space)
D11	R-K-Q-G-pS-S-Q-K-V-A-A-S-A-P-K-K-N-T-N-S
D12	R-K-Q-G-S-pS-Q-K-V-A-A-S-A-P-K-K-N-T-N-S
D13	R-K-Q-G-S-S-Q-K-V-A-A-pS-A-P-K-K-N-T-N-S
D14	R-K-Q-G-S-S-Q-K-V-A-A-S-A-P-K-K-N-pT-N-S
D15	R-K-Q-G-S-S-Q-K-V-A-A-S-A-P-K-K-N-T-N-pS
D16	R-K-Q-G-pS-E-Q-K-V-A-A-S-A-P-K-K-N-T-N-S
D17	R-K-Q-G-pS-S-Q-K-V-A-A-pS-A-P-K-K-N-T-N-S
D18	R-K-Q-G-pS-S-Q-K-V-A-A-S-A-P-K-K-N-pT-N-S
D19	R-K-Q-G-pS-S-Q-K-V-A-A-S-A-P-K-K-N-T-N-pS
D20	R-K-Q-G-S-pS-Q-K-V-A-A-pS-A-P-K-K-N-T-N-S
D21	R-K-Q-G-S-pS-Q-K-V-A-A-S-A-P-K-K-N-pT-N-S
D22	R-K-Q-G-S-pS-Q-K-V-A-A-S-A-P-K-K-N-T-N-pS
D23	R-K-Q-G-S-S-Q-K-V-A-A-pS-A-P-K-K-N-pT-N-S
D24	R-K-Q-G-S-S-Q-K-V-A-A-pS-A-P-K-K-N-T-N-pS
D25	R-K-Q-G-S-S-Q-K-V-A-A-S-A-P-K-K-N-pT-N-pS
D26	(space)
D27	Q-G-S-S-Q-K-V-A-A-S-A-P-K-K-N-T-N-S-N-N
D28	Q-G-pS-S-Q-K-V-A-A-S-A-P-K-K-N-T-N-S-N-N
D29	Q-G-S-pS-Q-K-V-A-A-S-A-P-K-K-N-T-N-S-N-N
D30	Q-G-S-S-Q-K-V-A-A-pS-A-P-K-K-N-T-N-S-N-N
E01	Q-G-S-S-Q-K-V-A-A-S-A-P-K-K-N-pT-N-S-N-N
E02	Q-G-S-S-Q-K-V-A-A-S-A-P-K-K-N-T-N-pS-N-N
E03	Q-G-pS-E-Q-K-V-A-A-S-A-P-K-K-N-T-N-S-N-N
E04	Q-G-pS-S-Q-K-V-A-A-pS-A-P-K-K-N-T-N-S-N-N
E05	Q-G-pS-S-Q-K-V-A-A-S-A-P-K-K-N-pT-N-S-N-N
E06	Q-G-pS-S-Q-K-V-A-A-S-A-P-K-K-N-T-N-pS-N-N

Location	Peptide
E07	Q-G-S-pS-Q-K-V-A-A-pS-A-P-K-K-N-T-N-S-N-N
E08	Q-G-S-pS-Q-K-V-A-A-S-A-P-K-K-N-pT-N-S-N-N
E09	Q-G-S-pS-Q-K-V-A-A-S-A-P-K-K-N-T-N-pS-N-N
E10	Q-G-S-S-Q-K-V-A-A-pS-A-P-K-K-N-pT-N-S-N-N
E11	Q-G-S-S-Q-K-V-A-A-pS-A-P-K-K-N-T-N-pS-N-N
E12	Q-G-S-S-Q-K-V-A-A-S-A-P-K-K-N-pT-N-pS-N-N
E13	(space)
E14	S-S-Q-K-V-A-A-S-A-P-K-K-N-T-N-S-N-N-S-I
E15	pS-S-Q-K-V-A-A-S-A-P-K-K-N-T-N-S-N-N-S-I
E16	S-pS-Q-K-V-A-A-S-A-P-K-K-N-T-N-S-N-N-S-I
E17	S-S-Q-K-V-A-A-pS-A-P-K-K-N-T-N-S-N-N-S-I
E18	S-S-Q-K-V-A-A-S-A-P-K-K-N-pT-N-S-N-N-S-I
E19	S-S-Q-K-V-A-A-S-A-P-K-K-N-T-N-pS-N-N-S-I
E20	S-S-Q-K-V-A-A-S-A-P-K-K-N-T-N-S-N-N-pS-I
E21	pS-E-Q-K-V-A-A-S-A-P-K-K-N-T-N-S-N-N-S-I
E22	pS-S-Q-K-V-A-A-pS-A-P-K-K-N-T-N-S-N-N-S-I
E23	pS-S-Q-K-V-A-A-S-A-P-K-K-N-pT-N-S-N-N-S-I
E24	pS-S-Q-K-V-A-A-S-A-P-K-K-N-T-N-pS-N-N-S-I
E25	pS-S-Q-K-V-A-A-S-A-P-K-K-N-T-N-S-N-N-pS-I
E26	S-pS-Q-K-V-A-A-pS-A-P-K-K-N-T-N-S-N-N-S-I
E27	S-pS-Q-K-V-A-A-S-A-P-K-K-N-pT-N-S-N-N-S-I
E28	S-pS-Q-K-V-A-A-S-A-P-K-K-N-T-N-pS-N-N-S-I
E29	S-pS-Q-K-V-A-A-S-A-P-K-K-N-T-N-S-N-N-pS-I
E30	S-S-Q-K-V-A-A-pS-A-P-K-K-N-pT-N-S-N-N-S-I
F01	S-S-Q-K-V-A-A-pS-A-P-K-K-N-T-N-pS-N-N-S-I
F02	S-S-Q-K-V-A-A-pS-A-P-K-K-N-T-N-S-N-N-pS-I
F03	S-S-Q-K-V-A-A-S-A-P-K-K-N-pT-N-pS-N-N-S-I
F04	S-S-Q-K-V-A-A-S-A-P-K-K-N-pT-N-S-N-N-pS-I
F05	S-S-Q-K-V-A-A-S-A-P-K-K-N-T-N-pS-N-N-pS-I
F06	(space)
F07	Q-K-V-A-A-S-A-P-K-K-N-T-N-S-N-N-S-I-L-K
F08	Q-K-V-A-A-pS-A-P-K-K-N-T-N-S-N-N-S-I-L-K
F09	Q-K-V-A-A-S-A-P-K-K-N-pT-N-S-N-N-S-I-L-K
F10	Q-K-V-A-A-S-A-P-K-K-N-T-N-pS-N-N-S-I-L-K
F11	Q-K-V-A-A-S-A-P-K-K-N-T-N-S-N-N-pS-I-L-K
F12	Q-K-V-A-A-pS-A-P-K-K-N-pT-N-S-N-N-S-I-L-K
F13	Q-K-V-A-A-pS-A-P-K-K-N-T-N-pS-N-N-S-I-L-K
F14	Q-K-V-A-A-pS-A-P-K-K-N-T-N-S-N-N-pS-I-L-K
F15	Q-K-V-A-A-S-A-P-K-K-N-pT-N-pS-N-N-S-I-L-K
F16	Q-K-V-A-A-S-A-P-K-K-N-pT-N-S-N-N-pS-I-L-K
F17	Q-K-V-A-A-S-A-P-K-K-N-T-N-pS-N-N-pS-I-L-K
F18	(space)
F19	V-A-A-S-A-P-K-K-N-T-N-S-N-N-S-I-L-K-I-Y

Location	Peptide
F20	V-A-A-pS-A-P-K-K-N-T-N-S-N-N-S-I-L-K-I-Y
F21	V-A-A-S-A-P-K-K-N-pT-N-S-N-N-S-I-L-K-I-Y
F22	V-A-A-S-A-P-K-K-N-T-N-pS-N-N-S-I-L-K-I-Y
F23	V-A-A-S-A-P-K-K-N-T-N-S-N-N-pS-I-L-K-I-Y
F24	V-A-A-pS-A-P-K-K-N-pT-N-S-N-N-S-I-L-K-I-Y
F25	V-A-A-pS-A-P-K-K-N-T-N-pS-N-N-S-I-L-K-I-Y
F26	V-A-A-pS-A-P-K-K-N-T-N-S-N-N-pS-I-L-K-I-Y
F27	V-A-A-S-A-P-K-K-N-pT-N-pS-N-N-S-I-L-K-I-Y
F28	V-A-A-S-A-P-K-K-N-pT-N-S-N-N-pS-I-L-K-I-Y
F29	V-A-A-S-A-P-K-K-N-T-N-pS-N-N-pS-I-L-K-I-Y
F30	(space)
G01	A-S-A-P-K-K-N-T-N-S-N-N-S-I-L-K-I-Y-S-D
G02	A-pS-A-P-K-K-N-T-N-S-N-N-S-I-L-K-I-Y-S-D
G03	A-S-A-P-K-K-N-pT-N-S-N-N-S-I-L-K-I-Y-S-D
G04	A-S-A-P-K-K-N-T-N-pS-N-N-S-I-L-K-I-Y-S-D
G05	A-S-A-P-K-K-N-T-N-S-N-N-pS-I-L-K-I-Y-S-D
G06	A-S-A-P-K-K-N-T-N-S-N-N-S-I-L-K-I-Y-pS-D
G07	A-pS-A-P-K-K-N-pT-N-S-N-N-S-I-L-K-I-Y-S-D
G08	A-pS-A-P-K-K-N-T-N-pS-N-N-S-I-L-K-I-Y-S-D
G09	A-pS-A-P-K-K-N-T-N-S-N-N-pS-I-L-K-I-Y-S-D
G10	A-pS-A-P-K-K-N-T-N-S-N-N-S-I-L-K-I-Y-pS-D
G11	A-S-A-P-K-K-N-pT-N-pS-N-N-S-I-L-K-I-Y-S-D
G12	A-S-A-P-K-K-N-pT-N-S-N-N-pS-I-L-K-I-Y-S-D
G13	A-S-A-P-K-K-N-pT-N-S-N-N-S-I-L-K-I-Y-pS-D
G14	A-S-A-P-K-K-N-T-N-pS-N-N-pS-I-L-K-I-Y-S-D
G15	A-S-A-P-K-K-N-T-N-pS-N-N-S-I-L-K-I-Y-pS-D
G16	A-S-A-P-K-K-N-T-N-S-N-N-pS-I-L-K-I-Y-pS-D
G17	(space)
G18	A-P-K-K-N-T-N-S-N-N-S-I-L-K-I-Y-S-D-E-A
G19	A-P-K-K-N-pT-N-S-N-N-S-I-L-K-I-Y-S-D-E-A
G20	A-P-K-K-N-T-N-pS-N-N-S-I-L-K-I-Y-S-D-E-A
G21	A-P-K-K-N-T-N-S-N-N-pS-I-L-K-I-Y-S-D-E-A
G22	A-P-K-K-N-T-N-S-N-N-S-I-L-K-I-Y-pS-D-E-A
G23	A-P-K-K-N-pT-N-pS-N-N-S-I-L-K-I-Y-S-D-E-A
G24	A-P-K-K-N-pT-N-S-N-N-pS-I-L-K-I-Y-S-D-E-A
G25	A-P-K-K-N-pT-N-S-N-N-S-I-L-K-I-Y-pS-D-E-A
G26	A-P-K-K-N-T-N-pS-N-N-pS-I-L-K-I-Y-S-D-E-A
G27	A-P-K-K-N-T-N-pS-N-N-S-I-L-K-I-Y-pS-D-E-A
G28	A-P-K-K-N-T-N-S-N-N-pS-I-L-K-I-Y-pS-D-E-A
G29	(space)
G30	K-K-N-T-N-S-N-N-S-I-L-K-I-Y-S-D-E-A-T-G
H01	K-K-N-pT-N-S-N-N-S-I-L-K-I-Y-S-D-E-A-T-G
H02	K-K-N-T-N-pS-N-N-S-I-L-K-I-Y-S-D-E-A-T-G

Location	Peptide
H03	K-K-N-T-N-S-N-N-pS-I-L-K-I-Y-S-D-E-A-T-G
H04	K-K-N-T-N-S-N-N-S-I-L-K-I-Y-pS-D-E-A-T-G
H05	K-K-N-T-N-S-N-N-S-I-L-K-I-Y-S-D-E-A-pT-G
H06	K-K-N-pT-N-pS-N-N-S-I-L-K-I-Y-S-D-E-A-T-G
H07	K-K-N-pT-N-S-N-N-pS-I-L-K-I-Y-S-D-E-A-T-G
H08	K-K-N-pT-N-S-N-N-S-I-L-K-I-Y-pS-D-E-A-T-G
H09	K-K-N-pT-N-S-N-N-S-I-L-K-I-Y-S-D-E-A-pT-G
H10	K-K-N-T-N-pS-N-N-pS-I-L-K-I-Y-S-D-E-A-T-G
H11	K-K-N-T-N-pS-N-N-S-I-L-K-I-Y-pS-D-E-A-T-G
H12	K-K-N-T-N-pS-N-N-S-I-L-K-I-Y-S-D-E-A-pT-G
H13	K-K-N-T-N-S-N-N-pS-I-L-K-I-Y-pS-D-E-A-T-G
H14	K-K-N-T-N-S-N-N-pS-I-L-K-I-Y-S-D-E-A-pT-G
H15	K-K-N-T-N-S-N-N-S-I-L-K-I-Y-pS-D-E-A-pT-G
H16	(space)
H17	N-T-N-S-N-N-S-I-L-K-I-Y-S-D-E-A-T-G-L-R
H18	N-pT-N-S-N-N-S-I-L-K-I-Y-S-D-E-A-T-G-L-R
H19	N-T-N-pS-N-N-S-I-L-K-I-Y-S-D-E-A-T-G-L-R
H20	N-T-N-S-N-N-pS-I-L-K-I-Y-S-D-E-A-T-G-L-R
H21	N-T-N-S-N-N-S-I-L-K-I-Y-pS-D-E-A-T-G-L-R
H22	N-T-N-S-N-N-S-I-L-K-I-Y-S-D-E-A-pT-G-L-R
H23	N-pT-N-pS-N-N-S-I-L-K-I-Y-S-D-E-A-T-G-L-R
H24	N-pT-N-S-N-N-pS-I-L-K-I-Y-S-D-E-A-T-G-L-R
H25	N-pT-N-S-N-N-S-I-L-K-I-Y-pS-D-E-A-T-G-L-R
H26	N-pT-N-S-N-N-S-I-L-K-I-Y-S-D-E-A-pT-G-L-R
H27	N-T-N-pS-N-N-pS-I-L-K-I-Y-S-D-E-A-T-G-L-R
H28	N-T-N-pS-N-N-S-I-L-K-I-Y-pS-D-E-A-T-G-L-R
H29	N-T-N-pS-N-N-S-I-L-K-I-Y-S-D-E-A-pT-G-L-R
H30	N-T-N-S-N-N-pS-I-L-K-I-Y-pS-D-E-A-T-G-L-R
I01	N-T-N-S-N-N-pS-I-L-K-I-Y-S-D-E-A-pT-G-L-R
I02	N-T-N-S-N-N-S-I-L-K-I-Y-pS-D-E-A-pT-G-L-R
I03	(space)
I04	N-S-N-N-S-I-L-K-I-Y-S-D-E-A-T-G-L-R-V-D
I05	N-pS-N-N-S-I-L-K-I-Y-S-D-E-A-T-G-L-R-V-D
I06	N-S-N-N-pS-I-L-K-I-Y-S-D-E-A-T-G-L-R-V-D
I07	N-S-N-N-S-I-L-K-I-Y-pS-D-E-A-T-G-L-R-V-D
I08	N-S-N-N-S-I-L-K-I-Y-S-D-E-A-pT-G-L-R-V-D
I09	N-pS-N-N-pS-I-L-K-I-Y-S-D-E-A-T-G-L-R-V-D
I10	N-pS-N-N-S-I-L-K-I-Y-pS-D-E-A-T-G-L-R-V-D
I11	N-pS-N-N-S-I-L-K-I-Y-S-D-E-A-pT-G-L-R-V-D
I12	N-S-N-N-pS-I-L-K-I-Y-pS-D-E-A-T-G-L-R-V-D
I13	N-S-N-N-pS-I-L-K-I-Y-S-D-E-A-pT-G-L-R-V-D
I14	N-S-N-N-S-I-L-K-I-Y-pS-D-E-A-pT-G-L-R-V-D
I15	(space)

Location	Peptide
I16	N-N-S-I-L-K-I-Y-S-D-E-A-T-G-L-R-V-D-P-L
I17	N-N-pS-I-L-K-I-Y-S-D-E-A-T-G-L-R-V-D-P-L
I18	N-N-S-I-L-K-I-Y-pS-D-E-A-T-G-L-R-V-D-P-L
I19	N-N-S-I-L-K-I-Y-S-D-E-A-pT-G-L-R-V-D-P-L
I20	N-N-pS-I-L-K-I-Y-pS-D-E-A-T-G-L-R-V-D-P-L
I21	N-N-pS-I-L-K-I-Y-S-D-E-A-pT-G-L-R-V-D-P-L
I22	N-N-S-I-L-K-I-Y-pS-D-E-A-pT-G-L-R-V-D-P-L
I23	(space)
I24	M-A-A-S-V-P-P-G-G-Q-R-I-L-Q-K-R-R-Q-A-Q
I25	A-S-V-P-P-G-G-Q-R-I-L-Q-K-R-R-Q-A-Q-S-I
I26	V-P-P-G-G-Q-R-I-L-Q-K-R-R-Q-A-Q-S-I-K-E
I27	P-G-G-Q-R-I-L-Q-K-R-R-Q-A-Q-S-I-K-E-K-Q
I28	G-Q-R-I-L-Q-K-R-R-Q-A-Q-S-I-K-E-K-Q-A-K
I29	R-I-L-Q-K-R-R-Q-A-Q-S-I-K-E-K-Q-A-K-Q-T
I30	L-Q-K-R-R-Q-A-Q-S-I-K-E-K-Q-A-K-Q-T-P-T
J01	K-R-R-Q-A-Q-S-I-K-E-K-Q-A-K-Q-T-P-T-S-T
J02	R-Q-A-Q-S-I-K-E-K-Q-A-K-Q-T-P-T-S-T-R-Q
J03	A-Q-S-I-K-E-K-Q-A-K-Q-T-P-T-S-T-R-Q-A-G
J04	S-I-K-E-K-Q-A-K-Q-T-P-T-S-T-R-Q-A-G-Y-G
J05	K-E-K-Q-A-K-Q-T-P-T-S-T-R-Q-A-G-Y-G-G-S
J06	K-Q-A-K-Q-T-P-T-S-T-R-Q-A-G-Y-G-G-S-S-S
J07	A-K-Q-T-P-T-S-T-R-Q-A-G-Y-G-G-S-S-S-S-I
J08	Q-T-P-T-S-T-R-Q-A-G-Y-G-G-S-S-S-S-I-L-K
J09	P-T-S-T-R-Q-A-G-Y-G-G-S-S-S-S-I-L-K-L-Y
J10	S-T-R-Q-A-G-Y-G-G-S-S-S-S-I-L-K-L-Y-T-D
J11	R-Q-A-G-Y-G-G-S-S-S-S-I-L-K-L-Y-T-D-E-A
J12	A-G-Y-G-G-S-S-S-S-I-L-K-L-Y-T-D-E-A-N-G
J13	Y-G-G-S-S-S-S-I-L-K-L-Y-T-D-E-A-N-G-F-R
J14	G-S-S-S-S-I-L-K-L-Y-T-D-E-A-N-G-F-R-V-D
J15	S-S-S-I-L-K-L-Y-T-D-E-A-N-G-F-R-V-D-S-L
J16	(newline)
J17	(newline)
J18	(newline)
J19	(newline)
J20	(newline)
J21	(newline)
J22	(newline)
J23	(newline)
J24	(newline)
J25	(newline)
J26	(newline)
J27	(newline)
J28	(newline)

Location	Peptide
J29	(newline)
J30	(newline)
K01	acS-S-P-T-P-P-G-G-Q-R-T-L-Q-K-R-K-Q-G-S-S
K02	acS-pS-P-T-P-P-G-G-Q-R-T-L-Q-K-R-K-Q-G-S-S
K03	acS-S-P-pT-P-P-G-G-Q-R-T-L-Q-K-R-K-Q-G-S-S
K04	acS-S-P-T-P-P-G-G-Q-R-pT-L-Q-K-R-K-Q-G-S-S
K05	acS-S-P-T-P-P-G-G-Q-R-T-L-Q-K-R-K-Q-G-pS-S
K06	acS-S-P-T-P-P-G-G-Q-R-T-L-Q-K-R-K-Q-G-S-pS
K07	acS-pS-P-pT-P-P-G-G-Q-R-T-L-Q-K-R-K-Q-G-S-S
K08	acS-pS-P-T-P-P-G-G-Q-R-pT-L-Q-K-R-K-Q-G-S-S
K09	acS-pS-P-T-P-P-G-G-Q-R-T-L-Q-K-R-K-Q-G-pS-S
K10	acS-pS-P-T-P-P-G-G-Q-R-T-L-Q-K-R-K-Q-G-S-pS
K11	acS-S-P-pT-P-P-G-G-Q-R-pT-L-Q-K-R-K-Q-G-S-S
K12	acS-S-P-pT-P-P-G-G-Q-R-T-L-Q-K-R-K-Q-G-pS-S
K13	acS-S-P-pT-P-P-G-G-Q-R-T-L-Q-K-R-K-Q-G-S-pS
K14	acS-S-P-T-P-P-G-G-Q-R-pT-L-Q-K-R-K-Q-G-pS-S
K15	acS-S-P-T-P-P-G-G-Q-R-pT-L-Q-K-R-K-Q-G-S-pS
K16	acS-S-P-T-P-P-G-G-Q-R-T-L-Q-K-R-K-Q-G-pS-E
K17	M-pS-S-P-T-P-P-G-G-Q-R-T-L-Q-K-R-K-Q-G-S
K18	M-pS-E-P-T-P-P-G-G-Q-R-T-L-Q-K-R-K-Q-G-S
K19	M-pS-S-P-pT-P-P-G-G-Q-R-T-L-Q-K-R-K-Q-G-S
K20	M-pS-S-P-T-P-P-G-G-Q-R-pT-L-Q-K-R-K-Q-G-S
K21	M-pS-S-P-T-P-P-G-G-Q-R-T-L-Q-K-R-K-Q-G-pS
K22	M-S-S-P-T-P-P-G-G-Q-R-T-L-Q-K-R-K-Q-G-S
K23	M-S-pS-P-T-P-P-G-G-Q-R-T-L-Q-K-R-K-Q-G-S
K24	M-S-S-P-pT-P-P-G-G-Q-R-T-L-Q-K-R-K-Q-G-S
K25	M-S-S-P-T-P-P-G-G-Q-R-pT-L-Q-K-R-K-Q-G-S
K26	M-S-S-P-T-P-P-G-G-Q-R-T-L-Q-K-R-K-Q-G-pS
K27	M-S-pS-P-pT-P-P-G-G-Q-R-T-L-Q-K-R-K-Q-G-S
K28	M-S-pS-P-T-P-P-G-G-Q-R-pT-L-Q-K-R-K-Q-G-S
K29	M-S-pS-P-T-P-P-G-G-Q-R-T-L-Q-K-R-K-Q-G-pS
K30	M-S-S-P-pT-P-P-G-G-Q-R-pT-L-Q-K-R-K-Q-G-S
L01	M-S-S-P-pT-P-P-G-G-Q-R-T-L-Q-K-R-K-Q-G-pS
L02	M-S-S-P-T-P-P-G-G-Q-R-pT-L-Q-K-R-K-Q-G-pS
L03	(space)
L04	P-T-P-P-G-G-Q-R-T-L-Q-K-R-K-Q-G-S-S-Q-K
L05	P-pT-P-P-G-G-Q-R-T-L-Q-K-R-K-Q-G-S-S-Q-K
L06	P-T-P-P-G-G-Q-R-pT-L-Q-K-R-K-Q-G-S-S-Q-K
L07	P-T-P-P-G-G-Q-R-T-L-Q-K-R-K-Q-G-pS-S-Q-K
L08	P-T-P-P-G-G-Q-R-T-L-Q-K-R-K-Q-G-S-pS-Q-K
L09	P-pT-P-P-G-G-Q-R-pT-L-Q-K-R-K-Q-G-S-S-Q-K
L10	P-pT-P-P-G-G-Q-R-T-L-Q-K-R-K-Q-G-pS-S-Q-K
L11	P-pT-P-P-G-G-Q-R-T-L-Q-K-R-K-Q-G-S-pS-Q-K

Location	Peptide
L12	P-T-P-P-G-G-Q-R-pT-L-Q-K-R-K-Q-G-pS-S-Q-K
L13	P-T-P-P-G-G-Q-R-pT-L-Q-K-R-K-Q-G-S-pS-Q-K
L14	P-T-P-P-G-G-Q-R-T-L-Q-K-R-K-Q-G-pS-E-Q-K
L15	P-P-G-G-Q-R-T-L-Q-K-R-K-Q-G-S-S-Q-K-V-A
L16	P-P-G-G-Q-R-pT-L-Q-K-R-K-Q-G-S-S-Q-K-V-A
L17	P-P-G-G-Q-R-T-L-Q-K-R-K-Q-G-pS-S-Q-K-V-A
L18	P-P-G-G-Q-R-T-L-Q-K-R-K-Q-G-S-pS-Q-K-V-A
L19	P-P-G-G-Q-R-pT-L-Q-K-R-K-Q-G-pS-S-Q-K-V-A
L20	P-P-G-G-Q-R-pT-L-Q-K-R-K-Q-G-S-pS-Q-K-V-A
L21	P-P-G-G-Q-R-T-L-Q-K-R-K-Q-G-pS-E-Q-K-V-A
L22	(space)
L23	G-G-Q-R-T-L-Q-K-R-K-Q-G-S-S-Q-K-V-A-A-S
L24	G-G-Q-R-pT-L-Q-K-R-K-Q-G-S-S-Q-K-V-A-A-S
L25	G-G-Q-R-T-L-Q-K-R-K-Q-G-pS-S-Q-K-V-A-A-S
L26	G-G-Q-R-T-L-Q-K-R-K-Q-G-S-pS-Q-K-V-A-A-S
L27	G-G-Q-R-T-L-Q-K-R-K-Q-G-S-S-Q-K-V-A-A-pS
L28	G-G-Q-R-pT-L-Q-K-R-K-Q-G-pS-S-Q-K-V-A-A-S
L29	G-G-Q-R-pT-L-Q-K-R-K-Q-G-S-pS-Q-K-V-A-A-S
L30	G-G-Q-R-pT-L-Q-K-R-K-Q-G-S-S-Q-K-V-A-A-pS
M01	G-G-Q-R-T-L-Q-K-R-K-Q-G-pS-E-Q-K-V-A-A-S
M02	G-G-Q-R-T-L-Q-K-R-K-Q-G-pS-S-Q-K-V-A-A-pS
M03	G-G-Q-R-T-L-Q-K-R-K-Q-G-S-pS-Q-K-V-A-A-pS
M04	(space)
M05	Q-R-T-L-Q-K-R-K-Q-G-S-S-Q-K-V-A-A-S-A-P
M06	Q-R-pT-L-Q-K-R-K-Q-G-S-S-Q-K-V-A-A-S-A-P
M07	Q-R-T-L-Q-K-R-K-Q-G-pS-S-Q-K-V-A-A-S-A-P
M08	Q-R-T-L-Q-K-R-K-Q-G-S-pS-Q-K-V-A-A-S-A-P
M09	Q-R-T-L-Q-K-R-K-Q-G-S-S-Q-K-V-A-A-pS-A-P
M10	Q-R-pT-L-Q-K-R-K-Q-G-pS-S-Q-K-V-A-A-S-A-P
M11	Q-R-pT-L-Q-K-R-K-Q-G-S-pS-Q-K-V-A-A-S-A-P
M12	Q-R-pT-L-Q-K-R-K-Q-G-S-S-Q-K-V-A-A-pS-A-P
M13	Q-R-T-L-Q-K-R-K-Q-G-pS-E-Q-K-V-A-A-S-A-P
M14	Q-R-T-L-Q-K-R-K-Q-G-pS-S-Q-K-V-A-A-pS-A-P
M15	Q-R-T-L-Q-K-R-K-Q-G-S-pS-Q-K-V-A-A-pS-A-P
M16	(space)
M17	T-L-Q-K-R-K-Q-G-S-S-Q-K-V-A-A-S-A-P-K-K
M18	pT-L-Q-K-R-K-Q-G-S-S-Q-K-V-A-A-S-A-P-K-K
M19	T-L-Q-K-R-K-Q-G-pS-S-Q-K-V-A-A-S-A-P-K-K
M20	T-L-Q-K-R-K-Q-G-S-pS-Q-K-V-A-A-S-A-P-K-K
M21	T-L-Q-K-R-K-Q-G-S-S-Q-K-V-A-A-pS-A-P-K-K
M22	pT-L-Q-K-R-K-Q-G-pS-S-Q-K-V-A-A-S-A-P-K-K
M23	pT-L-Q-K-R-K-Q-G-S-pS-Q-K-V-A-A-S-A-P-K-K
M24	pT-L-Q-K-R-K-Q-G-S-S-Q-K-V-A-A-pS-A-P-K-K

Location	Peptide
M25	T-L-Q-K-R-K-Q-G-pS-E-Q-K-V-A-A-S-A-P-K-K
M26	T-L-Q-K-R-K-Q-G-pS-S-Q-K-V-A-A-pS-A-P-K-K
M27	T-L-Q-K-R-K-Q-G-S-pS-Q-K-V-A-A-pS-A-P-K-K
M28	(space)
M29	Q-K-R-K-Q-G-S-S-Q-K-V-A-A-S-A-P-K-K-N-T
M30	Q-K-R-K-Q-G-pS-S-Q-K-V-A-A-S-A-P-K-K-N-T
N01	Q-K-R-K-Q-G-S-pS-Q-K-V-A-A-S-A-P-K-K-N-T
N02	Q-K-R-K-Q-G-S-S-Q-K-V-A-A-pS-A-P-K-K-N-T
N03	Q-K-R-K-Q-G-S-S-Q-K-V-A-A-S-A-P-K-K-N-pT
N04	Q-K-R-K-Q-G-pS-E-Q-K-V-A-A-S-A-P-K-K-N-T
N05	Q-K-R-K-Q-G-pS-S-Q-K-V-A-A-pS-A-P-K-K-N-T
N06	Q-K-R-K-Q-G-pS-S-Q-K-V-A-A-S-A-P-K-K-N-pT
N07	Q-K-R-K-Q-G-S-pS-Q-K-V-A-A-pS-A-P-K-K-N-T
N08	Q-K-R-K-Q-G-S-pS-Q-K-V-A-A-S-A-P-K-K-N-pT
N09	Q-K-R-K-Q-G-S-S-Q-K-V-A-A-pS-A-P-K-K-N-pT
N10	(space)
N11	R-K-Q-G-pS-S-Q-K-V-A-A-S-A-P-K-K-N-T-N-S
N12	R-K-Q-G-S-pS-Q-K-V-A-A-S-A-P-K-K-N-T-N-S
N13	R-K-Q-G-S-S-Q-K-V-A-A-pS-A-P-K-K-N-T-N-S
N14	R-K-Q-G-S-S-Q-K-V-A-A-S-A-P-K-K-N-pT-N-S
N15	R-K-Q-G-S-S-Q-K-V-A-A-S-A-P-K-K-N-T-N-pS
N16	R-K-Q-G-pS-E-Q-K-V-A-A-S-A-P-K-K-N-T-N-S
N17	R-K-Q-G-pS-S-Q-K-V-A-A-pS-A-P-K-K-N-T-N-S
N18	R-K-Q-G-pS-S-Q-K-V-A-A-S-A-P-K-K-N-pT-N-S
N19	R-K-Q-G-pS-S-Q-K-V-A-A-S-A-P-K-K-N-T-N-pS
N20	R-K-Q-G-S-pS-Q-K-V-A-A-pS-A-P-K-K-N-T-N-S
N21	R-K-Q-G-S-pS-Q-K-V-A-A-S-A-P-K-K-N-pT-N-S
N22	R-K-Q-G-S-pS-Q-K-V-A-A-S-A-P-K-K-N-T-N-pS
N23	R-K-Q-G-S-S-Q-K-V-A-A-pS-A-P-K-K-N-pT-N-S
N24	R-K-Q-G-S-S-Q-K-V-A-A-pS-A-P-K-K-N-T-N-pS
N25	R-K-Q-G-S-S-Q-K-V-A-A-S-A-P-K-K-N-pT-N-pS
N26	(space)
N27	Q-G-S-S-Q-K-V-A-A-S-A-P-K-K-N-T-N-S-N-N
N28	Q-G-pS-S-Q-K-V-A-A-S-A-P-K-K-N-T-N-S-N-N
N29	Q-G-S-pS-Q-K-V-A-A-S-A-P-K-K-N-T-N-S-N-N
N30	Q-G-S-S-Q-K-V-A-A-pS-A-P-K-K-N-T-N-S-N-N
O01	Q-G-S-S-Q-K-V-A-A-S-A-P-K-K-N-pT-N-S-N-N
O02	Q-G-S-S-Q-K-V-A-A-S-A-P-K-K-N-T-N-pS-N-N
O03	Q-G-pS-E-Q-K-V-A-A-S-A-P-K-K-N-T-N-S-N-N
O04	Q-G-pS-S-Q-K-V-A-A-pS-A-P-K-K-N-T-N-S-N-N
O05	Q-G-pS-S-Q-K-V-A-A-S-A-P-K-K-N-pT-N-S-N-N
O06	Q-G-pS-S-Q-K-V-A-A-S-A-P-K-K-N-T-N-pS-N-N
O07	Q-G-S-pS-Q-K-V-A-A-pS-A-P-K-K-N-T-N-S-N-N

Location	Peptide
O08	Q-G-S-pS-Q-K-V-A-A-S-A-P-K-K-N-pT-N-S-N-N
O09	Q-G-S-pS-Q-K-V-A-A-S-A-P-K-K-N-T-N-pS-N-N
O10	Q-G-S-S-Q-K-V-A-A-pS-A-P-K-K-N-pT-N-S-N-N
O11	Q-G-S-S-Q-K-V-A-A-pS-A-P-K-K-N-T-N-pS-N-N
O12	Q-G-S-S-Q-K-V-A-A-S-A-P-K-K-N-pT-N-pS-N-N
O13	(space)
O14	S-S-Q-K-V-A-A-S-A-P-K-K-N-T-N-S-N-N-S-I
O15	pS-S-Q-K-V-A-A-S-A-P-K-K-N-T-N-S-N-N-S-I
O16	S-pS-Q-K-V-A-A-S-A-P-K-K-N-T-N-S-N-N-S-I
O17	S-S-Q-K-V-A-A-pS-A-P-K-K-N-T-N-S-N-N-S-I
O18	S-S-Q-K-V-A-A-S-A-P-K-K-N-pT-N-S-N-N-S-I
O19	S-S-Q-K-V-A-A-S-A-P-K-K-N-T-N-pS-N-N-S-I
O20	S-S-Q-K-V-A-A-S-A-P-K-K-N-T-N-S-N-N-pS-I
O21	pS-E-Q-K-V-A-A-S-A-P-K-K-N-T-N-S-N-N-S-I
O22	pS-S-Q-K-V-A-A-pS-A-P-K-K-N-T-N-S-N-N-S-I
O23	pS-S-Q-K-V-A-A-S-A-P-K-K-N-pT-N-S-N-N-S-I
O24	pS-S-Q-K-V-A-A-S-A-P-K-K-N-T-N-pS-N-N-S-I
O25	pS-S-Q-K-V-A-A-S-A-P-K-K-N-T-N-S-N-N-pS-I
O26	S-pS-Q-K-V-A-A-pS-A-P-K-K-N-T-N-S-N-N-S-I
O27	S-pS-Q-K-V-A-A-S-A-P-K-K-N-pT-N-S-N-N-S-I
O28	S-pS-Q-K-V-A-A-S-A-P-K-K-N-T-N-pS-N-N-S-I
O29	S-pS-Q-K-V-A-A-S-A-P-K-K-N-T-N-S-N-N-pS-I
O30	S-S-Q-K-V-A-A-pS-A-P-K-K-N-pT-N-S-N-N-S-I
P01	S-S-Q-K-V-A-A-pS-A-P-K-K-N-T-N-pS-N-N-S-I
P02	S-S-Q-K-V-A-A-pS-A-P-K-K-N-T-N-S-N-N-pS-I
P03	S-S-Q-K-V-A-A-S-A-P-K-K-N-pT-N-pS-N-N-S-I
P04	S-S-Q-K-V-A-A-S-A-P-K-K-N-pT-N-S-N-N-pS-I
P05	S-S-Q-K-V-A-A-S-A-P-K-K-N-T-N-pS-N-N-pS-I
P06	(space)
P07	Q-K-V-A-A-S-A-P-K-K-N-T-N-S-N-N-S-I-L-K
P08	Q-K-V-A-A-pS-A-P-K-K-N-T-N-S-N-N-S-I-L-K
P09	Q-K-V-A-A-S-A-P-K-K-N-pT-N-S-N-N-S-I-L-K
P10	Q-K-V-A-A-S-A-P-K-K-N-T-N-pS-N-N-S-I-L-K
P11	Q-K-V-A-A-S-A-P-K-K-N-T-N-S-N-N-pS-I-L-K
P12	Q-K-V-A-A-pS-A-P-K-K-N-pT-N-S-N-N-S-I-L-K
P13	Q-K-V-A-A-pS-A-P-K-K-N-T-N-pS-N-N-S-I-L-K
P14	Q-K-V-A-A-pS-A-P-K-K-N-T-N-S-N-N-pS-I-L-K
P15	Q-K-V-A-A-S-A-P-K-K-N-pT-N-pS-N-N-S-I-L-K
P16	Q-K-V-A-A-S-A-P-K-K-N-pT-N-S-N-N-pS-I-L-K
P17	Q-K-V-A-A-S-A-P-K-K-N-T-N-pS-N-N-pS-I-L-K
P18	(space)
P19	V-A-A-S-A-P-K-K-N-T-N-S-N-N-S-I-L-K-I-Y
P20	V-A-A-pS-A-P-K-K-N-T-N-S-N-N-S-I-L-K-I-Y

Location	Peptide
P21	V-A-A-S-A-P-K-K-N-pT-N-S-N-N-S-I-L-K-I-Y
P22	V-A-A-S-A-P-K-K-N-T-N-pS-N-N-S-I-L-K-I-Y
P23	V-A-A-S-A-P-K-K-N-T-N-S-N-N-pS-I-L-K-I-Y
P24	V-A-A-pS-A-P-K-K-N-pT-N-S-N-N-S-I-L-K-I-Y
P25	V-A-A-pS-A-P-K-K-N-T-N-pS-N-N-S-I-L-K-I-Y
P26	V-A-A-pS-A-P-K-K-N-T-N-S-N-N-pS-I-L-K-I-Y
P27	V-A-A-S-A-P-K-K-N-pT-N-pS-N-N-S-I-L-K-I-Y
P28	V-A-A-S-A-P-K-K-N-pT-N-S-N-N-pS-I-L-K-I-Y
P29	V-A-A-S-A-P-K-K-N-T-N-pS-N-N-pS-I-L-K-I-Y
P30	(space)
Q01	A-S-A-P-K-K-N-T-N-S-N-N-S-I-L-K-I-Y-S-D
Q02	A-pS-A-P-K-K-N-T-N-S-N-N-S-I-L-K-I-Y-S-D
Q03	A-S-A-P-K-K-N-pT-N-S-N-N-S-I-L-K-I-Y-S-D
Q04	A-S-A-P-K-K-N-T-N-pS-N-N-S-I-L-K-I-Y-S-D
Q05	A-S-A-P-K-K-N-T-N-S-N-N-pS-I-L-K-I-Y-S-D
Q06	A-S-A-P-K-K-N-T-N-S-N-N-S-I-L-K-I-Y-pS-D
Q07	A-pS-A-P-K-K-N-pT-N-S-N-N-S-I-L-K-I-Y-S-D
Q08	A-pS-A-P-K-K-N-T-N-pS-N-N-S-I-L-K-I-Y-S-D
Q09	A-pS-A-P-K-K-N-T-N-S-N-N-pS-I-L-K-I-Y-S-D
Q10	A-pS-A-P-K-K-N-T-N-S-N-N-S-I-L-K-I-Y-pS-D
Q11	A-S-A-P-K-K-N-pT-N-pS-N-N-S-I-L-K-I-Y-S-D
Q12	A-S-A-P-K-K-N-pT-N-S-N-N-pS-I-L-K-I-Y-S-D
Q13	A-S-A-P-K-K-N-pT-N-S-N-N-S-I-L-K-I-Y-pS-D
Q14	A-S-A-P-K-K-N-T-N-pS-N-N-pS-I-L-K-I-Y-S-D
Q15	A-S-A-P-K-K-N-T-N-pS-N-N-S-I-L-K-I-Y-pS-D
Q16	A-S-A-P-K-K-N-T-N-S-N-N-pS-I-L-K-I-Y-pS-D
Q17	(space)
Q18	A-P-K-K-N-T-N-S-N-N-S-I-L-K-I-Y-S-D-E-A
Q19	A-P-K-K-N-pT-N-S-N-N-S-I-L-K-I-Y-S-D-E-A
Q20	A-P-K-K-N-T-N-pS-N-N-S-I-L-K-I-Y-S-D-E-A
Q21	A-P-K-K-N-T-N-S-N-N-pS-I-L-K-I-Y-S-D-E-A
Q22	A-P-K-K-N-T-N-S-N-N-S-I-L-K-I-Y-pS-D-E-A
Q23	A-P-K-K-N-pT-N-pS-N-N-S-I-L-K-I-Y-S-D-E-A
Q24	A-P-K-K-N-pT-N-S-N-N-pS-I-L-K-I-Y-S-D-E-A
Q25	A-P-K-K-N-pT-N-S-N-N-S-I-L-K-I-Y-pS-D-E-A
Q26	A-P-K-K-N-T-N-pS-N-N-pS-I-L-K-I-Y-S-D-E-A
Q27	A-P-K-K-N-T-N-pS-N-N-S-I-L-K-I-Y-pS-D-E-A
Q28	A-P-K-K-N-T-N-S-N-N-pS-I-L-K-I-Y-pS-D-E-A
Q29	(space)
Q30	K-K-N-T-N-S-N-N-S-I-L-K-I-Y-S-D-E-A-T-G
R01	K-K-N-pT-N-S-N-N-S-I-L-K-I-Y-S-D-E-A-T-G
R02	K-K-N-T-N-pS-N-N-S-I-L-K-I-Y-S-D-E-A-T-G
R03	K-K-N-T-N-S-N-N-pS-I-L-K-I-Y-S-D-E-A-T-G

Location	Peptide
R04	K-K-N-T-N-S-N-N-S-I-L-K-I-Y-pS-D-E-A-T-G
R05	K-K-N-T-N-S-N-N-S-I-L-K-I-Y-S-D-E-A-pT-G
R06	K-K-N-pT-N-pS-N-N-S-I-L-K-I-Y-S-D-E-A-T-G
R07	K-K-N-pT-N-S-N-N-pS-I-L-K-I-Y-S-D-E-A-T-G
R08	K-K-N-pT-N-S-N-N-S-I-L-K-I-Y-pS-D-E-A-T-G
R09	K-K-N-pT-N-S-N-N-S-I-L-K-I-Y-S-D-E-A-pT-G
R10	K-K-N-T-N-pS-N-N-pS-I-L-K-I-Y-S-D-E-A-T-G
R11	K-K-N-T-N-pS-N-N-S-I-L-K-I-Y-pS-D-E-A-T-G
R12	K-K-N-T-N-pS-N-N-S-I-L-K-I-Y-S-D-E-A-pT-G
R13	K-K-N-T-N-S-N-N-pS-I-L-K-I-Y-pS-D-E-A-T-G
R14	K-K-N-T-N-S-N-N-pS-I-L-K-I-Y-S-D-E-A-pT-G
R15	K-K-N-T-N-S-N-N-S-I-L-K-I-Y-pS-D-E-A-pT-G
R16	(space)
R17	N-T-N-S-N-N-S-I-L-K-I-Y-S-D-E-A-T-G-L-R
R18	N-pT-N-S-N-N-S-I-L-K-I-Y-S-D-E-A-T-G-L-R
R19	N-T-N-pS-N-N-S-I-L-K-I-Y-S-D-E-A-T-G-L-R
R20	N-T-N-S-N-N-pS-I-L-K-I-Y-S-D-E-A-T-G-L-R
R21	N-T-N-S-N-N-S-I-L-K-I-Y-pS-D-E-A-T-G-L-R
R22	N-T-N-S-N-N-S-I-L-K-I-Y-S-D-E-A-pT-G-L-R
R23	N-pT-N-pS-N-N-S-I-L-K-I-Y-S-D-E-A-T-G-L-R
R24	N-pT-N-S-N-N-pS-I-L-K-I-Y-S-D-E-A-T-G-L-R
R25	N-pT-N-S-N-N-S-I-L-K-I-Y-pS-D-E-A-T-G-L-R
R26	N-pT-N-S-N-N-S-I-L-K-I-Y-S-D-E-A-pT-G-L-R
R27	N-T-N-pS-N-N-pS-I-L-K-I-Y-S-D-E-A-T-G-L-R
R28	N-T-N-pS-N-N-S-I-L-K-I-Y-pS-D-E-A-T-G-L-R
R29	N-T-N-pS-N-N-S-I-L-K-I-Y-S-D-E-A-pT-G-L-R
R30	N-T-N-S-N-N-pS-I-L-K-I-Y-pS-D-E-A-T-G-L-R
S01	N-T-N-S-N-N-pS-I-L-K-I-Y-S-D-E-A-pT-G-L-R
S02	N-T-N-S-N-N-S-I-L-K-I-Y-pS-D-E-A-pT-G-L-R
S03	(space)
S04	N-S-N-N-S-I-L-K-I-Y-S-D-E-A-T-G-L-R-V-D
S05	N-pS-N-N-S-I-L-K-I-Y-S-D-E-A-T-G-L-R-V-D
S06	N-S-N-N-pS-I-L-K-I-Y-S-D-E-A-T-G-L-R-V-D
S07	N-S-N-N-S-I-L-K-I-Y-pS-D-E-A-T-G-L-R-V-D
S08	N-S-N-N-S-I-L-K-I-Y-S-D-E-A-pT-G-L-R-V-D
S09	N-pS-N-N-pS-I-L-K-I-Y-S-D-E-A-T-G-L-R-V-D
S10	N-pS-N-N-S-I-L-K-I-Y-pS-D-E-A-T-G-L-R-V-D
S11	N-pS-N-N-S-I-L-K-I-Y-S-D-E-A-pT-G-L-R-V-D
S12	N-S-N-N-pS-I-L-K-I-Y-pS-D-E-A-T-G-L-R-V-D
S13	N-S-N-N-pS-I-L-K-I-Y-S-D-E-A-pT-G-L-R-V-D
S14	N-S-N-N-S-I-L-K-I-Y-pS-D-E-A-pT-G-L-R-V-D
S15	(space)
S16	N-N-S-I-L-K-I-Y-S-D-E-A-T-G-L-R-V-D-P-L

Location	Peptide
S17	N-N-pS-I-L-K-I-Y-S-D-E-A-T-G-L-R-V-D-P-L
S18	N-N-S-I-L-K-I-Y-pS-D-E-A-T-G-L-R-V-D-P-L
S19	N-N-S-I-L-K-I-Y-S-D-E-A-pT-G-L-R-V-D-P-L
S20	N-N-pS-I-L-K-I-Y-pS-D-E-A-T-G-L-R-V-D-P-L
S21	N-N-pS-I-L-K-I-Y-S-D-E-A-pT-G-L-R-V-D-P-L
S22	N-N-S-I-L-K-I-Y-pS-D-E-A-pT-G-L-R-V-D-P-L
S23	(space)
S24	M-A-A-S-V-P-P-G-G-Q-R-I-L-Q-K-R-R-Q-A-Q
S25	A-S-V-P-P-G-G-Q-R-I-L-Q-K-R-R-Q-A-Q-S-I
S26	V-P-P-G-G-Q-R-I-L-Q-K-R-R-Q-A-Q-S-I-K-E
S27	P-G-G-Q-R-I-L-Q-K-R-R-Q-A-Q-S-I-K-E-K-Q
S28	G-Q-R-I-L-Q-K-R-R-Q-A-Q-S-I-K-E-K-Q-A-K
S29	R-I-L-Q-K-R-R-Q-A-Q-S-I-K-E-K-Q-A-K-Q-T
S30	L-Q-K-R-R-Q-A-Q-S-I-K-E-K-Q-A-K-Q-T-P-T
T01	K-R-R-Q-A-Q-S-I-K-E-K-Q-A-K-Q-T-P-T-S-T
T02	R-Q-A-Q-S-I-K-E-K-Q-A-K-Q-T-P-T-S-T-R-Q
T03	A-Q-S-I-K-E-K-Q-A-K-Q-T-P-T-S-T-R-Q-A-G
T04	S-I-K-E-K-Q-A-K-Q-T-P-T-S-T-R-Q-A-G-Y-G
T05	K-E-K-Q-A-K-Q-T-P-T-S-T-R-Q-A-G-Y-G-G-S
T06	K-Q-A-K-Q-T-P-T-S-T-R-Q-A-G-Y-G-G-S-S-S
T07	A-K-Q-T-P-T-S-T-R-Q-A-G-Y-G-G-S-S-S-S-I
T08	Q-T-P-T-S-T-R-Q-A-G-Y-G-G-S-S-S-S-I-L-K
T09	P-T-S-T-R-Q-A-G-Y-G-G-S-S-S-S-I-L-K-L-Y
T10	S-T-R-Q-A-G-Y-G-G-S-S-S-S-I-L-K-L-Y-T-D
T11	R-Q-A-G-Y-G-G-S-S-S-S-I-L-K-L-Y-T-D-E-A
T12	A-G-Y-G-G-S-S-S-S-I-L-K-L-Y-T-D-E-A-N-G
T13	Y-G-G-S-S-S-S-I-L-K-L-Y-T-D-E-A-N-G-F-R
T14	G-S-S-S-S-I-L-K-L-Y-T-D-E-A-N-G-F-R-V-D
T15	S-S-S-I-L-K-L-Y-T-D-E-A-N-G-F-R-V-D-S-L
T16	(space)
T17	(space)
T18	(space)
T19	(space)
T20	S-pS-P-T-P-P-G-G-Q-R-G-L
T21	(space)
T22	G-R-L-V-K-E-G-G-D-I-A-F
T23	(space)
T24	S-pS-P-T-P-P-G-G-Q-R-G-L
T25	(space)
T26	G-R-L-V-K-E-G-G-D-I-A-F
T27	(newline)
T28	(newline)
T29	(newline)

Location	Peptide		
T30		(newline)	